Signal processing and machine learning contributions to rhythm analysis during cardiopulmonary resuscitation

By

Iraia Isasi Liñero

Supervisors:

Unai Irusta Zarandona

Elisabete Aramendi Ecenarro

Doctoral Thesis

eman ta zabal zazu

Universidad del País Vasco   Euskal Herriko Unibertsitatea

Dedicated to my family,
for their endless support.

To Asier,
for always being there.

ACKNOWLEDGMENTS

To my "cuadrilla", for all the moments together. Thank you for those long coffees and confidences. These hard months of confinement made me realize how much I need you.

I am extremely grateful to my parents for their love, caring and sacrifices for educating and preparing me for my future. I owe you everything. To my sister, thanks for keeping me afloat in the bad moments, thanks for being my role model.

Finally, I would like to express my deepest gratitude to Asier for making these last 9 years the best experience of my life. I hope to keep sharing new adventures with you in this new chapter of our life.

ABSTRACT

Out-of-hospital cardiac arrest (OHCA) is characterized by the sudden loss of the cardiac function, and causes around 10% of the total mortality in developed countries. The estimated average annual incidence of OHCA is 55 cases per 100 000 persons, with low survival rates of around 10%.

Survival from OHCA depends largely on two factors: early defibrillation (electrical shock) and early cardiopulmonary resuscitation (CPR). The electrical shock is delivered using a defibrillator, an electromedical device which includes a shock advice algorithm (SAA) to detect if a shockable rhythm is present. Unfortunately, CPR must be stopped for a reliable SAA analysis because chest compressions introduce artefacts in the ECG. These interruptions in CPR have an adverse effect on OHCA survival.

Since the early 1990s, many efforts have been made to reliably analyze the rhythm during CPR. Strategies have mainly focused on adaptive filters to suppress the CPR artefact. Once the artefact is removed, SAAs of commercial defibrillators have been widely used for the shock/no-shock decision. However, these solutions did not meet the American Heart Association's (AHA) accuracy requirements for shock/no-shock decisions made analyzing artefact-free ECGs. A recent approach, which replaces the commercial SAA by machine learning classifiers, has demonstrated that a reliable rhythm analysis during CPR is possible. However, defibrillation is not the only treatment needed during OHCA, and depending on the clinical context a finer rhythm classification is needed. Indeed, an optimal OHCA scenario would allow the classification of the five cardiac arrest rhythm types that may be present during resuscitation. Unfortunately, multiclass classifiers that allow a reliable rhythm analysis during CPR have not yet been demonstrated.

In all of these studies artifacts originate from manual compressions delivered by rescuers. Mechanical compression devices, such as the LUCAS or the AutoPulse, are increasingly used in resuscitation. Thus, a reliable rhythm analysis during mechanical CPR is becoming critical. Unfortunately, no AHA compliant algorithms have yet been demonstrated during mechanical CPR.

The focus of this thesis work is to provide new or improved solutions for rhythm analysis during CPR, including shock/no-shock decision during manual and mechanical CPR and multiclass classification during manual CPR. The work started with the development of the first AHA compliant shock/no-shock decision algorithm during mechanical CPR. The method consisted of an adaptive filter to remove chest compression artefacts followed by a multistage shock/no-shock classifier based on a commercial SAA. These results were further improved in a second study where the commercial SAA was replaced by a machine learning classifier. Efforts were then focused on manual CPR. First, a reliable algorithm for multiclass OHCA rhythm classification was introduced in the presence of CPR artefacts. Second, deep learning techniques were firstly introduced to improve the accuracy of the machine learning based shock/no-shock algorithms proposed in the literature. The thesis concludes with an additional study where the performance of different mechanical CPR artefact suppression filters is evaluated in terms of ECG waveform restoration, clinically relevant ECG characteristics, and shock/no-shock diagnostic accuracy.

CONTENTS

LIST OF FIGURES

LIST OF TABLES

LIST OF ABBREVIATIONS

Acc	Total accuracy
AED	Automated external defibrillator
AF	Atrial fibrillation
AHA	American Heart Association
ANN	Artificial neural network
AS	Asystole
AV	Atrioventricular
BAC	Balanced accuracy
BLS	Basic life support
CAO	Coronary artery occlusion
CD	Compression depth
CO_2	Carbon dioxide
CPR	Cardiopulmonary resuscitation
DFA	Detrended fluctuation analysis
DWT	Discrete Wavelet transform
ECG	Electrocardiogram
EMD	Empirical mode decomposition
EMS	Emergency medical system
ERC	European Resuscitation Council
EuReCa	European Registry of Cardiac Arrest
Expmod	Standard exponential algorithm
FN	False negative
FP	False positive

FS	Feature selection
HILB	Hilbert transform
ID	Idioventricular
IHCA	In-hospital cardiac arrest
KNN	k-nearest neighbour
LEA	Low electrical activity
LMS	Least mean squares
MAV	Mean absolute value
MC-RAMP	Multi-channel Recursive Adaptive Matching Pursuit
MSA	Multistage algorithm
NPV	Negative predictive value
NSR	Normal sinus rhythm
OHCA	Out-of-hospital cardiac arrest
PAD	Public access defibrillation
PCA	Principal component analysis
PCI	Percutaneous coronary intervention
PEA	Pulseless electrical activity
PPV	Positive predictive value
PR	Pulse-generating rhythm
PSD	Power spectral density
PSR	Phase space reconstruction
PTA	Plus-l Minus-r selection
PVC	Premature ventricular contraction
RCWT	Raised-Cosine Wavelet transform
RF	Random forest
RFE	Recursive feature elimination
RLS	Recursive least squares
ROC	Resuscitation Outcome Consortium

ROSC	Restoration of spontaneous circulation
SA	Sinoatrial
SAA	Shock advice algorithm
SB	Sinus bradycardia
SBS	Sequential backward selection
SCA	Sudden cardiac arrest
SCD	Sudden cardiac death
Se	Sensitivity
SFS	Sequential floating selection
SNR	Signal-to-noise ratio
SOM	Self organizing maps
Sp	Specificity
SVM	Support vector machine
SVT	Supraventricular tachycardia
SWT	Stationary Wavelet transform
TCSC	Threshold crossing sample count
TI	Transthoracic impedance
TN	True negative
TP	True positive
UMS	Unweighted mean of sensitivities
VF	Ventricular fibrillation
VFleak	VF filter leakage
VT	Ventricular tachycardia

1 | THESIS OVERVIEW

1.1 THE HEART

The heart is a hollow muscular organ that, by rhythmic contraction, effectively pumps oxygenated blood throughout the circulatory system. As shown in Figure 1.1, the heart consists of four chambers split into two halves, the left and right sides. Each side contains an upper chamber called the atrium responsible of picking up the blood that comes into the heart, and a lower chamber called the ventricle that pumps the blood out. The right side receives oxygen-depleted blood from the circulatory system and delivers it to the lungs for oxygenation. The left side of the heart receives oxygen-rich blood from the lungs and pumps it out to the rest of the body tissues. These two actions are conducted simultaneously in two different phases which define the cardiac cycle: a filling phase called diastole, and a pumping phase called systole.

The pumping action involves a muscle contraction which originates from the electrical stimulation of the cardiac cells. This electrical activity can be recorded on the surface of the body by placing two electrodes, a signal known as the electrocardiogram (ECG). In a healthy heart, the cardiac cycle is initiated by the sinoatrial (SA) node, which is located in the upper part of the right atrium. The SA is a natural pacemaker and therefore sets the basic pace for the heart rate with a trigger rate of 60 to 100 impulses per minute. The electrical impulse propagates from the SA node through both the right and the left atria, causing their depolarization. The contraction induced by the depolarization of atrial cells pumps blood into the ventricles.
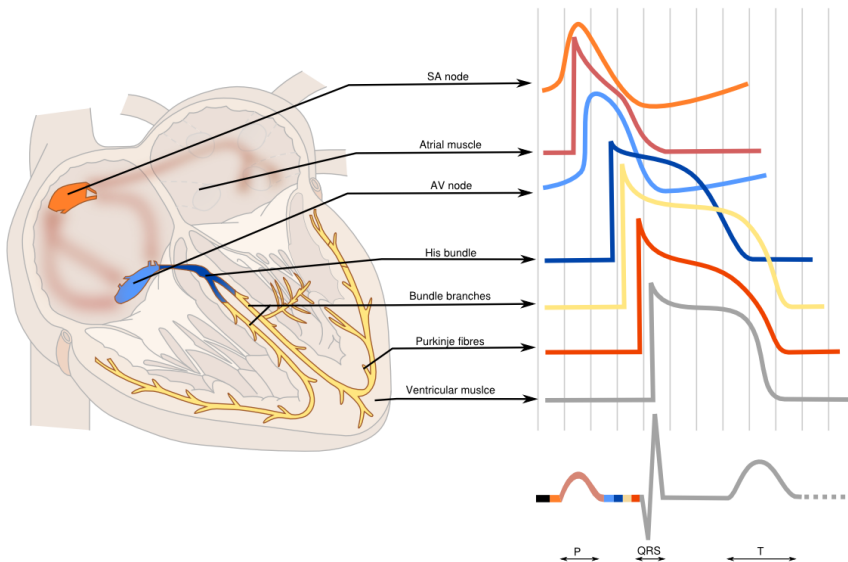
Figure 1.1. Formation of a QRS complex corresponding to a NSR in relation to the cardiac conduction system. Figure extracted from www.textbookofcardiology.org

This impulse is responsible for the P-wave of the electrocardiogram (see Figure 1.1) and, in turn, causes the atrioventricular (AV) node to depolarize (contract). The main task of the AV node is to collect and delay the propagation of the SA impulse so that the ventricles can be completely filled with blood. This delay in the transmission of the electrical impulse is reflected in the P-R interval of the ECG. The impulse is then spread through the left and the right ventricles using a fast conduction network composed of the bundle of His and the Purkinje fibers. This causes the depolarization of the ventricles and a rapid and coordinated mechanical contraction which generates enough pressure to pump the blood to the lungs or the rest of the tissues. As shown in Figure 1.1, the ventricular depolarization appears as the QRS complex in the ECG. The ventricular cells are then repolarized and returned back to their original state following a refractory period, during which they cannot be depolarized again. Ventricular repolarization produces the final deflection in the ECG called T wave. There is no distinctly visible wave representing atrial repolarization in the ECG because it occurs during ventricular depolarization and it is therefore masked by the QRS complex.

The aforementioned cardiac cycle sequence is continuously repeated producing an uninterruped blood flow and constitues the normal functioning of the heart, a state referred to as normal sinus rhythm (NSR). An arrhythmia is a heart rhythm disturbance from the NSR, either because the heart beats too fast (tachycardia), too slow (bradycardia), or irregularly. Although most arrhythmia are harmless, some can be dangerous and even lethal. The most life-threatening arrhythmia originate in the ventricles and are known as ventricular tachycardia (VT) and ventricular fibrillation (VF). During these lethal arrhytmia blood pumping is inefficient causing damage to vital organs. This is an emergency situation that requires immediate intervention to revert the arrhythmia.

1.2   Out-of-hospital cardiac arrest (OHCA)

Sudden cardiac arrest (SCA) is defined by the unexpected cessation of the mechanical activity of the heart, which leads to the abrupt loss of spontaneous and effective blood circulation [1]. Death resulting from a cardiac arrest occurs shortly after the onset of acute symptons (< 1 h), and is known as sudden cardiac death (SCD) [2, 3]. The high incidence, its sudden nature, and the low survival rates make SCD a major public health problem. Most cardiac arrest are unexpected and occur out of hospital, an event known as out-of-hospital cardiac arrest (OHCA). The efforts to revert cardiac arrest and recover spontaneous pulse are frequently referred to as resuscitation.

Coronary artery disease is the most common cause of sudden cardiac death, accounting for up to 80% of all cases [4]. The remaining 20% corresponds to cardiomyopathies and genetic channelopathies [4, 5]. These heart disorders predispose patients to VF which frequently starts as VT [6, 7]. VF is characterized by rapid and irregular electrical impulses which cause the loss of coordination in the contraction of the ventricles. The pumping function is therefore lost leading to an immediate cessation of the spontaneous blood circulation. Electrical defibrillation is the only effective treatment to revert VF and achieve pulse-generating rhythms (PR), i.e. organized cardiac electrical and mechanical activity that generates blood flow [8]. A critical factor to return to a PR, that is to achieve restoration of

4

spontaneous circulation (ROSC), is the time from onset of VF to defibrillation [9]. Untreated VF gradually deteriorates as time elapses leading to either asystole (AS), i.e. the absence of electrical activity, or pulseless electrical activity (PEA) characterized by the presence of organized electrical activity without an effective mechanical contraction that generates blood flow [10]. During AS and PEA there is no oxygenation of the cardiac cells leading to myocardial ischemia. Therefore, the probability of a successful defibrillation and subsequent survival is quite low for this kind of rhythms [11, 12]. Figure 1.2 shows examples of the ECG for the five cardiac arrest rhythm types that can be present during cardiac arrest.

The precise incidence of OHCA is unknown since it varies depending on its definition and the inclusion criteria. The overall
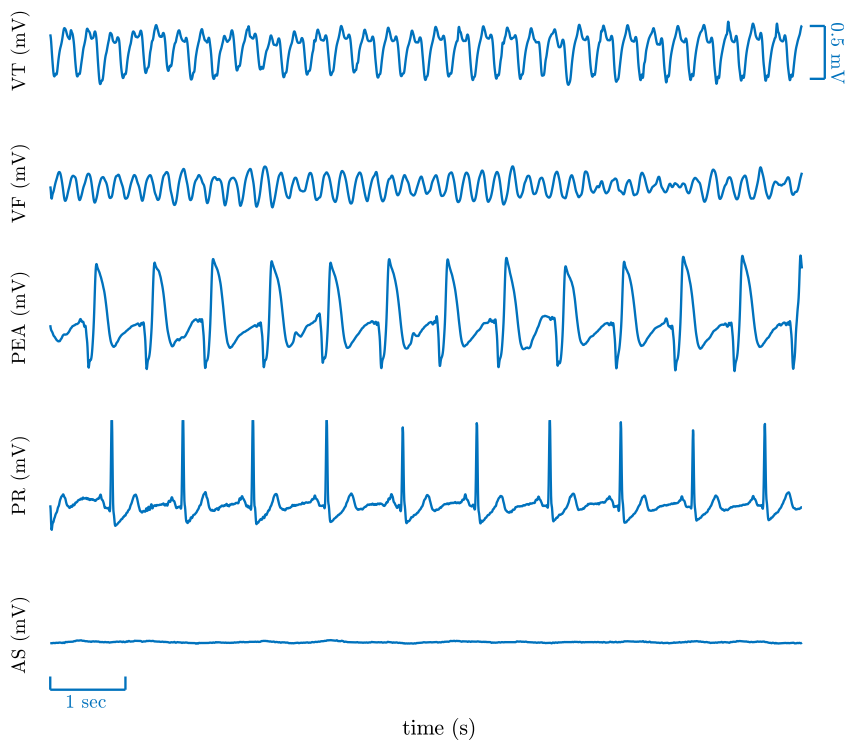
Figure 1.2. Examples of the five different cardiac rhythms during resuscitation. The vertical axes was equally scaled for every plot.

estimates per year range from 150 000 to 530 000 in the Unitated States [2, 13] and 275 000 in Europe [14, 15], with an incidence of 55 and 38 cases per 100 000 person-years, respectively. Incidences are similar in Spain with 29-40 cases per 100 000 persons every year [16, 17]. Finally, the Basque Country has a reported incidence of 33.9 OHCA cases per 100 000 person-years [18].

Despite advances in resuscitation therapies, survival rates of both in-hospital and OHCA remain poor. Rates ranging from 8.4% to 10.7% have been reported for OHCA [19, 14], and 10.4% for in-hospital cardiac arrest (IHCA) [20]. OHCA survival rates are higher for patients presenting VF as initial rhtyhm [19]. VF/VT is present as the initial rhythm in 46% of OHCA cases, PEA in 17% and AS in 37%, with respective survival rates of 27%, 3% and 1% [21]. However, prevalences for initial rhythms and reported outcomes differ considerably depending on the study and on the geographic region, ranging from less than 2% in some rural areas to more than 20% in certain cities with dedicated cardiopulmonary resuscitation (CPR) training programs [22, 23, 24].

1.3   KEY THERAPIES FOR OHCA

The chain of survival metaphor is the standard of care used across the world for OHCA victims. The latest version of the chain of survival was published in the 2005 European Resuscitation Council (ERC) [25] and American Heart Association (AHA) guidelines [26]. It was based on a review of previous iterations, starting with the first version in 1991 [27]. The chain of survival consists of 4 links:

- *Early access*: the first link in the chain of survival includes the early recognition of the cardiac arrest and the rapid activation of the Emergency Medical System (EMS) by calling the local emergency number. The early identification of cardiac arrest symptoms is critical, since EMS activation before the collapse is associated with higher survival rates [29].

- *Early CPR:* CPR combines chest compressions and rescue breathings in order to maintain a minimum blood flow essential to oxygenate the vital organs until the delivery of

an electrical shock. The immediate hands-on response of bystanders to cardiac arrest is critical to increase the likelihood of survival [30, 31, 32]. CPR and first aid training programs are therefore of great importance to increase the number of bystanders who know how to perform the basic CPR manoeuvres. The AHA has suggested that a 20% prevalence of CPR training among adults might significantly reduce mortality from OHCA [33].

- *Early defibrillation*: Defibrillation is the only effective way to revert VF and obtain ROSC. The time from onset of VF to defibrillation is critical for OHCA survival [34, 35]. Public Access Defibrillation (PAD) programs play a very important role in this step of the chain of survival [36]. They make defibrillation accessible to the general public through automated external defibrillators (AED) [36] in order to reduce the time to defibrillation as much as possible.

- *Early advanced cardiac life support (ACLS)*: The combination of CPR and defibrillation is sometimes not enough to restore a perfusing rhythm, and even less to sustain ROSC over time and stabilise the patient. Therefore, treatment provided by healthcare personnel is crucial to increase OHCA survival after defibrillation. ACLS includes intubation, administration of drugs and defibrillation as main interventions [37].

Figure 1.3. The four links of the chain of survival: early access, early CPR, rapid defibrillation and post resuscitation care. Figure extracted from ERC guidelines 2015 [28].

The mean time until the ambulance arrival and the first ACLS shock after EMS activation varies widely between areas, but they are within 5-9 min for ambulance arrival and 11 min for first ACLS shock in most cases [38, 39]. During this time, bystander CPR and defibrillation are determinant to increase the likelihood of survival. When no bystander CPR is provided, the survival rate decreases by $10 - 12\%$ for every minute delay in defibrillation [40, 41]. However, this rate is reduced to $3 - 4\%$ if CPR is provided [42, 43, 9]. Figure 1.4 shows the influence of early CPR and early defibrillation in OHCA survival. If CPR starts more than 5 min (the average minimum time of ambulance arrival) after the collapse and defibrillation is not provided within the first 11 min (mean time until the first EMS shock), the probability of survival is below 20%. Survival rates can be doubled (above 40%) if bystander CPR starts within the first 4 min from collapse and defibrillation is delivered within the first 8 min [44]. The role of the OHCA witness is therefore crucial for survival.

1.4 CARDIOPULMONARY RESUSCITATION

CPR consists of chest compressions interspaced with ventilations to maintain a small but critical oxygenated blood flow to the vital organs [45]. The positioning of the rescuer to provide chest
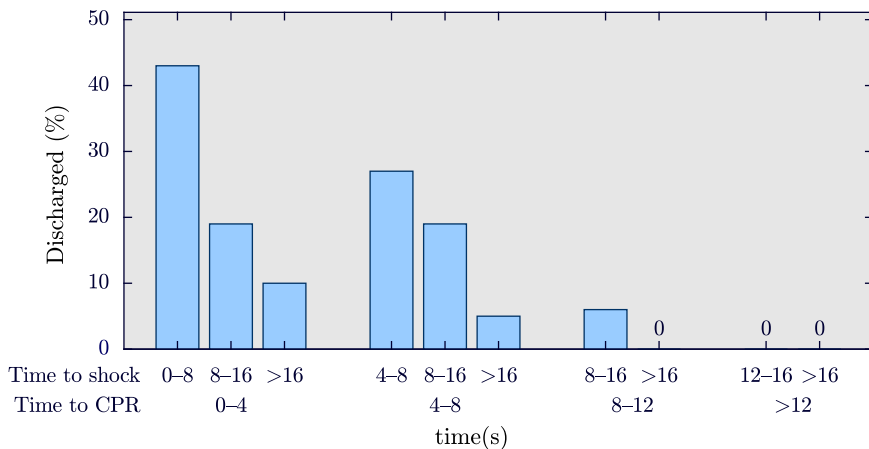
Figure 1.4. Percentage of survival to hospital discharge in OHCA, as a function of time to CPR and defibrillation. Adapted from Eisenberg et al. [44].

8

compressions and ventilations during CPR is shown in Figure 1.5.
CPR should occur immediately after witnesses recognize a cardiac
arrest and simultaneously with their efforts to activate the EMS
system. CPR alone is unlikely to terminate VF and achieve ROSC, so
it must be followed quickly by defibrillation, intubation, and drug
administration.

Resuscitation guidelines describe how CPR should be provided,
both in basic life support (BLS) and in ACLS settings [28, 46].
BLS comprises the non-invasive emergency interventions intended
to assist the immediate survival of an OHCA victim until the
arrival of ACLS. It is usually provided by trained or untrained
cardiac arrest witnesses, emergency medical technicians or public
safety professionals [47]. ACLS-level prehospital care is tipically
implemented by physicians and include invasive interventions to
support the airway, breathing and circulation [48].

The basic BLS therapy that all rescuers, trained or not, should
perform are chest compressions [28]. Furthermore, if the rescuer is
trained in CPR, ventilations (mouth-to-mouth rescue breaths) should
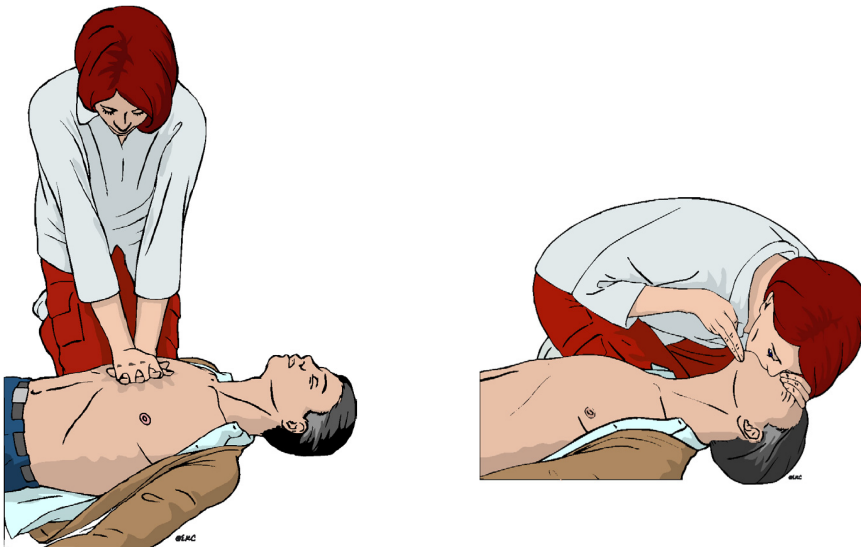
Figure 1.5. Positioning of the rescuer to provide chest compressions and ventilations during CPR. Source: ERC 2015 [28].

also be performed, alternating series of 30 chest compressions with 2 ventilations. CPR should be continuously administered until an AED is available. The AED analyzes the rhythm of the patient providing an electrical shock if necessary.

ACLS healthcare professionals should attempt laryngoscopy and intubation, minimizing interruptions of chest compressions during its placement [46]. After intubation, the patient should be ventilated at 10 breaths per minute whilst chest compressions are administered. Rhythm assessment is performed every two minutes through monitor-defibrillators which are able to provide an electrical shock if the physician considers it necessary.

Resuscitation guidelines emphasize the importance of high-quality chest compressions to improve outcome from OHCA [28, 46]. Optimal chest compressions imply rates and depths between 100-120 compressions per minute (cpm) and 5-6 cm, respectively [28, 49, 50]. Furthermore, a complete chest recoil should be allowed between each compression and interruptions in compressions must be minimized.

High-quality CPR is associated with an increase in OHCA survival [51]. Studies reveal that each 5 mm increase in compression depth portends an approximate two-fold increase in the likelihood of shock success [52]. However, compression depths exceeding 6 cm increase the rate of injuries such as rib fractures [53]. Regarding chest compression rate, Idris et al. [54] found that the likelihood of ROSC peaks at a rate of $\sim$ 125 cpm during the first 5 minutes of CPR. However, depth declined with higher compression rates decreasing the effectiveness of CPR [54]. Patients receiving less than 75 cpm were associated with decreased likelihood of ROSC [54].

Studies in OHCA have shown that providing high quality CPR is very challenging for untrained first responders [55], but also for health care professionals [20, 56, 57, 58]. In many cases, compressions are not continued for long enough periods of time, and compressions are too fast or too shallow, and with interruptions. Rescuer fatigue due to prolonged CPR, the lack of feedback systems or unstable conditions during ambulance transportation are the most important factors explaining low quality CPR.

Several mechanical chest compression devices have been introduced in ACLS settings to optimize the delivery of CPR. These devices deliver compressions at a constant rate and depth in adherence with current resuscitation guidelines. There are two types of automated compressors: pneumatically driven pistons like the LUCAS-3 (Physio-Control Inc/Jolife, AB, Lund, Sweeden), and load distributing bands like the AutoPulse (Zoll Circulation, Chelmsford, Massachusetts, USA) [46]. Both the LUCAS-3 and the AutoPulse are shown in Figure 1.6 and their technical specifications are detailed in Table 1.1.

Mechanical compression devices provide high quality chest compressions which are associated to higher OHCA survival. However, the results of the main randomized control trials for

Table 1.1. Technical specifications of the LUCAS-3 and the AutoPulse devices.

	LUCAS-3	AutoPulse
Compression rate	$102 \pm 2\,\mathrm{min}^{-1}$	$80 \pm 2\,\mathrm{min}^{-1}$
Compression depth	$40 - 55\,\mathrm{mm}$ based on chest height	20% of chest depth
Duty cycle	50%	50%
Full chest recoil	Yes	Yes

Figure 1.6. The LUCAS-2 and AutoPulse devices. The LUCAS-2 uses a pneumatically driven piston to compress the patient's chest whereas the AutoPulse uses a distributing band placed around the chest to deliver the chest compressions.

mechanical CPR show inconclusive evidences on the effect of these devices on survival [59, 60]. Rubertsson et al. [59] reported that there was no significant difference in 4-hour survival between patients treated with the LUCAS device or those treated with high-quality manual CPR. Neurological outcomes after 6 months were also the same for both groups. According to Wik et al. [60] there was also no statistical difference in survival to hospital discharge and neurological outcome between patients treated with the AutoPulse device and patients treated with manual CPR. Since the use of mechanical CPR devices is not associated to improved survival, the ERC guidelines recommend the use of automated compressors in prolonged CPR, and in scenarios where manual chest compressions are impractical or compromise rescuer's safety [46].

Treatment of the underlying cause of cardiac arrest is not always possible at the scene, e.g. hypothermia or intoxication [61, 62, 63, 64]. In these situations, the patient should be transferred to the hospital while receiving CPR therapy [65]. However, manual chest compressions are risky for unbelted rescuers and ineffective due to transport motion [66, 67]. Mechanical devices could therefore be a suitable alternative to manual CPR for providing high quality chest compressions during transport [68, 69, 70, 71, 72, 73].

Sometimes early CPR and defibrillation are not enough to achieve ROSC. In these cases it is necessary to first deal with the underlying source of the cardiac arrest. Coronary artery occlusion (CAO) is often the responsible for not achieving a perfusing rhythm as it causes recurrent VF or persistent PEA. Percutaneous coronary intervention (PCI) is usually required to restore an effective circulation in patients with CAO, but this must be performed whilst chest compressions are continued. As the delivery of manual CPR is unfeasible during this kind of interventions, mechanical devices have been extensively used during PCI [74, 75, 76, 77].

1.5 EARLY DEFIBRILLATION

In OHCA defibrillation is achieved through an electrical current to the cardiac muscle which enables the SA node to regain control and establish an organized perfusing rhythm. BLS provides electrical

therapy using AEDs while ACLS makes use of more sophisticated devices called monitor-defibrillators.

The AED is a portable, lightweight and easy-to-use device that allows bystanders with no training to assist OHCA victims, guiding them in CPR and defibrillation by visual and audio messages [78]. First, self-adhesive defibrillation patches need to be attached to the chest of the victim. These pads are used to record the ECG and transthoracic impedance (TI) signals, and to induce the current needed for the electrical shock. Once the pads are correctly attached, the AED automatically initiates the ECG rhythm analysis through the use of a shock advice algorithm (SAA). If the SAA detects a VF or a pulseless VT (i.e. a shockable rhythm) the AED prompts the rescuer to provide an electrical shock. In case that other rhythms (i.e. nonshockable rhythms) are detected, the AED will instruct rescuer to continue CPR for the next 2 minutes, after which another rhythm analysis will be done using the SAA of the device.

In 1997, the AHA published a statement which describes the requirements that SAAs must meet to be safely integrated into commercial AEDs [79]. This includes, among other items, specifications about the database used in the development and testing of the SAA, as well as minimum performance requisites of the algorithm. This statement later led to the ANSI/AAMI/IEC 60601-2-04 standard [80], which specifies the requirements for the safety of cardiac defibrillators and defines performance targets for SAAs.

The AHA statement divided OHCA arrhythmia into three categories:

- *Shockable rhythms:* lethal rhythms requiring prompt defibrillation to avoid SCD. These rhythms include coarse VF (peak-to-peak amplitude $> 200\,\mu V$) and rapid VT, with a heart rate usually greater than $120\,min^{-1}$ (depends on the manufacturer).

- *Nonshockable rhythms:* benign (or even normal) rhythms that must not be shocked, especially in patients with a pulse, because no benefit will follow and deterioration in rhythm may result. Nonshockable rhythms include NSR, supraventricular

tachycardia (SVT), sinus bradycardia (SB), atrial fibrillation and flutter (AF), heart block, idioventricular rhythms (IV), premature ventricular contractions (PVC), and other rhythms accompanied by a palpable pulse and/or occurring in a conscious patient. Asystole (peak-to-peak amplitudes below 100 µV) is unlikely to benefit from defibrillation [81]. Moreover, the ERC guidelines discourage interrupting CPR for shock delivery during asystole [46]. So, to maximize safety in the event of misapplication of the device/electrode, asystole was also included in this category.

- *Intermediate rhythms:* rhythms for which the benefits of defibrillation are limited or uncertain. This category includes slow or low-amplitude VF (peak to peak amplitudes within $100 - 200$ µV) and VT not fulfilling criteria for rapid VT.

The ECG rhythm databases to develop and test SAA algorithms should contain rhythms annotated into these three categories. As different physicians may differ in the annotation of certain rhythms, the AHA recommends that classification requires agreement among at least three qualified OHCA rhythm reviewers. Rhythm segments on which reviewers fail to reach 100% agreement can be classified, but the expert disagreement should be reported.

The performance of the SAA is evaluated by comparing its shock/no-shock decisions with the annotations of the reviewers, and defining shockable as the positive class. In this way, the number of true positive (TP), false positive (FP), false negative (FN) and true negative (TN) detections can be calculated. The AHA only demands a minimum value in two performance metrics, sensitivity (Se) and specificity (Sp), that is, the proportion of correctly classified shockable and nonshockable rhythms, respectively. However, positive and negative predictive values are also extensively used as SAA performance metrics. PPV and NPV determine the probability that a shock is needed when it is advised or not needed when it is not indicated. Total (Acc) and balanced accuracy (BAC) are also typically reported measures, although both can be derived from Se and Sp values and rhythm prevalences. Mathematically, these performance metrics are defined as:

$$Se = \frac{TP}{TP + FN} \qquad\qquad PPV = \frac{TP}{TP + FP} \qquad (1.1)$$

$$Sp = \frac{TN}{TN + FP} \qquad\qquad NPV = \frac{TN}{TN + FN} \qquad (1.2)$$

$$Acc = \frac{TP+TN}{TP+FN+TN+FP} \qquad BAC = \frac{1}{2}(Se + Sp) \qquad (1.3)$$

Table 1.2 indicates the minimum number of ECG samples per category required to test the algorithm, and the minimum values of sensitivity and specificity for each rhythm type established by the AHA. The SAAs implemented in commercial AEDs have been extensively tested on adults [82, 83] and more recently on pediatric patients [84, 85, 86, 87] and have reported sensitivities above 96% and specificities around 100% [88, 89].

Table 1.2. Performance goals for SAAs. Extracted from Kerber et al. [79].

Rhythms	Minimum test sample size	Performance goal	90% lowerCI
Shockable			
Coarse VF	200	> 90% Se	87%
Rapid VT	50	> 75% Se	67%
Non-shockable	300		
NSR	100	> 99% Sp	97%
AF, SB, SVT, blocks, IV, PVC	30	> 95% Sp	88%
Asystole	100	> 95% Sp	92%
Intermediate			
Fine VF	25	Report only	-
Other VT	30	Report only	-

1.6 DEFIBRILLATION AND CPR

The mechanical activity from the chest compressions introduces artefacts in the ECG that substantially lower the accuracy of SAAs to values below those recommended by the AHA [90]. Therefore, CPR must be interrupted for a reliable rhythm analysis. These

interruptions, which take between 5.2 s and 28.4 s [91], adversely affect the probability of shock success and subsequent survival [92, 93, 52, 94, 95]. As Figure 1.7 shows, successful defibrillation is associated with shorter preshock pauses [52]: the probability of shock success is greater than 90% for pre-shock pauses of less than 10 s, but drops to 38% if the pause is longer than 30 s. These findings are consistent with those of Chestkes et al. [95] which showed an 18% and 14% decrease in survival to hospital discharge for every 5 s increase in preshock and perishock (preshock plus postshock) pause, respectively.

ACLS clinicians use monitor/defibrillators instead of AEDs to analyze the ECG and provide defibrillation. Monitor/defibrillators have two operating modes: manual and automatic/semiautomatic mode, i.e. AED mode. They are mostly used in manual mode, in which clinicians visually assess the ECG and decide whether the patient should be shocked or not based on their knowledge. The rhythm is assesssed every 2 min cycle of CPR, and chest compressions are interrupted to view the ECG without artefacts.

The monitor/defibrillators allow a more comprehensive patient monitoring through the acquisition of multiple signals in addition to the ECG and TI, such as, pulse oximetry or capnography. Pulse
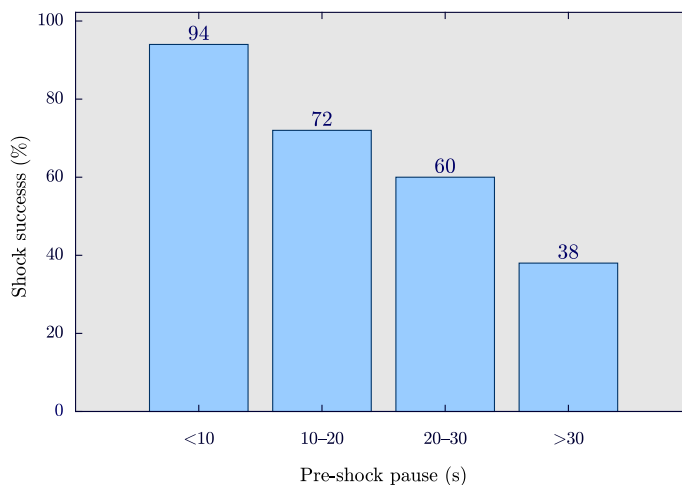
Figure 1.7. Probability of shock success as a function of the duration of the pre-shock pause. Adapted from Edelson et al. [52].

oximetry measures the oxygen saturation of arterial blood making use of a sensor typically attached to a finger, toe, or ear. It has been used as an hemodynamic marker of CPR efficiency [96] and as an indicator of ROSC [97, 98]. The capnogram is a continuous non-invasive measure of the carbon dioxide (CO_2) in respiratory gases. Its use is recommended to confirm tracheal tube placement [99, 100, 101], to monitor CPR quality [102, 103, 104] and to detect ROSC [105, 106, 107]. Furthermore, monitor/defibrillators often include sternal assist pads fitted with accelerometers and force sensors which allow real time CPR feedback. These sensors enable the calculation of the compression depth (CD) signal from which CPR quality measures, such as, compression depth and rate can be calculated [108, 109, 110]. Figure 1.8 shows an example of ECG, TI, CD and capnography signals recorded by a monitor/defibrillator.

Electronic files including signals extracted from AEDs and monitor/defibrillators along with the associated clinical data are often collected on centralized and multi-centre OHCA repositories.
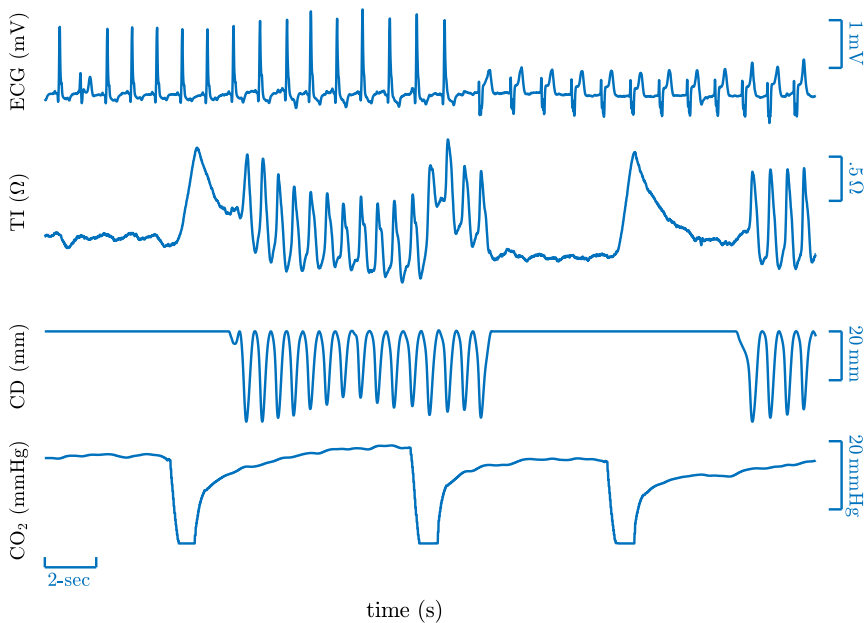
Figure 1.8. Example of signals available from monitor/defibrillators. From top to bottom: ECG, TI, CD and CO_2 (capnogram).

The clinical information needs to be compiled in the standard cardiac arrest reporting format (Utstein style) [111], and includes information from the emergency medical system's coordination centers, ambulances, and hospitals, and follow-up information about the patients discharged alive from hospital. OHCA registries play a vital role in the improvement of resuscitation therapy, since they provide large and standardized databases that enable communities to retrospectively compare patient populations, EMS response times, treatments, and outcomes with the goal of identifying factors associated with improved OHCA survival. The Resuscitation Outcome Consortium (ROC) [112] constitutes the major OHCA registry worldwide involving the efforts of eleven regional clinical centers distributed in Canada and the United States. In Europe, the European Registry of Cardiac Arrest (EuReCa) [113] is the largest OHCA dabase which collects data from EMSs in more than 27 nations.

1.7   AUTOMATIC RHYTHM CLASSIFICATION IN OHCA

Many algorithms based on signal processing and machine learning have been published in the scientific literature to improve OHCA therapy. The objective of these algorithms is to automate difficult clinical decisions in a reliable and accurate way. One of the critical applications is the identification of the patient's rhythm during OHCA.

Considering the critical role of defibrillation in OHCA survival, much of the research has focused on developing algorithms that discriminate between shockable and nonshockable rhythms. The ECG of shockable rhythms has some distinctive characteristics such as: greater waveform irregularity, higher ventricular rates, absence of QRS complexes and smaller bandwidths. Consequently, initial studies focused on the development of ECG features to identify shockable rhythms [114, 115, 116, 117, 118, 87, 119, 120, 121]. Although advanced signal processing techniques were used to identify these features, classification was at first simply achieved by means of a threshold. Consequently, the focus of research was later moved to improve the classification stage by efficiently combining VF

detection features through machine learning classifiers [122, 123, 124, 125, 126, 127]. Recently, the performance of VF detection algorithms has been further improved by the use of deep learning algorithms obtaining accuracies above 98.5% [128, 129].

However, defibrillation is not the only treatment needed during OHCA, and depending on the clinical context a finer rhythm classification is needed. One such setting would be the detection of ROSC, that is the detection of pulse. In OHCA, pulse detection is treated as a PEA/PR discrimination algorithm after an ECG with visible QRS complexes is detected. Pulse detection is crucial for early recognition of the cardiac arrest and early initiation of post-resuscitation efforts. Therefore, several signal processing and machine/deep learning algorithms have been developed for the detection of ROSC based solely on the ECG [130, 131] or TI [132], or on the combination of the ECG and TI [133] or the ECG, TI and the capnogram [134]. Other secondary rhythm classifications have also been studied, such as, the discrimination of VF/VT [135]. VT treatment may benefit from synchronized electrical cardioversion whereas VF will not [136].

General rhythm classification in OHCA should therefore address the classification into the five cardiac arrest rhythms. Knowing the patient's cardiac rhythm during resuscitation is important for two reasons. First, awareness of the patient's rhythm would allow to decide on the optimal OHCA treatment as well as to continuously adequate the treatment to the patient response in rhythm. Second, in retrospective analyses, the rhythm transitions of the patient during CPR provide important information about the interplay between therapy and patient response [137, 138, 139]. This can lead to the identification of treatment patterns that improve OHCA survival. However, a limiting factor in such analyses is that labeled OHCA data are scarce, and obtaining quality controlled rhythm annotations is time consuming. A multiclass classifier would allow the immediate annotation of OHCA episodes. Rad et al. [140, 141, 142] developed the first algorithms for 5-class OHCA rhythm classification, obtaining an unweighted mean of sensitivities (UMS) of 75% [142].

Signal processing and machine learning algorithms have also been useful in other OHCA fields that are not related to rhythm classification. For instance, tools for shock outcome prediction instruct the rescuer to defibrillate only when the probability of shock success is very high, thus avoiding unnecessary CPR interruptions that decrease OHCA survival. The ECG has been the most widely used signal to predict shock success [143, 144], although there is evidence that the prediction could be improved if the capnogram is used along with the ECG [145]. Finally, signal processing techniques have also been necessary for the estimation of CPR quality. The computation of CPR metrics is essential to monitor CPR performance in real-time, as well as to retrospectively identify CPR patterns associated with improved OHCA survival. The CD signal provides the most reliable measures of chest compression rate and depth [108, 109, 110]. The TI signal can also be used for the computation of chest compression rate [146, 147, 110] but not for the depth [148]. Metrics associated with ventilations are usually extracted from the TI or the capnogram [149, 150].

1.8   MOTIVATION

Artefacts introduced by the mechanical activity of chest compressions make the aforementioned CPR support tools unreliable. For instance, sensitivity/specificity values of 58.4%/90.8% and 81.5%/67.2% have been reported for SAAs in the presence of CPR artefacts [151, 152]. In addition, the UMS of the multiclass algorithm implemented by Rad et al. [142] dropped by more than 20 points when it was tested in intervals during compressions. Therefore, chest compressions must be interrupted for an accurate rhythm analysis. But as described in Section 1.6, interruptions in CPR clearly decrease the probability of survival. Consequently, the development of reliable methods that eliminate these hands-off intervals would be of great value.

During the last 15 years efforts have been made to allow a reliable rhythm analysis during chest compressions, and in particular to allow an accurate shock/no-shock diagnosis. At present algorithms meeting AHA performance goals during chest compressions have

been demonstrated, albait with accuracies lower than those for artefact free ECGs [153, 154]. Moreover, all those algorithms were demonstrated for manual CPR, but at the time this thesis started no AHA compliant algorithm had been demonstrated during mechanical CPR. Preliminary studies on shock/no-shock decision during mechanical CPR had reported sensitivities and specificities of 97.9% and 84.1%, respectively [155]. In addition, no algorithms for 5-class rhythm classification during manual or mechanical CPR had been demonstrated.

The objective of this thesis is to fill those unexplored topics in rhythm analysis during CPR. The focus of this work is on the systematic application of signal processing and machine learning techniques to provide new or improved solutions for rhythm analysis during CPR, including shock/no-shock decision during manual and mechanical CPR and 5-class classification during manual CPR. The methods developed are general and can be adapted to most context in rhythm analysis during CPR. The demonstration of their validity for the different CPR scenarios and rhythm classification problems depended largely on the data available for research.

2 | STATE OF THE ART

2.1 MACHINE LEARNING FOR OHCA CLASSIFICATION

The central problem in cardiac arrest rhythm classification has been the distinction of life-threatening arrhythmia (VF/VT) from nonshockable rhythms. In other words, the design of shock/no-shock decision algorithms for defibrillators.

The first studies on the topic proposed VF detection features obtained from the ECG. The extracted features quantified the distinctive characteristics of VF/VT rhythms and were obtained from different domains, such as, the time domain [117, 118], waveform morphology features [115], spectral features [114, 156], or measures of signal complexity [157, 158, 159]. Jekova et al. [160] and Amann et al. [157] conducted a comparative assessment of several single feature based SAAs. However, VF/VT detection performance is limited if only one feature is used [123]. Consequently, machine learning classifiers that efficiently combine the information from various VF features became common place [161, 162]. These classifiers need to be preceded by feature selection algorithms to identify a subset of features that optimize the classifier's performance [163, 123, 124, 122]. The architecture of a machine learning based SAA is graphically summarized in Figure 2.1. It consists of 4 stages: feature extraction, feature selection and a shock/no-shock classification stage based on a machine learning algorithm.
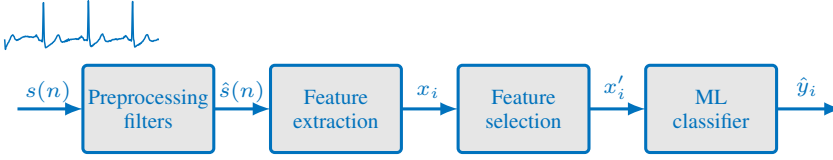
Figure 2.1. Building blocks of a SAA: preprocessing filters, feature extraction and selection stages and a machine learning based classifier for a shock/no-shock decision.

First, the ECG, $s(n)$[1], is filtered to eliminate noise, such as baseline wander or powerline interference. Then, features are extracted from the filtered ECG, $\hat{s}(n)$, to obtain a vector x_i which contains the values of K features, that is the signal is mapped into a K dimensional feature space. Then the feature selection stage reduces the dimensionality of x_i to K'. Thus, an OHCA database composed of N ECG signal segments could be represented as a set of instance-label pairs $\{(x'_1, y_1), ..., (x'_N, y_N)\}$ where y_i are the class labels $\{0, 1\}$ for a shock/no-shock classification problem.

As shown in Figure 2.2, data should be divided into two subsets: a training dataset which contains the examples used to fit the parameters of the machine learning classifier, and the test set to provide an unbiased evaluation of the final model. The training set is usually further divided into two subsets: a training subset to fit the model, and a validation subset to provide an unbiased evaluation of the fitted model while tuning the hyperparameters of the classifier. The selection of the features should also be computed in the training/validation sets.

The following subsections review the main features, the feature selection techniques and the shock/no-shock machine learning based decision algorithms found in the literature.

2.1.1 FEATURE EXTRACTION

To date, a plethora of features (well exceeding 100) have been described to discriminate fatal ventricular arrhythmia. These features quantify the distinctive characteristics of the arrhythmia, which

---

1 In this manuscript we will denote digital signals as $s(n)$. That is time is $t = nT_s$, where n is the sample index and T_s the sampling period.
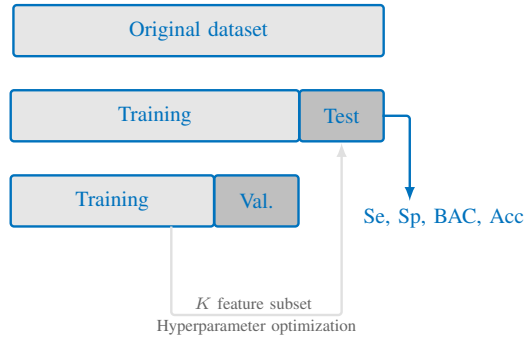
Figure 2.2. Train, validation and test sets in machine learning.

are usually better observed by transforming the ECG to a new domain. For instance, in the frequency domain, narrower bandwidths are observed for shockable than for nonshockable rhythms (see Figure 2.3). However, the waveform irregularity of VF or the lower content around the isoelectric line of VT is better identified in the time domain. What follows is a brief summary of the features designed to date in shock/no-shock classification problems, grouped by domain:

- *Time domain*: These features were designed to characterize the amplitude, slope, sample distribution, periodicity or heart rate of the rhythm. Calculations of heart rate and periodicitiy can be done using the autocorrelation function as proposed by Chen et al. [116], or simply by analyzing time events or threshold crossing intervals (TCI) as introduced by Thakor et al [117]. An improved version of the TCI, the threshold crossing sample count (TCSC) was later developed by Arafat et al [118]. In 2005, Amman et al. [157] introduced two features to estimate the heart rate based on exponentially decaying functions: the Standard Exponential Algorithm (Exp) and its modified version called the Modified Exponential Algorithm (Expmod). In 2004, Jekova et al. [114] introduced three features to quantify sample counts at different amplitude levels after bandpass filtering. Later, Anas et al. [115] demonstrated that distinguishable morphological characteristics of shockable and nonshockable rhythms could be quantified using the mean of the absolute value (MAV) of the signal. Absolute amplitudes

a) Nonshockable PR
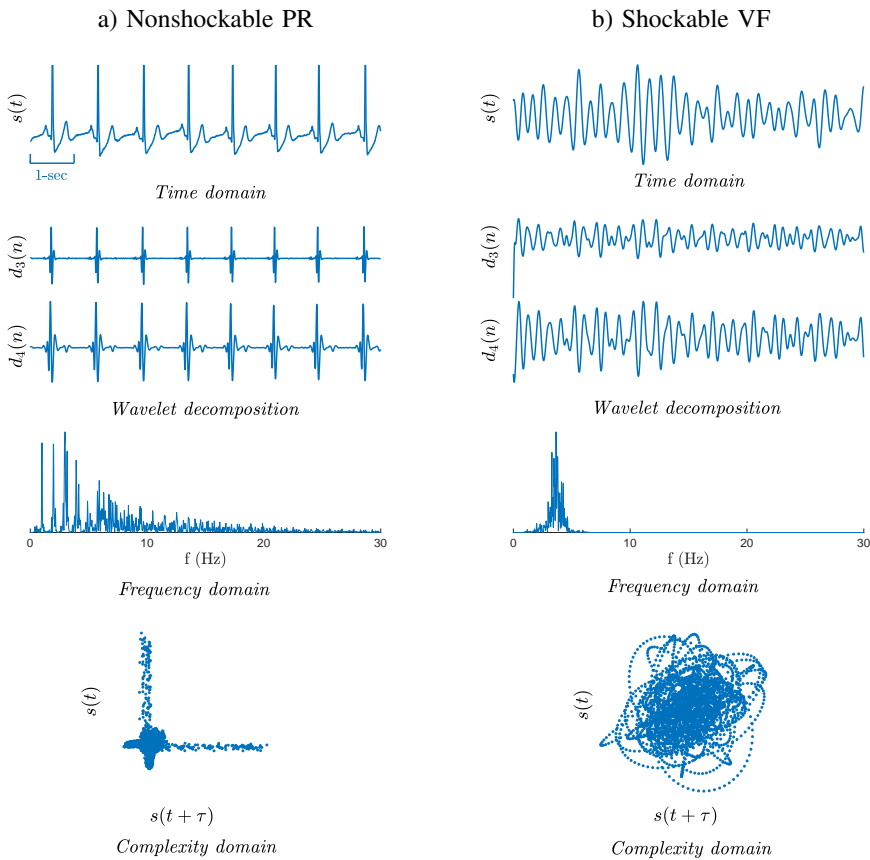
b) Shockable VF

Figure 2.3. From top to bottom: time domain, wavelet domain, frequency domain and the PSR representation of a nonshockable (left panel) and a shockable (right panel) rhythms.

corresponding to organized rhythms (ORG)[2] are most of the time low due to the isoelectric lines around QRS complexes, whereas VF and VT rhythms present on average higher signal amplitudes. Based on this observation Irusta et al. [87] designed a feature (bWT) to calculate the proportion of samples falling in a certain amplitude range around the isoelectric lines. More recently, Irusta et al. [87] and Ayala et al. [153] introduced three features based on the slope of the signal to exploit that rapid variations of the ECG during QRS complexes cause large values

---

2 Rhythms with visible QRS complexes, regardless of being associated to effective pulse or not. This category brings together PR and PEA rhythms in OHCA

of the ECG slope. The first feature (bCP) [87] was defined as the proportion of time the slope signal is below a predefined threshold. The second feature, called slope baseline (x1), was computed as the 10th percentile of the slope, and the last feature (x2) corresponds to the number of peaks above a fixed threshold in the slope [153].

- *Frequency domain*: The dominant frequency of ventricular arrhytmia fall between 2.5 – 7.5 Hz with a total bandwidth rarely exceeding 10 Hz. Rhythms with QRS complexes concentrate their frequency components around the harmonics of the cardiac frequency (1-2 Hz) and their bandwidth can reach 40 Hz due to fast-changing QRS complexes. The VF filter leakage (VFleak) was one of the first VF detection features and relies on approximating VF to a sinusoidal waveform using a bandpass filter around its dominant frequency [119]. In 1989, Barro et al. [156] developed four features to measure the energy content around the dominant frequency (M) and different frequency bands (A1, A2, A3) by means of Fourier analysis. Later, in 1999, Minami et al. [120] successfully detected ventricular arrhythmia by analyzing the frequency content of the QRS complex in five predefined frequency bands. In 2005, bispectral analysis of the ECG was explored in order to preserve phase coupling information between the frequency components of the ECG [121]. More recently, Irusta et al. [87] estimated the ECG bandwidth (bW) and included it as feature in the classifier. More recently, Ayala et al. [164] designed a set of three features that measured the location of the largest spectral peak in the 1-10 Hz band (x3), the power proportion around VF fibrillation band (2.5 – 7.5 Hz) (x4), and in the high spectral bands (above 12 Hz) (x5).

- *Time-frequency domain*: In 1995, Afonso et al. [165] suggested that the concomitant analysis of the spectral and temporal domains could be useful for arrhytmia classification. They compared the contour plots of different time-frequency distributions and showed the superiority of the smoothed Wigner–Ville and the cone-shaped kernel distributions over the short-time Fourier transform. The smoothed Wigner-Ville distribution

was further explored by Clayton et al [166]. In 1997, Khadra et al. [121] introduced the Raised-Cosine Wavelet Transform (RCWT) for the time-frequency analysis of the ECG, and compared the differences in density for various time-frequency regions across rhythms. This work was extended by Fahoum et al. [167] who extracted 6 energy descriptors from nine different continuous and discrete wavelet transforms. The Discrete Wavelet Transform (DWT) has also been used to characterize the complexity of VF using features like Tsallis or Shannon multiresolution entropy [168]. More recently, Arafat et al. [170] proposed the empirical mode decomposition (EMD) as an alternative to time-frequency distributions.

- *Signal complexity*: It is increasingly recognized that many cardiac arrhythmia can be characterized using techniques from non-linear dynamics [171]. Nonlinear signal analysis methods used in OHCA rhythm classification include reconstructed phase space analysis (PSR) [172, 173, 174], Lyapunov exponents [175], correlation dimension [166, 176], detrended fluctuation analysis (DFA) [177], recurrence plot [166], Poincaré plot [178], Hilbert transform (HILB) [179, 157], Hurst indices [169] and different type of entropies [180, 181, 182, 183, 184] among others. However, the nonlinear analysis of ventricular arrhythmia is computationally expensive, limiting their applicability in low-end hardware AEDs. A computationally simpler method is the complexity measure (CM) developed by Zhang et al. [158], a measure obtained from the Lempel-Ziv analysis of a binarized ECG. Jekova et al [163] further explored feature extraction from binarized ECGs introducing the covariance (CVbin), area (abin), frequency (Frqbin) and Kurtosis (Kurt) of the binarized ECG.

2.1.2 Feature selection

Given the large amount of available shock/no-shock decision features, efficient feature selection (FS) methods are needed. The performance of machine learning classifiers is strongly affected by the feature subsets fed to the models. FS techniques look for an optimal feature subset by removing non-informative, redundant or

correlated variables from the model. These techniques fall into three categories: filter, wrapper and embedded methods.

Filter-based FS techniques use statistical measures to score the correlation or dependence between input variables and are independent to the classification algorithm. Variables are ranked according to a predefined relevance score, and low scoring variables are removed.

Wrapper methods use the performance of a classification algorithm as quality criterion for evaluating the relevant information derivable from a subset of features. Thus, wrapper methods involve the selection of a classification algorithm, a criteria to evaluate the capacity of a given subset of features, and a searching procedure in the space of all possible feature subsets. Since an exhaustive search is not practical, heuristic search methods are used. These methods can be broadly classified as deterministic and randomized search algorithms. Deterministc methods include a set of sequential search techniques like Sequential Forward Selection (SFS), Sequential Backward Selection (SBS), Plus-ℓ Minus-r Selection (PTA) or Sequential Floating Selection (SFS). Randomized search algorithms include techniques such as Genetic Algorithms or Simulated Annealing.

Finally, embedded methods integrate the search for an optimal subset of features into the classifier contruction. The best known example of embedded FS is probably the feature importance embedded in random forest (RF) classifiers.

A wide variety of FS techniques have been used for shock/non-shock classification problems. In 2002, Rosado et al. [185] compared the efficiency of 2 filter-based FS methods: principal component analysis (PCA) and Self-organizing Maps (SOM-Ward). Later, in 2007, Jekova et al.[163] used a filter-based method based on F-values to stepwise add up to 10 features into a linear regression model [163]. More recently, Tripathy et al. [127] used a mutual information-based feature selection method (filter-based method) to evaluate the performance of the classifier as a function of the number of features.

Wrapper based FS methods were introduced in shock/no-shock decision problems by Jekova et al [161], who used the SFS search method using the accuracy of a K-nearest neighbour (KNN) classifier. SFS starts with an empty set of features and sequentially adds the feature (from the remaining ones) that improves accuracy the most. The procedure is continued until the addition of a feature does not improve the classification accuracy. Wrapper methods based on randomized search have also been used to identify lethal arrhythmia, and all of them rely on Genetic Algorithms [186, 187].

A widely used approach to improve the efficiency of FS techniques is to use hybrid models which combine embedded or filter-based FS techniques with wrapper methods. In these cases, SFS or SBS search methods (wrappers) are used to find the optimal subset of features, but the criterion to exclude or include a feature in the model is based on a feature relevance ranking provided by filter-based methods or by classifiers with intrinsic feature selection capability (embedded FS methods). For instance, in 2012 Alonso et al. [162] proposed the so-called Support Vector Machine (SVM) recursive feature elimination (SVM-RFE) technique which uses the weights of a linear SVM as exclusion criterion in each step of the SBS search. Later, in 2014, they replaced the SVM-based feature relevance scoring by the ranking obtained through a filter-based method [123]. More recently, Figuera et al. [122] combined the embedding FS of regularized logistic regression and boosting of decision trees with SBS.

Finally, nested architectures combining deterministic and randomized wrapper search methods have also been explored. For instance, Nguyen et al. [125] used a genetic algorithm-based feature ranking as feature inclusion criterion in a SFS search method.

2.1.3 MACHINE LEARNING CLASSIFIER

A wide variety of machine learning classifiers have been used to obtain a shock/no-shock decision algorithm, ranging from very simple approaches like logistic regression to more complex ones such as SVM or neural networks.

Logistic regression was used in two studies conducted by Sharma et al. [188] and Figuera et al. [122]. Logistic regression is

an extension of linear regression to solve classification problems and its representation can be simply obtained by applying a logit function to the linear regression model:

$$h_\theta(x_i) = \frac{1}{1 + e^{\theta x_i^T}} \quad \text{where} \quad \theta x_i^T = \sum_{k=1}^{K'} \theta_k x_i^k \tag{2.1}$$

The prediction of the model, $\hat{y}_i$, will be 1 if $h_\theta(x_i) \geq 0.5$ and 0 instead. The task in Equation 2.1 is to choose the best parameters θ in order to minimize errors between the predicted values y_i and the true labels. For that purpose the following cost function must be minimized:

$$J(\theta) = -\frac{1}{m} \left[\sum_{i=1}^{m} y_i \log h_\theta(x_i) + (1 - y^i) \log(1 - h_\theta(x_i)) \right] \tag{2.2}$$

This process could be extended for almost all machine learning classifiers. First, the model is built as in Equation 2.1, then a cost funtion is defined in order to find the hyperparameters (the weights θ). Then the cost function $J(\theta)$ is minimized, thus minimizing the errors between the predicted values $\hat{y}_i$ and true labels in the training set, y_i. Once the model is trained the training data can be set aside.

Another simple approach to classification is the KNN classifier, which was used by Sharma et al. [188] and Nguyen et al. [125]. In this method, the sample to be classified is assigned to the majority class among its K closest samples from the training set, and distances are measured in the multidimensional feature space. Unlike the logistic regression classifier, KNN classifiers need to store the samples from the training data to evaluate their predictions, which are based on distance comparisons to those samples.

Neural networks [189, 174, 120, 190] and SVM [191, 192, 123, 162, 124] have been by far the most widely used learners in shock/no-shock classification problems. The structure of an ANN consists of a set of interconnected units, or *neurons* that estimate the non-linear correlations between variables. The input neurons, which represent

predictor variables, x_i, are connected to a single or multiple layer(s) of hidden neurons, which are then linked to the output neurons for the final classification, $\hat{y}_i$. The SVM classifier is a learner that is designed to construct an optimal separating hyperplane, in the feature space, between the various classes. In the case of binary classification SVM detects the closest points between two classes in the feature space, and assigns a margin based on the distance between the hyperplane and the points. The margin between classes is maximized by the *support vectors* (the optimal points that should be lying on the boundary) in order to estimate an optimal separating hyperplane between the two classes. The SVM applies a kernel trick to transform the original feature space into a higher-dimensional space using a polynomial, linear or a gaussian kernel. The kernel trick is very important because in most cases data is not linearly separable, but by transforming it into a higher dimensional space it may become linearly separable.

Ensemble methods have also been implemented for ventricular arrhythmia detection, and they were systematically applied in this context by Figuera et al. [122]. The goal of ensemble methods is to combine the predictions of several weak learners in order to improve generalizability, and thus prediction performance. Figuera et al. [122] explored three approaches for ensemble methods: bagging, random forest and boosting. In bagging, B decision trees are built from B bootstrap samples of the training database. The final decision is the majority vote of those B trees. Random forest is a particular implementation of bagging for decision trees, where only a random subset of features is used at each tree split. Random Forest has also been successfully applied in some other studies for ventricular arrhythmia classification [192, 127]. Finally, boosting consists in sequentially training several $h_m(x_i)$ weak classifiers, each trying to correct its predecessor, $h_{m-1}(x_i)$. So $h_m(x_i)$ focuses on those samples misclassified by $h_{m-1}(x_i)$. The final classification is obtained by a weighted vote of the M classifiers:

$$y = \text{sign}\left(\sum_{m=1}^{M} \alpha_m h_m(x_i) \right) \tag{2.3}$$

2.2 CPR ARTEFACT

Mechanical and manual chest compressions introduce artefacts in the ECG, substantially altering its waveform. Figure 2.4 shows three examples of OHCA ECG segments recorded during manual CPR (panel a) and mechanical CPR (panels b and c). During the first 15 s the mechanical activity of the chest compressions masks the underlying rhythm of the patient. This rhythm is revealed in the last 5 s where no chest compressions are provided. OHCA rhythm classification is therefore unreliable during chest compressions. For instance, Figure 2.5 shows 3 examples of misclassified segments by the SAA of an AED during manual (panel a) and mechanical chest compressions (panels b and c). In panels a and b, chest compressions
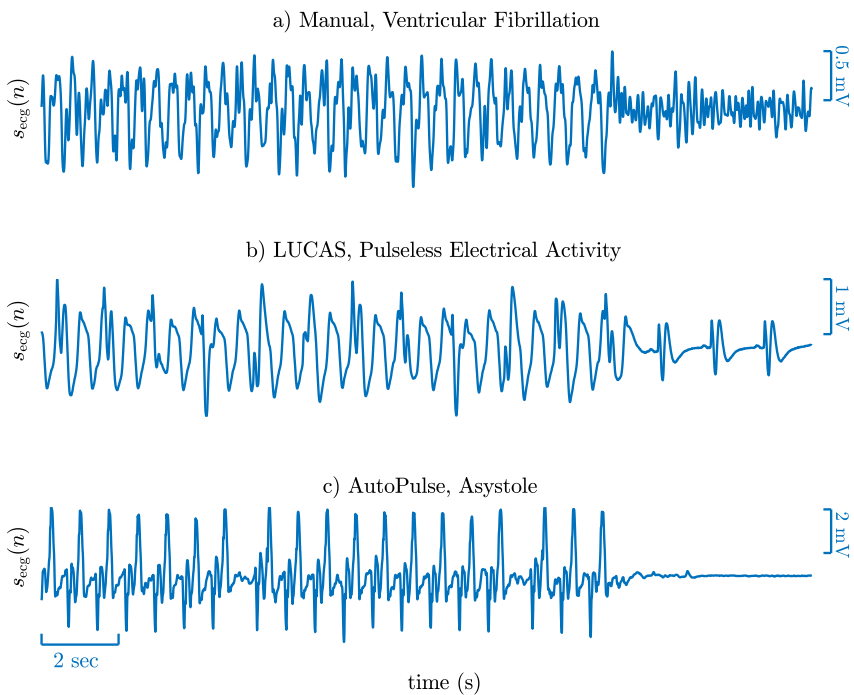
Figure 2.4. Three ECG examples of 20 s recorded in patients in OHCA. The initial 15 s are corrupted by chest compressions provided manually (a) and by the LUCAS-2 (b) and the AutoPulse (c) devices. The last 5 s show the underlying rhythm of the patient: VF (a), PEA (b) and AS (c).

introduce fast and disorganized artefacts in the ECG that make the nonshockable ORG rhythm resemble a VF. This leads to an erroneous shock decision of the SAA. In panel c, the chest compression artefact shows an organized activity locked to the compression frequency of the mechanical device (80 cpm). This makes VF resemble an ORG rhythm, thereby causing an incorrect no-shock decision. Therefore, the accuracy of rhythm analysis algorithms substantially decreases in the presence of chest compression artefacts. For instance, Se/Sp values of 58.4%/90.8% and 81.5%/67.2% have been reported for commercial SAAs during manual chest compressions [151, 152]. Aramendi et al. [155] reported Se/Sp values of 52.8%/81.5% for SAAs during LUCAS-2 use. In addition, the UMS of the multiclass
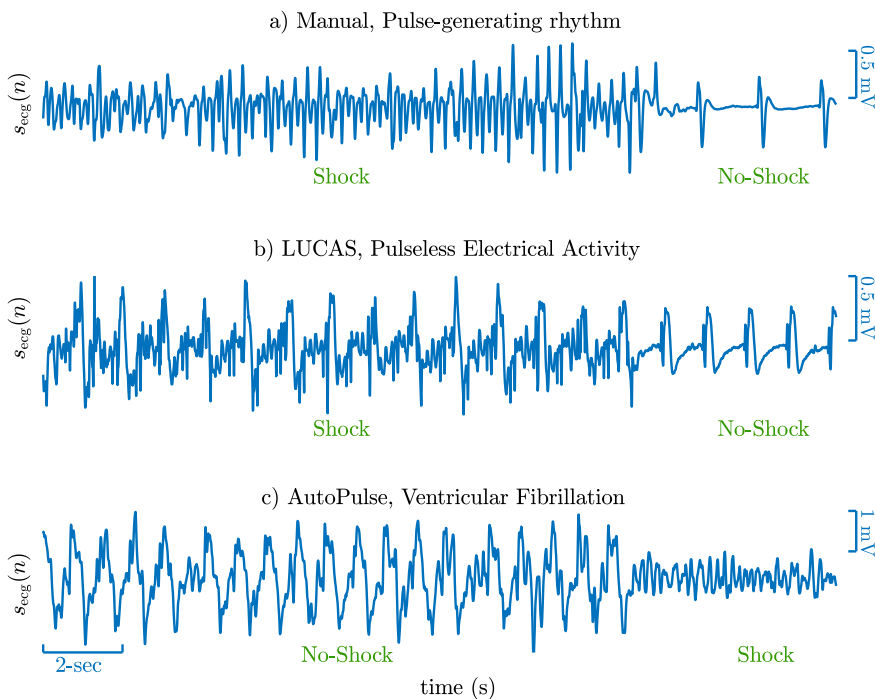
Figure 2.5. Three ECG examples of classification errors in a SAA during compressions (first 15 s) provided by different sources: manually by a rescuer (a), LUCAS-2 (b) and AutoPulse (c). In the first two panels nonshockable ORG rhythms (visible in the last 5 s) are corrupted with fast and disorganized artefacts resulting in an incorrect shock decision. In the last panel, the VF rhythm is completely masked by a slow and organized artefact, thus making the SAA diagnose it as nonshockable.

algorithm implemented by Rad et al. [142] for clean ECGs dropped by more than 20 points when it was tested in corrupted ECGs.

Although manual and mechanical CPR artefacts affect the ECG, their characteristics are very different both in time and frequency. These differences are analyzed in the following paragraphs, and the results presented here are derived from the datasets and results presented in various studies conducted during the thesis work [155, 193].

Figure 2.6 shows the normalized power spectral density (PSD) for manual CPR (panel a) and mechanical CPR (panels b and c) artefacts. The PSD reveals a very stable compression frequency (f_{cc}) for the LUCAS-2 (f_{cc} = 1.694 Hz=101.7 cpm) and the AutoPulse (f_{cc} = 1.335 Hz = 80.1 cpm) devices, and a very clear concentration of the power around its harmonics. In contrast, manual compressions show a great variability in compression frequency that results in a spread PSD. In addition, mechanical artefacts show higher bandwidths than manual ones. In the time domain, there were no significant differences in median (90% confidence interval, CI) amplitude between artefacts generated by manual chest compressions 1.29 (0.86 – 2.13) mV and the LUCAS-2 device 1.22 (0.70-1.86) mV according to Aramendi et al. [155]. However, artefacts generated by the AutoPulse device presented significantly greater median (90% CI) amplitudes 4.4 (1.0-16.7) mV and a higher variability between episodes [193]. Finally, mechanical artefacts showed significantly more stable waveforms (more periodic) than manual ones [155, 193]. The Pearson correlation coefficient (ρ) was similar for artefacts generated by the AutoPulse and the LUCAS-2 devices with median values of 0.983 (0.736 – 0.999) and 0.981 (0.585 – 0.999), respectively. Manual artefacts showed correlation coefficients of 0.896 (0.305 – 0.989), significantly smaller ($p < 3 \times 10^{-7}$ for the Wilcoxon Rank-Sum test) than for the mechanical artefacts.

According to Aramendi et al. [155] artefact waveform patterns induced by manual and mechanical chest compressions show a large variability within and between resuscitation episodes. This variability may be due to differences in chest characteristics, skin-electrode contact and on the relative position of the compression point and the
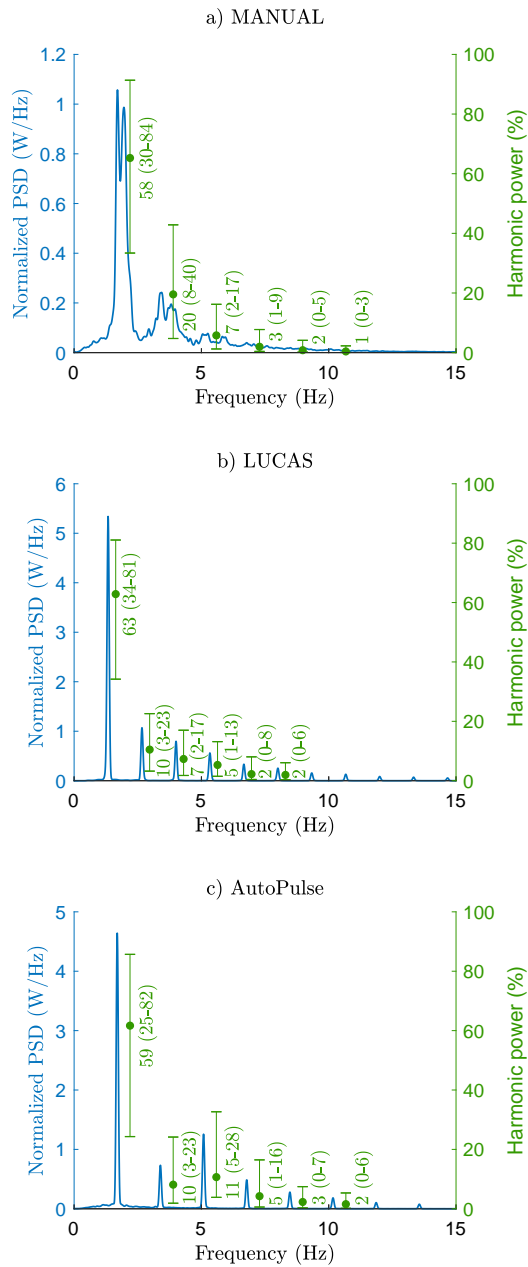
Figure 2.6. Normalized PSD for manual (a) and mechanical (b, c) artefacts recorded during asystole. The errorbars represent the median (80% CI) of the proportion of power concentrated in that harmonic.

defibrillation pads [194, 195]. When chest compressions are delivered manually, these variations may also be due to changes on how CPR is administered by the rescuer, rescuer fatigue, or the intervention of several rescuers [196]. In addition to this variability, both manual and mechanical artefacts present, on average, an spectral overlap with the different OHCA rhythm types. Figure 2.7 shows the PSD of the different OHCA rhythms overlapped with the PSDs of manual and mechanical artefacts shown in Figure 2.6. The overlap is larger for non-shockable rhythms like PEA and PR. In addition, these non-shockable rhythms present higher overlap with the spectrum corresponding to manual chest compressions.

In conclusion, two key aspects should be adressed to obtain a reliable rhythm analysis during CPR for both the manual and
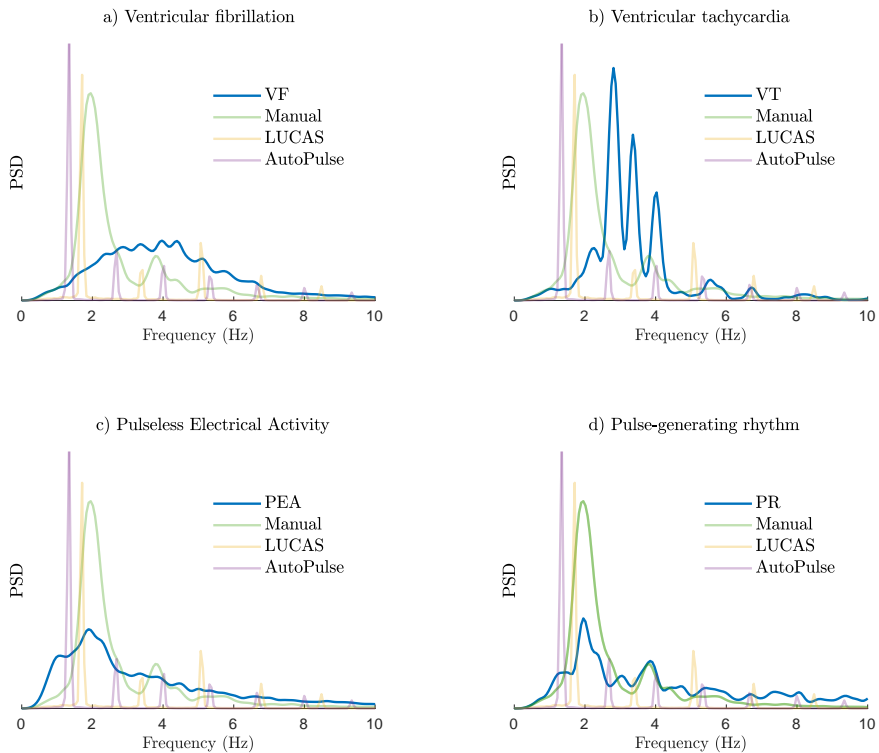
Figure 2.7. Normalized PSD of mechanical/manual artefacts recorded during asystole and the five OHCA rhythm types. Top panels correspond to shockable rhythms (VF, VT) and bottom panels to nonshockable rhythms.

mechanical cases: the time-frequency variability of the artefact and its spectral overlap with OHCA rhythms. Filtering the chest compression artefact to restore the underlying rhythm of the patient has been the major approach to rhythm analysis during CPR. These techniques are described in the following section.

2.3 Rhythm analysis during chest compressions

As stated in Section 1.7, the ideal rhythm analysis algorithm should allow the classification into the five cardiac arrest rhythms without the cessation of CPR therapy. However, considering the importance of defibrillation in OHCA survival and that the widespread use of mechanical CPR devices is recent, efforts in the last 15 years have focused on accurate shock/no-shock diagnosis methods during manual chest compressions.

Although different approaches to shock/no-shock decision during CPR have been explored [197, 198], filtering the CPR artefact has been the main line of study [196]. In early attempts, CPR artefacts were successfully removed from porcine ECG by means of fixed coefficient high-pass digital filters [199, 200]. In human data however, the artefacts cannot be efficiently suppressed by high pass filters as the spectral components of the CPR artefact overlap the dominant frequency of the ECG signal (see Section 2.2). Since then, studies have focused on the development of adaptive filters to model the CPR artefact and remove it from the ECG.

2.3.1 Evaluation methodology

The methodology followed to test those adaptive filters depended largely on the data available to the researchers. Early adaptive filtering approaches were tested on databases obtained from the artificial mixture of human ECG and CPR artefacts recorded during asystole, either in humans or in pigs. The mixture model was introduced early in 2000 by Langhelle et al. [194] and Aase et al. [201]. This model assumes that the CPR artefact, $s_{\mathrm{cpr}}(n)$, is an additive noise independent of the underlying ECG, $s_{\mathrm{ecg}}(n)$. Based on this assumption filtering methods can be tested using independently

recorded human ECG and CPR artefacts, added at different signal-to-noise ratios (SNRs):

$$s_{\text{cor}}(n) = s_{\text{ecg}}(n) + \alpha \cdot s_{\text{cpr}}(n), \quad \text{with} \quad \alpha = \sqrt{\frac{P_{\text{ecg}}}{P_{\text{cpr}} \cdot 10^{\text{SNR}/10}}} \quad (2.4)$$

The SNR in dB is adjusted in the artificial mixture, $s_{\text{cor}}(n)$, using the α coefficient, where P_{ecg} and P_{cpr} are the power of the underlying ECG and the CPR artefact, respectively. Typically, these mixtures are formed with SNR values in the -10 dB (strong corruption) to 10 dB (low corruption) range. Figure 2.8 shows an example of the corrupted ECG, $s_{\text{cor}}(n)$, obtained by mixing ORG (a) and VF (b) rhythms with manual CPR at SNR = 0 dB and SNR = -10dB.
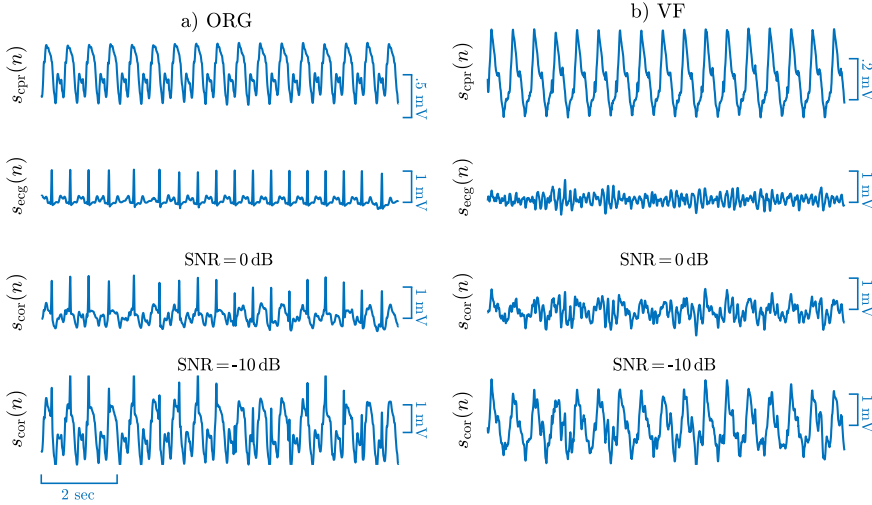
Figure 2.8. Examples of artificially mixed corrupted ECGs. From top to bottom: CPR artefacts, $s_{\text{cpr}}(n)$, recorded during asystole, clean ORG and VF rhythms, $s_{\text{ecg}}(n)$, and mixed signals, $s_{\text{cor}}(n)$, at SNR of 0 dB and -10 dB.

This testing method allowed a straight comparison between the restored ECG signal after filtering, $\hat{s}_{\text{ecg}}(n)$, and the original signal, $s_{\text{ecg}}(n)$. The increase in SNR caused by filtering (ΔSNR) was the first metric proposed to evaluate filtering performance on artificial mixtures. Although ΔSNR gives a direct and interpretable measure of filter performance useful to optimize the filter's parameters, it does

38

not give information about the final clinical decision, that is, whether the patient should be shocked or not. To address this limitation, Aase et al. [201] proposed to evaluate filtering techniques in terms of the accuracy of a SAA, as shown in Figure 2.9. The shock/no-shock decisions obtained by analyzing the filtered ECG using a SAA were compared with the ground truth labels to obtain the accuracy of the filtering method.

When human OHCA data became available to researchers, i.e. data recorded during resuscitation efforts, the artificial mixture model was virtually left aside due to two main drawbacks. First, the SNR in real cardiac arrest data is not known, and how improvements in SNR are translated to the more clinically relevant Se/Sp values is not fully understood [202]. Second, the mixture model may not accurately reflect the effect of CPR on heart dynamics. So in subsequent studies based on OHCA data, the performance of adaptive filters was evaluated through the accuracy of SAAs in commercial defibrillators, as shown in Figure 2.9.
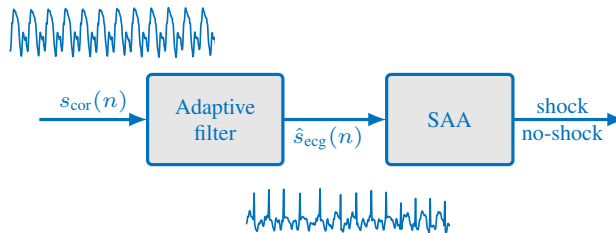
Figure 2.9. Main evaluation methodology of adaptive filters to remove CPR artefacts from the ECG. The filtered ECG, $\hat{s}_{\text{ecg}}(n)$, is diagnosed as shock/no-shock by the SAA of a commercial defibrillator designed for artefact-free ECGs.

2.3.2 ADAPTIVE CPR ARTEFACT CANCELLERS

MULTICHANNEL APPROACHES

The first approaches to remove artefacts from the ECG were based on the multichannel modeling of the chest compression artefact. Figure 2.10 shows the typical block diagram of multichannel methods in which the estimated artefact is:

$$\hat{s}_{\text{cpr}}(n) = \sum_{p=1}^{P} \sum_{k=0}^{K_p-1} h_p(n-k) s_{\text{ref},p}(k) \tag{2.5}$$

where P is the number of reference channels and $s_{\text{ref},p}(n)$ is the p-th channel, which must be correlated with the chest compression artefact. For each reference channel, $h_p(n)$ and K_p are the filter coefficients and the number of coefficients, respectively.

The objective of this approach is to find $\hat{s}_{\text{cpr}}(n)$ as the best possible estimate of the artefact in the corrupted ECG, $s_{\text{cor}}(n)$. Then the clean ECG can be obtained by subtracting the estimated artefact from the corrupt ECG:

$$\hat{s}_{\text{ecg}}(n) = s_{\text{cor}}(n) - \hat{s}_{\text{cpr}}(n) \tag{2.6}$$

which assumes an additive noise model. This is a classical problem in adaptive filtering and is commonly solved through finding the K_p filter coefficients of $h_p(n)$ for each time instant n that minimize the error between $s_{\text{cor}}(n)$ and $\hat{s}_{\text{cpr}}(n)$. Assuming no correlation between the uncorrupted ECG, $s_{\text{ecg}}(n)$, and the artefact, $s_{\text{cpr}}(n)$, this error, $\hat{s}_{\text{ecg}}(n)$, would approach the underlying rhythm of the patient.
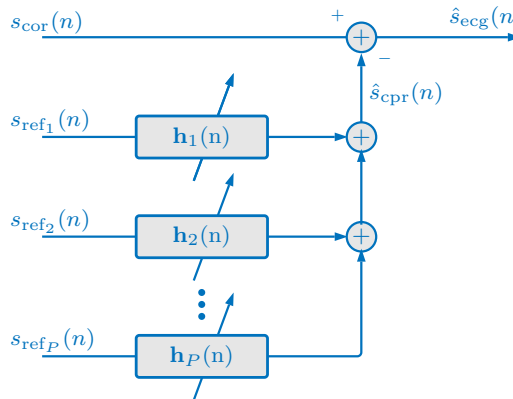
Figure 2.10. Block diagram of a multi-channel CPR artefact canceller. Filter coefficients can be estimated by different adaptive algorithms.

The multichannel approaches proposed in the literature mostly differ in the number and type of reference signals used to model the artefact, and in the algorithmic approach or filter type to find the optimal filter coefficients. The first multichannel approach was proposed by Aase et al. [201]. They used a Wiener filter and two reference signals, the TI and CD, to remove artefacts from the corrupted ECG. The data used in this study were obtained from the artificial mixture of human rhythms and mechanical chest compression artefacts from animal recordings. Later, Husøy et al. [203] proposed the Multi-Channel Recursive Adaptive Matching Pursuit (MC-RAMP) algorithm. This method updated filter coefficients using a Matching Pursuit algorithm, which in each iteration finds the reference channel with the highest correlation to the CPR artefact. The MC-RAMP substantially lowered the computational demands of the Wiener filter and yielded comparable SNR results in a similar database. In 2004, Eilevstjøn et al. [151] pioneered the development of adaptive filters using real OHCA data from human victims. They adapted the MC-RAMP filter to use four reference signals to model the artefact: TI, ECG common mode, acceleration and CD signals.

The main drawback of multichannel approaches is the need to acquire multiple external channels, which demands important defibrillator hardware modifications. Most defibrillators only record the surface ECG together with the TI signal (used to check pad placement), although possibilities to record compression depth or acceleration from CPR feedback devices is becoming common place. Moreover, multichannel schemes are computationally expensive, which limits their implementation in low-end hardware devices.

Simplified architectures

Since the study published by Eilevstjøn et al. [151], researchers have focused on reducing or eliminating the need for additional reference signals. These studies can be roughly divided into two main approaches: filters based solely on the ECG, and filters based on the ECG with minimal information on CPR. In addition to adaptive filters, methods based on the direct analysis of the corrupted ECG have also been explored.

The first attempts to reduce the complexity of multichannel filters were based on methods that remove the chest compression artefact using only the ECG signal. As shown in Figure 2.11, these filtering schemes follow two steps. In a first stage, the fundamental frequency of the chest compressions, f_0, is directly estimated from the corrupted ECG by means of spectral techniques. In a second stage, an adaptive filter is used to suppress the frequency components of the artefact by suppressing components at f_0 and its harmonics. Three different adaptive filters have been proposed in the literature for the second stage: an adaptive band-stop filter [204], a Kalman filter [90], and a coherent line removal algorithm [205].

The band-stop filter was proposed by Aramendi et al. [204] in 2007. This notch filter was centred on f_0, which was estimated as the frequency of the largest spectral component in the $1-3$ Hz range. The filter adapted to the time-varying characteristics of the artefact by updating f_0 every 4.8 s, which was the window size of the SAA used to test the performance of the filter.

In 2008, Ruiz de Gauna et al. [90] presented a more complex filter based on a more elaborate model of the artefact composed of two harmonically related sinusoids:

$$\hat{s}_{\text{cpr}}(n) = c_0(n)\cos(\omega_0 n + \theta_0(n)) + K c_1(n)\cos(2\omega_0 + \theta_1(n)) \quad (2.7)$$
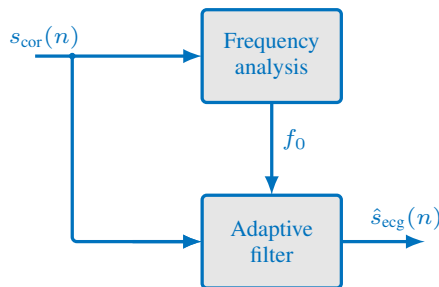
Figure 2.11. Block diagram of single-channel adaptive filters. The fundamental frequency of the artefact, f_0, extracted from the corrupted ECG, $s_{\text{cor}}(n)$, is the only information used to characterize the artefact.

where $\omega_0 = 2\pi f_0 T_s$ is the discrete frequency and K is a binary coefficient that controls whether or not the second harmonic is considered. The time-varying amplitudes and phases of the sinusoidal components ($c_0(n), c_1(n), \theta_0(n)$ and $\theta_1(n)$) were recursively estimated as the state variables of a four-state Kalman filter.

In 2010, Amann et al. [205] studied the feasibility of a coherent line removal algorithm for the suppression of the chest compression artefacts using only the ECG. The chest compression frequency was estimated from the sum of the power at each frequency f and its harmonics, taking f_0 as:

$$f_0 = \arg\max_{f} \left\{ \sum_{k=1}^{M} |X_{\text{cor}}(kf)^2| \right\} \tag{2.8}$$

where X_{cor} is the Fourier Transform of $s_{\text{cor}}(n)$. Once f_0 was estimated, the coherent line removal algorithm removed the artefact, assuming a periodic artefact of strong harmonic components.

The Kalman filter proposed by Ruiz de Gauna et al. [196] obtained the best SAA performance in terms of Se and Sp. However, accuracies were below those obtained by the MC-RAMP, underlying the importance of using additional reference information to model the CPR artefact.

In order to improve the poor performance obtained by ECG only approaches, Irusta et al. [152] proposed a filter based on the surface ECG with minimal additional information on CPR. Their first hypothesis was that the frequency of the compressions was enough to construct an accurate model of the CPR artefact. This would reduce the hardware modifications demanded by multichannel approaches, since recording the frequency of the compressions can be directly obtained from CPR feedback devices.

The CPR artefact was modeled as a quasi-periodic interference using a Fourier series truncated to N harmonics. The fundamental frequency of the artefact, f_0, was that of the chest compressions, which was assumed constant during a chest compression but variable

from compression to compression. This means that for an interval between two successive compressions at time points, t_{k-1} and t_k, the frequency can be expressed as:

$$f_0(n) = \frac{1}{t_k - t_{k-1}} \quad t_{k-1} \leq nT_s < t_k \qquad (2.9)$$

and the N-term Fourier series representations is then:

$$\hat{s}_{\text{cpr}}(n) = A(n) \sum_{k=1}^{N} \left[a_k(n) \cos(k\phi(n)) + b_k(n) \sin(k\phi(n)) \right] \quad (2.10)$$

where $a_k(n)$ and $b_k(n)$ are the time varying in-phase and quadrature amplitudes of each harmonic, $\phi(n) = 2\pi f_0(n)nT_s$, is the instantaneous phase of the fundamental harmonic, and $A(n)$ is an amplitude envelope to model intervals with compressions, $A(n) = 1$, and without compressions, $A(n) = 0$, such as hands-off intervals for ventilations. The chest compression instants, t_k, were automatically identified through negative peak detection in the CD signal (see bottom panel in Figure 2.12). An example of the intantaneous phase and the amplitude envelope used in the model of the artefact is shown in Figure 2.12. The CD signal is also visible with the chest compression instants marked.

Figure 2.13 shows the structure of the adaptive filter proposed by Irusta et al. [152]. In addition to the ECG, the only information fed into the adaptive filter are the t_k instants needed for the computation of $A(n)$ and $f_0(n)$. The time-varying $a_k(n)$ and $b_k(n)$ coefficients are updated using the Least Mean Squares (LMS) algorithm to minimize the error between $s_{\text{cor}}(n)$ and $\hat{s}_{\text{cpr}}(n)$ at the harmonics of f_0.

Irusta et al. [152] showed that the multiharmonic modeling of the CPR artefact based on the chest compression frequency can be as accurate as the four reference channels used by the MC-RAMP filter. Since then, several studies have been developed based on the Fourier series modeling of the artefact. Ruiz et al. [206] estimated the time-varying Fourier series coefficients by means of a Kalman filter. Later, Aramendi et al. [207] demonstrated that the instantaneous frequency
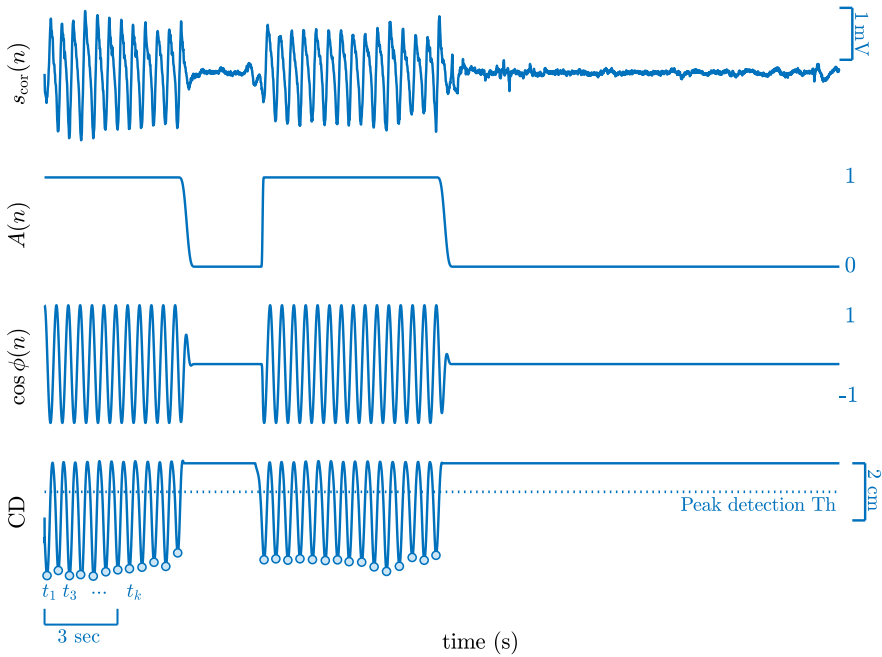
Figure 2.12. From top to bottom: the corrupted ECG, $s_{cor}(n)$, the amplitude envelope, $A(n)$, the time-varying phase of the Fourier series model, $\cos\phi(n)$, and the CD signal with the chest compressions, t_k, marked.

used by the LMS filter could also be derived from the TI signal, which is recorded by most current AEDs. This was a big step forward, since it demonstrated the possibility of incorporating the multiharmonic model to any device without the need of sternal CPR assist pads.

A new approach to rhythm analysis during CPR was introduced by Li et al. [197] in 2008, the direct analysis of the corrupted ECG. Li et al. [197] proposed a shock/no-shock discrimination algorithm using ECG features marginally affected by the artefact, that is filtering was embedded in the feature extraction phase. These features were obtained from the wavelet subband analysis of the ECG, and the analysis of the correlation accross subbands. Shortly after, Krasteva et al. [198] presented a second method. In this case, the shock/no-shock decision features were extracted from the corrupted ECG and from a reconstructed version of the ECG, which was equivalent to the filtered ECG.
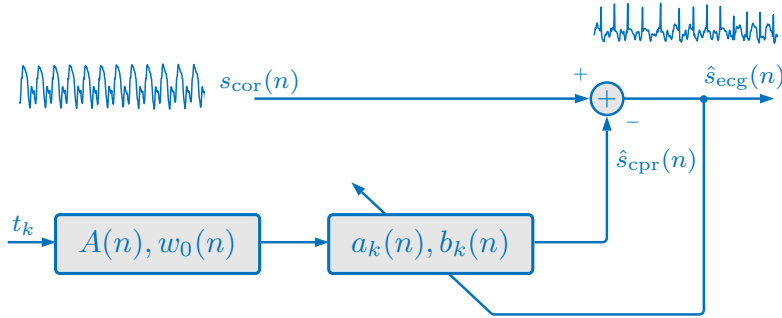
Figure 2.13. Block diagram of the adaptive filter proposed by Irusta et al. [152]. The filter takes as reference the Fourier series model of the artefact built using the chest compression instants, t_k. The $a_k(n)$ and $b_k(n)$ coefficients of the model are adaptively estimated using an LMS filter to minimize the error between the corrupted and the filtered ECG at the harmonics of f_0.

2.3.3 SUMMARY OF THE RESULTS

Table 2.1 shows the results of the best performing studies within each of the above-mentioned approaches. All these studies were tested on human cardiac arrest data, so performances were reported in terms of the Se and Sp of a SAA. Although it is not entirely fair to compare these results due to differences in the database and the SAA used for evaluation, these results provide an insight on which could be the optimal approach to rhythm analysis during CPR.

The performance reported by Ruiz de Gauna et al. [90] for a filter based only on the ECG is well below the performance presented by other authors, particularly the sensitivity, which is 5 to 6 points lower. The direct analysis of the corrupted ECG proposed by Li et al. [197] improved those results but did not consider asystole. Asystole is one of the causes of low Se and Sp values, since one of the critical distinctions after filtering is between VF and AS [87, 90]. This underlines the importance of additional reference information to obtain an accurate rhythm analysis. The multichannel MC-RAMP filter used four reference channels directly fed to the adaptive algorithm, obtaining better performance than ECG only approaches on a representative OHCA database. The filter based only on chest compression instants introduced by Irusta et al.[152], obtained similar

results while substantially reducing the computational burden and hardware requirements of the solution.

Table 2.1. Comparison of four representative approaches to rhythm analysis during CPR tested with real OHCA data. In the nonshockable (NSh) column the proportion in parenthesis refers to the prevalence of AS within the class.

		Accuracy		Datasets	
Authors	Method	Se (%)	Sp (%)	Sh	NSh
Eilevstjøn et al. [151]	MC-RAMP	96.7	79.9	92	174 (30%)
Ruiz de Gauna et al [90]	Kalman filter	90.1	80.4	131	347 (43%)
Irusta et al. [152]	LMS filter	95.6	86.4	89	292 (30%)
Li et al. [197]	Direct analysis	93.3	88.6	1256	964 (4%)

All the methods presented sensitivities above 90%, the minimum value recommended by the AHA for SAA on artefact-free ECG. However, the specificity was at best [152] 9 points below the 95% recommended by the AHA. A low specificity would result in a large number of false shock diagnoses during CPR, which would unnecessarily increase the number of interruptions in CPR. The main source of the low Sp are filtering residuals in nonshockable rhythms. As shown in Figure 2.14a, these residuals often resemble a disorganized rhythm and are frequently misdiagnosed as shockable by commercial SAAs. Most of the false negatives are also due to filtering residuals. In these cases (see Figure 2.14b), the filter is unable to remove the spiky artefact introduced by each compression, and these spikes are interpreted as the QRS complexes of an ORG rhythm by the SAA.

In conclusion, the performance of the shock/no-shock decision algorithms during CPR is limited by the use of SAAs from commercial defibrillators. These SAAs were designed to classify clean ECG, but filtering residuals act as a major confounding factor. Recently, a new line of research has focused on developing ad-hoc algorithms for shock/no-shock decision that analyze the filtered ECG.
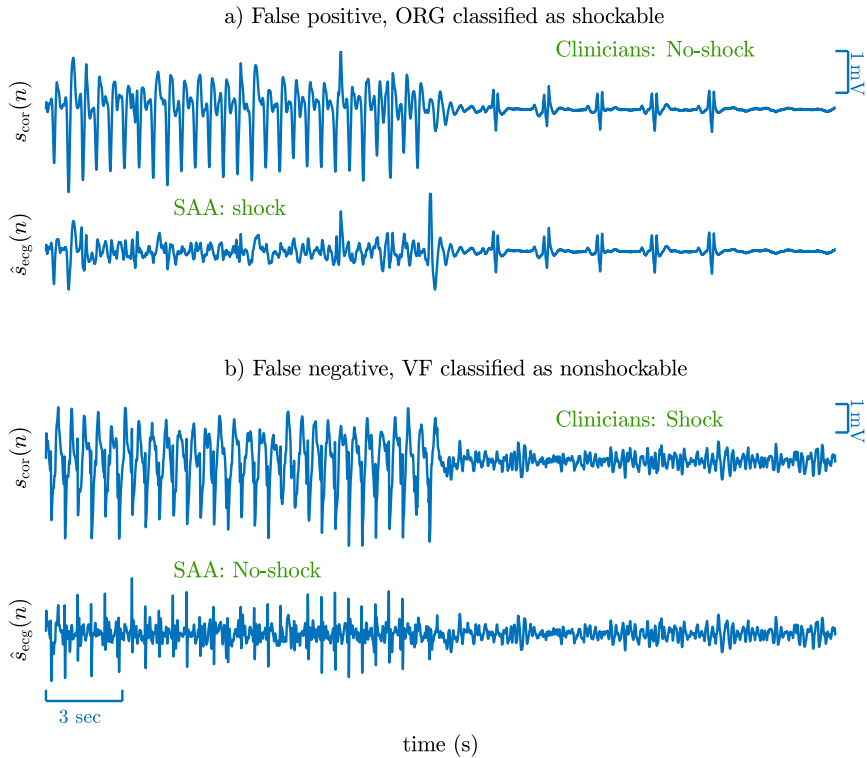
Figure 2.14. Two examples in which the SAA incorrectly classifies the filtered ECG, $\hat{s}_{ecg}(n)$. In both examples, the top panels show the ECG recorded by the defibrillator, $s_{cor}(n)$, and the bottom panels show the ECG after filtering the chest compression artefact, $\hat{s}_{ecg}(n)$. In the top panels, the initial 15 s of the ECG are corrupted by the chest compressions, whereas the following 15 s show the underlying rhythm in an interval free of artefact. In both cases the SAA produces an erroneous shock/no-shock analysis of the filtered ECG due to the strong filtering residuals.

2.3.4 ANALYSIS OF THE FILTERED ECG

In 2014, Ayala et al. [110] introduced a novel approach to improve rhythm analysis during CPR. They proposed the use of machine learning classifiers to design shock/no-shock algorithms using information derived from the filtered ECG. Figure 2.15 summarizes the architecture of this new approach which combines the adaptive filtering stage with a machine learning based shock/no-shock decision algorithm, a synthesis of the methods described in sections 2.3.2 and 2.1. As shown in Figure 2.15, the machine learning
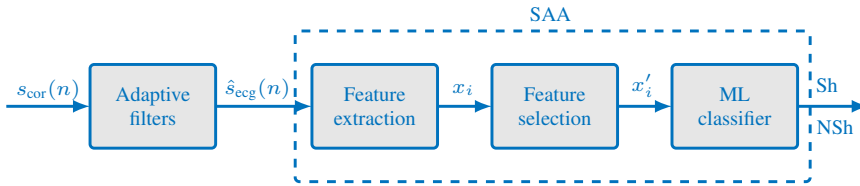
Figure 2.15. New approach to rhythm analysis during CPR. It consists of two main stages: an adaptive filter to suppress chest compression artefacts followed by a machine learning shock/no-shock classification algorithm trained using information derived from the filtered ECG.

based classifier is fed with the features extracted from the filtered ECG. In this way, the SAA learns the characteristics of the filtered ECG including those of the filtering residuals. Moreover, the SAA's feature selection stage provides the classifier with the feature set best suited for classification, i.e. the feature subset that minimizes the adverse effect of filtering residuals.

First, Ayala et al. [110] used the adaptive filter proposed by Irusta et al. [152] to remove the chest compression artefact. Then, two features were extracted from the filtered ECG and threholding was used to identify rhythms with low electrical activity (LEA) like asystole. Signal segments that were not identified as LEA were further classified as VF or ORG using features obtained from the time domain and the spectral domain. Finally, these features were fed into a SVM classifier for the final shock/no-shock classification.

This method was the first to provide a shock/no-shock diagnosis during CPR compliant with AHA recommendations, obtaining a Se and a Sp of 91% and 96.6%, respectively. Although there was a slight drop in Se, the algorithm corrected most of the false positives which were common in previous solutions. This novel approach provided a solid foundation for further improvements on rhythm analysis during CPR, which should explore new approaches to feature extraction, feature selection, and classification using machine learning algorithms.

3 | HYPOTHESIS AND OBJECTIVES

At the time this thesis started, several knowledge gaps were identified in rhythm analysis during CPR. The main hypothesis of this thesis work was that given appropriate data, the systematic use of machine learning and advanced signal processing techniques could help cover those gaps. In an attempt to address those gaps the following objectives were defined:

- *Objective 1*: The development of methods for a reliable shock/no-shock decision during mechanical CPR, a field in which no AHA compliant solutions existed. This objective was divided into two secondary goals:

  – To adapt filtering schemes to the suppression of mechanical artefacts. The results associated to this goal were published in a conference paper ($C1_1$) and in an indexed journal, $J1_1$.

  – To improve the results of decision algorithms during mechanical CPR by introducing machine learning classifiers. This secondary goal led to a conference and a journal paper, $C2_1$ and $J2_1$.

- *Objective 2*: The introduction of a new method for the classification of the five OHCA rhythm types during manual CPR. This work was an extension of the multiclass OHCA classifier developed by Rad et al. [141] for ECGs free of artefacts. All the work done to reach this objective was published in an international journal, $J1_2$.

- *Objective 3*: The development of the first deep learning solution to improve the accuracy of machine learning based shock/no-shock classifiers during manual CPR. This goal led to two conference papers, $C1_3$ and $C2_3$, and a journal paper, $J1_3$.

- *Objective 4*: To analyze the effectiveness of mechanical CPR artefact supression filters in restoring clinically relevant ECG information beyond the shock/no-shock decision. The results related to this goal were published in an indexed paper, $J1_4$.

4 | RESULTS AND CONCLUSIONS

4.1 RESULTS AND DISCUSSION

This section discusses the results obtained in the studies conducted to reach the goals defined in Chapter 4. We will focus on the results obtained in the indexed journals, as they extend and improve the contributions published preliminarly in conferences.

4.1.1 RESULTS RELATED TO OBJECTIVE 1

Objective one was split into two secondary goals and each of them led to a journal publication:

- $J1_1$: This solution proposed an improved filter for the suppresion of LUCAS-2 artefacts based on the multiharmonic modeling of the artefact proposed by Irusta et al. [152]. Two features contributed to an increased decision accuracy. First, the Generalized Goertzel algorithm was used to calculate the number of harmonics N to be used in the Fourier Series model individually for each ECG segment. Second, a Recursive Least Squares (RLS) filter was used instead of the LMS filter. This improved CPR artefact filter led to a Se and a Sp of 98.1% and 87.0% when evaluated using the SAA of a commercial AED. Although this approach outperformed the results obtained in preliminary studies [155], the algorithm did not meet AHA performance goals. Thus, a more complex architecture named multistage algorithm (MSA) was introduced to analyze the

filtered ECG. The MSA was composed of three shock/no-shock decision stages based on a commercial SAA and on an ECG-slope decision stage. The method obtained a Se of 91.8% and a Sp of 98.1%. Although the MSA method was computationally demanding, it was the first method to give a shock/no-shock diagnosis compliant with AHA recommendations during piston-driven chest compressions.

- $J2_1$: In this study, the commercial SAA was replaced by a machine learning based shock/no-shock decision algorithm. This approach consisted of a high-resolution feature extraction method based on the Stationary Wavelet Transform (SWT), a wrapper-based feature selection algorithm and a SVM classifier for the final shock/no-shock classification. The algorithm obtained a Se and a Sp of 97.5% and 98.2%, improving by 3 points the BAC of the MSA solution. There were two main reasons for this improvement. First, the feature extraction phase based on the SWT resulted in new and improved discriminating features. Second, extracting the features after removing the CPR artefact and feeding those features to the SVM improved the accuracy considerably, because the machine learning algorithm was able to learn the characteristics of filtering residuals. Very importantly, this improvement was achieved along with a drastic reduction of the computation demands when compared to the MSA.

4.1.2 RESULTS RELATED TO OBJECTIVE 2

In $J1_2$ we introduced the first framework for multiclass OHCA rhythm classification in the presence of manual CPR artefacts. More than 93 state-of-the-art VF detection features were computed from the SWT analysis of the filtered ECG, and a RF was used for classification. A hybrid FS algorithm combining wrapper and embedded FS methods was used to select the most discriminative subset of features. The FS was based on a SBS approach using the permutation importance provided by the RF classifier as a ranking criterion. Four levels of clinical detail were studied: shock/no-shock, shock/AS/ORG, VF/VT/AS/ORG, and VF/VT/AS/PEA/PR. The

median UMS for the 2, 3, 4, and 5-class classifiers were: 95.4%, 87.6%, 80.6%, and 71.9%, respectively. For shock/no-shock decisions sensitivities were 93.5% and 97.2%, meeting AHA standards and outperforming the results obtained by Ayala et al. [110] (see Section 2.3.4). Our 5-class classifier had a median UMS of 71.9% during manual CPR, which is only 5.8-points lower than the 5-class OHCA rhythm classifier on artefact-free ECG proposed by Rad et al. [142]. Furthermore, when Rad et al. [142] used their algorithms to annotate complete OHCA episodes, the UMS during artefact-free segments was 75%, but dropped to 52.5% in intervals during chest compressions, even after filtering the CPR artefact.

4.1.3 RESULTS RELATED TO OBJECTIVE 3

The objective of $J1_3$ was to improve the accuracy of previous methods by designing the first deep learning solution to discriminate shockable from nonshockable rhythms during manual CPR. The method comprised two stages, an adaptive RLS filter to remove CPR artefacts from the ECG followed by a convolutional neural network (CNN) to classify the ECG after filtering. The CNN was composed of three convolutional blocks to extract the high level features of the ECG, and two fully connected layers for shock/no-shock classification. The CNN obtained a Se and a Sp of 95.8% and 96.1%, respectively. The algorithm outperformed the performance of the clasical machine learning algorithm published in $J1_2$, showing the potential of deep learning methods to provide a reliable shock/no-shock diagnosis during manual chest compression therapy.

4.1.4 RESULTS RELATED TO OBJECTIVE 4

This study, published as $J1_4$, evaluated the performance of the best known adaptive filters during piston-driven chest compressions in terms of ECG waveform restoration, clinically relevant ECG characteristics and shock/no-shock diagnostic accuracy. The mixture model was used to evaluate filter performance in terms of ECG waveform restoration (see Section 2.3.1 for details). The preservation of signal integrity is of vital importance during CPR since ALS clinicians visually evaluate the ECG to decide suitable therapeutic

interventions. The integrity of the filtered signal was measured in terms of restored SNR and correlation-based similarity measures. Moreover, it is important to know to what extent filters degrade the features that are clinically relevant for different diagnostic scenarios other than the shock/no-shock decision, such as, the prediction of defibrillation success [143] or the detection of pulse [131]. For that, the following ECG features were assessed before and after filtering: heartbeat detection accuracy for ORG rhythms, and dominant frequency (DF), mean amplitude (MA) and waveform irregularity for VF. The RLS filter produced the largest correlation coefficient, average increase in SNR and largest heartbeat detection accuracy. The LMS filter best restored VF with lower errors in DF, MA and waveform irregularity. This was the first time a mixture model was used to make an exhaustive evaluation of adaptive filters during mechanical CPR.

4.2 Conclusions

This thesis work has addressed the overall objective of designing new strategies that allow a reliable rhythm analysis during manual and mechanical CPR.

In the context of mechanical CPR, we introduced the first AHA compliant shock/no-shock decision algorithm using an enhanced adaptive filter and a multistage shock/no-shock decision algorithm based on a commercial SAA. These results were further improved when the commercial SAA was replaced by a machine learning classifier. Moreover, the mixture model was used for the first time to determine the most suitable adaptive filter for evaluating ECG waveform restoration in diferent OHCA clinical contexts.

Regarding manual CPR, two main contributions were carried out:

- First, we introduced the first multiclass OHCA framework which accounts for four levels of clinical detail: shock/no-shock, shock/AS/ORG, VF/VT/AS/ORG and VF/VT/AS/PEA/PR. The shock/no-shock algorithm improved the results of the machine learning based classifier proposed by Ayala et al. [110]. The 5-class classifier, which was the main goal of the study,

presented a performance similar to that of the multiclass classifier proposed by Rad et al [142] for artefact free ECGs.

- Second, we improved the performance of classical machine learning shock/no-shock decision algorithms by the introduction of deep learning techniques.

Although great progress has been made in the field of rhythm analysis during CPR, there are still many challenges ahead. First, methods that allow a reliable rhythm analysis during piston-driven chest compressions should be recast to mechanical CPR devices based on load distributing bands, like the AutoPulse. As shown in 2.2 the artefact generated by the AutoPulse device presents larger amplitudes and a higher variability between episodes than the LUCAS-2 artefact. So, we foresee a more challenging adaptive filtering problem. Second, the multiclass OHCA rhythm classifiers should also be adapted to mechanical CPR. Finally, based on the results reported in J1$_3$, we foresee that deep learning models could improve the performance of machine learning based multiclass classifiers and shock/no-shock decision algorithms during mechanical CPR.

BIBLIOGRAPHY

[1] R. Cummins, D. Chamberlain, N. Abramson, M. Allen, P. Baskett, L. Becker *et al.*, "A statement for health professionals from a task force of the American Heart Association, the European Resuscitation Council, the Heart and Stroke Foundation of Canada, and the Australian Resuscitation Council. Recommended guidelines for uniform reporting of data from out-of-hospital cardiac arrest: the Utstein style," *Circulation*, vol. 84, no. 2, pp. 960–975, 1991.

[2] Z.-J. Zheng, J. B. Croft, W. H. Giles, and G. A. Mensah, "Sudden cardiac death in the United States, 1989 to 1998," *Circulation*, vol. 104, no. 18, pp. 2158–2163, 2001.

[3] D. P. Zipes and H. J. Wellens, "Sudden cardiac death," in *Professor Hein JJ Wellens*. Springer, 2000, pp. 621–645.

[4] S. S. Chugh, K. Reinier, C. Teodorescu, A. Evanado, E. Kehr, M. Al Samara *et al.*, "Epidemiology of sudden cardiac death: clinical and research implications," *Progress in cardiovascular diseases*, vol. 51, no. 3, pp. 213–228, 2008.

[5] M. Luu, W. G. Stevenson, L. W. Stevenson, K. Baron, and J. Walden, "Diverse mechanisms of unexpected cardiac arrest in advanced heart failure." *Circulation*, vol. 80, no. 6, pp. 1675–1680, 1989.

[6] R. Cummins and W. Thies, "Automated external defibrillators and the Advanced Cardiac Life Support Program: a new initiative from the American Heart Association," *Am J Emerg Med*, vol. 9, pp. 91–3, 1991.

[7] A. B. de Luna, P. Coumel, and J. F. Leclercq, "Ambulatory sudden cardiac death: mechanisms of production of fatal arrhythmia on the basis of data from 157 cases," *American Heart Journal*, vol. 117, no. 1, pp. 151–159, 1989.

[8] P. M. Zoll, "Resuscitation of the heart in ventricular standstill by external electric stimulation," *New England Journal of Medicine*, vol. 247, no. 20, pp. 768–771, 1952.

[9] R. A. Waalewijn, M. A. Nijpels, J. G. Tijssen, and R. W. Koster, "Prevention of deterioration of ventricular fibrillation by basic life support during out-of-hospital cardiac arrest," *Resuscitation*, vol. 54, no. 1, pp. 31–36, 2002.

[10] M. L. Weisfeldt and L. B. Becker, "Resuscitation after cardiac arrest: a 3-phase time-sensitive model," *JAMA*.

[11] M. Holmberg, S. Holmberg, and J. Herlitz, "Incidence, duration and survival of ventricular fibrillation in out-of-hospital cardiac arrest patients in Sweden," *Resuscitation*, vol. 44, no. 1, pp. 7–17, 2000.

[12] L. Wik, T. B. Hansen, F. Fylling, T. Steen, P. Vaagenes, B. H. Auestad *et al.*, "Delaying defibrillation to give basic cardiopulmonary resuscitation to patients with out-of-hospital ventricular fibrillation: a randomized trial," *JAMA*, vol. 289, no. 11, pp. 1389–1395, 2003.

[13] L. A. Cobb, C. E. Fahrenbruch, M. Olsufka, and M. K. Copass, "Changing incidence of out-of-hospital ventricular fibrillation, 1980-2000," *JAMA*, vol. 288, no. 23, pp. 3008–3013, 2002.

[14] C. Atwood, M. S. Eisenberg, J. Herlitz, and T. D. Rea, "Incidence of EMS-treated out-of-hospital cardiac arrest in Europe," *Resuscitation*, vol. 67, no. 1, pp. 75–80, 2005.

[15] S. Sans, H. Kesteloot, D. O. Kromhout, and T. Force, "The burden of cardiovascular diseases mortality in Europe: Task Force of the European Society of Cardiology on Cardiovascular Mortality and Morbidity Statistics in Europe," *European Heart Journal*, vol. 18, no. 8, pp. 1231–1248, 1997.

[16] J.-A. Álvarez-Fernández and R. J. Gazmuri, "Mortalidad evitable por parada cardíaca extrahospitalaria," *Medicina Clínica*, vol. 130, no. 18, pp. 710–714, 2008.

[17] J. Cosin, "Muerte súbita extrahospitalaria en España," in *Muerte súbita cardíaca*. Doyma Barcelona, 1991, pp. 13–21.

[18] K. Ibarguren, J. M. Unanue, D. Alonso, I. Vaqueriza, U. Irusta, E. Aramendi *et al.*, "Difference in survival from pre-hospital cardiac arrest between cities and villages in the Basque Autonomous Community," *Resuscitation*, vol. 96, p. 114, 2015.

[19] T. D. Rea, M. S. Eisenberg, G. Sinibaldi, and R. D. White, "Incidence of EMS-treated out-of-hospital cardiac arrest in the United States,"

Resuscitation, vol. 63, no. 1, pp. 17–24, 2004.

[20] B. S. Abella, J. P. Alvarado, H. Myklebust, D. P. Edelson, A. Barry, N. O'Hearn *et al.*, "Quality of cardiopulmonary resuscitation during in-hospital cardiac arrest," *Jama*, vol. 293, no. 3, pp. 305–310, 2005.

[21] M. Wolbinski, A. H. Swain, S. A. Harding, and P. D. Larsen, "Out-of-hospital cardiac arrest patient characteristics: comparing ventricular arrhythmia and pulseless electrical activity," *Heart, Lung and Circulation*, vol. 25, no. 7, pp. 639–644, 2016.

[22] J. Berdowski, R. A. Berg, J. G. P. Tijssen, and R. W. Koster, "Global incidences of out-of-hospital cardiac arrest and survival rates: Systematic review of 67 prospective studies," *Resuscitation*, vol. 81, no. 11, pp. 1479–1487, Nov. 2010.

[23] M. Eisenberg and R. D. White, "The unacceptable disparity in cardiac arrest survival among American communities," *Annals of Emergency Medicine*, vol. 54, no. 2, p. 258, 2009.

[24] J. Herlitz, J. Bahr, M. Fischer, M. Kuisma, K. Lexow, and G. Thorgeirsson, "Resuscitation in Europe: a tale of five European regions," *Resuscitation*, vol. 41, no. 2, pp. 121–131, 1999.

[25] A. J. Handley, R. Koster, K. Monsieurs, G. D. Perkins, S. Davies, and L. Bossaert, "European Resuscitation Council Guidelines for Resuscitation 2005: Section 2. Adult basic life support and use of automated external defibrillators," *Resuscitation*, vol. 67, pp. S7–S23, 2005.

[26] E. Committee *et al.*, "2005 American Heart Association guidelines for cardiopulmonary resuscitation and emergency cardiovascular care." *Circulation*, vol. 112, no. 24 Suppl, p. IV1, 2005.

[27] R. O. Cummins, J. P. Ornato, W. H. Thies, and P. E. Pepe, "Improving survival from sudden cardiac arrest: the chain of survival concept. a statement for health professionals from the Advanced Cardiac Life Support Subcommittee and the Emergency Cardiac Care Committee, American Heart Association." *Circulation*, vol. 83, no. 5, pp. 1832–1847, 1991.

[28] G. D. Perkins, A. J. Handley, R. W. Koster, M. Castrén, M. A. Smyth, T. Olasveengen *et al.*, "European resuscitation council guidelines for resuscitation 2015: Section 2. adult basic life support and automated external defibrillation," *Resuscitation*, vol. 95, pp. 81–99, 2015.

[29] C. Sasson, M. A. Rogers, J. Dahl, and A. L. Kellermann, "Predictors of survival from out-of-hospital cardiac arrest: a systematic review

and meta-analysis," *Circulation: Cardiovascular Quality and Outcomes*, vol. 3, no. 1, pp. 63–81, 2010.

[30] R. M. Sutton, B. French, A. Nishisaki, D. E. Niles, M. R. Maltese, L. Boyle *et al.*, "American Heart Association cardiopulmonary resuscitation quality targets are associated with improved arterial blood pressure during pediatric cardiac arrest," *Resuscitation*, vol. 84, no. 2, pp. 168–172, 2013.

[31] M. Holmberg, S. Holmberg, and J. Herlitz, "Effect of bystander cardiopulmonary resuscitation in out-of-hospital cardiac arrest patients in Sweden," *Resuscitation*, vol. 47, no. 1, pp. 59–70, 2000.

[32] J. Herlitz, L. Svensson, S. Holmberg, K.-A. Ängquist, and M. Young, "Efficacy of bystander CPR: intervention by lay people and by health care professionals," *Resuscitation*, vol. 66, no. 3, pp. 291–295, 2005.

[33] M. L. Selby, J. A. Kautz, T. J. Moore, W. R. Gombeski Jr, A. G. Ramirez, E. J. Farge *et al.*, "Indicators of response to a mass media CPR recruitment campaign." *American Journal of Public Health*, vol. 72, no. 9, pp. 1039–1042, 1982.

[34] T. D. Valenzuela, D. J. Roe, G. Nichol, L. L. Clark, D. W. Spaite, and R. G. Hardman, "Outcomes of rapid defibrillation by security officers after cardiac arrest in casinos," *New England Journal of Medicine*, vol. 343, no. 17, pp. 1206–1209, 2000.

[35] R. D. White, T. J. Bunch, and D. G. Hankins, "Evolution of a community-wide early defibrillation programme: experience over 13 years using police/fire personnel and paramedics as responders," *Resuscitation*, vol. 65, no. 3, pp. 279–283, 2005.

[36] M. L. Weisfeldt, R. E. Kerber, R. P. McGoldrick, A. J. Moss, G. Nichol, J. P. Ornato *et al.*, "Public access defibrillation: a statement for healthcare professionals from the American Heart Association Task Force on automatic external defibrillation," *Circulation*, vol. 92, no. 9, pp. 2763–2763, 1995.

[37] K. Sunde, M. Pytte, D. Jacobsen, A. Mangschau, L. P. Jensen, C. Smedsrud *et al.*, "Implementation of a standardised treatment protocol for post resuscitation care after out-of-hospital cardiac arrest," *Resuscitation*, vol. 73, no. 1, pp. 29–39, 2007.

[38] M. L. Weisfeldt, C. M. Sitlani, J. P. Ornato, T. Rea, T. P. Aufderheide, D. Davis *et al.*, "Survival after application of automatic external defibrillators before arrival of the emergency medical system: evaluation in the resuscitation outcomes consortium population of 21

million," *Journal of the American College of Cardiology*, vol. 55, no. 16, pp. 1713–1720, 2010.

[39] A. P. van Alem, R. H. Vrenken, R. de Vos, J. G. Tijssen, and R. W. Koster, "Use of automated external defibrillator by first responders in out of hospital cardiac arrest: prospective controlled trial," *British Medical Journal*, vol. 327, no. 7427, p. 1312, 2003.

[40] P. S. Chan, H. M. Krumholz, G. Nichol, B. K. Nallamothu, and A. H. A. N. R. of Cardiopulmonary Resuscitation Investigators, "Delayed time to defibrillation after in-hospital cardiac arrest," *New England Journal of Medicine*, vol. 358, no. 1, pp. 9–17, 2008.

[41] T. D. Valenzuela, D. J. Roe, S. Cretin, D. W. Spaite, and M. P. Larsen, "Estimating effectiveness of cardiac arrest interventions: a logistic regression survival model," *Circulation*, vol. 96, no. 10, pp. 3308–3313, 1997.

[42] M. P. Larsen, M. S. Eisenberg, R. O. Cummins, and A. P. Hallstrom, "Predicting survival from out-of-hospital cardiac arrest: a graphic model," *Annals of Emergency Medicine*, vol. 22, no. 11, pp. 1652–1658, 1993.

[43] R. A. Waalewijn, R. de Vos, J. G. Tijssen, and R. W. Koster, "Survival models for out-of-hospital cardiopulmonary resuscitation from the perspectives of the bystander, the first responder, and the paramedic," *Resuscitation*, vol. 51, no. 2, pp. 113–122, 2001.

[44] M. S. Eisenberg, L. Bergner, and A. Hallstrom, "Cardiac resuscitation in the community: importance of rapid provision and implications for program planning," *JAMA*, vol. 241, no. 18, pp. 1905–1907, 1979.

[45] J. Kramer-Johansen, D. P. Edelson, H. Losert, K. Köhler, and B. S. Abella, "Uniform reporting of measured quality of cardiopulmonary resuscitation (CPR)," *Resuscitation*, vol. 74, no. 3, pp. 406–417, 2007.

[46] J. Soar, J. P. Nolan, B. W. Böttiger, G. D. Perkins, C. Lott, P. Carli *et al.*, "European Resuscitation Council guidelines for resuscitation 2015: Section 3. Adult advanced life support," *Resuscitation*, vol. 95, pp. 100–147, 2015.

[47] J.-L. Vincent and J. B. Hall, *Encyclopedia of Intensive Care Medicine*. SpringerLink (Online service), 2012, no. 616.028.

[48] V. Wenzel, "Advanced life support," in *Drowning*. Springer, 2014, pp. 635–639.

[49] R. A. Berg, R. Hemphill, B. S. Abella, T. P. Aufderheide, D. M. Cave, M. F. Hazinski *et al.*, "Part 5: adult basic life support: 2010 American

Heart Association guidelines for cardiopulmonary resuscitation and emergency cardiovascular care," *Circulation*, vol. 122, no. 18_suppl_3, pp. S685–S705, 2010.

[50] M. R. Sayre, R. W. Koster, M. Botha, D. M. Cave, M. T. Cudnik, A. J. Handley *et al.*, "Part 5: adult basic life support: 2010 international consensus on cardiopulmonary resuscitation and emergency cardiovascular care science with treatment recommendations," *Circulation*, vol. 122, no. 16_suppl_2, pp. S298–S324, 2010.

[51] R.-P. Lukas, J. T. Gräsner, S. Seewald, R. Lefering, T. P. Weber, H. Van Aken *et al.*, "Chest compression quality management and return of spontaneous circulation: a matched-pair registry study," *Resuscitation*, vol. 83, no. 10, pp. 1212–1218, 2012.

[52] D. P. Edelson, B. S. Abella, J. Kramer-Johansen, L. Wik, H. Myklebust, A. M. Barry *et al.*, "Effects of compression depth and pre-shock pauses predict defibrillation failure during cardiac arrest," *Resuscitation*, vol. 71, no. 2, pp. 137–145, Nov. 2006.

[53] E. Simpson, "In-hospital resuscitation: recognising and responding to adults in cardiac arrest." *Nursing Standard*, vol. 30, no. 51, 2016.

[54] A. H. Idris, D. Guffey, T. P. Aufderheide, S. Brown, L. J. Morrison, P. Nichols *et al.*, "Relationship between chest compression rates and outcomes from cardiac arrest," *Circulation*, vol. 125, no. 24, pp. 3004–3012, 2012.

[55] E. J. Gallagher, G. Lombardi, and P. Gennis, "Effectiveness of bystander cardiopulmonary resuscitation and survival following out-of-hospital cardiac arrest," *JAMA*, vol. 274, no. 24, pp. 1922–1925, 1995.

[56] D. A. Fried, M. Leary, D. A. Smith, R. M. Sutton, D. Niles, D. L. Herzberg *et al.*, "The prevalence of chest compression leaning during in-hospital cardiopulmonary resuscitation," *Resuscitation*, vol. 82, no. 8, pp. 1019–1024, 2011.

[57] J. Kramer-Johansen, H. Myklebust, L. Wik, B. Fellows, L. Svensson, H. Sørebø *et al.*, "Quality of out-of-hospital cardiopulmonary resuscitation with real time automated feedback: a prospective interventional study," *Resuscitation*, vol. 71, no. 3, pp. 283–292, 2006.

[58] L. Wik, J. Kramer-Johansen, H. Myklebust, H. Sørebø, L. Svensson, B. Fellows *et al.*, "Quality of cardiopulmonary resuscitation during out-of-hospital cardiac arrest," *JAMA*, vol. 293, no. 3, pp. 299–304, 2005.

[59] S. Rubertsson, E. Lindgren, D. Smekal, O. Östlund, J. Silfverstolpe, R. A. Lichtveld *et al.*, "Mechanical Chest Compressions and Simultaneous Defibrillation vs Conventional Cardiopulmonary Resuscitation in Out-of-Hospital Cardiac Arrest: The LINC Randomized Trial," *JAMA*, vol. 311, no. 1, pp. 53–61, Jan. 2014.

[60] L. Wik, J.-A. Olsen, D. Persse, F. Sterz, M. Lozano, M. A. Brouwer *et al.*, "Manual vs. integrated automatic load-distributing band CPR with equal survival after out of hospital cardiac arrest. The randomized CIRC trial," *Resuscitation*, vol. 85, no. 6, pp. 741–748, Jun. 2014.

[61] L. Wik and S. Kiil, "Use of an automatic mechanical chest compression device (LUCAS) as a bridge to establishing cardiopulmonary bypass for a patient with hypothermic cardiac arrest," *Resuscitation*, vol. 66, no. 3, pp. 391–394, 2005.

[62] P. Holmström, J. Boyd, M. Sorsa, and M. Kuisma, "A case of hypothermic cardiac arrest treated with an external chest compression device (lucas) during transport to re-warming," *Resuscitation*, vol. 67, no. 1, pp. 139–141, 2005.

[63] H. Friberg and M. Rundgren, "Submersion, accidental hypothermia and cardiac arrest, mechanical chest compressions as a bridge to final treatment: a case report," *Scandinavian Journal of Trauma, Resuscitation and Emergency Medicine*, vol. 17, no. 1, p. 7, 2009.

[64] T. T. Vatsgar, O. Ingebrigtsen, L. O. Fjose, B. Wikstrøm, J. E. Nilsen, and L. Wik, "Cardiac arrest and resuscitation with an automatic mechanical chest compression device (LUCAS) due to anaphylaxis of a woman receiving caesarean section because of pre-eclampsia," *Resuscitation*, vol. 68, no. 1, pp. 155–159, 2006.

[65] J. Soar, G. D. Perkins, G. Abbas, A. Alfonzo, A. Barelli, J. J. Bierens *et al.*, "European Resuscitation Council Guidelines for Resuscitation 2010 Section 8. Cardiac arrest in special circumstances: electrolyte abnormalities, poisoning, drowning, accidental hypothermia, hyperthermia, asthma, anaphylaxis, cardiac surgery, trauma, pregnancy, electrocution," *Resuscitation*, vol. 81, no. 10, p. 1400, 2010.

[66] K. Sunde, L. Wik, and P. A. Steen, "Quality of mechanical, manual standard and active compression–decompression cpr on the arrest site and during transport in a manikin model," *Resuscitation*, vol. 34, no. 3, pp. 235–242, 1997.

[67] T. M. Olasveengen, L. Wik, and P. A. Steen, "Quality of cardiopulmonary resuscitation before and during transport in out-of-hospital cardiac arrest," *Resuscitation*, vol. 76, no. 2, pp. 185–190,

2008.

[68] M. E. H. Ong, K. E. Mackey, Z. C. Zhang, H. Tanaka, M. H.-M. Ma, R. Swor *et al.*, "Mechanical CPR devices compared to manual CPR during out-of-hospital cardiac arrest and ambulance transport: a systematic review," *Scandinavian Journal of Trauma, Resuscitation and Emergency Medicine*, vol. 20, no. 1, p. 39, Jun. 2012.

[69] G. Putzer, P. Braun, A. Zimmermann, F. Pedross, G. Strapazzon, H. Brugger *et al.*, "LUCAS compared to manual cardiopulmonary resuscitation is more effective during helicopter rescue—a prospective, randomized, cross-over manikin study," *The American Journal of Emergency Medicine*, vol. 31, no. 2, pp. 384–389, Feb. 2013.

[70] H. Gässler, S. Kümmerle, M.-M. Ventzke, L. Lampl, and M. Helm, "Mechanical chest compression: an alternative in helicopter emergency medical services?" *Internal and Emergency Medicine*, vol. 10, no. 6, pp. 715–720, 2015.

[71] H. Gässler, M.-M. Ventzke, L. Lampl, and M. Helm, "Transport with ongoing resuscitation: a comparison between manual and mechanical compression," *Emergency Medicine Journal*, vol. 30, no. 7, pp. 589–592, 2013.

[72] M.-M. Ventzke, H. Gässler, L. Lampl, and M. Helm, "Cardio pump reloaded: in-hospital resuscitation during transport," *Internal and Emergency Medicine*, vol. 8, no. 7, pp. 621–626, 2013.

[73] J. Fox, R. Fiechter, P. Gerstl, A. Url, H. Wagner, T. F. Lüscher *et al.*, "Mechanical versus manual chest compression CPR under ground ambulance transport conditions," *Acute cardiac care*, vol. 15, no. 1, pp. 1–6, 2013.

[74] A. I. Larsen, s. S. Hjørnevik, C. L. Ellingsen, and D. W. T. Nilsen, "Cardiac arrest with continuous mechanical chest compression during percutaneous coronary intervention: A report on the use of the LUCAS device," *Resuscitation*, vol. 75, no. 3, pp. 454–459, Dec. 2007.

[75] H. Wagner, C. J. Terkelsen, H. Friberg, J. Harnek, K. Kern, J. F. Lassen *et al.*, "Cardiac arrest in the catheterisation laboratory: a 5-year experience of using mechanical chest compressions to facilitate PCI during prolonged resuscitation efforts," *Resuscitation*, vol. 81, no. 4, pp. 383–387, 2010.

[76] J. M. Venturini, E. Retzer, J. R. Estrada, J. Friant, D. Beiser, D. Edelson *et al.*, "Mechanical chest compressions improve rate of return of spontaneous circulation and allow for initiation of percutaneous

circulatory support during cardiac arrest in the cardiac catheterization laboratory," *Resuscitation*, vol. 115, pp. 56–60, 2017.

[77] Z.-P. Zhang, X. Su, C.-W. Liu, D. Song, J. Peng, and H. Yan, "Continuous mechanical chest compression-assisted percutaneous coronary intervention in a patient with cardiac arrest complicating acute myocardial infarction," *Chinese medical journal*, vol. 128, no. 6, p. 846, 2015.

[78] R. W. Neumar, M. Shuster, C. W. Callaway, L. M. Gent, D. L. Atkins, F. Bhanji *et al.*, "Part 1: executive summary: 2015 American Heart Association guidelines update for cardiopulmonary resuscitation and emergency cardiovascular care," *Circulation*, vol. 132, no. 18_suppl_2, pp. S315–S367, 2015.

[79] R. E. Kerber, L. B. Becker, J. D. Bourland, R. O. Cummins, A. P. Hallstrom, M. B. Michos *et al.*, "Automatic external defibrillators for public access defibrillation: recommendations for specifying and reporting arrhythmia analysis algorithm performance, incorporating new waveforms, and enhancing safety: a statement for health professionals from the American Heart Association Task Force on Automatic External Defibrillation, Subcommittee on AED Safety and Efficacy," *Circulation*, vol. 95, no. 6, pp. 1677–1682, 1997.

[80] "AAMI/IEC 60601-2-04/Ed.5, Medical electrical equipment - Part 2-4: Particular requirements for basic safety and essential performance of cardiac defibrillators. Technical report, association for the advancement of medical instrumentation 2011."

[81] D. R. Martin, T. Gavin, J. Bianco, C. G. Browns, H. Stueven, P. E. Pepe *et al.*, "Initial countershock in the treatment of asystole," *Resuscitation*, vol. 26, no. 1, pp. 63–68, 1993.

[82] A. Clifford, "Comparative assessment of shockable ECG rhythm detection algorithms in automated external defibrillators," *Resuscitation*, vol. 32, no. 3, pp. 217–225, 1996.

[83] A. Murray, R. Clayton, and R. Campbell, "Assessment of the ventricular fibrillation detection algorithm in the semi-automatic cardio-aid defibrillator," *Resuscitation*, vol. 29, no. 2, pp. 113–117, 1995.

[84] F. Cecchin, D. B. Jorgenson, C. I. Berul, J. C. Perry, A. A. Zimmerman, B. W. Duncan *et al.*, "Is arrhythmia detection by automatic external defibrillator accurate for children? sensitivity and specificity of an automatic external defibrillator algorithm in 696 pediatric arrhythmias," *Circulation*, vol. 103, no. 20, pp. 2483–2488, 2001.

[85] E. Atkinson, B. Mikysa, J. A. Conway, M. Parker, K. Christian, J. Deshpande *et al.*, "Specificity and sensitivity of automated external defibrillator rhythm analysis in infants and children," *Annals of Emergency Medicine*, vol. 42, no. 2, pp. 185–196, 2003.

[86] D. L. Atkins, W. A. Scott, A. D. Blaufox, I. H. Law, M. Dick II, F. Geheb *et al.*, "Sensitivity and specificity of an automated external defibrillator algorithm designed for pediatric patients," *Resuscitation*, vol. 76, no. 2, pp. 168–174, Feb. 2008.

[87] U. Irusta, J. Ruiz, E. Aramendi, S. Ruiz de Gauna, U. Ayala, and E. Alonso, "A high-temporal resolution algorithm to discriminate shockable from nonshockable rhythms in adults and children," *Resuscitation*, vol. 83, no. 9, pp. 1090–1097, Sep. 2012.

[88] W. D. Weaver, L. A. Cobb, D. Dennis, R. RAY, A. P. HALLSTROM, and M. K. COPASS, "Amplitude of ventricular fibrillation waveform and outcome after cardiac arrest," *Annals of internal medicine*, vol. 102, no. 1, pp. 53–55, 1985.

[89] R. L. Page, J. A. Joglar, R. C. Kowal, J. D. Zagrodzky, L. L. Nelson, K. Ramaswamy *et al.*, "Use of automated external defibrillators by a us airline," *New England Journal of Medicine*, vol. 343, no. 17, pp. 1210–1216, 2000.

[90] S. Ruiz de Gauna, J. Ruiz, U. Irusta, E. Aramendi, T. Eftestøl, and J. Kramer-Johansen, "A method to remove CPR artefacts from human ECG using only the recorded ECG," *Resuscitation*, vol. 76, no. 2, pp. 271–278, Feb. 2008.

[91] D. Snyder and C. Morgan, "Wide variation in cardiopulmonary resuscitation interruption intervals among commercially available automated external defibrillators may affect survival despite high defibrillation efficacy," *Critical Care Medicine*, vol. 32, no. 9, p. S421, Sep. 2004.

[92] R. A. Berg, A. B. Sanders, K. B. Kern, R. W. Hilwig, J. W. Heidenreich, M. E. Porter *et al.*, "Adverse hemodynamic effects of interrupting chest compressions for rescue breathing during cardiopulmonary resuscitation for ventricular fibrillation cardiac arrest," *Circulation*, vol. 104, no. 20, pp. 2465–2470, 2001.

[93] Eftestøl Trygve, Sunde Kjetil, and Steen Petter Andreas, "Effects of Interrupting Precordial Compressions on the Calculated Probability of Defibrillation Success During Out-of-Hospital Cardiac Arrest," *Circulation*, vol. 105, no. 19, pp. 2270–2273, May 2002.

[94] T. J. Mader, A. T. Paquette, D. D. Salcido, B. H. Nathanson, and J. J. Menegazzi, "The effect of the preshock pause on coronary perfusion pressure decay and rescue shock outcome in porcine ventricular fibrillation," *Prehospital Emergency Care*, vol. 13, no. 4, pp. 487–494, 2009.

[95] S. Cheskes, R. H. Schmicker, J. Christenson, D. D. Salcido, T. Rea, J. Powell *et al.*, "Perishock pause: an independent predictor of survival from out-of-hospital shockable cardiac arrest," *Circulation*, vol. 124, no. 1, pp. 58–66, 2011.

[96] C. N. Pozner, A. Almozlino, J. Elmer, S. Poole, D. McNamara, and D. Barash, "Cardiopulmonary resuscitation feedback improves the quality of chest compression provided by hospital health care professionals," *The American Journal of Emergency Medicine*, vol. 29, no. 6, pp. 618–625, 2011.

[97] C. Li, J. Xu, F. Han, L. Zheng, Y. Fu, D. Yao *et al.*, "The role of pulse oximetry plethysmographic waveform monitoring as a marker of restoration of spontaneous circulation: a pilot study," *Zhonghua wei zhong bing ji jiu yi xue*, vol. 27, no. 3, pp. 203–208, 2015.

[98] R. W. Wijshoff, T. van der Sar, W. H. Peeters, R. Bezemer, P. Aelen, I. W. Paulussen *et al.*, "Detection of a spontaneous pulse in photoplethysmograms during automated cardiopulmonary resuscitation in a porcine model," *Resuscitation*, vol. 84, no. 11, pp. 1625–1632, 2013.

[99] K. Tanigawa, T. Takeda, E. Goto, and K. Tanaka, "Accuracy and reliability of the self-inflating bulb to verify tracheal intubation in out-of-hospital cardiac arrest patients," *Anesthesiology: The Journal of the American Society of Anesthesiologists*, vol. 93, no. 6, pp. 1432–1436, 2000.

[100] T. Takeda, K. Tanigawa, H. Tanaka, Y. Hayashi, E. Goto, and K. Tanaka, "The assessment of three methods to verify tracheal tube placement in the emergency setting," *Resuscitation*, vol. 56, no. 2, pp. 153–157, 2003.

[101] S. Silvestri, G. A. Ralls, B. Krauss, J. Thundiyil, S. G. Rothrock, A. Senn *et al.*, "The effectiveness of out-of-hospital use of continuous end-tidal carbon dioxide monitoring on the rate of unrecognized misplaced intubation within a regional emergency medical services system," *Annals of Emergency Medicine*, vol. 45, no. 5, pp. 497–503, 2005.

[102] K. R. Ward, J. J. Menegazzi, R. R. Zelenak, R. J. Sullivan, and N. E. McSwain Jr, "A comparison of chest compressions between

mechanical and manual CPR by monitoring end-tidal pco2 during human cardiac arrest," *Annals of Emergency Medicine*, vol. 22, no. 4, pp. 669–674, 1993.

[103] J. L. Falk, E. C. Rackow, and M. H. Weil, "End-tidal carbon dioxide concentration during cardiopulmonary resuscitation," *New England Journal of Medicine*, vol. 318, no. 10, pp. 607–611, 1988.

[104] Z. Kalenda, "The capnogram as a guide to the efficacy of cardiac massage," *Resuscitation*, vol. 6, no. 4, pp. 259–263, 1978.

[105] M. Pokorná, E. Nečas, J. Kratochvíl, R. Skřipský, M. Andrlík, and O. Franěk, "A sudden increase in partial pressure end-tidal carbon dioxide (PETCO2) at the moment of return of spontaneous circulation," *The Journal of Emergency Medicine*, vol. 38, no. 5, pp. 614–621, 2010.

[106] M. S. Bhende, D. G. Karasic, and R. B. Karasic, "End-tidal carbon dioxide changes during cardiopulmonary resuscitation after experimental asphyxial cardiac arrest," *The American Journal of Emergency Medicine*, vol. 14, no. 4, pp. 349–350, 1996.

[107] A. R. Garnett, J. P. Ornato, E. R. Gonzalez, and E. B. Johnson, "End-tidal carbon dioxide monitoring during cardiopulmonary resuscitation," *JAMA*, vol. 257, no. 4, pp. 512–515, 1987.

[108] S. R. de Gauna, D. M. Gonzalez-Otero, J. Ruiz, and J. K. Russell, "Feedback on the rate and depth of chest compressions during cardiopulmonary resuscitation using only accelerometers," *PloS one*, vol. 11, no. 3, 2016.

[109] M. H. Jung, J. H. Oh, C. W. Kim, S. E. Kim, D. H. Lee, and W. J. Chang, "Does accelerometer feedback on high-quality chest compression improve survival rate? an in-hospital cardiac arrest simulation," *The American Journal of Emergency Medicine*, vol. 33, no. 8, pp. 993–997, 2015.

[110] U. Ayala, T. Eftestøl, E. Alonso, U. Irusta, E. Aramendi, S. Wali *et al.*, "Automatic detection of chest compressions for the assessment of CPR-quality parameters," *Resuscitation*, vol. 85, no. 7, pp. 957–963, 2014.

[111] I. Jacobs, V. Nadkarni, I. T. F. on Cardiac Arrest, C. R. Outcomes, C. PARTICIPANTS, J. Bahr *et al.*, "Cardiac arrest and cardiopulmonary resuscitation outcome reports: update and simplification of the Utstein templates for resuscitation registries: a statement for healthcare professionals from a task force of the international

liaison committee on resuscitation (American Heart Association, European Resuscitation Council, Australian Resuscitation Council, New Zealand Resuscitation Council, Heart and Stroke Foundation of Canada, InterAmerican Heart Foundation, Resuscitation Councils of Southern Africa)," *Circulation*, vol. 110, no. 21, pp. 3385–3397, 2004.

[112] L. J. Morrison, G. Nichol, T. D. Rea, J. Christenson, C. W. Callaway, S. Stephens *et al.*, "Rationale, development and implementation of the resuscitation outcomes consortium epistry—cardiac arrest," *Resuscitation*, vol. 78, no. 2, pp. 161–169, 2008.

[113] J.-T. Gräsner, R. Lefering, R. W. Koster, S. Masterson, B. W. Böttiger, J. Herlitz *et al.*, "EuReCa ONE–27 Nations, ONE Europe, ONE Registry: A prospective one month analysis of out-of-hospital cardiac arrest outcomes in 27 countries in Europe," *Resuscitation*, vol. 105, pp. 188–195, Aug. 2016.

[114] I. Jekova and V. Krasteva, "Real time detection of ventricular fibrillation and tachycardia," *Physiological Measurement*, vol. 25, no. 5, pp. 1167–1178, Aug. 2004.

[115] E. M. A. Anas, S. Y. Lee, and M. K. Hasan, "Sequential algorithm for life threatening cardiac pathologies detection based on mean signal strength and EMD functions," *BioMedical Engineering OnLine*, vol. 9, no. 1, p. 43, Sep. 2010.

[116] S. Chen, N. V. Thakor, and M. M. Mower, "Ventricular fibrillation detection by a regression test on the autocorrelation function," *Medical and Biological Engineering and Computing*, vol. 25, no. 3, pp. 241–249, 1987.

[117] N. V. Thakor, Y.-S. Zhu, and K.-Y. Pan, "Ventricular tachycardia and fibrillation detection by a sequential hypothesis testing algorithm," *IEEE Transactions on Biomedical Engineering*, vol. 37, no. 9, pp. 837–843, 1990.

[118] M. A. Arafat, A. W. Chowdhury, and M. K. Hasan, "A simple time domain algorithm for the detection of ventricular fibrillation in electrocardiogram," *Signal, Image and Video Processing*, vol. 5, no. 1, pp. 1–10, 2011.

[119] S. KUO, "Computer Detection of Ventricular Fibrillation," *Proc. of Computers in Cardiology, IEEE Comuputer Society*, pp. 347–349, 1978.

[120] K.-i. Minami, H. Nakajima, and T. Toyoshima, "Real-time discrimination of ventricular tachyarrhythmia with Fourier-transform neural network," *IEEE transactions on Biomedical Engineering*, vol. 46,

no. 2, pp. 179–185, 1999.

[121] L. Khadra, A. Al-Fahoum, and H. Al-Nashash, "Detection of life-threatening cardiac arrhythmias using the Wavelet transformation," *Medical and Biological Engineering and Computing*, vol. 35, no. 6, pp. 626–632, 1997.

[122] C. Figuera, U. Irusta, E. Morgado, E. Aramendi, U. Ayala, L. Wik *et al.*, "Machine learning techniques for the detection of shockable rhythms in automated external defibrillators," *PloS one*, vol. 11, no. 7, 2016.

[123] F. Alonso-Atienza, E. Morgado, L. Fernandez-Martinez, A. García-Alberola, and J. L. Rojo-Alvarez, "Detection of life-threatening arrhythmias using feature selection and support vector machines," *IEEE Transactions on Biomedical Engineering*, vol. 61, no. 3, pp. 832–840, 2013.

[124] Q. Li, C. Rajagopalan, and G. D. Clifford, "Ventricular fibrillation and tachycardia classification using a machine learning approach," *IEEE Transactions on Biomedical Engineering*, vol. 61, no. 6, pp. 1607–1613, 2013.

[125] M. T. Nguyen, B. Van Nguyen, and K. Kim, "Shockable rhythm diagnosis for automated external defibrillators using a modified variational mode decomposition technique," *IEEE Transactions on Industrial Informatics*, vol. 13, no. 6, pp. 3037–3046, 2017.

[126] P. Cheng and X. Dong, "Life-Threatening Ventricular Arrhythmia Detection With Personalized Features," *IEEE Access*, vol. 5, pp. 14 195–14 203, 2017.

[127] R. Tripathy, L. Sharma, and S. Dandapat, "Detection of shockable ventricular arrhythmia using variational mode decomposition," *Journal of Medical Systems*, vol. 40, no. 4, p. 79, 2016.

[128] U. R. Acharya, H. Fujita, O. S. Lih, Y. Hagiwara, J. H. Tan, and M. Adam, "Automated detection of arrhythmias using different intervals of tachycardia ECG segments with convolutional neural network," *Information Sciences*, vol. 405, pp. 81–90, Sep. 2017.

[129] A. Picon, U. Irusta, A. Álvarez Gila, E. Aramendi, F. Alonso-Atienza, C. Figuera *et al.*, "Mixed convolutional and long short-term memory network for the detection of lethal ventricular arrhythmia," *PLoS ONE*, vol. 14, no. 5, May 2019.

[130] A. Elola, E. Aramendi, U. Irusta, A. Picón, E. Alonso, P. Owens *et al.*, "Deep Neural Networks for ECG-Based Pulse Detection during Out-

of-Hospital Cardiac Arrest," *Entropy*, vol. 21, no. 3, p. 305, Mar. 2019.

[131] A. Elola, E. Aramendi, U. Irusta, J. Del Ser, E. Alonso, and M. Daya, "ECG-based pulse detection during cardiac arrest using random forest classifier," *Medical & Biological Engineering & Computing*, vol. 57, no. 2, pp. 453–462, Feb. 2019.

[132] J. Ruiz, E. Alonso, E. Aramendi, J. Kramer-Johansen, T. Eftestøl, U. Ayala *et al.*, "Reliable extraction of the circulation component in the thoracic impedance measured by defibrillation pads," *Resuscitation*, vol. 84, no. 10, pp. 1345–1352, Oct. 2013.

[133] E. Alonso, E. Aramendi, M. Daya, U. Irusta, B. Chicote, J. K. Russell *et al.*, "Circulation detection using the electrocardiogram and the thoracic impedance acquired by defibrillation pads," *Resuscitation*, vol. 99, pp. 56–62, 2016.

[134] A. Elola, E. Aramendi, U. Irusta, E. Alonso, Y. Lu, M. P. Chang *et al.*, "Capnography: A support tool for the detection of return of spontaneous circulation in out-of-hospital cardiac arrest," *Resuscitation*, vol. 142, pp. 153–161, 2019.

[135] Y. Alwan, Z. Cvetković, and M. J. Curtis, "Methods for Improved Discrimination Between Ventricular Fibrillation and Tachycardia," *IEEE Transactions on Biomedical Engineering*, vol. 65, no. 10, pp. 2143–2151, Oct. 2018.

[136] M. S. Link, L. C. Berkow, P. J. Kudenchuk, H. R. Halperin, E. P. Hess, V. K. Moitra *et al.*, "Part 7: adult advanced cardiovascular life support: 2015 American Heart Association guidelines update for cardiopulmonary resuscitation and emergency cardiovascular care," *Circulation*, vol. 132, no. 18_suppl_2, pp. S444–S464, 2015.

[137] T. Nordseth, D. E. Niles, T. Eftestøl, R. M. Sutton, U. Irusta, B. S. Abella *et al.*, "Rhythm characteristics and patterns of change during cardiopulmonary resuscitation for in-hospital paediatric cardiac arrest," *Resuscitation*, vol. 135, pp. 45–50, Feb. 2019.

[138] T. Nordseth, D. Bergum, D. P. Edelson, T. M. Olasveengen, T. Eftestøl, R. Wiseth *et al.*, "Clinical state transitions during advanced life support (ALS) in in-hospital cardiac arrest," *Resuscitation*, vol. 84, no. 9, pp. 1238–1244, Sep. 2013.

[139] J. T. Kvaløy, E. Skogvoll, T. Eftestøl, K. Gundersen, J. Kramer-Johansen, T. M. Olasveengen *et al.*, "Which factors influence spontaneous state transitions during resuscitation?" *Resuscitation*, vol. 80, no. 8, pp. 863–869, Aug. 2009.

[140] A. B. Rad, K. Engan, A. K. Katsaggelos, J. T. Kvaløy, L. Wik, J. Kramer-Johansen *et al.*, "Automatic cardiac rhythm interpretation during resuscitation," *Resuscitation*, vol. 102, pp. 44–50, May 2016.

[141] A. B. Rad, T. Eftestøl, K. Engan, U. Irusta, J. T. Kvaløy, J. Kramer-Johansen *et al.*, "ECG-Based Classification of Resuscitation Cardiac Rhythms for Retrospective Data Analysis," *IEEE Transactions on Biomedical Engineering*, vol. 64, no. 10, pp. 2411–2418, Oct. 2017.

[142] A. B. Rad, T. Eftestøl, U. Irusta, J. T. Kvaløy, L. Wik, J. Kramer-Johansen *et al.*, "An automatic system for the comprehensive retrospective analysis of cardiac rhythms in resuscitation episodes," *Resuscitation*, vol. 122, pp. 6–12, Jan. 2018.

[143] B. Chicote, U. Irusta, R. Alcaraz, J. J. Rieta, E. Aramendi, I. Isasi *et al.*, "Application of entropy-based features to predict defibrillation outcome in cardiac arrest," *Entropy*, vol. 18, no. 9, p. 313, 2016.

[144] B. Chicote, U. Irusta, E. Aramendi, R. Alcaraz, J. J. Rieta, I. Isasi *et al.*, "Fuzzy and sample entropies as predictors of patient survival using short ventricular fibrillation recordings during out of hospital cardiac arrest," *Entropy*, vol. 20, no. 8, p. 591, 2018.

[145] B. Chicote, E. Aramendi, U. Irusta, P. Owens, M. Daya, and A. Idris, "Value of capnography to predict defibrillation success in out-of-hospital cardiac arrest," *Resuscitation*, vol. 138, pp. 74–81, 2019.

[146] H. Zhang, Z. Yang, Z. Huang, B. Chen, L. Zhang, H. Li *et al.*, "Transthoracic impedance for the monitoring of quality of manual chest compression during cardiopulmonary resuscitation," *Resuscitation*, vol. 83, no. 10, pp. 1281–1286, 2012.

[147] D. M. González-Otero, S. R. de Gauna, J. Ruiz, M. R. Daya, L. Wik, J. K. Russell *et al.*, "Chest compression rate feedback based on transthoracic impedance," *Resuscitation*, vol. 93, pp. 82–88, 2015.

[148] E. Alonso, D. González-Otero, E. Aramendi, S. R. de Gauna, J. Ruiz, U. Ayala *et al.*, "Can thoracic impedance monitor the depth of chest compressions during out-of-hospital cardiopulmonary resuscitation?" *Resuscitation*, vol. 85, no. 5, pp. 637–643, 2014.

[149] E. Aramendi, A. Elola, E. Alonso, U. Irusta, M. Daya, J. K. Russell *et al.*, "Feasibility of the capnogram to monitor ventilation rate during cardiopulmonary resuscitation," *Resuscitation*, vol. 110, pp. 162–168, 2017.

[150] M. Risdal, S. O. Aase, M. Stavland, and T. Eftestol, "Impedance-based ventilation detection during cardiopulmonary resuscitation," *IEEE*

transactions on biomedical engineering, vol. 54, no. 12, pp. 2237–2245, 2007.

[151] J. Eilevstjønn, T. Eftestøl, S. O. Aase, H. Myklebust, J. H. Husøy, and P. A. Steen, "Feasibility of shock advice analysis during CPR through removal of CPR artefacts from the human ECG," *Resuscitation*, vol. 61, no. 2, pp. 131–141, May 2004.

[152] U. Irusta, J. Ruiz, S. R. de Gauna, T. EftestØl, and J. Kramer-Johansen, "A least mean-square filter for the estimation of the cardiopulmonary resuscitation artifact based on the frequency of the compressions," *IEEE Transactions on Biomedical Engineering*, vol. 56, no. 4, pp. 1052–1062, Jan. 2009.

[153] U. Ayala, U. Irusta, J. Ruiz, T. Eftestøl, J. Kramer-Johansen, F. Alonso-Atienza *et al.*, "A reliable method for rhythm analysis during cardiopulmonary resuscitation," *BioMed research international*, vol. 2014, 2014.

[154] G. Zhang, T. Wu, Z. Wan, Z. Song, M. Yu, D. Wang *et al.*, "A method to differentiate between ventricular fibrillation and asystole during chest compressions using artifact-corrupted ECG alone," *Computer Methods and Programs in Biomedicine*, vol. 141, pp. 111–117, Apr. 2017.

[155] E. Aramendi, U. Irusta, U. Ayala, H. Naas, J. Kramer-Johansen, and T. Eftestøl, "Filtering mechanical chest compression artefacts from out-of-hospital cardiac arrest data," *Resuscitation*, vol. 98, pp. 41–47, Jan. 2016.

[156] S. Barro, R. Ruiz, D. Cabello, and J. Mira, "Algorithmic sequential decision-making in the frequency domain for life threatening ventricular arrhythmias and imitative artefacts: a diagnostic system," *Journal of Biomedical Engineering*, vol. 11, no. 4, pp. 320–328, Jul. 1989.

[157] A. Amann, R. Tratnig, and K. Unterkofler, "Reliability of old and new ventricular fibrillation detection algorithms for automated external defibrillators," *BioMedical Engineering OnLine*, vol. 4, no. 1, p. 60, Oct. 2005.

[158] X.-S. Zhang, Y.-S. Zhu, N. V. Thakor, and Z.-Z. Wang, "Detecting ventricular tachycardia and fibrillation by complexity measure," *IEEE Transactions on Biomedical Engineering*, vol. 46, no. 5, pp. 548–555, 1999.

[159] A. Amann, R. Tratnig, and K. Unterkofler, "Detecting Ventricular Fibrillation by Time-Delay Methods," *IEEE Transactions on Biomedical Engineering*, vol. 54, no. 1, pp. 174–177, Jan. 2007.

[160] I. Jekova, "Comparison of five algorithms for the detection of ventricular fibrillation from the surface ECG," *Physiological measurement*, vol. 21, no. 4, p. 429, 2000.

[161] I. Jekova and P. Mitev, "Detection of ventricular fibrillation and tachycardia from the surface ECG by a set of parameters acquired from four methods," *Physiological Measurement*, vol. 23, no. 4, p. 629, 2002.

[162] F. Alonso-Atienza, J. L. Rojo-Álvarez, A. Rosado-Muñoz, J. J. Vinagre, A. García-Alberola, and G. Camps-Valls, "Feature selection using support vector machines and bootstrap methods for ventricular fibrillation detection," *Expert Systems with Applications*, vol. 39, no. 2, pp. 1956–1967, 2012.

[163] I. Jekova, "Shock advisory tool: Detection of life-threatening cardiac arrhythmias and shock success prediction by means of a common parameter set," *Biomedical Signal Processing and Control*, vol. 2, no. 1, pp. 25–33, Jan. 2007.

[164] U. Ayala, T. Eftestøl, E. Alonso, U. Irusta, E. Aramendi, S. Wali *et al.*, "Automatic detection of chest compressions for the assessment of CPR-quality parameters," *Resuscitation*, vol. 85, no. 7, pp. 957–963, Jul. 2014.

[165] V. X. Afonso and W. J. Tompkins, "Detecting ventricular fibrillation," *IEEE Engineering in Medicine and Biology Magazine*, vol. 14, no. 2, pp. 152–159, 1995.

[166] R. Clayton and A. Murray, "Linear and non-linear analysis of the surface electrocardiogram during human ventricular fibrillation shows evidence of order in the underlying mechanism," *Medical & Biological Engineering & Computing*, vol. 37, no. 3, pp. 354–358, 1999.

[167] A. Al-Fahoum and I. Howitt, "Combined wavelet transformation and radial basis neural networks for classifying life-threatening cardiac arrhythmias," *Medical & biological engineering & computing*, vol. 37, no. 5, pp. 566–573, 1999.

[168] H. Huang, H. Xie, and Z. Wang, "The analysis of vf and vt with wavelet-based tsallis information measure," *Physics Letters A*, vol. 336, no. 2-3, pp. 180–187, 2005.

[169] Y. Sun, K. L. Chan, and S. M. Krishnan, "Life-threatening ventricular arrhythmia recognition by nonlinear descriptor," *BioMedical Engineering OnLine*, vol. 4, no. 1, p. 6, 2005.

[170] M. A. Arafat, J. Sieed, and M. K. Hasan, "Detection of ventricular fibrillation using empirical mode decomposition and bayes decision theory," *Computers in Biology and Medicine*, vol. 39, no. 11, pp. 1051–1057, 2009.

[171] L. Glass, "Dynamics of cardiac arrhythmias." *Physics Today*, vol. 49, no. 8, pp. 40–45, 1996.

[172] A. Amann, R. Tratnig, and K. Unterkofler, "Detecting ventricular fibrillation by time-delay methods," *IEEE Transactions on Biomedical Engineering*, vol. 54, no. 1, pp. 174–177, 2006.

[173] M. Roopaei, R. Boostani, R. R. Sarvestani, M. A. Taghavi, and Z. Azimifar, "Chaotic based reconstructed phase space features for detecting ventricular fibrillation," *Biomedical Signal Processing and Control*, vol. 5, no. 4, pp. 318–327, 2010.

[174] S.-H. Lee, "Development of ventricular fibrillation diagnosis method based on neuro-fuzzy systems for automated external defibrillators," *International Journal of Fuzzy Systems*, vol. 19, no. 2, pp. 440–451, 2017.

[175] M. I. Owis, A. H. Abou-Zied, A.-B. Youssef, and Y. M. Kadah, "Study of features based on nonlinear dynamical modeling in ECG arrhythmia detection and classification," *IEEE transactions on Biomedical Engineering*, vol. 49, no. 7, pp. 733–736, 2002.

[176] M. Small, D. Yu, J. Simonotto, R. G. Harrison, N. Grubb, and K. Fox, "Uncovering non-linear structure in human ecg recordings," *Chaos, Solitons & Fractals*, vol. 13, no. 8, pp. 1755–1762, 2002.

[177] H. Hai, X. Hongbo, and W. Zhizhong, "Discrimination of VF and VT with method of detrended fluctuation analysis," in *2004 International Conference on Intelligent Mechatronics and Automation, 2004. Proceedings.* IEEE, 2004, pp. 881–884.

[178] K. Chua, V. Chandran, U. Acharya, and C. Lim, "Computer-based analysis of cardiac state using entropies, recurrence plots and poincare geometry," *Journal of Medical Engineering & Technology*, vol. 32, no. 4, pp. 263–272, 2008.

[179] S.-H. Lee, K.-Y. Chung, and J. S. Lim, "Detection of ventricular fibrillation using Hilbert transforms, phase-space reconstruction, and time-domain analysis," *Personal and ubiquitous computing*, vol. 18, no. 6, pp. 1315–1324, 2014.

[180] S. C. Schuckers, "Approximate entropy as a measure of morphologic variability for ventricular tachycardia and fibrillation," in *Computers in Cardiology 1998. Vol. 25 (Cat. No. 98CH36292).* IEEE, 1998, pp.

265–268.

[181] S. C. Schuckers and P. Raphisak, "Distinction of arrhythmias with the use of approximate entropy," in *Computers in Cardiology 1999. Vol. 26 (Cat. No. 99CH37004)*.   IEEE, 1999, pp. 347–350.

[182] H. Li, W. Han, C. Hu, and M. Q.-H. Meng, "Detecting ventricular fibrillation by fast algorithm of dynamic sample entropy," in *2009 IEEE International Conference on Robotics and Biomimetics (ROBIO)*. IEEE, 2009, pp. 1105–1110.

[183] H.-B. Xie, G. Zhong-Mei, and H. Liu, "Classification of ventricular tachycardia and fibrillation using fuzzy similarity-based approximate entropy," *Expert Systems with Applications*, vol. 38, no. 4, pp. 3973–3981, 2011.

[184] D.-R. Kong and H.-B. Xie, "Use of modified sample entropy measurement to classify ventricular tachycardia and fibrillation," *Measurement*, vol. 44, no. 4, pp. 653–662, 2011.

[185] A. Rosado-Muñoz, G. Camps-Valls, J. Guerrero-Martínez, J. Francés-Villora, J. Muñoz-Marí, and A. Serrano-López, "Enhancing feature extraction for VF detection using data mining techniques," in *Computers in Cardiology*.   IEEE, 2002, pp. 209–212.

[186] Q. Li, C. Rajagopalan, and G. D. Clifford, "Ventricular Fibrillation and Tachycardia Classification Using a Machine Learning Approach," *IEEE Transactions on Biomedical Engineering*, vol. 61, no. 6, pp. 1607–1613, Jun. 2014.

[187] M. T. Nguyen, A. Shahzad, B. Van Nguyen, and K. Kim, "Diagnosis of shockable rhythms for automated external defibrillators using a reliable support vector machine classifier," *Biomedical Signal Processing and Control*, vol. 44, pp. 258–269, 2018.

[188] M. Sharma, S. Singh, A. Kumar, R. San Tan, and U. R. Acharya, "Automated detection of shockable and non-shockable arrhythmia using novel wavelet-based ECG features," *Computers in Biology and Medicine*, vol. 115, p. 103446, 2019.

[189] R. Clayton, A. Murray, and R. Campbell, "Recognition of ventricular fibrillation using neural networks," *Medical and Biological Engineering and Computing*, vol. 32, no. 2, pp. 217–220, 1994.

[190] J. Pardey, "Detection of ventricular fibrillation by sequential hypothesis testing of binary sequences," in *2007 Computers in Cardiology*.   IEEE, 2007, pp. 573–576.

[191] Y. Alwan, Z. Cvetković, and M. Curtis, "Structured prediction for differentiating between normal rhythms, ventricular tachycardia, and ventricular fibrillation in the ECG," in *2015 37th Annual International Conference of the IEEE Engineering in Medicine and Biology Society (EMBC)*.   IEEE, 2015, pp. 310–314.

[192] M. Sharma, R.-S. Tan, and U. R. Acharya, "Detection of shockable ventricular arrhythmia using optimal orthogonal wavelet filters," *Neural Computing and Applications*, pp. 1–16, 2019.

[193] I. Isasi, U. Irusta, E. Aramendi, J. Age, and L. Wik, "Characterization of the ECG compression artefact caused by the AutoPulse device," *Resuscitation*, vol. 118, p. e38, Sep. 2017.

[194] A. Langhelle, T. Eftestøl, H. Myklebust, M. Eriksen, B. Terje Holten, and P. Andreas Steen, "Reducing CPR artefacts in ventricular fibrillation in vitro," *Resuscitation*, vol. 48, no. 3, pp. 279–291, Mar. 2001.

[195] E. Fitzgibbon, R. Berger, J. Tsitlik, and H. R. Halperin, "Determination of the noise source in the electrocardiogram during cardiopulmonary resuscitation," *Critical Care Medicine*, vol. 30, no. 4, p. S148, Apr. 2002.

[196] S. Ruiz de Gauna, U. Irusta, J. Ruiz, U. Ayala, E. Aramendi, and T. Eftestøl, "Rhythm analysis during cardiopulmonary resuscitation: past, present, and future," *BioMed Research International*, vol. 2014, 2014.

[197] Y. Li, J. Bisera, F. Geheb, W. Tang, and M. H. Weil, "Identifying potentially shockable rhythms without interrupting cardiopulmonary resuscitation," *Critical Care Medicine*, vol. 36, no. 1, pp. 198–203, Jan. 2008.

[198] V. Krasteva, I. Jekova, I. Dotsinsky, and J.-P. Didon, "Shock Advisory System for Heart Rhythm Analysis During Cardiopulmonary Resuscitation Using a Single ECG Input of Automated External Defibrillators," *Annals of Biomedical Engineering*, vol. 38, no. 4, pp. 1326–1336, Apr. 2010.

[199] M. Noc, M. H. Weil, W. Tang, S. Sun, A. Pernat, and J. Bisera, "Electrocardiographic prediction of the success of cardiac resuscitation," *Critical Care Medicine*, vol. 27, no. 4, pp. 708–714, 1999.

[200] H.-U. Strohmenger, K. H. Lindner, A. Keller, I. M. Lindner, and E. G. Pfenninger, "Spectral analysis of ventricular fibrillation and closed-chest cardiopulmonary resuscitation," *Resuscitation*, vol. 33, no. 2, pp. 155–161, 1996.

[201] S. Aase, T. Eftestøl, J. Husoy, K. Sunde, and P. Steen, "CPR artifact removal from human ECG using optimal multichannel filtering," *IEEE Transactions on Biomedical Engineering*, vol. 47, no. 11, pp. 1440–1449, Nov. 2000.

[202] S. R. de Gauna, J. Ruiz, U. Irusta, and U. Ayala, "Filtering the cardiopulmonary resuscitation artifact: influence of the signal-to-noise-ratio on the accuracy of the shock advice algorithm," in *2010 Computing in Cardiology*. IEEE, 2010, pp. 681–684.

[203] J. Husoy, J. Eilevstjonn, T. Eftestøl, S. Aase, H. Myklebust, and P. Steen, "Removal of cardiopulmonary resuscitation artifacts from human ECG using an efficient matching pursuit-like algorithm," *IEEE Transactions on Biomedical Engineering*, vol. 49, no. 11, pp. 1287–1298, Nov. 2002.

[204] E. Aramendi, S. R. de Gauna, U. Irusta, J. Ruiz, M. F. Arcocha, and J. M. Ormaetxe, "Detection of ventricular fibrillation in the presence of cardiopulmonary resuscitation artefacts," *Resuscitation*, vol. 72, no. 1, pp. 115–123, Jan. 2007.

[205] A. Amann, A. Klotz, T. Niederklapfer, A. Kupferthaler, T. Werther, M. Granegger *et al.*, "Reduction of CPR artifacts in the ventricular fibrillation ECG by coherent line removal," *BioMedical Engineering OnLine*, vol. 9, no. 1, p. 2, Jan. 2010.

[206] J. Ruiz, U. Irusta, S. Ruiz de Gauna, and T. Eftestøl, "Cardiopulmonary resuscitation artefact suppression using a Kalman filter and the frequency of chest compressions as the reference signal," *Resuscitation*, vol. 81, no. 9, pp. 1087–1094, Sep. 2010.

[207] E. Aramendi, U. Ayala, U. Irusta, E. Alonso, T. Eftestøl, and J. Kramer-Johansen, "Suppression of the cardiopulmonary resuscitation artefacts using the instantaneous chest compression rate extracted from the thoracic impedance," *Resuscitation*, vol. 83, no. 6, pp. 692–698, Jun. 2012.

A | PUBLISHED PAPERS

A.1 Publications associated to objective 1

A.1.1 First conference paper: C1$_1$

Table A.1. Conference paper associated to objective 1.

Publication in international conference
Reference: I. Isasi, U. Irusta, E. Aramendi, U.Ayala, E. Alonso, J. Kramer-Johansen, T. Eftestøl,"Removing piston-driven mechanical chest compression artefacts from the ECG", *Proceedings of the Conference IEEE Computing in Cardiology 2017*, vol.44, pp. 1-4.
Quality indices: • **Type of publication**: Indexed Congress in SJR • **Area**: Cardiology and Cardiovascular Medicine • **SJR factor**: 0.191

Removing Piston-driven Mechanical Chest Compression Artefacts from the ECG

Iraia Isasi[1], Unai Irusta[1], Elisabete Aramendi[1], Unai Ayala[2], Erik Alonso[3], Jo Kramer-Johansen[4], Trygve Eftestøl[5]

[1] Communications Engineering, University of the Basque Country (UPV/EHU), Bilbao, Spain
[2] Signal Processing and Communications, Mondragon University, Mondragon, Spain
[3] Department of Applied Mathematics, University of the Basque Country (UPV/EHU), Bilbao, Spain
[4] Norwegian National Advisory Unit on Prehospital Emergency Medicine,
Oslo University Hospital and University of Oslo, Norway
[5] Electrical Engineering and Computer Science. University of Stavanger, Stavanger, Norway

Abstract

Piston-driven mechanical chest compression (CC) devices induce a quasi-periodic artefact in the ECG, making rhythm diagnosis unreliable. Data from 230 out-of-hospital cardiac arrest (OHCA) patients were collected in which CCs were delivered using the piston driven LUCAS-2 device. Underlying rhythms were annotated by expert reviewers in artefact-free intervals. Two artefact removal methods (filters) were introduced: a static solution based on Goertzel's algorithm, and an adaptive solution based on a Recursive Least Squares (RLS) filter. The filtered ECG was diagnosed by a shock/no-shock decision algorithm used in a commercial defibrillator and compared with the rhythm annotations. Filter performance was evaluated in terms of balanced accuracy (BAC), the mean of sensitivity (shockable) and specificity (nonshockable). Compared to the unfiltered signal, the static filter increased BAC by 20 points, and the RLS filter by 25 points. Adaptive filtering results in 99.0% sensitivity and 87.3% specificity.

1. Introduction

Early defibrillation and high-quality cardiopulmonary resuscitation (CPR) are crucial to improve chances of survival from out of hospital cardiac arrest (OHCA) [1]. Chest compressions (CCs) provided during CPR introduce artefacts in the ECG, invalidating the diagnosis of any rhythm analysis algorithm. Currently compressions are interrupted for the analysis, but these hands-off intervals compromise circulation and thus reduce the probability of restoration of spontaneous circulation (ROSC) and survival [2]. Although solutions to analyse the rhythm

during pauses in CC exist [3, 4], rhythm analysis during CCs requires a filter to remove CC artefacts. Many such filters have been proposed to permit a reliable diagnosis during CCs [5, 6], but no effective solution has been integrated into current defibrillators yet.

Piston-driven mechanical CC devices are increasingly used in resuscitation. These devices deliver CCs with a constant rate and depth ensuring CPR is delivered according to resuscitation guidelines. Their use is especially recommended during transportation, invasive procedures or prolonged CPR. One such device is the LUCAS 2 (Physio-Control/Jolife AB, Lund, Sweden). The LUCAS 2 provides chest compressions in a fixed position, constant depth (40-53 mm depending on chest height), constant rate ($102 \pm 2 \, \mathrm{min}^{-1}$, 1.694 Hz), 50% duty-cycle and full chest recoil after each compression [7]. We should expect the artefact caused by LUCAS 2 to have a periodical pattern at the constant frequency of the CCs.

This study evaluates the feasibility of analyzing the rhythm during mechanical CCs provided by LUCAS 2 on OHCA data. Two artefact removal alternatives were compared: an adaptive filtering method based on a Recursive Least Square (RLS) algorithm and a non-adaptive (static) filtering method which uses Goertzel's algorithm to model the artefact.

2. Materials and methods

2.1. Materials

The data used for this study were gathered by the emergency services of Oslo and Akershus (Norway) with the LifePak 15 defibrillators (Physio-Control Inc., Redmond, WA, USA). The recorded ECG and thoracic
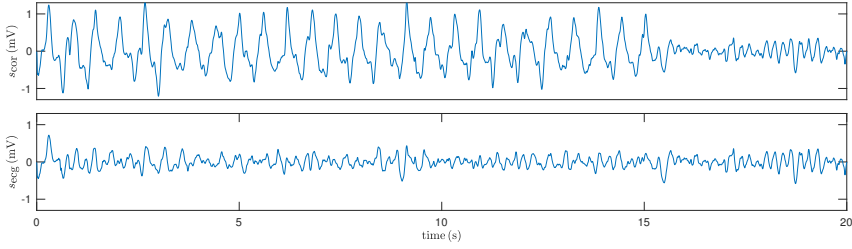
Figure 1. A 20 s episode of a patient in ventricular fibrillation (VF), before filtering (top) and after filtering (bottom). The initial 15 s show ECG records during CCs delivered by the LUCAS 2 (quasi-periodic artefact). The last 5 s show the underlying VF, in an interval without CCs. Filtering (bottom pannel) reveals the underlying rhythm.

impedance (TI) signals were exported to Matlab using the Codestat (Physio-Control Inc.) research tool, and resampled to 250 Hz. Details on the dataset are further described in [7].

The dataset contains 1045 segments of 20 s from 230 patients. The first 15 s included continuous CCs, the last 5 s were free of artefacts and were used by expert reviewers to assess the underlying rhythm. The dataset contains 201 shockable and 844 nonshockable rhythms (270 asystole, 574 organized) [7].

2.2. Methods

ECG segments were band-pass filtered to a typical automatic external defibrillator (AED) bandwidth, using an order 8 Butterworth filter (0.5-40 Hz).

Model of the compression artefact

The CC artefact in the ECG is customarily modelled as additive noise:

$$s_{\mathrm{cor}}(n) = s_{\mathrm{ecg}}(n) + s_{\mathrm{cc}}(n) \tag{1}$$

where s_{cor} is the ECG corrupted by the CC artefact, s_{cc}, and s_{ecg} is the ECG which reflects the underlying heart rhythm. For a piston-driven compression device the artefact, s_{cc}, can be approximated by a (quasi)-periodic signal in term of N harmonics of the fundamental frequency, $f_0 = 1.694$ Hz. Assuming a model with N Fourier coefficients $c_k = |c_k|e^{j\theta_k}$, the artefact can be simply written as:

$$s_{\mathrm{cc}}(n) = A(n) \sum_{k=1}^{N} |c_k| \cos(k\omega_0 n T_s + \theta_k) = \tag{2}$$

$$= A(n) \sum_{k=1}^{N} a_k \cos(k\omega_0 n T_s) + b_k \sin(k\omega_0 n T_s) \tag{3}$$

where T_s is the sampling period, $\omega_0 = 2\pi f_0$ and $A(n)$ is an amplitude envelope to differentiate intervals with ($A = 1$) and without compressions ($A = 0$).

The two methods proposed in this paper assume different natures for the Fourier coefficients. In the static solution, $c_k = |c_k|e^{j\theta_k}$ are constant over time. In the adaptive solution the coefficients are assumed to be time-varying $c_k(n) = |c_k(n)|e^{j\theta_k(n)}$, with small changes every sample. Once s_{cc} is estimated, the underlying rhythm s_{ecg} is obtained by subtraction using equation (1), and then fed to a shock/no-shock decision algorithm for diagnosis.

Static solution

The static solution assumes the N Fourier coefficients are constant. Since only just a few frequency components of s_{cor} signal are of interest, Goertzel's algorithm can be used to estimate those spectral components instead of analyzing all frequency components of the Discrete-Time Fourier Transform (DTFT). However, since for an L point signal the frequency resolution of Goertzel's algorithm is $\Delta f = f_s/L$, the fundamental frequency of the signal must be an integer multiple of Δf. This is not the case for $f_0 = 1.694$ Hz (LUCAS 2), so, the Generalized Goertzel algorithm was used. This generalization allows the calculation of spectral components at any frequency, by extending the DTFT to any real frequency $\omega_\ell = 2\pi\ell/L$. Then the frequency component is estimated as:

$$X(\omega_\ell) = e^{-j2\pi\ell} \sum_{n=0}^{L-1} x(n) e^{-j2\pi\ell \frac{n-L}{L}} \tag{4}$$

to which the custom Goertzel's algorithm is applied [8]:

$$s(n) = x(n) + 2\cos\left(\frac{2\pi\ell}{N}\right)s(n-1) - s(n-2) \tag{5}$$

$$y(n) = \left(s(n) - e^{-j\frac{2\pi\ell}{N}}s(n-1)\right)e^{-j2\pi\ell} \tag{6}$$

and $y(L-1) = X(\omega_\ell)$. In our case the signal was first windowed using a Kaiser window $w_\beta(n)$, to form

Page 2

$x_w(n) = s_{cor}(n) \cdot w_\beta(n)$, so the spectral component was obtained as:

$$c_k = \frac{2}{W_\beta(0)} X_w(\omega_\ell), \quad \ell \in \mathbb{R} \quad (7)$$

where W_β is the Fourier transform of the Kaiser window, and $X_w(\omega_\ell)$ is the Fourier transform of $x_w(n)$ as shown in equation (4) and computed using Goertzel's algorithm. In the Kaiser window the form factor β controls the window trade-off between side-lobe level and main-lobe width. For each segment, the c_k coefficients were estimated using an interval of 5 s with uninterrupted CCs.

Adaptive solution

In the adaptive solution the time-varying Fourier coefficients, $a_k(n)$, $b_k(n)$, were estimated using an RLS filter that tracks the spectral components of the artefact [9].

The in-phase, $a_k(n)$, and quadrature, $b_k(n)$, components model the artefact as described by equation (8), which is equation (3) in vector notation:

$$s_{cc}(n) = \Theta_{n-1}^T \Phi_n \quad (8)$$

where,

$$\Theta_n = [a_1(n)\, b_1(n)\, \ldots\, a_N(n)\, b_N(n)]^T \quad (9)$$
$$\Phi_n = [\cos(\omega_0 n T_s)\, \sin(\omega_0 n T_s)\, \ldots$$
$$\cos(N\omega_0 n T_s)\, \sin(N\omega_0 n T_s)]^T \quad (10)$$

The model of the artefact is updated through the $a_k(n)$ and $b_k(n)$ coefficients in each iteration. The filtered s_{ecg} and the filter coefficients are computed as follows:

$$s_{ecg}(n) = s_{cor}(n) - s_{cc}(n) \quad (11)$$
$$\Theta_n = \Theta_{n-1} + F_n \Phi_n s_{ecg}(n) \quad (12)$$
$$F_n = \frac{1}{\lambda}\left[F_{n-1} - \frac{F_{n-1}\Phi_n \Phi_n^T F_{n-1}}{\lambda + \Phi_n^T F_{n-1}\Phi_n} \right] \quad (13)$$

where the forgetting factor λ is usually close to one, and defines the convergence rate, the tracking power, misadjustement and stability of the RLS filter.

2.3. Evaluation

The ECG filtered through both methods was diagnosed by a shock/no-shock decision algorithm, the Matlab version of the algorithm designed for the Reanibex R-series defibrillators (Bexen Cardio, Ermua, Spain). This algorithm diagnoses the ECG in less than 9.6 s by analyzing 2 or 3 consecutive 3.2 s intervals of the ECG [10]. The interval from 3.4 s to 13 s of

each segment was diagnosed in order to avoid filtering transients. The diagnoses were compared with the rhythm annotations to obtain the proportion of correctly classified shockable (sensitivity, SE) and nonshockable (specificity, SP) rhythms.

Filter performance was evaluated in terms of the balanced accuracy (BAC), BAC = 0.5(SE + SP), within the following working ranges: $10 < N < 30$ and $0 < \beta < 15$ for the static filter, and $10 < N < 30$ and $0.965 < \lambda < 0.999$ for the adaptive filter. Finally, within those ranges a 100 bootstrapped patient-wise 5-fold cross validation approach was used to obtain an estimate of the statistical distribution of SE and SP. SE/SP values will be reported as mean (CI, 95% confidence interval).

3. Results

Figure 2 shows the BAC for the static (left) and adaptive (right) filters within the working ranges for three significant values of N. As seen in figure 2, both filters showed a working range in which the performance was close to optimal in terms of BAC. In the case of the static filter, the best results were obtained for $4 < \beta < 5$ and $N > 20$. The range for the RLS filter was $0.989 < \lambda < 0.993$ and $N > 20$. In fact, for smaller values of N (see figure 2) the BAC in the optimal β and λ ranges is smaller in both cases.

Table 1 shows the bootstraped SE/SP and BAC after filtering, compared to the values obtained before filtering.

	unfilt	Goertzel	RLS
SE (%)	50.7	97.0 (95.5–97.5)	99.0 (97.0–99.5)
SP (%)	83.9	80.2 (79.5–81.0)	87.3 (86.5–87.6)
BAC (%)	67.3	88.6 (87.8–89.3)	93.0 (91.9–93.5)

Table 1. Accuracy before and after filtering.

Both filters resulted in an increase of over 30 points in SE with a slight change in SP. The shock/no-shock decision after applying the adaptive filter were more accurate than those obtained after applying the static filter.

4. Discussion

This study introduces two different filtering techniques to remove CPR artefact from the ECG during mechanical compressions. Both methods represent the artefact as a (quasi)-periodic signal with a fundamental frequency equal to the frequency of the compressions and N harmonics. Whereas the static method assumes that the artefact is periodic, the adaptive method considers slow fluctuations from cycle to cycle.

Mechanically delivered compressions have very stable frequency, depth and duty cycle. We might assume little

Page 3
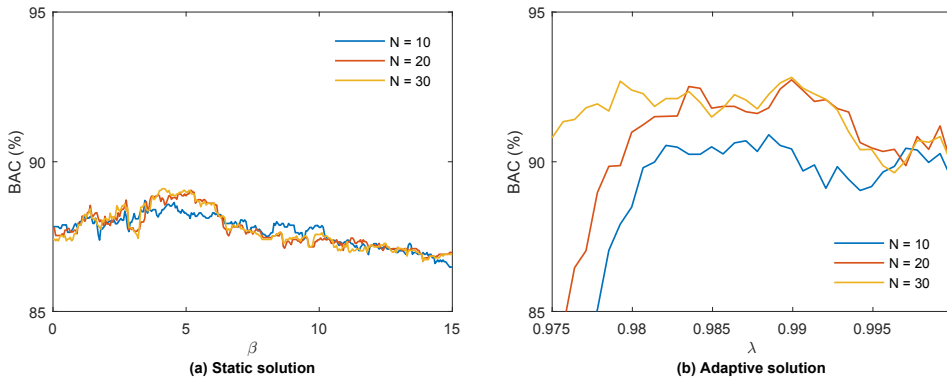
Figure 2. Performance of the static and the adaptive filtering methods in terms of N and β for the Goertzel filter (panel a), and in terms of N and λ for the RLS filter (panel b).

change in the artefact from CC cycle to cycle, but the results of this study show the need of an adaptive solution. Both methods resulted in a significant increase in BAC but the RLS filter produced better results than the static solution (approximately 2 points more in SE and 7 points more in SP). The adaptive solution was able to track the small fluctuations of the artefact from cycle to cycle.

In conclusion, the results showed that the adaptive filtering provided acceptable values for an acccurate rhythm diagnosis during compressions, particularly for shockable rhythms (SE>98%). However, further analysis is recommended to increase the accuracy, mainly, for nonshockable rhythms. The results reported in this and in previous studies [7] are still below the 95% recommended for nonshockable rhythms by the American Heart Association.

Acknowledgements

References

[1] Perkins GD, et al. European resuscitation council guidelines for resuscitation 2015: Section 2. adult basic life support and automated external defibrillation 2015;.

[2] Eftestøl T, Sunde K, Steen PA. Effects of interrupting precordial compressions on the calculated probability of defibrillation success during out-of-hospital cardiac arrest. Circulation 2002;105(19):2270–2273.

[3] Ruiz J, Ayala U, de Gauna SR, Irusta U, González-Otero D, Alonso E, Kramer-Johansen J, Eftestøl T. Feasibility of automated rhythm assessment in chest compression pauses during cardiopulmonary resuscitation. Resuscitation 2013; 84(9):1223–1228.

[4] Ayala U, Irusta U, Ruiz J, de Gauna SR, González-Otero D, Alonso E, Kramer-Johansen J, Naas H, Eftestøl T. Fully automatic rhythm analysis during chest compression pauses. Resuscitation 2015;89:25–30.

[5] Irusta U, Ruiz J, de Gauna SR, Eftestøl T, Kramer-Johansen J. A least mean-square filter for the estimation of the cardiopulmonary resuscitation artifact based on the frequency of the compressions. IEEE Transactions on Biomedical Engineering 2009;56(4):1052–1062.

[6] Gong Y, Gao P, Wei L, Dai C, Zhang L, Li Y. An enhanced adaptive filtering method for suppressing cardiopulmonary resuscitation artifact. IEEE Transactions on Biomedical Engineering 2016;.

[7] Aramendi E, Irusta U, Ayala U, Naas H, Kramer-Johansen J, Eftestøl T. Filtering mechanical chest compression artefacts from out-of-hospital cardiac arrest data. Resuscitation 2016;98:41–47.

[8] Sysel P, Rajmic P. Goertzel algorithm generalized to non-integer multiples of fundamental frequency. EURASIP Journal on Advances in Signal Processing 2012;2012(1):56.

[9] Xiao Y, Ma L, Ward RK. Fast RLS fourier analyzers capable of accommodating frequency mismatch. Signal Processing 2007;87(9):2197–2212.

[10] Irusta U, Ruiz J, Aramendi E, de Gauna SR, Ayala U, Alonso E. A high-temporal resolution algorithm to discriminate shockable from nonshockable rhythms in adults and children. Resuscitation 2012;83(9):1090–1097.

Address for correspondence:

Name: Iraia Isasi Liñero
Full postal address: Alda Urquijo s/n, 48013,Bilbao,Spain
E-mail address: iraia.isasi@ehu.eus

Page 4

A.1.2 FIRST JOURNAL PAPER: J1₁

Table A.2. Journal paper associated to objective 1.

Publication in international magazine
Reference — I. Isasi, U. Irusta, E. Aramendi, U.Ayala, E. Alonso, J. Kramer-Johansen, T. Eftestøl,"A Multistage Algorithm for ECG Rhythm Analysis During Piston-Driven Mechanical Chest Compressions", *IEEE Transactions on Biomedical Engineering*, vol. 48, no. 3, pp. 279-291, 2019.

Quality indices

- **Type of publication:** Journal paper idexed in JCR and SJR
- **Area:** Biomedical Engineering
- **Ranking:** 14/87 (Q1) based on JCR 2019
- **Impact factor SJR:** 1.410
- **Impact factor JCR:** 4.424

A Multistage Algorithm for ECG Rhythm Analysis During Piston-Driven Mechanical Chest Compressions

Iraia Isasi , Unai Irusta , *Member, IEEE*, Elisabete Aramendi, Unai Ayala , Erik Alonso , Jo Kramer-Johansen , and Trygve Eftestøl, *Member, IEEE*

Abstract—Goal: An accurate rhythm analysis during cardiopulmonary resuscitation (CPR) would contribute to increase the survival from out-of-hospital cardiac arrest. Piston-driven mechanical compression devices are frequently used to deliver CPR. The objective of this paper was to design a method to accurately diagnose the rhythm during compressions delivered by a piston-driven device. *Methods:* Data was gathered from 230 out-of-hospital cardiac arrest patients treated with the LUCAS 2 mechanical CPR device. The dataset comprised 201 shockable and 844 nonshockable ECG segments, whereof 270 were asystole (AS) and 574 organized rhythm (OR). A multistage algorithm (MSA) was designed, which included two artifact filters based on a recursive least squares algorithm, a rhythm analysis algorithm from a commercial defibrillator, and an ECG-slope-based rhythm classifier. Data was partitioned randomly and patient-wise into training (60%) and test (40%) for optimization and validation, and statistically meaningful results were obtained repeating the process 500 times. *Results:* The mean (standard deviation) sensitivity (SE) for shockable rhythms, specificity (SP) for nonshockable rhythms, and the total accuracy of the MSA solution were: 91.7 (6.0), 98.1 (1.1), and 96.9 (0.9), respectively. The SP for AS and OR were 98.0 (1.7) and 98.1 (1.4), respectively. *Conclusions:* The SE/SP were above the 90%/95% values recommended by the American Heart Association for shockable and nonshockable rhythms other than sinus rhythm, respectively. *Significance:* It is possible to accurately diagnose the rhythm during mechanical chest compressions and the results considerably improve those obtained by previous algorithms.

Index Terms—Artifact suppression, cardiac arrest, cardiopulmonary resuscitation (CPR), electrocardiogram (ECG), mechanical chest compressions, piston-driven compressions, recursive least squares (RLS).

I. INTRODUCTION

EARLY electrical defibrillation and high-quality chest compressions during cardiopulmonary resuscitation (CPR) are key for the outcome of out-of-hospital cardiac arrest patients [1]. Current treatment guidelines for cardiac arrest highlight the importance of minimizing interruptions in compressions during CPR [1]. However, for a reliable shock/no-shock decision, current defibrillators require interrupting compressions to avoid artifacts in the ECG. An accurate shock/no-shock decision during CPR would improve therapy in two ways. For nonshockable rhythms it would do away with unnecessary interruptions in CPR to check the rhythm. These interruptions, which compromise coronary perfusion pressure, worsen chest compression fraction and may result in decreased survival [2]. For ventricular fibrillation (VF) it would contribute to a quicker identification of the need to shock the patient, which is important given the high oxygen demands of VF [3].

Strategies to allow an accurate shock/no-shock decision without interrupting CPR therapy include analyzing the rhythm during pauses in compressions for ventilation, and using signal processing techniques to allow a reliable shock/no-shock decision during compressions. Pauses in compressions for ventilations occur approximately every 20 s in 30:2 CPR, and an accurate rhythm analysis during those pauses has already been demonstrated [4], [5]. However, those techniques are inapplicable to compression only CPR.

Solutions based on digital signal processing for a reliable shock/no-shock decision during compressions have followed two main approaches [6]: the design of adaptive filters to suppress the artifact followed by a defibrillator's shock/no-shock decision algorithm, and shock/no-shock decision algorithms based on robust ECG features minimally affected by the artifact. Adaptive filters address the spectral overlap between

resuscitation cardiac rhythms and compression artifacts, and the time-varying spectral characteristics of the artifact. However, these filters require additional reference signals correlated to the artifact like compression force [7], thoracic impedance [8] or blood pressure [9]. Several solutions based on these signals have been developed including Wiener filters [10], recursive adaptive matching pursuit algorithms [11], [12] or Kalman state-space models [13]. Given the quasi-periodic nature of CPR artifacts, adaptive solutions to estimate a time-varying Fourier series model of the artifact have also been proposed, including Least Mean Squares (LMS) [14]–[16] or Kalman [17] solutions. Filtering schemes that use only the ECG to both characterize and remove the artifact include approaches based on coherent line removal [18], LMS [19] and Kalman filters [20].

Finally, two types of algorithms based on robust ECG-features have been proposed to classify the ECG during CPR: features computed without filtering like the morphological consistency algorithm [21], [22] and adaptive rhythm sequencing [23], or after filtering the artifact [24], [25]. Despite progress, current solutions do not allow a reliable rhythm analysis during CPR [6], either because filtering residuals may resemble VF in patients in asystole (AS), or because spiky residuals are interpreted as the QRS complexes of organized rhythms (OR) in patients in VF [15], [16].

In all of these studies artifacts originate from manual compressions delivered by rescuers. Mechanical compression devices are increasingly used in resuscitation although evidences of improved survival are not conclusive [26], [27], and have become popular in scenarios such as transportation, invasive-procedures or prolonged CPR [28]–[31]. Mechanical devices deliver compressions at a constant rate and depth in adherence with current resuscitation guidelines. There are two types of automated compressors available: pneumatically driven pistons like the LUCAS 2 (Physio-Control Inc/Jolife AB, Lund, Sweeden), and load distributing bands like the Auto Pulse (Zoll Circulation, Chelmsford, Massachusetts, USA) [32]. Preliminary attempts to remove the LUCAS 2 artifact with simple comb filters were promising on a limited dataset [33], even though filtering was later shown to be as challenging as for manual CPR artifacts when tested on a more comprehensive dataset [34]. Although mechanical CPR artifacts have a fixed frequency, they present larger amplitudes, significant filtering residuals, and many harmonics that make filtering the artifact challenging [34].

This study introduces a new method for a reliable shock/no-shock decision during piston-driven mechanical compressions. The approach uses two recursive least-squares (RLS) filters to reduce CPR artifacts, followed by three shock/no-shock decision stages based on a standard defibrillator algorithm and on an ECG-slope decision stage. The complete solution is therefore named multistage algorithm (MSA). The manuscript is organized as follows: Section II describes the study dataset; Section III introduces the time-varying Fourier series model of the artifact, an algorithm to estimate the order of the model, and the adaptive filter to track the time-varying Fourier coefficients; Section IV describes the building blocks and the general architecture of the MSA solution; Section V describes the performance metrics, data partition and optimization/test

procedures; and the results, conclusions and discussion are presented in Sections VI to VIII.

II. DATA COLLECTION AND PREPARATION

Data from 263 out-of-hospital cardiac arrest patients treated with the LUCAS 2 piston-driven chest compression device (Physio-Control Inc., Redmond, WA, USA) were reviewed. The cardiac arrest episodes were collected by the advanced life support responders of the emergency services of Oslo and Akershus (Norway) during 18 months in 2012 and 2013. Responders used Physio-Control's Lifepack 15 defibrillators that continuously record the ECG and impedance signals. The LUCAS 2 device delivers compressions in a fixed position, with constant depth (40–53 mm depending on chest height), at a constant rate (102 ± 2 min^{-1}), with a 50% duty cycle, and allowing full chest recoil after each compression [35].

Anonymized data from the defibrillators was exported to Matlab (MathWorks Inc., Naick, MA) using Physio-Control's Code Stat data review software, and resampled to a sampling frequency of 250 Hz. The data included the ECG and impedance signals of each episode together with the compression instants detected by the Code Stat software.

The start of use of the LUCAS-2 device was marked when the compression rate stabilized at the device's fixed rate of 102 min^{-1} [34]. Then, 20 s signal segments with the same underlying rhythm were extracted during the device usage. The segments contained an initial 15 s interval during compressions to develop and evaluate our solution for the shock/no-shock decision during chest compressions, followed by a 5 s interval without compression artifacts to annotate the patient's rhythm. Fig. 1 shows two examples. Ground truth rhythm labels were adjudicated by consensus among two independent reviewers, a clinical researcher and a biomedical engineer, both specialized in resuscitation data science [34]. The rhythm annotators, who were not involved in the conception and development of the methods, examined the 5 s interval without artifacts (see Fig. 1) to annotate the rhythms. Segments were annotated as: VF and ventricular tachycardia (VT) in the shockable rhythm category, and OR and AS in the nonshockable category. Presence of pulse could not annotated because patient charts with clinical pulse annotations and/or capnography levels were not available. So the OR category includes both pulseless electrical activity and pulsed rhythms. Intermediate rhythms like fine VF (amplitude< 200 μV) were discarded. The American Heart Association (AHA) does not establish a shock/no-shock recommendation for intermediate rhythms because the benefits of defibrillation are unclear for those rhythms [36].

The final annotated dataset consisted of 1045 segments from 230 patients, segments like the two examples shown in Fig. 1. There were 201 shockable segments (5 VT and 196 VF) from 62 patients, 270 AS segments from 99 patients and 574 OR segments from 160 patients. In what follows rhythms will be grouped into three categories: shockable (VF/VT), OR and AS. This is the typical rhythm class definition used in the literature on shock/no-shock decisions during CPR [15], [23]–[25]. The prevalence of VT in our dataset is low, although it is comparable
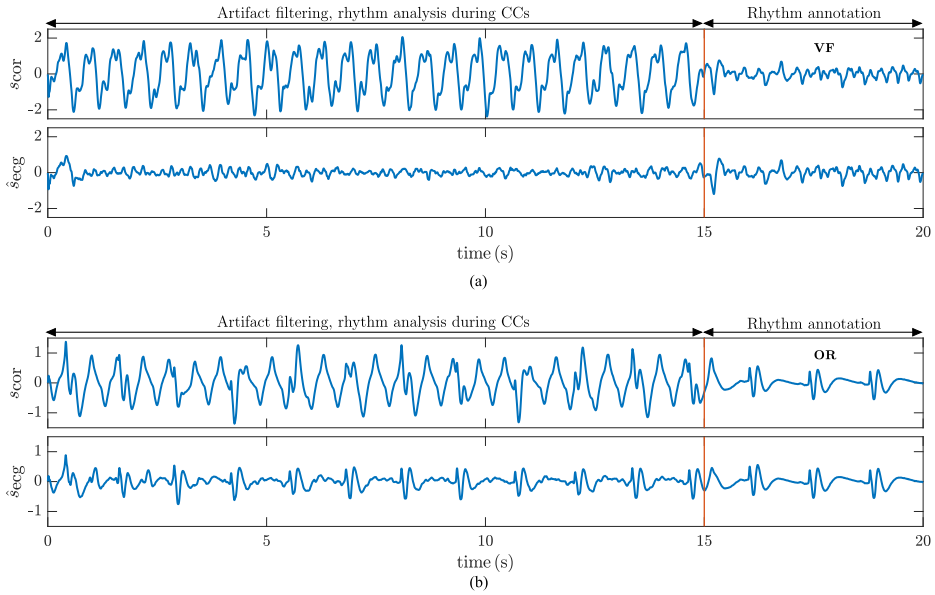
Fig. 1. Two examples of 20 s ECG segments corresponding to a patient in VF [example (a)] and to a patient in OR [example (b)]. In both examples, the top panels show the ECG recorded by the device (the corrupt ECG, s_{cor}), and the bottom panels show the ECG after filtering the compression artifact (the estimated rhythm, $\hat{s}_{ecg}$). In the top panels, the initial 15 s of the ECG are corrupted by the LUCAS 2 artifact. The last 5 s show the underlying rhythm in an interval free of artifact. Filtering (bottom pannel in both examples) reveals the underlying rhythm.

to that of most similar studies [15], [16], [23], so a separate analysis for VT would not be meaningful.

III. QUASI-PERIODIC MODEL OF THE ARTIFACT

A. Signal model

During chest compressions the ECG signal recorded by the defibrillator, $s_{cor}(n)$, is corrupted by additive chest compression artifacts, $s_{cc}(n)$, resulting in [11], [15]:

$$s_{cor}(n) = s_{ecg}(n) + s_{cc}(n) \qquad (1)$$

where $s_{ecg}(n)$ is the patient's clean ECG reflecting the actual underlying heart rhythm. Methods focus on estimating the artifact $s_{cc}(n)$. An extensively used approach is to assume $s_{cc}(n)$ to be quasi-periodic and thus model the artifact as a truncated Fourier series of N terms [14]–[16] with no DC-component. The Fourier series can be expressed in terms of the amplitude and phase coefficients, $c_k(n)$ and $\theta_k(n)$, or as a sine-cosine series with in-phase and cuadrature amplitudes, $a_k(n)$ and $b_k(n)$, in the following way:

$$s_{cc}(n) = A(n) \sum_{k=1}^{N} c_k(n) \cos(k\omega_0 n + \theta_k(n)) \qquad (2)$$

$$= A(n) \sum_{k=1}^{N} \left(a_k(n) \cos(k\omega_0 n) + b_k(n) \sin(k\omega_0 n) \right) \qquad (3)$$

where $A(n)$ is an amplitude term to model intervals with compressions, $A(n) = 1$, and without compressions, $A(n) = 0$,

such as hands-off intervals for ventilations. Smooth transitions between intervals were defined as described in [15], [37]. The spectral components of the artifact, its Fourier coefficients, are considered time-varying and will be tracked using an adaptive RLS filter (see Subsection III-C). The frequency ω_0 is the fundamental discrete frequency of the compressions which for a piston-driven compression device is constant:

$$\omega_0 = 2\pi f_{LUCAS} T_s \qquad (4)$$

with $f_{LUCAS} = 1.694 \, \text{Hz} \equiv 101.6 \, \text{min}^{-1}$ [34], and T_s the sampling period.

B. Estimating the number of harmonics N

Previous works have assumed the number of harmonics N to be fixed for all cases. However, the spectral content of the artifact is very variable from case to case both in manual [15] and mechanical compressions [34], and depends on factors like the rescuer, the patient or electrode placement. Estimating N in manual CPR is unfeasible or inaccurate because compression frequency changes with every compression. In mechanical CPR the frequency is fixed and simple spectral methods can be used to estimate the number of significant coefficients in (2). Assuming constant c_k coefficients, which suffices for approximate power computations but not for rhythm analysis, we can express the power of the artifact in short ECG intervals using Parseval's theorem:

$$P_{cc} \approx \sum_{k=1}^{N} c_k^2 = \sum_{k=1}^{N} \left(a_k^2 + b_k^2 \right) \qquad (5)$$

In this work we determined the number of significant harmonics as the first integer $N \leq 30$ for which the following inequality holds:

$$100 \cdot \frac{P_{\mathrm{cc},N+3} - P_{\mathrm{cc},N}}{P_{\mathrm{cc},N}} \leq \gamma \quad \mathrm{with} \quad P_{\mathrm{cc},K} = \sum_{k=1}^{K} c_k^2 \quad (6)$$

i.e., when the addition of 3 new harmonics increased the relative power by less than the threshold γ, optimized in the simulation phase. The problem then reduces to efficiently estimating the amplitudes c_k located at fixed frequencies $k\omega_0$.

The Fourier coefficients were estimated using the Generalized Goertzel Algorithm. The standard Goertzel algorithm allows the direct evaluation of isolated terms of the discrete Fourier transform. Its generalization extends the method to compute spectral components at any frequency [38], in our case the $k\omega_0$ frequencies. Therefore, $X(k\omega_0)$, the spectral components of the signal $x(n)$ at our frequencies of interest were computed using the following equations [38]:

$$s(n) = x(n) + 2\cos(k\omega_0)s(n-1) - s(n-2) \quad (7)$$

$$X(k\omega_0) = \left(s(L_g) - e^{-jk\omega_0}s(L_g - 1) \right)e^{-jk\omega_0 L_g} \quad (8)$$

where L_g is the length of the signal $x(n)$. For mechanical chest compression artifacts we assume that the ECG components at $k\omega_0$ are negligible when compared to the harmonics of the artifact, and therefore $x(n) = s_{\mathrm{cor}}(n)$. We used the initial 5 s window ($L_g = 5 \cdot f_s$) with compressions to estimate the c_k, and formed a windowed signal $x_w(n) = s_{\mathrm{cor}}(n) \cdot w_\beta(n)$, where $w_\beta(n)$ is a Kaiser window with form factor $\beta = 4.5$ to reduce spectral leakage. The c_k coefficients were obtained as:

$$c_k = |X(k\omega_0)| = \left| \frac{2}{W_{4.5}(0)}X_w(k\omega_0) \right| \quad (9)$$

Here $W_{4.5}(0)$ is the spectral component of the Kaiser window at the origin, and $X_w(k\omega_0)$ are the spectral components of $x_w(n)$ at the harmonic frequencies.

C. Estimation of the $a_k(n)$ and $b_k(n)$ Coefficients

Constant Fourier coefficients were assumed to determine N, the order of the model for each case. However, a proper rhythm analysis requires tracking the time-varying characteristics of the spectral components of the artifact, the coefficients in (3). These were estimated using an RLS Fourier analyzer [39], adapted to estimate mechanical CPR artifacts [40]. The RLS filter presents improved convergence and adaptability characteristics when compared to the LMS approach formerly used for CPR artifact suppression [14]–[16]. First we define two vectors for the coefficients and reference signals (the harmonic components):

$$\boldsymbol{\Theta}(n) = [a_1(n)\, b_1(n)\, \ldots\, a_N(n)\, b_N(n)]^T \quad (10)$$

$$\boldsymbol{\Phi}(n) = [\cos(\omega_0 n)\, \sin(\omega_0 n)\, \ldots\, \cos(N\omega_0 n)\, \sin(N\omega_0 n)]^T \quad (11)$$

Then the estimated chest compression artifact, $\hat{s}_{\mathrm{cc}}(n)$, is:

$$\hat{s}_{\mathrm{cc}}(n) = A(n)\boldsymbol{\Theta}^{\mathbf{T}}(n-1)\boldsymbol{\Phi}(n) \quad (12)$$

Filter coefficients are updated using the RLS algorithm to minimize the error between the corrupt ECG and the estimated artifact at the harmonics of the mechanical chest compression frequency. The error signal is the ECG of the estimated underlying rhythm, $\hat{s}_{\mathrm{ecg}}$, and the update equations are:

$$\hat{s}_{\mathrm{ecg}}(n) = s_{\mathrm{cor}}(n) - \hat{s}_{\mathrm{cc}}(n) \quad (13)$$

$$\mathbf{F}(n) = \frac{1}{\lambda}\left[\mathbf{F}(n-1) - \frac{\mathbf{F}(n-1)\boldsymbol{\Phi}(n)\boldsymbol{\Phi}^T(n)\mathbf{F}(n-1)}{\lambda + \boldsymbol{\Phi}^T(n)\mathbf{F}(n-1)\boldsymbol{\Phi}(n)} \right] \quad (14)$$

$$\boldsymbol{\Theta}(n) = \boldsymbol{\Theta}(n-1) + \mathbf{F}(n)\boldsymbol{\Phi}(n)\hat{s}_{\mathrm{ecg}}(n) \quad (15)$$

where the gain matrix and coefficient vector were initialized to $\mathbf{F}(0) = 0.03\mathbf{I}_{2N}$ and $\boldsymbol{\Theta}(0) = \mathbf{0}^T$. The forgetting factor of the RLS algorithm, λ, governs the performance of the filter and is set very close to unity. The choice of the forgetting factor is a compromise between the tracking capabilities and misadjustment and stability. Forgetting factors very close to unity ($\lambda > 0.995$) mean low misadjustments and good stability, but reduced tracking capabilities. This is desirable when the underlying rhythm (error signal) presents abrupt changes like QRS complexes, for instance in some OR rhythms. Smaller values of λ ($0.980 < \lambda < 0.995$) produce fast tracking capabilities but larger misadjustements and poorer stability. This may be desirable when the underlying rhythm is negligible, such as during AS. The different qualitative behaviors of the filter will be exploited by the MSA solution that uses two configurations of the RLS filter, as described in the following section.

IV. ARCHITECTURE OF THE SOLUTION

A. Rhythm Analysis

Filtering should reveal the underlying heart rhythm of the patient, consequently $\hat{s}_{\mathrm{ecg}}(n)$ was used to diagnose the rhythm as shockable or nonshockable. Two different approaches were used to diagnose the rhythm: an AHA compliant rhythm analysis algorithm designed to diagnose clean ECG, and an ECG feature designed to discriminate OR and VF rhythms after filtering the CPR artifact.

The rhythm analysis algorithm used was originally designed to diagnose artifact-free ECG, and uses 3 consecutive ECG intervals of 3.2 s to give a shock/no-shock decision. Succinctly, for an in depth description consult chapter 4 (pages 63-111) of [41], the decision is performed in three different stages. The first one discriminates asystole segments by identifying the absence of electrical activity based on the amplitude and power of the ECG. In the second stage, three parameters that identify the presence of QRS complexes are fed in a binary classifier based on a multiple logistic regression model to discriminate OR and shockable rhythms [42]. Finally a patch is added to discriminate fast ventricular from supraventricular rhythms [43]. The code for the computations of the features is avaliable through [44]. The algorithm was developed and tested following AHA recommendations for arrhythmia analysis algorithms in defibrillators [36], and is fully AHA compliant [41], [42]. Furthermore, it

is currently in use in the Reanibex R-series defibrillator (Bexen Cardio S. Coop., Ermua, Spain).

The algorithm was designed to diagnose artifact-free ECG, and uses 9.6 s ECG intervals to give a shock/no-shock decision. In this work we fed the rhythm analysis algorithm with a 9.6 s interval of the filtered ECG (from 3.4 s to 13 s), the first 3.4 s were left out to avoid RLS filter transients.

The OR/VF discrimination feature is based on the slope of the filtered ECG [25], and was computed using the same signal interval of $\hat{s}_{\mathrm{ecg}}(n)$ fed to the rhythm analysis algorithm (from 3.4 s to 13 s). The slope was obtained as the first difference, it was then squared and passed through a moving average filter of M samples (80 ms) and normalized by its maximum value, to obtain:

$$d(n) = \frac{1}{M} \sum_{m=0}^{M-1} (\hat{s}_{\mathrm{ecg}}(n-m) - \hat{s}_{\mathrm{ecg}}(n-m-1))^2 \quad (16)$$

$$\overline{d(n)} = \frac{d(n)}{\max\{d(n)\}} \quad n = 0, ..., L_a - 2 \quad (17)$$

where $L_a = 9.6 \cdot f_s$ is the length in samples of the interval. The discrimination feature is called slope baseline (bS) [25] and was obtained as the 10th percentile of $\overline{d(n)}$ in the analysis interval. OR rhythms present large slopes only around QRS complexes leading to low values of bS. In contrast, VF rhythms present evenly distributed slopes, thus larger values of bS. The averaging filter contributes to eliminate the effect of filtering residuals [25].

B. Architecture of the MSA Solution

The general architecture of the MSA solution for the shock/no-shock decision during mechanical chest compressions is shown in Fig. 2, and is composed of three stages. The process starts by determining the number of significant harmonics of the artifact using the generalized Goertzel method (Section III-B). In stage 1, the corrupt ECG is coarsely filtered using the RLS filter with a $\lambda_1 \sim 0.990$, to identify AS segments. If the rhythm analysis algorithm identifies a nonshockable rhythm the process ends, otherwise stage 2 is activated. In stage 2, the corrupt ECG is finely filtered using the RLS filter with a $\lambda_2 \sim 0.999$, in order to preserve quick ECG variations like QRS complexes. Again if the algorithm identifies a nonshockable rhythm the process ends, otherwise stage 3 is activated. In stage 3, the finely filtered ECG is used to compute bS and discriminate OR from VF. Four free parameters were left to optimize the performance of the solution: the threshold to determine the order of the CPR artifact model (γ), the forgetting factors of the filters (λ_1 and λ_2), and the bS threshold (ρ).

V. EVALUATION AND OPTIMIZATION

The performance of the method was evaluated by comparing the shock/no-shock decisions of our method for the filtered intervals with the clinicians' rhythm annotations for the artifact-free intervals. The following metrics were computed: sensitivity (SE), the proportion of correctly identified shockable segments; specificity (SP), the proportion of correctly identified
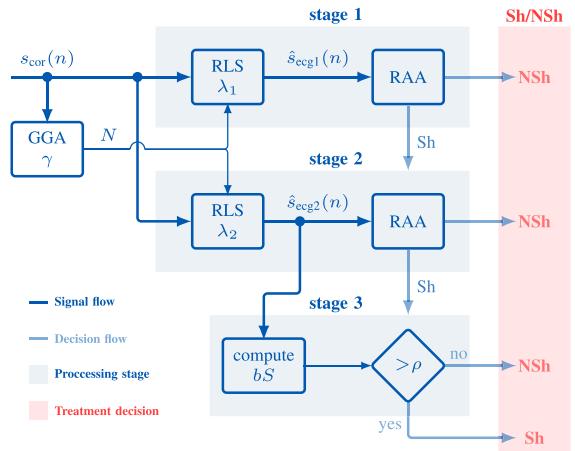
Fig. 2. Architecture of the MSA solution for shock (Sh) and no-shock (NSh) decisions during mechanical compressions. The solution is composed of three analysis stages: a first stage based on a coarse RLS adaptive filter ($\lambda_1 \sim 0.99$), a second stage with a fine RLS filter ($\lambda_2 \sim 0.999$), and a third stage based on the slope analysis (bS) of the filtered ECG. In stages 1 and 2, the decision is based on an AHA commpliant rhythm analysis algorithm (RAA). The order N of the RLS filters is determined using the generalized Goertzel algorithm (GGA). The stages are activated sequentially and the process ends when a no-shock decision is reached in stages 1 or 2, or with any diagnosis at stage 3.

nonshockable segments; accuracy (Acc), the proportion of correct decisions; and balanced accuracy (BAC). The BAC is the mean value of SE and SP,

$$\mathrm{BAC} = \tfrac{1}{2}(\mathrm{SE} + \mathrm{SP}) \quad (18)$$

and gives an unbiased measure of the method's perfomance which is desirable during optimization given the different prevalences of shockable and nonshockable segments in our dataset. BAC can be interpreted as a particular case of the unbiased mean of sensitivities for multiclass problems [45].

Data was partitioned patient-wise, 60% of patients were included in the training dataset to optimize the values of γ, λ_1, λ_2, and ρ, and 40% were left for testing to compute SE, SP, BAC and Acc. Since the partition of the data can have a significant impact on the results, the process was repeated for 500 random 60/40 patient-wise partitions to obtain statistically meaningful results. We used 500 bootstrap replicas because in our preliminary experiments a number of replicas above 300 ensured the repeatability and reliability of the estimates of the statistical distributions of the performance metrics. These distributions of the performance metrics were tested for normality using the Kolmogorov-Smirnov test, and were reported as mean value and standard deviation since they followed normal distributions.

For each of the 500 partitions the optimization process comprised three steps. First, the pair (γ, λ_1) that maximized the BAC for stage 1 of the training set was determined by doing a greedy search in the $0 < \gamma < 0.07$ and $0.985 < \lambda < 0.995$ ranges. Second, the value λ_2 that maximized the SP for OR in stage 2 was determined by searching the $0.9950 < \lambda < 0.9999$
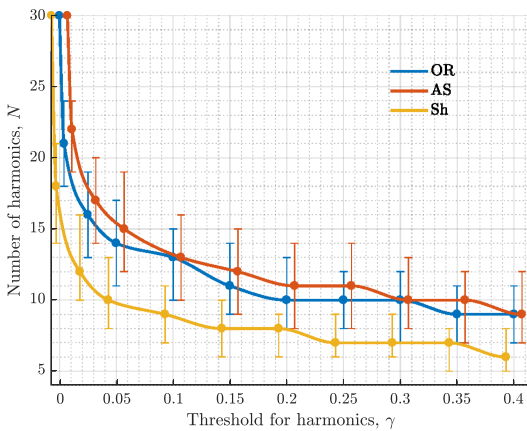
Fig. 3. Distribution of the number of harmonics as a function of the harmonic selection threshold (γ). The graph shows the median value and the 25–75 percentile range for the complete dataset. Data is shown for all cases differentiated by rhythm type: OR, AS, and shockable.

range. Third, two values of ρ were determined using the training segments that made it to stage 3. The first (ρ_1) and second (ρ_2) values set the threshold of correctly detected VF segments at 99% (high SE) and 95% (high SP), respectively.

The results were compared to those obtained for the filtering methods proposed in the literature to suppress chest compression artifacts from piston-driven devices: the LMS filter [15], [34] and the comb filter [33], [34]. For a fair comparative assessment, the training/test procedure used for the RLS was replicated. Therefore, the filters were optimized as in stage 1 of the solution proposed in this paper, that is by adjusting (γ, BW) in the comb filter and (γ, μ) in the LMS filter. In the comb filter BW refers to the bandwidth around each notch (multi-notch filter), and for the LMS filter μ is the step size of the LMS algorithm. The algorithmic details can be found in the original references [15], [33], [34].

VI. RESULTS

The dependence of the order of the model, i.e., the number of harmonics N, with the power threshold γ is shown in Fig. 3. For small values of the threshold, $\gamma < 0.005$, the median model order is above 20 but the variability is large. For instance, for $\gamma = 0.005$ model orders ranged from 8–30, and in 90% of cases were in the 11–27 range. This indicates that although many harmonics are required to accurately represent the piston-driven chest compression artifact ($N > 15$), the variability is large from case to case, and that it is important to adjust the order of the model in the prefiltering stage. Furthermore, Fig. 3 shows differences in model order depending on the underlying rhythm. Nonshockable rhythms (AS and OR) presented larger orders than shockable rhythms, because in the latter Goertzel's coefficient estimation may be affected by the spectral overlap of the underlying rhythm and the artifact.

Fig. 4 shows filtering examples for the three rhythm types, and the two filter configurations, coarse ($\lambda_1 = 0.990$) and fine

TABLE I
PERFORMANCE OF THE MSA SOLUTION PRESENTED STEP-WISE AND COMPARED TO PREVIOUS PROPOSALS BASED ON LMS AND COMB FILTERS

Method	SE (%)	SP (%)	BAC (%)	Acc (%)
Before filtering	50.7	83.9	67.3	77.5
MSA solution				
stage 1	98.1 (1.0)	87.0 (1.8)	92.5 (1.1)	89.1 (1.5)
stage 2	97.4 (2.0)	93.5 (1.2)	95.5 (1.0)	94.3 (1.0)
stage 3 (high SE)	95.0 (4.0)	95.4 (1.8)	**95.2** (1.4)	95.3 (1.1)
stage 3 (high SP)	91.7 (6.0)	**98.1** (1.1)	94.9 (2.6)	**96.9** (0.9)
LMS [34]	98.6 (1.0)	84.0 (1.8)	91.3 (1.2)	86.8 (1.6)
Comb [33], [34]	97.1 (2.0)	84.3 (1.8)	90.7 (1.3)	86.8 (1.6)

filtering ($\lambda_2 = 0.999$). Both filter configurations reveal the underlying VF equally well in the example in panel (a). For nonshockable rhythms, coarse filtering has a larger negative effect on signal amplitude in OR rhythms, as shown by the lower amplitude of the QRS complexes in the example of panel (b). However, fine filtering leaves a larger filtering residual than can mislead rhythm analysis during AS, as shown in the example of panel (c). So a compromise between both filtering characteristics is needed for an accurate rhythm analysis. For a better understanding of the filter characteristics (λ_1/λ_2) with OR rhythm the reader can consult the additional filtering examples in the supplementary materials, which also provide additional filtering experiments that explain the differences observed for OR rhythms for the two filter configurations.

The effectiveness of the RLS filter is summarized in Fig. 5, which shows the SE, SP and BAC of the rhythm analysis algorithm after filtering the chest compression artifact. This is equivalent to using only stage 1 in the filtering solution. The figure shows four implementations of the filter: for a fixed order ($N = 30, \gamma = 0$), and for three case dependent orders, with a small threshold ($\gamma = 0.002$, i.e., large N), intermediate treshold ($\gamma = 0.070$, i.e., intermediate N) and large threshold ($\gamma = 0.400$, i.e., small N). In addition the filter's optimal working range in the BAC sense is highlighted. The best results were obtained for small γ, and the figure shows that a case dependent order was particularly important to improve SP, which is where CPR suppression filters are known to fail [6].

The performance metrics for the 500 random patient-wise training/test partitions are shown in Table I. All metrics are reported as mean (standard deviation). Metrics were computed for different configurations of the filtering solution including only one, two or all three stages described in Fig. 2. The results are compared to the single stage LMS and comb filters proposed in the literature, and to the results obtained for the unfiltered ECG. Filtering increased the BAC by over 20-points in all cases. The RLS filter was the best single stage method, its BAC was 1.2-points above that of the LMS filter. Furthermore the addition of stages 2 and 3 increased the overall BAC by around 3-points and most importantly the SP by over 8-points. Stage 3 allows a trade-off between the SE and SP of the solution. The 3-stage MSA solution produced SE/SP pairs above the minimum 90/95 values recommended by the AHA [36] for rhythm analysis on clean ECGs. As in previous works on shock/no-shock decision during manual CPR, the performance goal for nonshockable
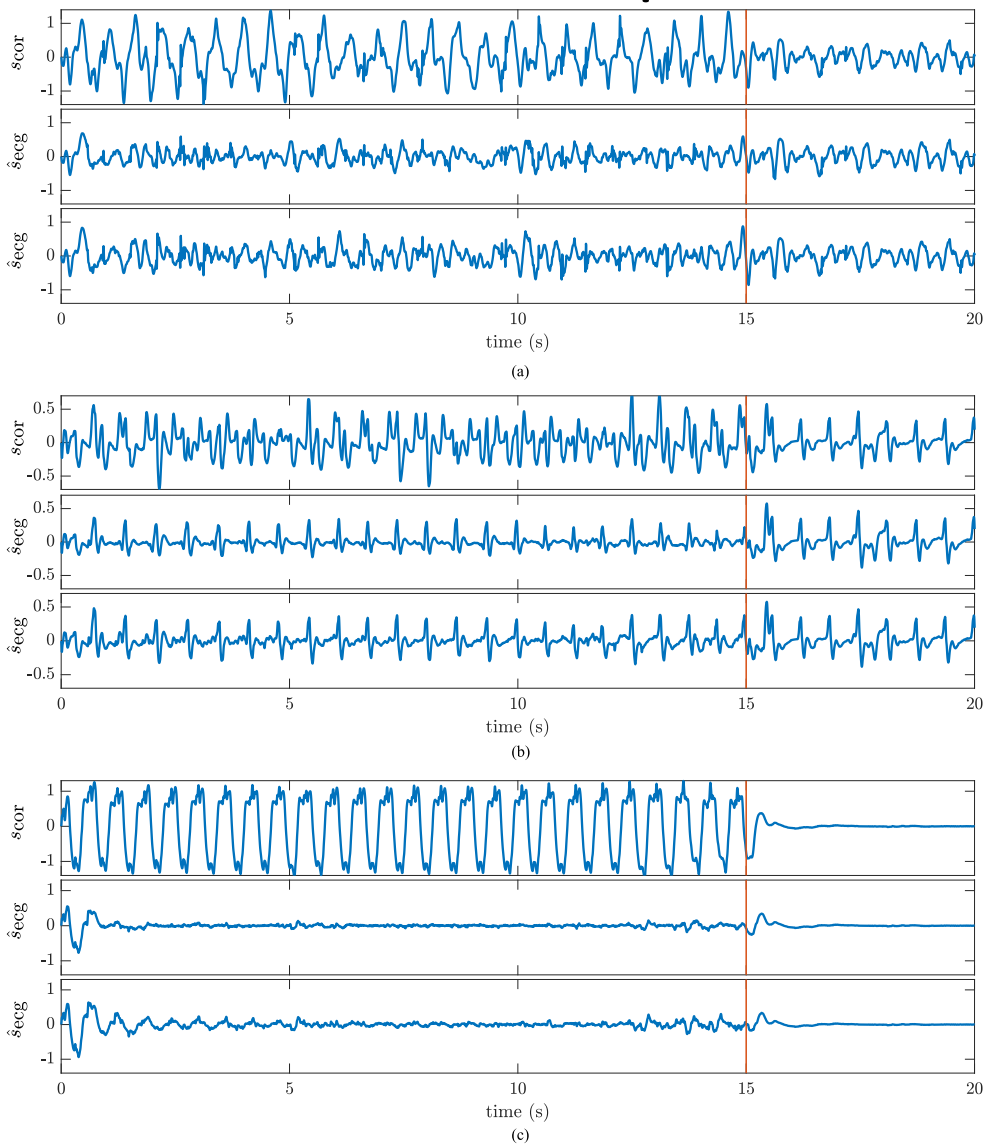
Fig. 4. An example of unfiltered and filtered (a) VF, (b) OR, and (c) AS rhythms. The first graph of each panel shows the unfiltered ECG, whereas the other two show the filtered ECG for both filtering stages, coarse filtering ($\lambda_1 = 0.990$) in the middle and fine filtering ($\lambda_2 = 0.999$) in the bottom graphs.

rhythms was fixed at 95% specificity [9], [14]–[16], [24]. This is the AHA performance goal for asystole and for rhythms other than normal sinus rhythm. For safety reasons, the AHA recommends a 99 % specificity for normal sinus rhythms. However, organized rhythms during cardiac arrest are rarely normal sinus rhythms, since restoration of a normal rhythm and pulse would imply ceasing chest compression therapy.

The average characteristics of the optimal MSA solution were $\lambda_1 = 0.9899\,(0.0006)$, $\gamma = 2.3\,(1.3) \cdot 10^{-3}$, $\lambda_2 = 0.9990$ (0.0003), $\rho_1 = 7.7\,(4.3) \cdot 10^{-3}$ and $\rho_2 = 16.7\,(4.4) \cdot 10^{-3}$. On average 70.7% of segments were diagnosed in stage 1, 5.4% in stage 2 and 23.9% in stage 3. The drawback of an RLS based solution is the processing time, and in particular the recursion formula for the gain matrix which involves the multiplication of $2N \times 2N$ matrices (14). Our Matlab implementation of the RLS filter (single stage) on an i7 3.2 GHz single-core processor and 16 GB of memory took on average 85 ms, considerably more than the 17 ms and 8 ms obtained for the LMS and the comb
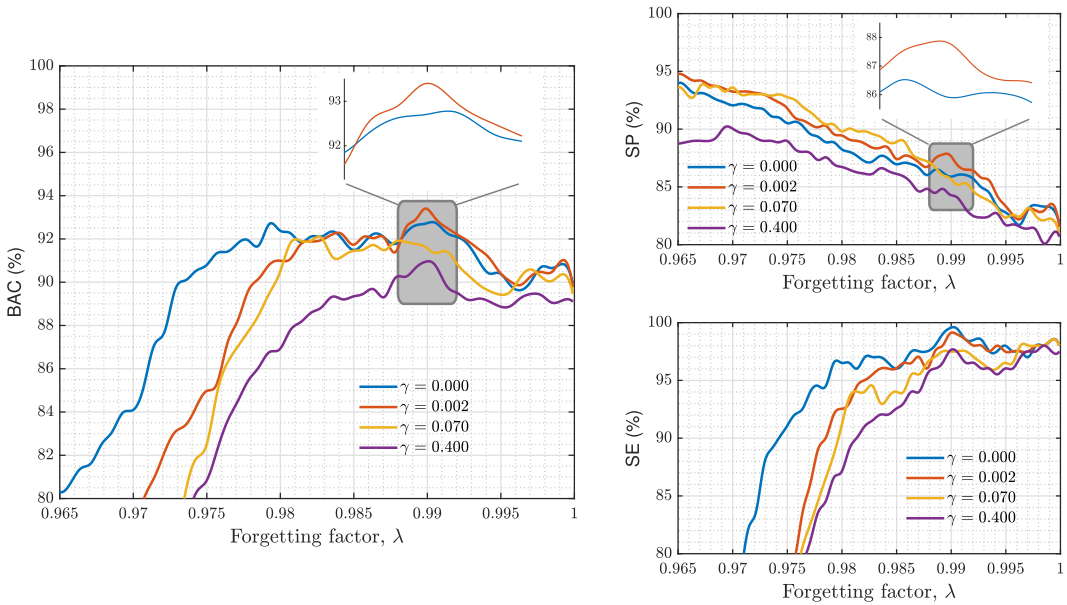
Fig. 5.   Performance metrics for a single stage RLS filter. Data was obtained for the whole dataset and is shown as a function of the forgetting factor of the filter (λ) for four thresholds: $\gamma = 0$ ($N = 30$ fixed), $\gamma = 0.002$ (large N), $\gamma = 0.07$ (intermediate N), and $\gamma = 0.4$ (small N). The highlighted region shows the optimal range of the filter in the BAC sense, and shows that the best results were obtained for small γ (red).

TABLE II
COMPARISON BETWEEN MSA SOLUTION BASED ON RLS, LMS AND COMB
FILTERS, INCLUDING PROCESSING TIMES

MSA solution	SE (%)	SP (%)		ptime (ms)
		AS	OR	
RLS based				
stage 1	98.1 (1.0)	93.0 (2.7)	84.2 (2.2)	85
stage 2	97.4 (2.0)	95.3 (2.2)	92.7 (1.5)	110
stage 3 (high SE)	95.0 (4.0)	96.3 (2.3)	95.0 (2.1)	111
stage 3 (high SP)	91.7 (6.0)	98.0 (1.7)	98.1 (1.4)	111
LMS based				
stage 1	98.6 (1.0)	87.7 (3.1)	82.3 (2.3)	16
stage 2	96.0 (2.0)	94.2 (2.3)	92.0 (1.6)	21
stage 3 (high SE)	94.4 (3.0)	95.0 (2.3)	92.3 (1.6)	21
stage 3 (high SP)	90.4 (5.0)	95.3 (2.2)	92.4 (1.5)	21
COMB based				
stage 1	97.1 (2.0)	86.7 (4.1)	83.2 (2.6)	8
stage 2	94.6 (2.0)	91.2 (3.4)	89.3 (2.1)	11
stage 3 (high SE)	92.4 (4.0)	93.6 (2.7)	93.1 (2.7)	11
stage 3 (high SP)	88.8 (6.0)	95.9 (2.4)	96.9 (1.7)	11

filters, respectively. The computational demands of the RLS filter are acceptable for the implementation on current monitor/defibrillators, but processing demands could be reduced by an order of magnitude using an MSA solution based on the comb filter, of five-fold using the LMS filter. We implemented those solutions, by replicating the optimization process used for the RLS filter and using for stage 2 a bandwidth range of $0.08 < BW < 0.2$ Hz for the comb filter, and a step size range of $0.0009 < \mu < 0.002$ for the LMS filter, which are equivalent to the range of large forgetting factors in the RLS filter. Table II compares the MSA solutions based on the RLS, LMS and comb filters, and shows there is a trade-off between diagnostic accuracy and computational demands. The table also shows the classification per rhythm type, to describe the effect of each stage of the MSA solution on the accuracy for each rhythm type. In fact, the AHA's requirements for all rhythm types were only met by the 3-stage RLS based solutions.

VII. DISCUSSION

This paper introduces a MSA solution for an accurate shock/no-shock decision during mechanical CPR. The solution introduces and/or combines several features that contribute to an increased decision accuracy: an improved CPR artifact filter with a per case filter order (genelarized Goertzel algorithm) and better tracking characteristics (RLS filter), a two-stage filtering approach to improve SP, and a final VF/OR discrimination algorithm to balance the SE and SP of the solution. It improves the BAC, SP and Acc of previous solutions by more than 5-points, 12-points and 10-points, respectively. The MSA is the first solution to meet AHA's criteria for SE/SP during mechanical compressions, with a specificity above the 95% AHA recommendation for nonshockable rhythms other than sinus rhythm.

Mechanical compressions are delivered at a fixed frequency, this allowed the realization of a simple and computationally efficient method to determine the order of the model. Previous attempts to remove the LUCAS 2 artifact focused on the identification of an overall optimal model order [33], [34], but our results show that model orders vary considerably from case to case and that a case dependent order contributes to an improved SP. RLS Fourier analyzers present improved convergence, shorter

transients and better tracking properties [39] than the previously used LMS [14], [15], [19] or Kalman filters [17]. The RLS filter improved the BAC of the LMS filter by 1.2-points, and the effect was larger on the SP (see Table I). The last two characteristics of the MSA solution were inspired by two recent solutions to allow accurate shock/no-shock decisions during manual CPR. Iterative artifact filtering was introduced within the enhanced adaptive filter (EAF) [16]. In our case, two filtering stages were sufficient, a coarse filter to maximize BAC (stage 1) and a fine filter to improve the detection of OR rhythms (stage 2). The analysis of the slope, an approach introduced by Ayala *et al.* [25] to classify the filtered ECG, improved the SP of our method by 2–4 points depending on the configuration of the detection threshold. These two additions boosted the SP above 95% and were particularly important to increase SP for OR rhythms by 10 to 14-points (see Table II).

Mechanical chest compression devices are popular in emergency services. Data from a US cardiac arrest registry indicated that 45% of participating services routinely used mechanical devices [46]. Current resuscitation guidelines for instance recommend their use in situations where sustained high quality manual chest compressions are impractical or unsafe [32]. It is therefore important to devise methods to reduce the compression artifact and allow an accurate shock/no-shock decision during therapy. When compared to filtering manual compression artifacts, mechanical compression artifacts present advantages and challenges. Mechanical artifact filtering is easier because the compression frequency is fixed and the artifact waveform pattern more stable [34]. Challenges include larger artifact amplitudes [33], [34], and larger harmonic content, producing models with very large orders and increased computational cost.

Many CPR artifact filters for manual chest compressions have used additional reference signals to model the artifact [7], [9], [11]–[13], [16]. The acquisition of signals like compression depth, acceleration or force makes defibrillator hardware more complex and expensive, so these reference signals are not universally available [6]. Irusta et al showed that chest compression rate derived from the depth signal was sufficient to accurately model the artifact [15]. In fact, when compared on the same data and with the same shock/no-shock decision algorithm, adaptive filters based only on chest compression rate were as accurate as adaptive filters using four reference channels [47]. Piston-driven mechanical chest compressions are delivered at a fixed frequency, so the problem is further simplified because depth or impedance are no longer needed to determine the chest compression rate. Furthermore, for manual CPR computing chest compression rate from signals like impedance, depth or force requires algorithms that accurately identify compression related fiducial points (maximum depth). These fiducial points cannot be always accurately determined, and this negatively affects the performance of the adaptive solutions based only on rate [14]. Our simulations for the MSA method on manual CPR data (see Section I of the supplementary materials) confirm this hypothesis. Artifact filtering during manual CPR based only on the ECG involves an additional stage to determine compression frequency for which methods using spectral analysis [20], [48], empirical

mode decomposition [19], or coherent line removal [18] have been devised. Some of these methods could be adapted in the future to implement a prefiltering stage to determine a case dependent model for manual CPR artifacts. Increasing the SP of shock/no-shock decisions during manual chest compressions remains a challenge but future solutions should probably include multistage filters and post-filtering stages such as spiky artifact detectors [16] and ad-hoc solutions to discriminate rhythms based on the filtered ECG [21], [24], [25].

This study has some limitations. First, the MSA method is computationally demanding. The filtering stages could be simplified using computationally efficient RLS Fourier analyzers [39], LMS filters, or comb filters, but the cost would be a lower accuracy. Second, compressions were delivered using a piston-driven device, and artifact characteristics may differ when load distribution bands are used. Third, data were gathered using only one monitor/defibrillator model and extrapolation of the results to other models may involve adjusting the method for different sampling frequencies, voltage resolutions and ECG acquisition bandwidth. And fourth, data was gathered from a single emergency service, and there may be differences in resuscitation protocols and device usage across services [46] that may alter the characteristics of the CPR artifacts.

VIII. Conclusion

This paper introduces the first method to give a shock/no-shock diagnosis compliant with AHA recommendations for shockable (SE above 90%) and nonshockable rhythms (SP above 95% for rhythms other than sinus rhythm) during mechanical chest compressions. The MSA method had an SE of 91.8% and an SP of 98.1%, for an accuracy of 96.9%. A two stage filtering approach combined with an ad-hoc algorithm to differentiate OR from VF were implemented to increase the SP, which was well below 90% in all previous studies. This new approach to rhythm diagnosis during chest compressions may open the possibility of diagnosing the rhythm without interrupting compression therapy.

References

[1] G. Perkins *et al.*, "European resuscitation council guidelines for resuscitation 2015: Section 2. Adult basic life support and automated external defibrillation," *Resuscitation*, vol. 95, pp. 81–99, 2015.

[2] C. Vaillancourt *et al.*, "The impact of increased chest compression fraction on return of spontaneous circulation for out-of-hospital cardiac arrest patients not in ventricular fibrillation," *Resuscitation*, vol. 82, no. 12, pp. 1501–1507, 2011.

[3] M. G. Hoogendijk *et al.*, "Ventricular fibrillation hampers the restoration of creatine-phosphate levels during simulated cardiopulmonary resuscitations," *Europace*, vol. 14, no. 10, pp. 1518–1523, 2012.

[4] J. Ruiz *et al.*, "Feasibility of automated rhythm assessment in chest compression pauses during cardiopulmonary resuscitation," *Resuscitation*, vol. 84, no. 9, pp. 1223–1228, 2013.

[5] U. Ayala *et al.*, "Fully automatic rhythm analysis during chest compression pauses," *Resuscitation*, vol. 89, pp. 25–30, 2015.

[6] S. Ruiz de Gauna *et al.*, "Rhythm analysis during cardiopulmonary resuscitation: Past, present, and future," *Biomed. Res. Int.*, vol. 2014, 2014, Art. no. 386010.

[7] R. D. Berger *et al.*, "Rhythm discrimination during uninterrupted CPR using motion artifact reduction system," *Resuscitation*, vol. 75, no. 1, pp. 145–152, 2007.

[8] S. Babaeizadeh *et al.*, "Analyzing cardiac rhythm in the presence of chest compression artifact for automated shock advisory," *J. Electrocardiol.*, vol. 47, no. 6, pp. 798–803, 2014.

[9] T. Werther *et al.*, "CPR artifact removal in ventricular fibrillation ECG signals using Gabor multipliers," *IEEE Trans. Biomed. Eng.*, vol. 56, no. 2, pp. 320–327, Feb. 2009.

[10] S. O. Aase *et al.*, "CPR artifact removal from human ECG using optimal multichannel filtering," *IEEE Trans. Biomed. Eng.*, vol. 47, no. 11, pp. 1440–1449, Nov. 2000.

[11] J. Eilevstjønn *et al.*, "Feasibility of shock advice analysis during CPR through removal of CPR artefacts from the human ECG," *Resuscitation*, vol. 61, no. 2, pp. 131–141, 2004.

[12] J. Husoy *et al.*, "Removal of cardiopulmonary resuscitation artifacts from human ECG using an efficient matching pursuit-like algorithm," *IEEE Trans. Biomed. Eng.*, vol. 49, no. 11, pp. 1287–1298, Nov. 2002.

[13] K. Rheinberger *et al.*, "Removal of CPR artifacts from the ventricular fibrillation ECG by adaptive regression on lagged reference signals," *IEEE Trans. Biomed. Eng.*, vol. 55, no. 1, pp. 130–137, Jan. 2008.

[14] E. Aramendi *et al.*, "Suppression of the cardiopulmonary resuscitation artefacts using the instantaneous chest compression rate extracted from the thoracic impedance," *Resuscitation*, vol. 83, no. 6, pp. 692–698, 2012.

[15] U. Irusta *et al.*, "A least mean-square filter for the estimation of the cardiopulmonary resuscitation artifact based on the frequency of the compressions," *IEEE Trans. Biomed. Eng.*, vol. 56, no. 4, pp. 1052–1062, Apr. 2009.

[16] Y. Gong *et al.*, "An enhanced adaptive filtering method for suppressing cardiopulmonary resuscitation artifact," *IEEE Trans. Biomed. Eng.*, vol. 64, no. 2, pp. 471–478, Feb. 2017.

[17] J. Ruiz *et al.*, "Cardiopulmonary resuscitation artefact suppression using a Kalman filter and the frequency of chest compressions as the reference signal," *Resuscitation*, vol. 81, no. 9, pp. 1087–1094, 2010.

[18] A. Amann *et al.*, "Reduction of CPR artifacts in the ventricular fibrillation ECG by coherent line removal," *Biomed. Eng. Online*, vol. 9, no. 1, 2010, Art. no. 2.

[19] G. Zhang *et al.*, "A method to differentiate between ventricular fibrillation and asystole during chest compressions using artifact-corrupted ECG alone," *Comput. Methods Programs Biomed.*, vol. 141, pp. 111–117, 2017.

[20] S. R. de Gauna *et al.*, "A method to remove CPR artefacts from human ECG using only the recorded ECG," *Resuscitation*, vol. 76, no. 2, pp. 271–278, 2008.

[21] Y. Li *et al.*, "Identifying potentially shockable rhythms without interrupting cardiopulmonary resuscitation," *J. Critical Care Med.*, vol. 36, no. 1, pp. 198–203, 2008.

[22] Y. Li *et al.*, "An algorithm used for ventricular fibrillation detection without interrupting chest compression," *IEEE Trans. Biomed. Eng.*, vol. 59, no. 1, pp. 78–86, Jan. 2012.

[23] H. Kwok *et al.*, "Adaptive rhythm sequencing: A method for dynamic rhythm classification during CPR," *Resuscitation*, vol. 91, pp. 26–31, Jun. 2015.

[24] V. Krasteva *et al.*, "Shock advisory system for heart rhythm analysis during cardiopulmonary resuscitation using a single ECG input of automated external defibrillators," *Ann. Biomed. Eng.*, vol. 38, no. 4, pp. 1326–1336, 2010.

[25] U. Ayala *et al.*, "A reliable method for rhythm analysis during cardiopulmonary resuscitation," *Biomed. Res. Int.*, vol. 2014, 2014, Art. no. 872470.

[26] S. Rubertsson *et al.*, "Mechanical chest compressions and simultaneous defibrillation vs conventional cardiopulmonary resuscitation in out-of-hospital cardiac arrest: The LINC randomized trial," *JAMA*, vol. 311, no. 1, pp. 53–61, 2014.

[27] L. Wik *et al.*, "Manual vs. integrated automatic load-distributing band CPR with equal survival after out of hospital cardiac arrest. The randomized CIRC trial," *Resuscitation*, vol. 85, no. 6, pp. 741–748, 2014.

[28] M. E. H. Ong *et al.*, "Mechanical CPR devices compared to manual CPR during out-of-hospital cardiac arrest and ambulance transport: A systematic review," *Scand. J. Trauma Resuscitation Emergency Med.*, vol. 20, no. 1, 2012, Art. no. 39.

[29] G. Putzer *et al.*, "LUCAS compared to manual cardiopulmonary resuscitation is more effective during helicopter rescue. A prospective, randomized, cross-over manikin study," *Amer. J. Emergency Med.*, vol. 31, no. 2, pp. 384–389, 2013.

[30] A. I. Larsen *et al.*, "Cardiac arrest with continuous mechanical chest compressions during percutaneous coronary intervention: a report on the use of the LUCAS device," *Resuscitation*, vol. 75, no. 3, pp. 454–459, 2007.

[31] K. Sunde *et al.*, "Quality of mechanical, manual standard and active compression–decompression CPR on the arrest site and during transport in a manikin model," *Resuscitation*, vol. 34, no. 3, pp. 235–242, 1997.

[32] J. Soar *et al.*, "European resuscitation council guidelines for resuscitation 2015: Section 3. Adult advanced life support," *Resuscitation*, vol. 95, pp. 100–147, 2015.

[33] J. Sullivan *et al.*, "A digital filter can effectively remove mechanical chest compression artifact," *Resuscitation*, vol. 85, 2014, Art. no. S41.

[34] E. Aramendi *et al.*, "Filtering mechanical chest compression artefacts from out-of-hospital cardiac arrest data," *Resuscitation*, vol. 98, pp. 41–47, 2016.

[35] *Instruction for use, Chest Compression System LUCAS*, Jolife AB/Physio-Control, Lund, Sweden, 2009.

[36] R. E. Kerber *et al.*, "Automatic external defibrillators for public access defibrillation: recommendations for specifying and reporting arrhythmia analysis algorithm performance, incorporating new waveforms, and enhancing safety," *Circulation*, vol. 95, no. 6, pp. 1677–1682, 1997.

[37] R. W. C. G. R. Wijshoff *et al.*, "Photoplethysmography-based algorithm for detection of cardiogenic output during cardiopulmonary resuscitation," *IEEE Trans. Biomed. Eng.*, vol. 62, no. 3, pp. 909–921, Mar. 2015.

[38] P. Sysel and P. Rajmic, "Goertzel algorithm generalized to non-integer multiples of fundamental frequency," *EURASIP J. Adv. Signal Process.*, vol. 2012, no. 1, 2012, Art. no. 56.

[39] Y. Xiao *et al.*, "Fast RLS Fourier analyzers capable of accommodating frequency mismatch," *Signal Process.*, vol. 87, no. 9, pp. 2197–2212, 2007.

[40] I. Isasi *et al.*, "Removing piston-driven mechanical chest compression artefacts from the ECG," *Comput. Cardiol.*, vol. 44, pp. 1–4, 2017.

[41] U. Irusta Zarandona, "New signal processing algorithms for automated external defibrillators," Ph.D. dissertation, Dept. Electron. Telecommun., Univ. Basque Country, Leioa, Spain, 2010. [Online]. Available: http://hdl.handle.net/10810/7990

[42] U. Irusta *et al.*, "A high-temporal resolution algorithm to discriminate shockable from nonshockable rhythms in adults and children," *Resuscitation*, vol. 83, no. 9, pp. 1090–1097, 2012.

[43] U. Irusta and J. Ruiz, "An algorithm to discriminate supraventricular from ventricular tachycardia in automated external defibrillators valid for adult and paediatric patients," *Resuscitation*, vol. 80, pp. 1229–1233, 2009.

[44] C. Figuera *et al.*, "Machine learning techniques for the detection of shockable rhythms in automated external defibrillators," *PloS one*, vol. 11, 2016, Art. no. e0159654.

[45] A. B. Rad *et al.*, "ECG-based classification of resuscitation cardiac rhythms for retrospective data analysis," *IEEE Trans. Biomed. Eng.*, vol. 64, no. 10, pp. 2411–2418, Oct. 2017.

[46] P. Govindarajan *et al.*, "Practice variability among the EMS systems participating in cardiac arrest registry to enhance survival (CARES)," *Resuscitation*, vol. 83, no. 1, pp. 76–80, 2012.

[47] U. Ayala *et al.*, "Are dual-channel methods as accurate as multi-channel methods to suppress the CPR artifact?" in *Proc. Comput. Cardiol.*, Sep. 2011, pp. 509–512.

[48] E. Aramendi *et al.*, "Detection of ventricular fibrillation in the presence of cardiopulmonary resuscitation artefacts," *Resuscitation*, vol. 72, no. 1, pp. 115–123, 2007.

Supplementary materials

Iraia Isasi, Unai Irusta*, *Member, IEEE* Elisabete Aramendi, Unai Ayala, Erik Alonso,
Jo Kramer-Johansen, and Trygve Eftestøl, *Member, IEEE*

I. THE MSA ALGORITHM FOR RHYTHM ANALYSIS DURING MANUAL CPR

The objective of this section is to describe the adaptations of the MSA solution for manual CPR, and to test those adaptations using out-of-hospital cardiac arrest data in which manual CPR was delivered. The results are also compared to previous solutions for rhythm analysis during CPR.

A. Data collection and preparation

The dataset used to optimize and test the performance of the MSA solution on manual CPR is the one used to introduce the LMS filter for manual CPR artifact [1], [2]. The interested reader can consult those references for further details on data extraction and annotation. In brief, the data was gathered from a prospective study conducted in Akershus (Norway), Stockholm (Sweden) and London (UK) between March 2002 and September 2004. ECG and compression depth (CD) signals were acquired using a modified version of Laerdal's Heartstast 4000 defibrillator and downsampled to 250 Hz.

For our simulations we used ECG segments composed of two consecutive 15.5 s intervals: an initial interval corrupted by CPR artefacts, and a second interval used to annotate the ground truth rhythm labels. Fig. 1 shows an example from the database. Rhythm labels were adjudicated by consensus among an anaesthesiologist and a biomedical engineer both specialized in resuscitation [3], [4]. The database is composed of 372 segments from 295 patients, of which 87 were shockable, (5 VT and 82 VF), and 285 nonshockable (88 AS and 197 OR).

B. Architecture of the MSA solution

The model of the artifact is the one described in section III-A of the manuscript, i.e. a truncated Fourier series of N harmonics:

$$s_{cc}(n) = A(n) \sum_{k=1}^{N} c_k(n) \cos(k\omega_0(n)n + \theta_k(n)) = \qquad (1)$$

$$= A(n) \sum_{k=1}^{N} a_k(n) \cos(k\omega_0(n)n) + b_k(n) \sin(k\omega_0(n)n) \quad (2)$$

For chest compressions delivered using the LUCAS-2 device $\omega_0 = 2\pi f_{\text{LUCAS}}$ is constant, and fixed by the device to $f_{\text{LUCAS}} = 1.694$ Hz. In manual CPR the frequency of the compressions delivered by a human rescuer changes from compression to compression and therefore it is time varying: $\omega_0 = 2\pi f_0(n)T_s$. In our model we assume $f_0(n)$

is fixed during a compression cycle but variable from cycle to cycle. We define the oscillation cycle as the interval between consecutive chest compression instants. As shown in Fig. 1, we denote as t_k the instant in which the k-th compression was delivered (maximum chest depletion), as measured in the CD. Then, the instantaneous frequency for compression cycle k can be calculated as:

$$f_0(n) = \frac{1}{t_k - t_{k-1}} \quad t_{k-1} < nTs \le t_k \qquad (3)$$

During manual chest compressions the spectral components of the artefact are not well localized since the frequency may change in every cycle. Consequently the initial stage of the MSA solution cannot be used, i.e. the per case estimation of the model's order (N) using Goertzel's Generalized Algorithm. We decided instead to test the algorithm using the same number of harmonics for all the cases, as done in [1], [2]. The architecture of the MSA solution is the one shown in Fig. 2, which is the same as the one used for mechanical CPR artifacts but eliminating the per case estimation of N. The rest of the processing blocks are the ones described in the manuscript including the RLS filter, the Rhythm Analysis Algorithm (RAA) and stage 3 based on the analysis of the slope of the filtered ECG. The only adaptation needed for the RLS filter equations are:

$$\mathbf{\Theta}(n) = [a_1(n)\, b_1(n)\, \ldots\, a_N(n)\, b_N(n)]^T \qquad (4)$$

$$\mathbf{\Phi}(n) = [\cos(\omega_0(n)\, n)\, \sin(\omega_0(n)\, n)\, \ldots$$
$$\cos(N\omega_0(n)\, n)\, \sin(N\omega_0(n)\, n)]^T \qquad (5)$$

$$\hat{s}_{cc}(n) = A(n)\mathbf{\Theta}^{\mathbf{T}}(n-1)\mathbf{\Phi}(n) \qquad (6)$$

where the $\mathbf{\Phi}(n)$ vector is now composed of the sinusoidal components of time-varying frequency, that accommodate a time-varying chest compression frequency $\omega_0(n)$.

C. Optimization and evaluation

The method was evaluated in terms of the performance metrics defined in Section V of the manuscript: sensitivity for shockable rhythms (SE), specificity for nonshockable rhythm (SP), Balanced Accuracy (BAC) and total accuracy (Acc). The optimization parameters of the MSA architecture were the order of the model N, the two forgetting factors λ_1 for the coarse RLS filter and λ_2 for the fine RLS filter, and the threshold ρ of the VF/OR discriminator in stage 3. Data was randomly partitioned patient-wise into training (60%) and test (40%) for optimization and validation, and statistically meaningful results were obtained repeating the process 500 times. For each partition the optimization process comprised the following steps:
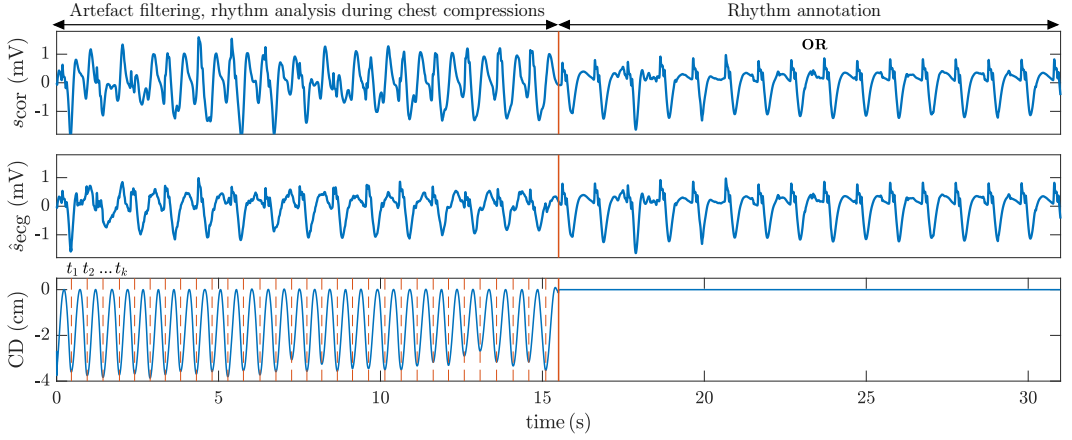
Fig. 1. Example of the 31 s segments in the manual CPR dataset. The top panel shows the ECG of a patient in OR, the middle panel shows the filtered ECG, and the bottom panel the CD signal. The chest compression instants are indicated by vertical lines in CD, the t_k instants.
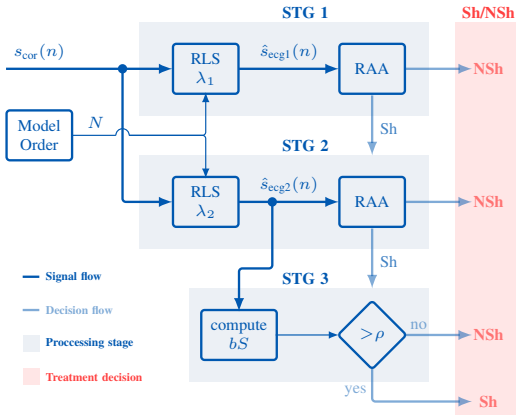
Fig. 2. Architecture of the MSA solution for rhythm analysis during manual CPR. In this case the order of the model N is fixed.

1) The pair (N, λ_1) that maximized the BAC for stage 1 of the training set was determined by doing a greedy search in the $3 \leq N \leq 7$ and $0.980 \leq \lambda_1 \leq 0.990$.
2) The value λ_2 that maximized the SP for OR in stage 2 was determined by searching the $0.995 \leq \lambda_2 \leq 1$ range.
3) Two values of ρ were determined using the training segments that made it to stage 3. The first (ρ_1) and second (ρ_2) values set the threshold of correctly detected VF segments at 99% (high SE) and 95% (high SP), respectively.

As reference, the MSA method was also adapted to use the LMS approach to estimate $a_k(n)$ and $b_k(n)$ [1], [2], which were the studies that introduced the Fourier series model of the artifact. The performance metrics were estimated using again 500 data partitions, and replicating the optimization procedure used for the MSA based on the RLS filter. The ranges for N

and μ in the greedy search procedures of stages 1 and 2 were: $2 \leq N \leq 7$ and $0.008 \leq \mu_1 \leq 0.06$, and $0.0013 \leq \mu_2 \leq 0.0080$, respectively.

D. Results

The RLS filter performance for a single stage is shown in Fig. 3. The figure shows the SE, SP and BAC of the RAA after filtering the artifact for four different model orders: $N = 1, 4, 5, 8$. The results for model orders 1 and 8 are shown to illustrate the effect of using few harmonics and an excessive number of harmonics to estimate the manual CPR artefact. Model orders 4-5 are the ones that have been previously been identified as optimal using other filtering approaches [1], [2]. The best results in terms of BAC were obtained for $0.980 < \lambda < 0.990$ and $4 \leq N \leq 6$. The optimal working range for λ is similar to that obtained for mechanical CPR (figure 5 of the manuscript). However, the optimal model order for the artifact is significantly smaller, $N \sim 4$ for manual CPR and $N \sim 25$ for the LUCAS-2 device. In line with previous findings, our results show that optimal CPR artifact filters for manual chest compressions involve fewer harmonics [5], [6].

The average characteristics of the optimal MSA solution using the RLS/LMS filter were:

stage 1: $\lambda_1 = 0.987 \, (0.002)$, $\mu_1 = 0.019 \, (0.008)$
stage 2: $\lambda_2 = 0.998 \, (0.002)$, $\mu_2 = 0.005 \, (0.002)$
stage 3, $\uparrow$ SE: $\rho_1 = 0.005 \, (0.001)$, $\rho_1 = 0.005 \, (0.002)$
stage 3, $\uparrow$ SP: $\rho_2 = 0.009 \, (0.002)$, $\rho_2 = 0.009 \, (0.003)$

In both cases, the order of the artifact model was between 3 an 5 in over 95% of the segments. Table I shows the performance metrics for the 500 random partitions reported as mean (standard deviation). Metrics were computed for different configurations of the MSA solution: stage 1, stage 2 and stage 3. The results are compared with the performance of the RAA before filtering, and are reported for both filtering methods the RLS and the LMS filters. Using a single RLS filtering stage the BAC is increased by around 12 points. The
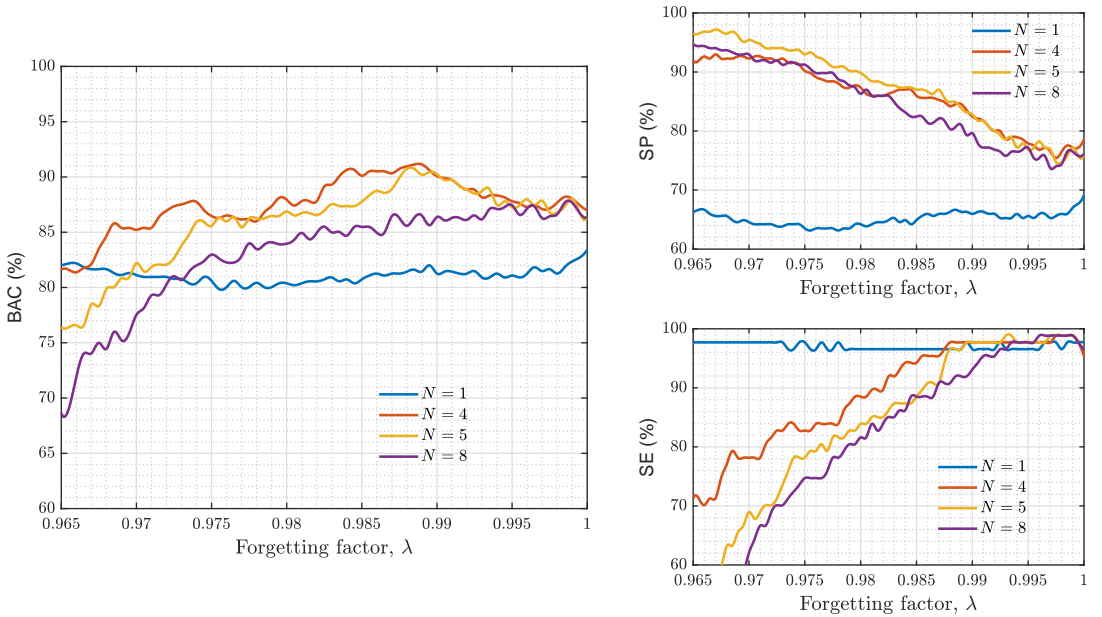
Fig. 3. Performance metrics for a single stage RLS filter. Data was obtained for the whole dataset and is shown as a function of λ for three values of the order of the artefact model: $N = 1, 4, 5, 8$.

addition of the stages 2 and 3 increases the BAC by 1.2 and 2.6 points, and the overall accuracy by 1.8 and over 5 points, respectively. This is because stages 2 and 3 boots the SP, which in the MSA solution is increased by at least 6 points over a single filtering stage.

Finally Fig. 4 shows three examples of manual CPR filtering using the RLS filter. The examples represent the typical situation for the three rhythm types, VF, AS and OR and also illustrate the differences in filtered signal between coarse (λ_1) and fine (λ_2) filtering. As with the LUCAS-2 device, coarse filtering may over attenuate QRS complexes (OR), and fine filtering may leave filtering residuals (AS).

E. Conclusions

The MSA solution improves the results presented in the past for single stage filtering solutions [1], [7]. When compared using the same dataset and RAA, the high MSA solutions improved the BAC and Acc of a single stage filtering method by over 2 and 4.5-points, respectively. Furthermore, we also show that RLS filtering improves the accuracy of the past LMS solution [1], [2] by at least 1-point. This difference is smaller than for the LUCAS-2 artifact, the RLS filter is more accurate for artifacts with harmonics of higher order. Most importantly the MSA architecture provides a framework to increase the SP of previous rhythm analysis solutions, since the SP increased by 6.5-9 points over a single stage solution. This is very important because the low SP has been identified as the main limitation of most methods for rhythm analysis during manual CPR [8]. Our SE/SP values for the MSA solution, both in the high SE 93.6%/91.0% or high SP 89.6%/93.8% configurations, are close to the AHA performance recommendations [9]. Currently the AHA recommends a 90 % SE for shockable rhythms (VF), and a 95 % SP for nonshockable rhythms other than normal sinus rhythm [9].

Finally, the MSA solution and two filter configurations can be further refined in the future by developing machine learning algorithms to classify the filtered ECG signals, in line with some recent developments [10], [11]. Such a research line is promising and should be explored in the future, for it may result in solutions that meet the AHA SE/SP recommendations for cardiac arrest rhythms.

TABLE I
PERFORMANCE OF THE MSA SOLUTION PRESENTED STEP-WISE AND
COMPARED WITH THE VALUES BEFORE FILTERING.

Method	SE (%)	SP (%)	BAC (%)	Acc (%)
Before filtering	74.7	80.9	77.8	79.6
MSA, with RLS				
STG 1	95.1 (4.0)	84.3 (3.1)	89.7 (2.5)	86.9 (2.5)
STG 2	95.0 (4.0)	86.7 (3.2)	90.9 (2.4)	88.7 (2.5)
STG 3, high SE	93.0 (5.0)	91.0 (2.9)	**92.0** (2.6)	91.4 (2.2)
STG 3, high SP	89.4 (6.0)	**93.6** (2.4)	91.5 (3.0)	**92.6** (1.9)
MSA, with LMS				
STG 1	95.4 (4.0)	81.0 (3.2)	88.2 (2.3)	84.4 (2.4)
STG 2	95.2 (4.0)	84.6 (3.0)	89.9 (2.5)	87.1 (2.4)
STG 3, high SE	93.1 (5.0)	89.6 (3.1)	91.3 (2.5)	90.4 (2.2)
STG 3, high SP	89.8 (6.0)	**93.0** (2.6)	**91.4** (2.9)	**92.2** (2.0)

Fig. 4. An example of unfiltered and filtered VF (a), OR (b) and AS (c) rhythms. The first graph of each panel shows the unfiltered ECG, whereas the other two show the filtered ECG for both filtering stages ($N = 4$), coarse filtering ($\lambda_1 = 0.990$) in the middle and fine filtering ($\lambda_2 = 0.999$) in the bottom graphs.

II. Additional examples and experiments for OR rhythms

This section provides additional filtering experiments and examples during mechanical chest compressions. The section was conceived to illustrate how the RLS filter solution, both coarse (λ_1) and fine (λ_2), performs for the subset of organized rhythms. These ex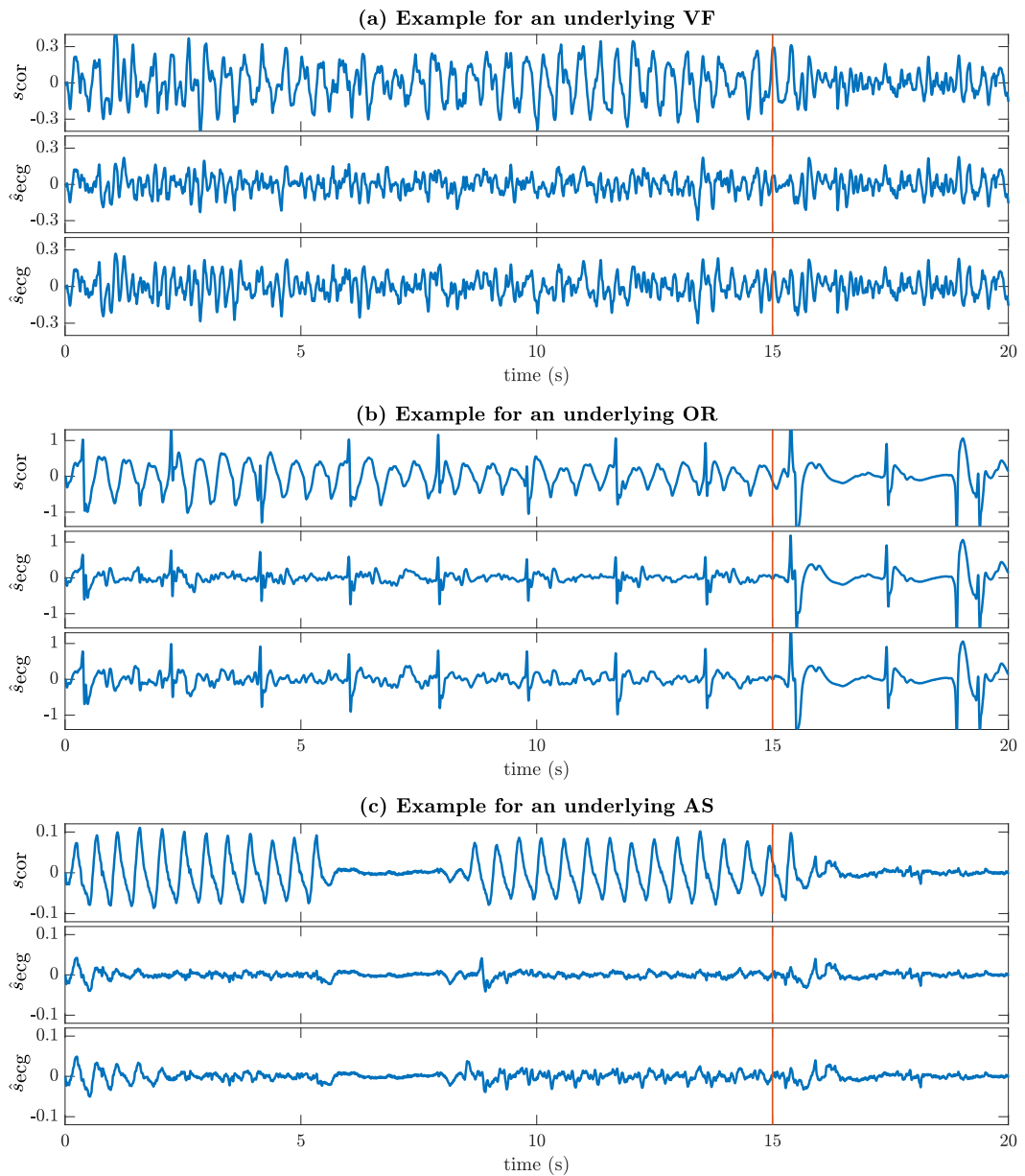periments and examples are important to understand why a multi-stage solution is needed for an accurate rhythm analysis during LUCAS-2 use, and thus extend and complete the description in the main manuscript of the rationale behind the solution. The section is divided in two parts. First, an experiment was conducted using artificial mixtures of LUCAS-2 CPR artifacts and ECG samples from patients in normal sinus rhythms. Second, additional time-domain traces of filtering examples are included for the subset of OR rhythms during LUCAS-2 use.

A. The RLS filter for strongly corrupted normal sinus rhythms

This section describes a controlled experiment to shed light into how the RLS filter performs with normal sinus rhythms. First, we controlled the signal input to the filter by creating artificial mixtures of artifact free ECGs during normal sinus rhythm and pure CPR artifacts recorded during LUCAS-2 use. This setup allows an a priory determination of the corruption level, in terms of signal to noise ratio (SNR), and a posteriori evaluation of how filtering improves the SNR, and of the SP for normal sinus rhythm after filtering in terms of the input corruption level.

1) Data preparation: data was gathered from two sources. First, artifact free ECGs during normal sinus rhythm were extracted from the MIT-BIH arrhythmia database [12]. The database contains 48 cases of 30 minutes, with various arrhythmias, and we extracted a sample per patient with 20 s annotated as normal sinus rhythm. This resulted in 42 samples. Second, we used the CPR artifacts from our LUCAS-2 dataset with AS annotated as underlying rhythm. The assumption in this case is that during the 15 s interval in which chest compressions were delivered the only component of the ECG signal was the CPR artifact, since there is no underlying electrical activity of the heart during AS [13]. From the complete dataset 50 samples were chosen at random, in this way we could have over 2000 different mixtures of clean ECG and CPR artifact for a particular corruption level.

Clean ECGs and CPR artifacts were artificially mixed following a well established model [14], [15]. The artificial mixture or corrupt ECG, $s_{\mathrm{cor}}(n)$, is formed by linearly mixing the artifact free ECG, $s_{\mathrm{ecg}}(n)$, and the mechanical CPR artifact, $s_{\mathrm{cpr}}(n)$, in the following way:

$$s_{\mathrm{cor}}(n) = s_{\mathrm{ecg}}(n) + \alpha s_{\mathrm{cpr}}(n) \tag{7}$$

where the mixture coefficient α is used to fix the SNR in decibel (dB) at the input of the filter, SNR_i, using the following equations:

$$\mathrm{SNR}_i = 10 \log_{10} \frac{P_{\mathrm{ecg}}}{P_{\mathrm{cpr}}} \, (\mathrm{dB})$$

$$\alpha = \sqrt{\frac{P_{\mathrm{ecg}}}{10^{\mathrm{SNR}_i/10}}} \tag{8}$$

where P_{ecg} and P_{cpr} denote the power of the clean ECG and the CPR artifact, respectively.

After filtering the estimated ECG signal, $\hat{s}_{\mathrm{ecg}}(n)$, can be compared to the actual underlying rhythm since in the mixture model is controlled and known to be $s_{\mathrm{ecg}}(n)$. The error signal, $e(n)$, or noise at the output of the filter, and consequently the recovered SNR at the output are simply calculated as:

$$e(n) = s_{\mathrm{ecg}}(n) - \hat{s}_{\mathrm{ecg}}(n) \tag{9}$$

$$\mathrm{SNR}_o = 10 \log_{10} \frac{P_{\mathrm{ecg}}}{P_{\mathrm{e}}} \, (\mathrm{dB}) \tag{10}$$

where P_{e} is the estimated noise power at the output of the filter. The SNR_o calculations were done in the interval spanning from 3.4 s to 13 s to be consistent with the signal interval used for the shock/no-shock decisions. This also avoids including filter transients in the SNR_o calculations, which as shown in the first example of Figure 6 can be large for very low SNR_i.

2) Experimental setup: Every ECG sample was mixed with every CPR artifact at different corruption levels, resulting in 2100 different mixtures for each corruption level. In order to test filter performance strong corruption levels were selected, since rhythm analysis in the absence of artifacts is known to be precise [16]. We tested the following corruption levels, $\mathrm{SNR}_i = -20, -15, -10, -5, 0 \, \mathrm{dB}$. That is, from very strong corruption up to the level in which the ECG and the artifact have the same power.

At each corruption level two filters were applied to obtain the filtered ECG, $\hat{s}_{\mathrm{ecg}}(n)$, the coarse RLS filter ($\lambda_1 = 0.990$) and the fine RLS filter ($\lambda_2 = 0.999$). Figure 5 shows two examples of how the corrupt signals were constructed for two corruption levels, and how filtering revealed the underlying normal sinus rhythm. The output SNR was determined using equations (9) and (10), and the improvement in SNR due to filtering as:

$$\Delta \, \mathrm{SNR} = \mathrm{SNR}_o - \mathrm{SNR}_i \, (\mathrm{dB}) \tag{11}$$

Finally both the corrupt mixtures and the filtered ECG signals were fed to the RAA and the shock/no-shock decisions of the algorithm were used to determine the specificity (SP) before and after the filter was applied.

3) Results: Figure 6 shows $\Delta \, \mathrm{SNR}$ in terms of the corruption level for the two filtering modes. In both cases the filters recovered the underlying rhythm sufficiently well. The worst case is that of the strongest input corruption level, but even for $\mathrm{SNR}_i = -20 \, \mathrm{dB}$ the restored SNR was close to, or above 0 dB. This means that in the estimated ECG, $\hat{s}_{\mathrm{ecg}}$, the underlying rhythm and the artifact would have equal power, despite the very high input corruption level. This results in a recovered ECG with clear QRS complexes, since in the time domain most ECG power is due to these complexes (or large T-waves), as shown in the examples in Figure 5.

The recovered SNR is larger for very high corruption levels ($\mathrm{SNR}_i < -15 \, \mathrm{dB}$) when the coarse filter is used. In this case over-filtering helps since the input signal is dominated by the CPR artifact, as shown in Figure 5 (a). For lower input corruption levels fine filtering produces a more accurate estimate of the underlying rhythm, this is the case in Figure 5 (b). And the difference in favor of fine filtering, in
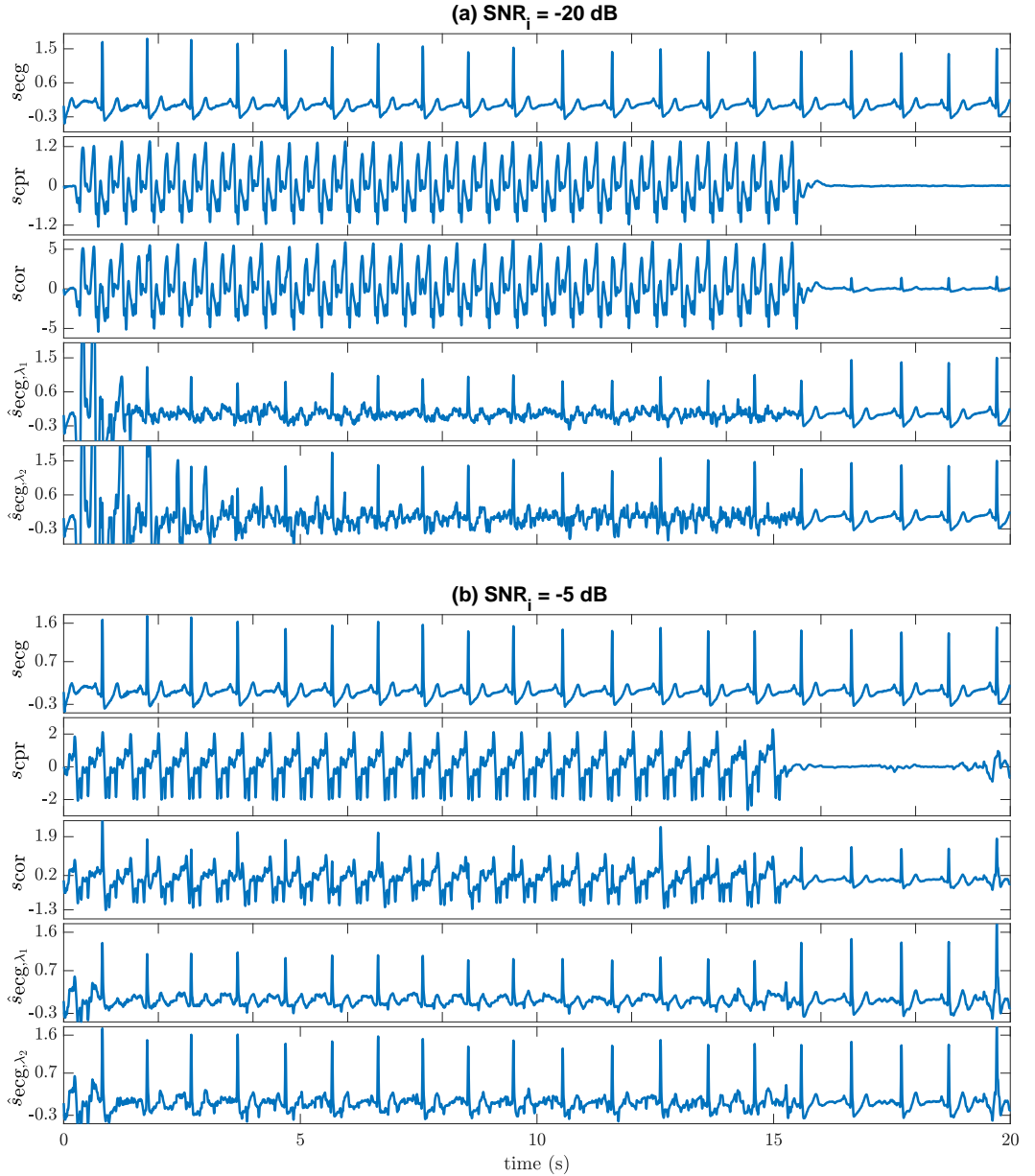
Fig. 5. Two examples of the construction of the artificial mixtures and the effects of RLS filtering for normal sinus rhythm. The top example shows the case of a strong corruption level, while the bottom example corresponds to medium corruption. Coarse filtering (λ_1, fourth subpanel) attenuates QRS amplitudes more than fine filtering (λ_1, fourth subpanel). Fine filtering however leaves a larger filtering residual between QRS complexes.

terms of Δ SNR, increases as the corruption level decreases. For very low corruption levels over-filtering may alter the amplitudes and waveform of the QRS complexes. This is shown in section II-B of these supplementary materials, with actual OHCA examples from the dataset used in the main manuscript.

Finally, table II shows the specificity results before and after filtering for all the input corruption levels and for both filters. As shown in the table there are practically no differences in specificity when using coarse or fine filtering,
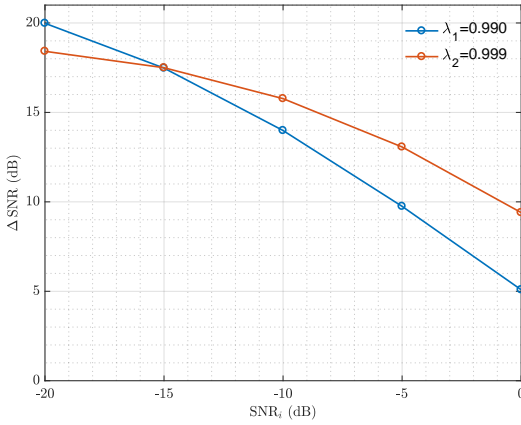
Fig. 6. Improvement in SNR after applying RLS filtering to artificial mixtures of normal sinus rhythm and mechanical CPR artifacts. The improvement is shown for strong corruption levels of the input signal and for the two filter configurations, coarse ($\lambda_1 = 0.990$) and fine filtering ($\lambda_2 = 0.999$).

and the specificity is above 95% for $\text{SNR}_i > -15\,\text{dB}$. The specificity meets the 99% AHA recommendation for normal sinus rhythms when $\text{SNR}_i > -10\,\text{dB}$. So even a single filtering stage is enough to meet AHA recommendations on normal sinus rhythms for most reasonable corruption levels. However, during cardiac arrest normal sinus rhythms are seldom observed during chest compressions, because a patient presenting normal sinus rhythm has recovered circulation and in those cases chest compression therapy is no longer needed. Consequently, the organized rhythms observed during cardiac arrest pose a bigger challenge for rhythm analysis during CPR since they frequently correspond to rhythms with lower heart rates and more aberrant QRS complexes. Figure 7 shows four such examples of OR rhythms recorded during chest compressions delivered by the LUCAS-2 device.

TABLE II
SPECIFICITY BEFORE/AFTER FILTERING.

	specificity (%)		
SNR_i (dB)	Before	RLS-λ_1	RLS-λ_2
-20	82.7	89.9	90.2
-15	83.3	96.9	97.4
-10	84.7	99.6	99.7
-5	89.1	99.8	99.9
0	95.4	100	100

B. Filtering examples for OHCA cases

The aim of this subsection is to provide additional time domain traces of filtering examples that add to the ones shown in the main manuscript. These are examples extracted from the OHCA database, and represent cases in which the LUCAS-2 device was used when the underlying rhythm was organized. These examples show the differences between the coarse (λ_1) filtering used in stage 1 and the fine filtering (λ_2) used in stage 2. It is important to stress that both fine and coarse filtering preserve the VF waveform as was demonstrated in the main manuscript, so the aim here is to show why two filtering stages help improving the accuracy for OR rhythms.

Most frequently, fine filtering reveals the underlying rhythm with smaller waveform and amplitude distortion of the QRS complexes. In general the differences are not large, as can be seen in the first two examples. In both examples the input SNR was large, but filtering revealed the underlying QRS complexes. However, occasionally coarse filtering may remove some of the QRS complexes and result in a disorganized filtered ECG that may be diagnosed as shockable by a RAA. This is the case shown in the third example, in which the input SNR is smaller than in the previous two examples. Finally, when the artifact presents higher frequency harmonics and the underlying OR rhythm has a low heart rate, fine filtering may result in a disorganized filtering residual during the intervals in which the heart rhythm returns to baseline. These residuals may confound the RAA which may diagnose the rhythm as shockable. This is shown in the fourth and last example. Combining fine and coarse filtering, which leave VF unaltered, helps to correctly identify OR in those limiting cases.

Finally, we briefly justify why coarse filtering is used first. The first stage was conceived to maximize the balanced accuracy using a single stage. In this sense, the best choice of filter is the one that better handles both nonshockable rhythm types jointly, that is OR and AS rhythms. The table shows the performance of the coarse and fine filters for all rhythm types when used in a single stage configuration, i.e. the filter followed by the RAA. It also shows the large increase in specificity, without compromising sensitivity, derived from using a two stage filter configuration. Coarse filtering was the best choice in stage 1 because for AS coarse it leaves much smaller filtering residuals while being adequate for most OR cases. In stage 2, once most AS cases have been correctly identified as nonshockable, the fine filter is targeted at identifying the limiting OR cases overfiltered by the coarse filter.

TABLE III
ACCURACY PER RHYTHM TYPE FOR TWO SINGLE STAGE RLS FILTERS
AND THE TWO STAGE RLS FILTER CONFIGURATIONS.

		SP (%)		
stages (γ, λ)	SE (%)	AS	OR	TOT
1-stage (0.0023, 0.990)	98.5	93.7	85.2	87.8
1-stage (0.0023, 0.999)	98.5	78.5	85.7	83.4
2-stage	97.0	95.2	93.4	94.0
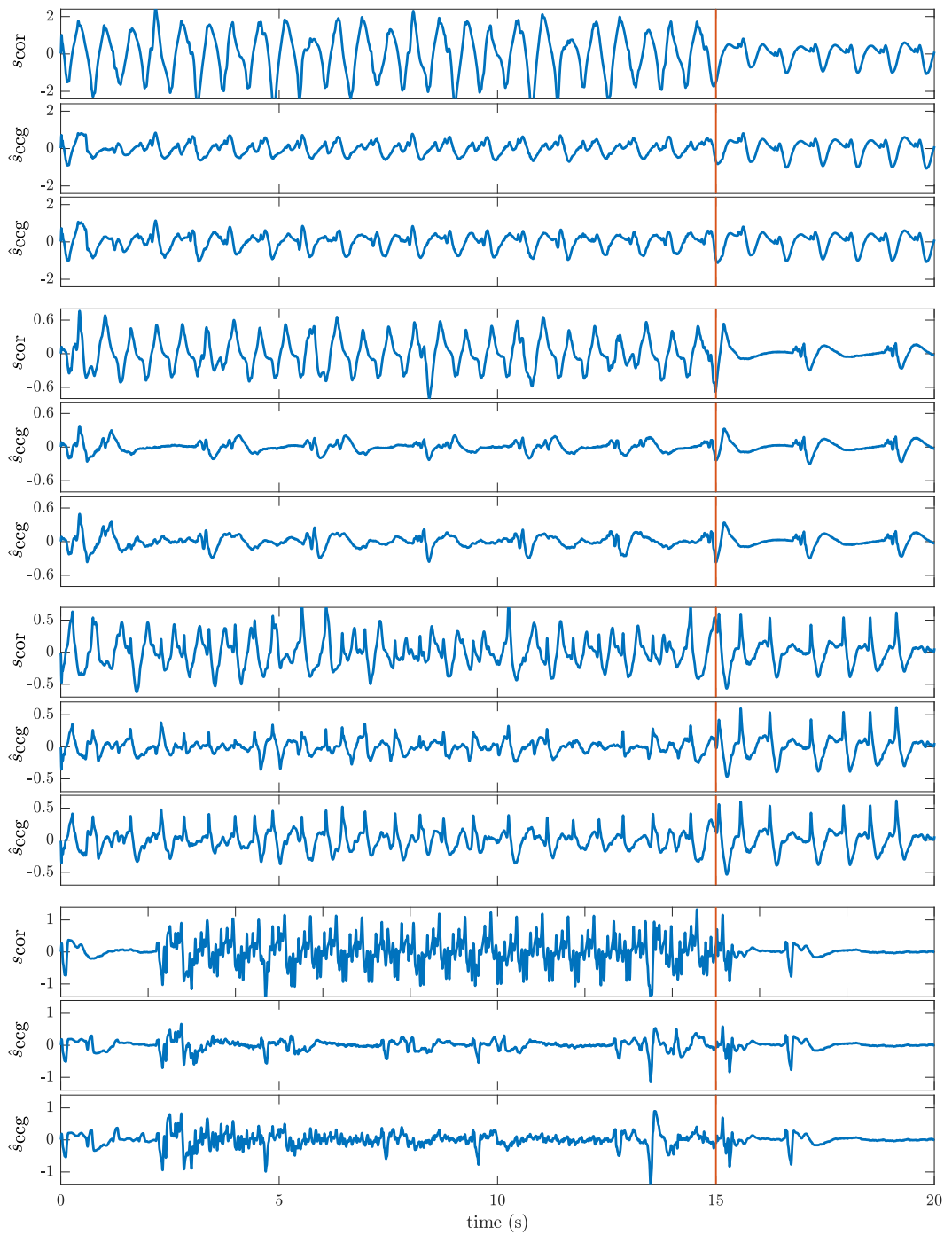
Fig. 7. Four filtering examples extracted from patients in OR. For each example the top panel shows the ECG before filtering, the middle panel the ECG after coarse filtering (λ_1), and the bottom panel the ECG after fine filtering e filtering (λ_2).

REFERENCES

[1] U. Irusta *et al.*, "A least mean-square filter for the estimation of the cardiopulmonary resuscitation artifact based on the frequency of the compressions," *IEEE Trans. Biomed. Eng.*, vol. 56, no. 4, pp. 1052–1062, 2009.

[2] E. Aramendi *et al.*, "Suppression of the cardiopulmonary resuscitation artefacts using the instantaneous chest compression rate extracted from the thoracic impedance," *Resuscitation*, vol. 83, no. 6, pp. 692–698, 2012.

[3] L. Wik *et al.*, "Quality of cardiopulmonary resuscitation during out-of-hospital cardiac arrest." *JAMA*, vol. 293, pp. 299–304, 2005.

[4] J. Kramer-Johansen *et al.*, "Quality of out-of-hospital cardiopulmonary resuscitation with real time automated feedback: a prospective interventional study." *Resuscitation*, vol. 71, pp. 283–292, 2006.

[5] J. Sullivan *et al.*, "A digital filter can effectively remove mechanical chest compression artifact," *Resuscitation*, vol. 85, p. S41, 2014.

[6] E. Aramendi *et al.*, "Filtering mechanical chest compression artefacts from out-of-hospital cardiac arrest data," *Resuscitation*, vol. 98, pp. 41–47, 2016.

[7] J. Eilevstjønn *et al.*, "Feasibility of shock advice analysis during CPR through removal of CPR artefacts from the human ECG," *Resuscitation*, vol. 61, no. 2, pp. 131–141, 2004.

[8] S. Ruiz de Gauna *et al.*, "Rhythm analysis during cardiopulmonary resuscitation: past, present, and future," *Biomed. Res. In.*, vol. 2014, 2014.

[9] R. E. Kerber *et al.*, "Automatic external defibrillators for public access defibrillation: recommendations for specifying and reporting arrhythmia analysis algorithm performance, incorporating new waveforms, and enhancing safety," *Circulation*, vol. 95, no. 6, pp. 1677–1682, 1997.

[10] V. Krasteva *et al.*, "Shock advisory system for heart rhythm analysis during cardiopulmonary resuscitation using a single ECG input of automated external defibrillators," *Ann. Biomed. Eng.*, vol. 38, no. 4, pp. 1326–1336, 2010.

[11] U. Ayala *et al.*, "A reliable method for rhythm analysis during cardiopulmonary resuscitation," *Biomed. Res. In.*, vol. 2014, 2014.

[12] A. L. Goldberger *et al.*, "Physiobank, physiotoolkit, and physionet: components of a new research resource for complex physiologic signals." *Circulation*, vol. 101, pp. E215–E220, 2000.

[13] E. Aramendi *et al.*, "Detection of ventricular fibrillation in the presence of cardiopulmonary resuscitation artefacts," *Resuscitation*, vol. 72, no. 1, pp. 115–123, 2007.

[14] S. O. Aase *et al.*, "CPR artifact removal from human ECG using optimal multichannel filtering," *IEEE Trans. Biomed. Eng.*, vol. 47, no. 11, pp. 1440–1449, 2000.

[15] A. Langhelle *et al.*, "Reducing CPR artefacts in ventricular fibrillation in vitro," *Resuscitation*, vol. 48, no. 3, pp. 279–291, 2001.

[16] U. Irusta *et al.*, "A high-temporal resolution algorithm to discriminate shockable from nonshockable rhythms in adults and children," *Resuscitation*, vol. 83, no. 9, pp. 1090–1097, 2012.

A.1.3 SECOND CONFERENCE PAPER: C2$_1$

Table A.3. Conference paper associated to objective 1.

Publication in international conference
Reference I. Isasi, U. Irusta, E. Aramendi, U.Ayala, E. Alonso, J. Kramer-Johansen, T. Eftestøl,"An accurate shock advise algorithm for use during piston-driven chest compressions", *Proceedings of the Conference IEEE Computing in Cardiology 2018*, vol. 45, pp. 1-4.
Quality indices • **Type of publication**: Indexed Congress in SJR • **Area**: Cardiology and Cardiovascular Medicine • **SJR factor**: 0.202

An Accurate Shock Advise Algorithm for Use During Piston-Driven Chest Compressions

Iraia Isasi[1], Unai Irusta[1], Elisabete Aramendi[1], Unai Ayala[2],
Erik Alonso[3], Jo Kramer-Johansen[4], Trygve Eftestøl[5]

[1] Communications Engineering, University of the Basque Country (UPV/EHU), Bilbao, Spain
[2] Signal Processing and Communications, Mondragon University, Mondragon, Spain
[3] Department of Applied Mathematics, University of the Basque Country (UPV/EHU), Bilbao, Spain
[4] Norwegian National Advisory Unit on Prehospital Emergency Medicine,
Oslo University Hospital and University of Oslo, Norway
[5] Electrical Engineering and Computer Science. University of Stavanger, Stavanger, Norway

Abstract

Mechanically delivered chest compressions induce artifacts in the ECG that can lead to an incorrect diagnosis of the shock advice algorithms implemented in the defibrillators. This forces the rescuer to stop cardiopulmonary resuscitation (CPR) compromising circulation and thus reducing the probability of survival. This paper introduces a new approach for a reliable rhythm analysis during mechanical compressions which consists of an artifact supression filter based on the recursive least squares algorithm, and a shock/no-shock decision algorithm based on machine learning techniques that uses features obtained from the filtered ECG. Data were collected from 230 out-of-hospital cardiac arrest patients treated with the LUCAS CPR device. The underlying rhythms were annotated in artifact-free intervals by consesus of expert resuscitation rhythm reviewers. Shock/no-shock diagnoses obtained through the decision algorithm were compared with the rhythm annotations to obtain the sensitivity (Se), specificity (Sp) and balanced accuracy (BAC) of the method. The results obtained were: 94.7% (Se), 97.1% (Sp) and 95.9% (BAC).

1. Introduction

High quality cardiopulmonary resuscitation (CPR) and early defibrillation are the most influential factors explaining survival from out of hospital cardiac arrest (OHCA)[1]. Current advanced life support guidelines state that minimum interruptions in chest compressions (CCs) are required during CPR to improve the chances of a successful defibrillation[1]. Unfortunately, current defibrillators require interrupting CPR during rhythm analysis because CCs produce artifacts in the ECG that can lead to an incorrect shock/no-shock diagnosis.

Adaptive filtering of the CC artifact has been the major approach to allow rhythm analysis during CCs, ranging from filters that use additional reference signals correlated with the artifact to simpler but less effective filters that analyze the ECG alone[2]. Taking advantage of the quasi-periodic nature of CC artifacts, adaptive filters based on the multiharmonic modelling of the artifact have also been explored[3]. Diagnosing the filtered ECG by a commercial shock advice algorithm (SAA) has become general practice to evaluate the performance of these algorithms[2]. This allows the estimation of the Sensitivity (Se) and Specificity (Sp), that is the proportion of correctly identified shockable and nonshockable rhythms, respectively. However, the SAAs used were originally designed to analyze artifact-free ECG and not to diagnose the filtered ECG.

Most rhythm analysis methods have been devoted to manual CPR[2]. However recently methods to analyze the rhythm during mechanical CCs delivered by piston driven devices have been developed[4–6]. These methods were based on the SAA of commercial AEDs[7, 8] for the shock advise decision, and either showed poor performance[4, 5] or involved several filtering stages and excessive computational demands[6].

This study proposes a method for a reliable shock advise during mechanical CCs provided by the LUCAS-2 (Physio Control/Jolife AN, Lund, Sweeden) piston driven device. The method combines an adaptive filter based on the recursive least-squares (RLS) algorithm to remove the artifact and a shock/no-shock decision algorithm based on a support vector machine (SVM) classifier to diagnose the rhythm after filtering.

2. Materials and methods
2.1. Materials

The data used for this study were gathered by the emergency services of Oslo and Akershus (Norway) using LifePak 15 defibrillators (Physio-Control Inc., Redmond, WA, USA). ECG and thoracic impedance (TI) signals were recorded and resampled to $250\,\mathrm{Hz}$ (see [4] for a detailed description of the data). The ECG was band limited to $0.5\text{-}40\,\mathrm{Hz}$ using an order 8 Butterworth filter.

The dataset extracted from this data consisted of 1045 segments of $20\,\mathrm{s}$ from 230 patients, whereof 201 were shockable rhythms and 844 nonshockable (270 asystole, 574 organized). The first $15\,\mathrm{s}$ of the segment included continuous CCs and were used to develop our solution. The last $5\,\mathrm{s}$, free of artifact, were used by the expert reviewers to annotate the patient's underlying rhythm as shockable/nonshockable and used as ground truth. Figure 1 shows an example of a $20\,\mathrm{s}$ ECG segment corresponding to an underlying nonshockable rhythm.

2.2. Methods
2.2.1. Filtering the CC Artifact

CC artifacts were removed from the ECG using a RLS filter based on the multiharmonic Fourier modelling of the artifact, the filter is described in detail in [5, 6]. In brief, during CCs the artifact is modelled as an N-term Fourier series with time varying coefficients ($a_k(n)$ and $b_k(n)$) and a constant fundamental frequency, $f_0 = 1.694\,\mathrm{Hz}$ (about 101 compressions min^{-1}), which is fixed by the LUCAS-2:

$$s_{cc}(n) = \sum_{k=1}^{N} a_k(n)\cos(k2\pi f_0 n T_s) + \qquad (1)$$
$$b_k(n)\sin(k2\pi f_0 n T_s) \qquad (2)$$

where T_s is the sampling period. The RLS filter estimates the time-varying coefficients ($a_k(n)$ and $b_k(n)$) and subtracts the estimated artifact from the corrupted ECG (s_{cor}) to give the filtered ECG ($\hat{s}_{ecg}$), see Figure 1.

In this paper we used the optimal configuration of the filter as described in [6], which has two degrees of freedom. First, a parameter to decide the number of harmonics to be used in the method, $\gamma = 0.0023$ which roughly corresponds to an average number of $N = 23$ harmonics. Second, the RLS solution's forgetting factor, $\lambda = 0.9899$.

2.2.2. Feature extraction

A set of 59 shock/no-shock decision features were extracted from the filtered ECG. Only the interval from $4\,\mathrm{s}$ to $12\,\mathrm{s}$ (see the highlighted interval in figure 1) was used for feature extraction. First $4\,\mathrm{s}$ were left out to avoid RLS filtering transients. These features have been comprehensively studied and described [9–11] to classify OHCA rhythms. The features are:

- **Time domain features**. TCI, TCSC, Exp, Expmod, MAV, count1, count2, count3, x1, x2 and bCP [9].
- **Spectral domain features**. vFleak, M, A1, A2, A3, x3, x4, x5, bWT and bW [9]; FuzzEn [11, 12].
- **Wavelet domain features**. IQR ($d_{3\text{-}7}$), Var ($d_{3\text{-}7}$), first quartile of $d_{3\text{-}7}$ (FQ ($d_{3\text{-}7}$)), IQR ($s(n)$), IQR ($\dot{s}(n)$), IQR ($\ddot{s}(n)$), $\mu_{2\text{-}4,s}$, $\mu_{3\text{-}4,\dot{s}}$, $a_{1\text{-}4}$ and σ_v^2 [10]; Li feature [9].
- **Complexity features**. CM, CVbin, abin, Frqbin, Kurt, PSR, HILB and SamEn [11, 12].

2.2.3. Architecture of the model and evaluation

A 10-fold cross-validation (CV) architecture was used for feature selection and model optimization and assessment. Folds were partitioned patient-wise and ensuring that the rhythm prevalences matched (to at least 90%) the prevalences for shockable and nonshockable

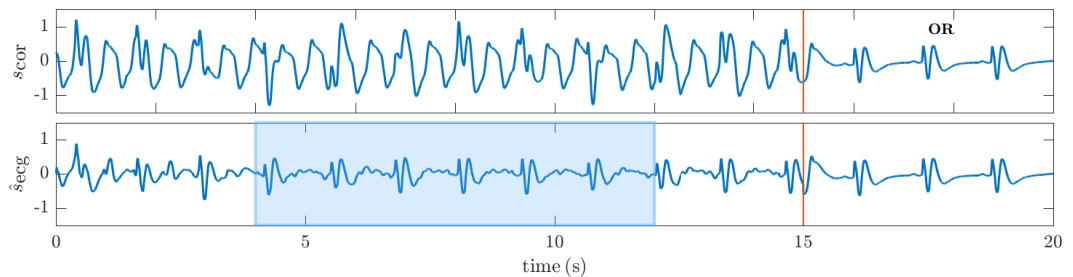Figure 1. Example of a $20\,\mathrm{s}$ episode of the database. The top panel shows the ECG of a patient with a nonshockable organized rhythm (OR): the first $15\,\mathrm{s}$ are corrupted by the CC artifact, and the last $5\,\mathrm{s}$ are free of artifact showing the patient's underlying rhythm. The bottom panel shows the filtered ECG which reveals the patient's rhythm during CCs.

Page 2

rhythms seen in the whole dataset (quasi-stratified). The main classifier used for the shock/no-shock decision was optimized using the most relevant subset of k features selected in the training data and used to classify the test segments. These diagnoses were compared with the ground truth to obtain the performance of the solution in terms of Se, Sp and BAC (the mean value of Se and Sp).

2.2.4. Feature selection

We used the ReliefF [13] feature selection method to choose the k features used in the main classifier. This supervised filter-based method is an extension of the well-known Relief [14] for multiclass and regression problems. The key idea of Relief is to estimate the relevance of features according to how well their values distinguish between the instances of the same and different classes that are near to each other (neighbours). Whereas Relief only relies in a single neighbour to calculate the importance of the features, RefliefF considers the contribution of several neighbours, making the algorithm more robust dealing with noisy data. In this study the number of neighbours was fixed to 50. Feature selection was performed for $k = 1, ...59$ so as to find which value of k offered the best compromise between dimensionality and performance.

2.2.5. Shock/no-shock classification algorithm

Support Vector Machine (SVM) classifier with a gaussian kernel was used for the shock/no-shock decision. Selecting an optimal SVM model involves selecting two parameters: γ and C, the width of the Gaussian Kernel and the flexibility of the decision boundary, respectively [15]. The values of C and γ that maximized the BAC were determined in the 10-fold CV loop doing a 25x25 logaritmic grid search in the ranges $10^{-1} < C < 10^{1.5}$ and $10^{-3} < \gamma < 10$. The procedure was repeated 50 times to estimate the statistical distributions of the performance metrics and the optimal parameters of the SVM model. These distributions will be reported as mean (95% CI, confidence interval).

3. Results

Figure 2 shows the mean values of Se, Sp and BAC obtained in the 50 random repetitions as a function of the number of features (k) selected in the training data. The best compromise between model simplicity and performance was obtained for $k = 24$ as the mean BAC slightly increases for a greater value of k. In this working point ($k = 24$), the mean value of the optimal configuration (C/γ) of the SVM classifier was 10.62/0.02 obtaining a Se, Sp and BAC of 94.7% (93.5-95.6), 97.1%

(95.5-97.8) and 95.9% (95.4-96.5), respectively. This is a considerable improvement over using the RLS filter followed by a commercial SAA [7, 8], which resulted in a Se, Sp and BAC of 98.1%, 87.0%, 92.5% respectively.
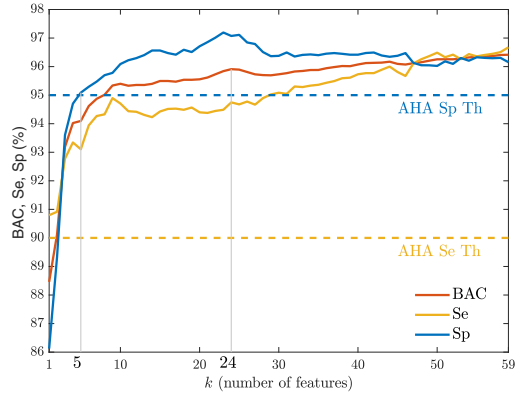
Figure 2. Mean values of the performance metrics as a function of the number of features (k) used in the classifier.

However, as shown in Figure 2, American Heart's Association's (AHA) requirements for a reliable rhythm diagnosis (Se>90% and Sp>95%) are met with as few as 5 features. In fact, the distributions of Se, Sp and BAC for $k = 5$ were: 93.1% (90.5-95.5), 95.1% (94.1-95.9) and 94.1% (92.7-95.4). Table 1 shows the 10 features selected in the 50 random repetitions of the 10-fold CV for $k = 5$:

Feature	N	Feature	N_f
x1	500	A1	169
vfleak	494	IQR (d_3)	86
x2	491	count3	75
x4	414	IQR (d_2)	24
FQ (d_3)	246	IQR (d_1)	1

Table 1. The features selected in 50 random repetitions ranked by the number of times (N_f) they were selected for $k = 5$.

4. Discussion

This work introduces a new method for a reliable rhythm analysis during mechanical CCs. It consists of an adaptive RLS filter designed to remove the CC artifact and a shock/no-shock decision algorithm using multiple ECG features and a state of the art machine learning classifiers. The results show that the best trade-off between model dimensionality and performance was obtained using 24 features, obtaining a BAC of 95.9%. However, AHA compliant performance was obtained with only 5 features.

Page 3

In our previous work [6] a single filtering stage followed by a commercial SAA yielded Se, Sp and BACs of 98.1%, 87.0% and 92.5% in this same dataset. By using a machine learning approach we were able to boost the BAC by 3.4 points with an increase in Se and Sp of -3.4 and 10.1 points respectively. This shows that it is possible to accurately decide whether to shock the patient during mechanical CCs using a single filtering stage. In the past we obtained AHA compliant results using 2 filtering stages and 3 decision stages [6], with lower BAC and higher computational demands.

In conclusion, the method presented in this paper is, to the best of our knowledge, the computationally cheapest method for a reliable rhythm analysis during mechanical CCs, according to AHA recommendations.

Acknowledgements

References

[1] Perkins GD, Handley AJ, Koster RW, Castrén M, Smyth MA, Olasveengen T, Monsieurs KG, Raffay V, Gräsner JT, Wenzel V, et al. European resuscitation council guidelines for resuscitation 2015: Section 2. adult basic life support and automated external defibrillation 2015;.

[2] Ruiz de Gauna S, Irusta U, Ruiz J, Ayala U, Aramendi E, Eftestøl T. Rhythm analysis during cardiopulmonary resuscitation: past, present, and future. BioMed Research International 2014;2014.

[3] Irusta U, Ruiz J, de Gauna SR, Eftestøl T, Kramer-Johansen J. A least mean-square filter for the estimation of the cardiopulmonary resuscitation artifact based on the frequency of the compressions. IEEE Transactions on Biomedical Engineering 2009;56(4):1052–1062.

[4] Aramendi E, Irusta U, Ayala U, Naas H, Kramer-Johansen J, Eftestøl T. Filtering mechanical chest compression artefacts from out-of-hospital cardiac arrest data. Resuscitation 2016;98:41–47.

[5] Isasi I, Irusta U, Aramendi E, Ayala U, Alonso E, Kramer-Johansen J, Eftestøl T. Removing piston-driven mechanical chest compression artefacts from the ECG. Computing 2017;44:1.

[6] Isasi I, Irusta U, Aramendi E, Ayala U, Alonso E, Kramer-Johansen J, Eftestol T. A multistage algorithm for ECG rhythm analysis during piston driven mechanical chest compressions. IEEE Transactions on Biomedical Engineering 2018;.

[7] Irusta U, Ruiz J, Aramendi E, de Gauna SR, Ayala U, Alonso E. A high-temporal resolution algorithm to discriminate shockable from nonshockable rhythms in adults and children. Resuscitation 2012;83(9):1090–1097.

[8] Irusta U, Ruiz J. An algorithm to discriminate supraventricular from ventricular tachycardia in automated external defibrillators valid for adult and paediatric patients. Resuscitation 2009;80(11):1229–1233.

[9] Figuera C, Irusta U, Morgado E, Aramendi E, Ayala U, Wik L, Kramer-Johansen J, Eftestøl T, Alonso-Atienza F. Machine learning techniques for the detection of shockable rhythms in automated external defibrillators. PloS One 2016;11(7):e0159654.

[10] Rad AB, Eftestøl T, Engan K, Irusta U, Kvaløy JT, Kramer-Johansen J, Wik L, Katsaggelos AK. ECG-based classification of resuscitation cardiac rhythms for retrospective data analysis. IEEE Transactions on Biomedical Engineering 2017;64(10):2411–2418.

[11] Chicote B, Irusta U, Alcaraz R, Rieta JJ, Aramendi E, Isasi I, Alonso D, Ibarguren K. Application of entropy-based features to predict defibrillation outcome in cardiac arrest. Entropy 2016;18(9):313.

[12] Chicote B, Irusta U, Aramendi E, Alcaraz R, Rieta J, Isasi I, Alonso D, Baqueriza M, Ibarguren K. Fuzzy and sample entropies as predictors of patient survival using short ventricular fibrillation recordings during out of hospital cardiac arrest. Entropy 2018;20:591.

[13] Kononenko I. Estimating attributes: analysis and extensions of RELIEF. In European conference on machine learning. Springer, 1994; 171–182.

[14] Kira K, Rendell LA. A practical approach to feature selection. In Machine Learning Proceedings 1992. Elsevier, 1992; 249–256.

[15] Ben-Hur A, Weston J. A user's guide to support vector machines. In Data mining techniques for the life sciences. Springer, 2010; 223–239.

Address for correspondence:

Name: Iraia Isasi Liñero
Full postal address: Ingeniero Torres Quevedo Plaza, 1, 48013 Bilbo, Bizkaia, Spain
E-mail address: iraia.isasi@ehu.eus

A.1.4 SECOND JOURNAL PAPER: J2$_1$

Table A.4. Journal paper associated to objective 1.

Publication in international magazine

Reference	I. Isasi, U. Irusta, A. Elola, E. Aramendi, U.Ayala, E. Alonso, J. Kramer-Johansen, T. Eftestøl,"A machine learning shock decision algorithm for use during piston-driven chest compressions", *IEEE Transactions on Biomedical Engineering*, vol. 66, no. 6, pp. 1752-1760, 2019.
Quality indices	• **Type of publication:** Journal paper idexed in JCR and SJR • **Area:** Biomedical Engineering • **Ranking:** 14/87 (Q1) based on JCR 2019 • **Impact factor SJR:** 1.410 • **Impact factor JCR:** 4.424

A Machine Learning Shock Decision Algorithm for Use During Piston-Driven Chest Compressions

Iraia Isasi ⓘ, Unai Irusta ⓘ, *Member, IEEE*, Andoni Elola, Elisabete Aramendi, Unai Ayala ⓘ,
Erik Alonso ⓘ, Jo Kramer-Johansen ⓘ, and Trygve Eftestøl, *Member, IEEE*

Abstract—Goal: Accurate shock decision methods during piston-driven cardiopulmonary resuscitation (CPR) would contribute to improve therapy and increase cardiac arrest survival rates. The best current methods are computationally demanding, and their accuracy could be improved. The objective of this work was to introduce a computationally efficient algorithm for shock decision during piston-driven CPR with increased accuracy. *Methods:* The study dataset contains 201 shockable and 844 nonshockable ECG segments from 230 cardiac arrest patients treated with the LUCAS-2 mechanical CPR device. Compression artifacts were removed using the state-of-the-art adaptive filters, and shock/no-shock discrimination features were extracted from the stationary wavelet transform analysis of the filtered ECG, and fed to a support vector machine (SVM) classifier. Quasi-stratified patient wise nested cross-validation was used for feature selection and SVM hyperparameter optimization. The procedure was repeated 50 times to statistically characterize the results. *Results:* Best results were obtained for a six-feature classifier with mean (standard deviation) sensitivity, specificity, and total accuracy of 97.5 (0.4), 98.2 (0.4), and 98.1 (0.3), respectively. The algorithm presented a five-fold reduction in computational demands when compared to the best available methods, while improving their balanced accuracy by 3 points. *Conclusions:* The accuracy of the best available methods was improved while drastically reducing the computational demands. *Significance:* An efficient and accurate method for shock decisions during mechanical CPR is now available to improve therapy and contribute to increase cardiac arrest survival.

Index Terms—Support vector machine (SVM), machine learning, stationary wavelet transform (SWT), cardiac arrest, cardiopulmonary resuscitation (CPR), electrocardiogram (ECG), mechanical chest compressions, piston-driven compressions, shock decision algorithm.

I. INTRODUCTION

HIGH quality cardiopulmonary resuscitation (CPR) and early defibrillation are key for the survival of out-of-hospital cardiac arrest (OHCA) patients [1]. During CPR, chest compressions and ventilations should be delivered according to international guidelines [1]. Interruptions in chest compressions decrease coronary perfusion pressure [2], and may compromise the survival of the patient [3]. Chest compressions induce an artifact in the ECG, so current defibrillators instruct the rescuers to stop chest compressions for a reliable shock decision [4].

Many efforts have been made to allow a reliable shock decision during CPR, with solutions that go from analyzing the rhythm during ventilation pauses [5], [6] to ad-hoc algorithms designed for a reliable shock decision in the presence of chest compression artifacts [7]–[9]. The best known solutions are based on adaptive filters that remove the CPR artifact before using the shock decision algorithm of the defibrillator. These filters model the artifact using additional reference channels recorded by the defibrillator such as compression depth, thoracic impedance, chest acceleration, or chest force/pressure. Several solutions have been proposed including Wiener filters [10], Matching Pursuit algorithms [11], [12], Kalman filters [13], [14], Gabor filters [15], Least Mean Squares (LMS) filters [16]–[18] and Recursive Least Squares (RLS) filters [19]. Reference channels are not always available and may increase the cost of defibrillators, fortunately filters based only on the frequency of chest compressions are as effective as complex filters based on several reference channels [16], [20]. For manual CPR, solutions based on adaptive filters followed by the shock decision algorithms of commercial defibrillators do not meet the accuracy requirements of the American Heart Association (AHA) [4]. The sensitivity (Se) for shockable rhythms is above the minimum 90% recommendation, but the

I. Isasi is with the Department of Communications Engineering, University of the Basque Country UPV/EHU, 48013 Bilbao, Spain (e-mail: iraia.isasi@ehu.eus).

U. Irusta, A. Elola, and E. Aramendi are with the Department of Communications Engineering, University of the Basque Country UPV/EHU.

U. Ayala is with the Department of Signal Processing and Communications, Mondragon University.

E. Alonso is with the Department of Applied Mathematics, University of the Basque Country UPV/EHU.

J. Kramer-Johansen is with the Norwegian National Advisory Unit on Prehospital Emergency Medicine (NAKOS) and the Department Of Anaesthesiology, Oslo University Hospital and University of Oslo.

T. Eftestøl is with the Department of Electrical Engineering and Computer Science, University of Stavanger.

specificity (Sp) for nonshockable rhythms is below the minimum recommended value of 95%. Filtering residuals have been identified as the main confounding factor for the shock decision algorithms of commercial defibrillators [12], [21], which are designed to classify ECGs free of artifacts [22].

Mechanical CPR is becoming increasingly popular to treat OHCA patients, even if it has not shown benefits in survival [23]–[25]. Mechanical devices guarantee high quality chest compressions, and have become important in scenarios where manual CPR is impractical, such as during transport or invasive procedures [24], [26]–[28]. There are two families of mechanical compressors available: pneumatically driven pistons and load distributing bands. According to the resuscitation guidelines the most popular/widespread devices are the LUCAS-2 (Physio-Control Inc/Jolife AB, Lund, Sweeden) piston-driven device and the Autopulse (Zoll Circulation, Chelmsford, Massachusetts, USA) load distributed band [29]. This study focuses on the LUCAS-2 device, whose impact on survival has been thoroughly studied on two of the three largest randomized controlled trials on mechanical chest compression devices [23], [25].

Mechanical chest compression artifacts have larger amplitudes and more harmonics than manual CPR artifacts [30], but their frequency is fixed and known [19]. So the methods to remove manual CPR artifacts have to be recast for piston-driven devices. In the last few years, methods based on comb filters [30], [31], LMS filters [30] and RLS filters [19] have been introduced. Unfortunately these filters followed by the shock decision algorithms of commercial defibrillators were strongly affected by filtering residuals and did not meet AHA goals [30]. Recently, a multi stage algorithm based on two RLS filters and three decision algorithms has been proven to meet the AHA Se/Sp goals [19], albeit with a complex solution and a high computational cost. There is a need to simplify the algorithms that allow an accurate shock decision during piston-driven chest compressions.

This study introduces a new method for shock decision during piston-driven compressions based on an adaptive filter followed by a machine learning algorithm designed to classify the filtered ECG. The machine learning algorithm learns the characteristics of the filtered ECG, including those of the filtering residuals that confound the shock decision algorithms designed for artifact free ECGs. This solution considerably simplifies the best current multistage solution, and improves its accuracy with a much lower computational cost. The paper is organized as follows: the study dataset is described in Section II; feature engineering including CPR artifact filtering, the Stationary Wavelet Transform (SWT) and feature extraction are described in Section III; Section IV describes the architecture used for feature selection and the optimization and evaluation of the classifier. Finally, results, conclusions and discussion are presented in Sections V to VI.

II. STUDY DATASET

The dataset used in this study was collected and annotated for a previous study, so further details on data collection and preparation are available in [19], [30]. In brief, data comes from 263 OHCA patients treated with the LUCAS-2 device by the Oslo and Akershus (Norway) emergency services between July 2012 and December 2013. Signals including ECG and thoracic impedance were recorded using the Lifepak 15 monitor-defibrillator (Physio Control, Redmond, WA, USA), exported to an open matlab format for processing, and resampled to 250 Hz. A 50 Hz notch filter was used to remove powerline interferences from the ECG.

The complete episodes were reviewed and 20-s segments were extracted for studies on mechanical CPR artifact removal. These segments, like the ones shown in Fig. 1, contain an initial 15-s interval during LUCAS-2 use, followed by a 5-s interval without compressions. Ground truth shock/no-shock decisions were adjudicated by consensus between two specialists on cardiac arrest data, a clinical researcher and a biomedical engineer, who inspected the 5-s artifact-free intervals. Nonshockable rhythms included organized rhythms (OR) and asystole (AS), and shockable rhythms were ventricular fibrillation (VF) and ventricular tachycardia (VT). The initial 15-s intervals were used to develop and test the shock decision methods during mechanical compressions. The final dataset contained 1045 20-s segments from 230 patients, whereof 201 were shockable (62 patients) and 844 were nonshockable (209 patients). For an extended description of the dataset and the annotation process consult [19], [30].

III. FEATURE ENGINEERING

Shock/no-shock decision features were extracted in three phases. First an adaptive CPR artifact filter was used to remove chest compression artifacts and obtain the filtered ECG, $\hat{s}_{ecg}(n)$, then a wavelet analysis provided the denoised signal, $\hat{s}_{den}(n)$, and the subband decomposition. Finally features were extracted from $\hat{s}_{den}(n)$ and the subband components. Filtering and wavelet analysis (denoising and the most relevant subband) are illustrated in Fig. 1 for a shockable and a nonshockable rhythm.

A. CPR Artifact Filtering

During compressions the corrupt ECG, $s_{cor}(n)$, was assumed to follow an additive artifact model [10], [32]:

$$s_{cor}(n) = s_{ecg}(n) + s_{cc}(n) \tag{1}$$

where $s_{ecg}(n)$ is the ECG containing the underlying rhythm and $s_{cc}(n)$ the chest compression artifact. Chest compressions given by the LUCAS-2 device have a constant rate of $100 \pm 2 \, \text{min}^{-1}$ ($f_0 = 1.694 \, \text{Hz}$), and a depth of 4.0–5.3 cm (depending on the chest height), with a 50% duty cycle at a fixed position on the chest. The pattern of the artifact is therefore quasi-periodic and can be represented as an N term Fourier series of fixed frequency and slowly time varying amplitudes:

$$s_{cc}(n) = A(n) \sum_{k=1}^{N} a_k(n) \cos(k\omega_0 n) + b_k(n) \sin(k\omega_0 n) \tag{2}$$
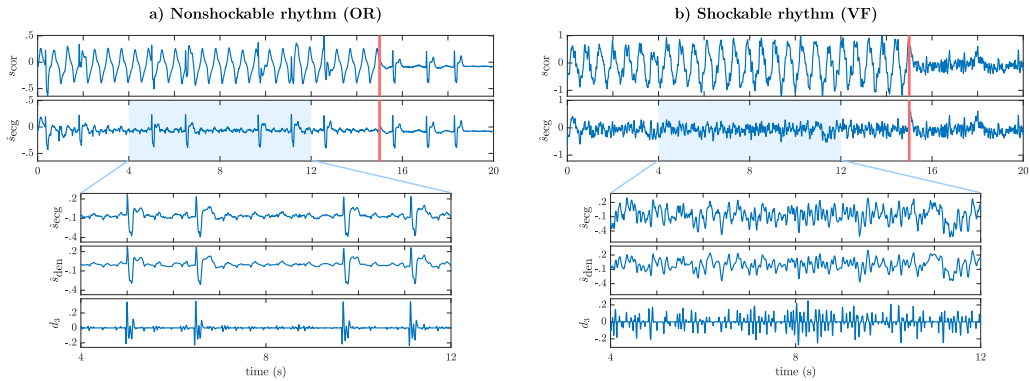
Fig. 1.   Two examples of 20-s ECG segments corresponding to a patient presenting a nonshockable rhythm (example a) and to a patient presenting a shockable rhythm (example b). The top panel depicts the corrupt ECG, $s_{cor}(n)$, and the panel below the ECG after adaptive filtering. The top panel has two intervals, the initial 15-s in which the chest compression artifact is visible, and the last 5-s without artifact in which the underlying rhythm is visible. Finally, the three panels at the bottom zoom in on the 8-s interval used by the shock decision algorithm, and show the filtered ECG, and two significant components obtained from the wavelet analysis of the filtered ECG: the denoised ECG, $\hat{s}_{den}(n)$, and the detail 3 coefficient, d_3.

where $\omega_0 = 2\pi f_0/f_s$ is the fundamental frequency of the LUCAS-2 device and f_s the sampling frequency. The amplitude envelope $A(n)$ was introduced to differentiate intervals with ($A = 1$) and without ($A = 0$) compressions.

In this work two adaptive methods, LMS [16] and RLS [19] filters, were examined to estimate the time varying in-phase, $a_k(n)$, and quadrature, $b_k(n)$, amplitudes. For each filter two degrees of freedom were adjusted: N the number of harmonics of the artifact model and μ/λ the coarseness of the filter [16], [19]. N can also be interpreted as the order of the filter. It determines the number of filter coefficients, which is $2N$ since there are a cuadrature and in-phase coefficient per harmonic. The coarseness of the filter is either μ, the step size of the LMS filter, or λ the forgetting factor of the RLS filter. Both these values offer a compromise between tracking capabilities and misadjustment and stability of the filter. A small forgetting factor in the RLS filter or a large step size in the LMS filter mean that a bigger change can occur in the filter coefficients for each new sample, i.e. a more coarse filter [16], [19]. This produces adaptive filters that follow changes in the input signal better, but also that filter coefficients can increase without bound if changes accumulate, resulting in an unstable filter.

B. Stationary Wavelet Transform

Feature extraction was based on the wavelet decomposition of the filtered ECG. Previous studies on OHCA rhythm classification have successfully applied feature extraction based on the Discrete Wavelet Transform (DWT) [33]. We chose instead a Stationary Wavelet Transform (SWT) approach [34], [35]. Unlike the DWT, the SWT is shift-invariant and better suited for edge detection, fiducial point location or denoising [36], [37]. The SWT is based on the same dyadic decomposition as the DWT, a typical architecture is shown in Fig. 2. Shift invariance is achieved by upsampling the filters instead of sub-sampling the signal at each level of decomposition. The DWT scaling and wavelet filters for signal decomposition, $g_0(n)$ and $h_0(n)$, are
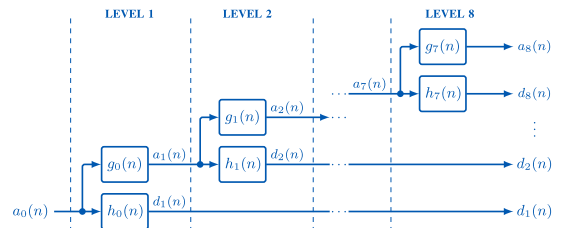
Fig. 2.   SWT implementation for eight levels of decomposition.

a pair of quadrature mirror lowpass and highpass filters. The filters at stage j are obtained by upsampling the original filters by a factor of 2^j, that is:

$$h_j(n) = (h_0 \uparrow 2^j)(n) = \begin{cases} h_0\left(\frac{n}{2^j}\right) & n = k \cdot 2^j \\ 0 & n \neq k \cdot 2^j \end{cases} \quad (3)$$

The detail, $d_j(n)$, and approximation, $a_j(n)$, coefficients at all levels from $j = 1, \ldots, J$ are then recursively obtained:

$$a_0(n) = \hat{s}_{ecg}(n) \quad (4)$$

$$a_{j+1}(n) = g_j(n) * a_j(n) \quad (5)$$

$$d_{j+1}(n) = h_j(n) * a_j(n) \quad (6)$$

where $*$ stands for convolution. The filter coefficients depend on the mother wavelet used. In this work a Daubechies-2 mother wavelet was adopted because it produced the best results (see supplementary materials). The filters for reconstruction are obtained by time reversion: $\overline{g}_j(n) = g_j(-n)$ and $\overline{h}_j(n) = h_j(-n)$. Therefore, the original signal can be reconstructed from the level J coefficients (ISWT) by recursively applying [35]:

$$a_{j-1}(n) = \tfrac{1}{2}\left(\overline{g}_j(n) * a_j(n) + \overline{h}_j(n) * d_j(n)\right) \quad (7)$$

from $j = J, \ldots, 1$.

Eight decomposition levels ($J = 8$) were used to generate nine sets of coefficients, a_8 and $d_8, \ldots d_1$. A signal interval of $M = 2048$ samples was analyzed, for a sampling frequency of $f_s = 250$ Hz it included the 8-s interval of the filtered ECG highlighted in Fig. 1. Since the analysis is based on a dyadic decomposition in which the available bandwidth is split in two at each successive decomposition level, and considering that the bandwidth of interest in defibrillators is commonly between 0.5–30 Hz, only detail coefficients d_3-d_8 were kept and d_1, d_2 and a_8 were set to zero [33]. A soft denoising was then applied to d_3-d_8 using a fixed treshold, ρ, and single estimation of level noise based on first-level detail coefficients [38]:

$$\rho = 1.483 \cdot \text{MAD}(d_1)\sqrt{2 \ln M} \qquad (8)$$

where $\text{MAD}(d_1)$ is the median absolute deviation of d_1. Finally, the denoised d_3-d_8 coefficients were used in equation (7) to reconstruct $\hat{s}_{\text{den}}(n)$ in the 0.5–31.25 Hz frequency range.

C. Feature Extraction

The denoised signal, $\hat{s}_{\text{den}}(n)$, and the detail coefficients, d_3-d_8, were used to obtain a set of 38 features for the shock decision algorithm, selected from the literature on the topic [33], [39]–[51].

The first 18 features were the interquartile range (IQR), first quartile (FQR) and the sample entropy (SampEn) of the detail coefficients d_3-d_8 [33]. The remaining 20 features were computed from $\hat{s}_{\text{den}}(n)$, and constitute a comprehensive set of features from the available methods on shock decision algorithms that included time domain, frequency domain and signal complexity characterizations of the ECG. The extracted features were TCSC [39], Expmod [40], MAV [41], count1-count3 [42], x1-x2 [43], bCP and bWT [44], A1-A3 [45], VFleak [46], SampEn [47], [48], the number of peaks in the 8-s interval (Np) [33], HILB [51], CM [50], Kurt and Frqbin [49]. A detailed description can be found in the references given above, and a Matlab implementation of the features derived from the denoised ECG is available in: https://github.com/FelipeURJC/ohca-vs-public-dbs/tree/master/ecg parameterscomputation/parameters.

IV. ARCHITECTURE OF THE MODEL AND EVALUATION

A nested cross-validation (CV) architecture was used for feature selection, and classifier hyperparameter optimization, and model assessment, as shown in Fig. 3. In the inner loop features were selected using a wrapper approach in a 5-fold CV [52]. In the outer loop, 10-fold CV was used for hyperparameter optimization and model assessment. Both inner and outer folds were partitioned patient-wise in a quasi-stratified way, by ensuring that the shock/no-shock case prevalences matched to at least 85% those of the whole dataset. The performance of the method was evaluated by comparing the shock/no-shock decisions of the classifier with ground truth labels in the outer test set. The following metrics were computed: Se, Sp, accuracy (Acc) and the Balanced Accuracy (BAC), i.e. the mean value of Se and Sp.
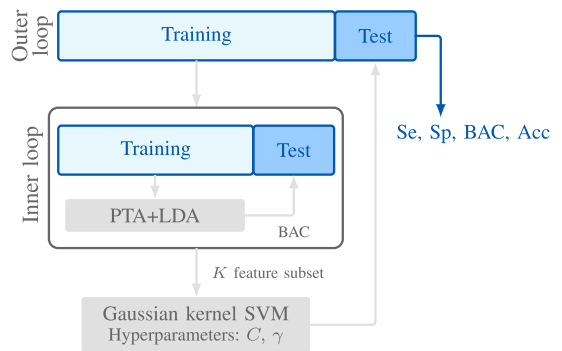
Fig. 3. Nested cross-validation architecture used for feature selection and for model optimization and evaluation.

A. Feature Selection

In the inner loop, a PTA(4, 3) (plus 4, take away 3) feature selection algorithm was used [53], [54]. The criterion to include or exclude a feature within each inner loop was the maximization of the BAC of a Linear Discriminant Analysis (LDA) classifier [33], see inner loop in Fig. 3. BAC values were obtained by comparing the shock/no-shock decisions obtained through the LDA classifier with ground truth labels of the inner test set. At each step of the PTA(4, 3) four features were included in the model using Sequential Forward Selection, and then three were removed from the model using Sequential Backward Selection. The feature selection method was run until K features were included, several values of K were tested in the experiments. A wrapper-based approach was adopted in order to address feature dependencies and hence select K features that altogether are the most discriminative ones. Finally, we chose the PTA algorithm to avoid the nesting effects of sequential feature selection [53].

B. Shock Decision Algorithm

The decision algorithm was designed in the outer loop, deploying a Support Vector Machine (SVM) classifier with a Gaussian kernel [55]. Features were standardized to zero mean and unit variance using the data in the training set, and the K features from the inner feature selection loop were used. This resulted in a training set of instance-label pairs $\{(\boldsymbol{x}_1, y_1), \ldots, (\boldsymbol{x}_n, y_n)\} \in \mathbb{R}^K \times \{\pm 1\}$, where $y_i = 1$ for shockable and $y_i = -1$ for nonshockable rhythms. The decision function of the SVM is found by solving the following maximization problem [55]:

$$W(\alpha) = \sum_{i=1}^{N} \alpha_i - \frac{1}{2} \sum_{i,j=1}^{N} \alpha_i \alpha_j y_i y_j \exp(-\gamma \|\boldsymbol{x}_i - \boldsymbol{x}_j\|^2) \quad (9)$$

$$\text{s.t.} : \ 0 \le \alpha_i \le C \quad \forall i, \quad \text{and} \quad \sum_i \alpha_i y_i = 0 \qquad (10)$$

where the α_i Lagrange multipliers are non-zero only for N_s support vectors, C is the soft margin parameter and γ the width of the gaussian kernel. Once the support vectors are determined

the decision function is:

$$f(\boldsymbol{x}) = \text{sign}\left[\sum_{i=1}^{N_s} \alpha_i y_i \exp(-\gamma \|\boldsymbol{x} - \boldsymbol{x}_i\|^2) + b\right] \qquad (11)$$

where the threshold b is determined in the optimization phase. A rhythm will be classified as shockable for $f(\boldsymbol{x}) = 1$ or non-shockable for $f(\boldsymbol{x}) = -1$.

Hyperparameter optimization for a gaussian kernel SVM involves selecting γ and C, and was carried out using the *libsvm* library [56]. The soft margin parameter C represents a trade-off between maximizing the margin and minimizing errors in the training data, and γ controls the flexibility of the decision boundary [57]. The values of C and γ that maximized the BAC were determined in the outer loop doing a 25×25 logarithmic grid search in the ranges $10^{-1} \leq C \leq 10^2$ and $10^{-3} \leq \gamma \leq 10^1$, respectively. The nested CV procedure was repeated 50 times to estimate the statistical distributions of the performance metrics that will be reported as mean (standard deviation).

V. RESULTS AND DISCUSSION

This section provides the main results for the shock decision algorithm; additional results are given in the supplementary materials and referenced in the manuscript. First the LMS/RLS filter was optimized; then the effect of two variables were analyzed, the number of features used by the classifier (K), and the length of the analysis segment used for the shock/no-shock decision (L). Finally the results are compared to all available solutions for shock decisions during piston-driven chest compressions. The results are reported for the C/γ pair with best average BAC in the 50 repetitions of the outer CV loop.

A. CPR Artifact Filter Configuration and Processing Times

Fig. 4 shows the mean values of the BAC obtained in the 50 random repetitions of the nested CV procedure for different configurations of the LMS and RLS filters, using an interval of $L = 8$ s for feature extraction and an SVM classifier with $K = 6$ features. Both filters showed near-optimal performance with a BAC above 96.5% for a wide range of configurations, that is, for different filter orders (N) and coarseness levels (μ, λ): $N \geq 10$ and $\mu \sim 3\text{–}12 \cdot 10^{-3}$ for the LMS filter and $N \geq 10$ and $\lambda \sim 0.970\text{–}0.990$ for the RLS filter. The accuracy of the solution is not very sensitive to the CPR artifact filter, so filters can be considerably simplified by decreasing their order N to reduce the computational cost. Table I shows the distribution of the performance metrics and the average computation time for different filter orders. The filters were configured at their optimal coarseness, $\mu = 8 \cdot 10^{-3}$ and $\lambda = 0.99$, as shown in Fig. 4. The computation time t_1 is the time required to suppress the CPR artifact and t_2 includes the wavelet decomposition, feature calculations ($K = 6$), and the decision of the SVM classifier obtained through Eq (11). All calculations were done in Matlab on an i7 3.2 GHz single-core processor and 16 GHz of memory.

AHA performance goals were met with the RLS and LMS filters with as few as $N = 5$ harmonics, but best results were obtained with $N = 20$, as shown in Table I. For $N = 5$ the computational demands of the complete algorithm were very low, 16 ms for the LMS or 38 ms for the RLS filter. Feature extraction including SWT/ISWT analysis and denoising consumed on average 6 ms, so the LMS filter is computationally very cheap and its computational cost negligible regardless of its order, it uses up 10 ms for $N = 5$, and 18 ms for $N = 30$. The RLS filter has a greater computational cost that increases considerably with its order, from 30 ms for $N = 5$ to over 140 ms for $N = 30$. This excessive computational cost is caused by the RLS recursion formula for the gain matrix which involves $2N \times 2N$ matrix multiplications for each signal sample [19]. The RLS filter has been shown to be more effective than the LMS filter to remove piston-driven compression artifacts when shock decision algorithms from commercial defibrillators are used in the classification stage [19], [58] (see also Table III). Shock decision algorithms in commercial defibrillators are designed to classify artifact free ECGs, so an effective suppression of the CPR artifact is critical. This is also important if the filtered ECG ($\hat{s}_{\text{ecg}}$ in Fig. 1 and Fig. 7) is shown in the screen of the monitor-defibrillator to serve as a decision support signal for the emergency clinician. However, our results show that the design of CPR artifact filters can be relaxed when a properly designed machine learning algorithm trained with the filtered ECG is used for classification. This is probably because the classification algorithm now learns the characteristics of filtering residuals that confound the shock decision algorithms of commercial defibrillators.

For all the analyses hereafter an LMS filter with $\mu = 8 \cdot 10^{-3}$ and $N = 20$ was used.

B. Classification Features and Feature Ranking

One of the pivotal aspects of a machine learning algorithm is the design of the classification features. The method proposed includes features extracted from the d_3-d_8 denoised SWT components and their reconstructed signals. Table II shows the ranking of the features by the number of times they were selected using the PTA(4, 3) feature selection scheme in the inner loop and 50 random repetitions of the outer CV loop ($50 \times 10 = 500$ feature selection loops). This ranking was obtained for a solution with $K = 6$ features. The features with the best ranking are a mixture of those derived from the detail coefficients and from the denoised signal, and represent a variety of signal analysis approaches that comprise signal regularity/complexity (SampEn, CM, Frqbin) [49], [50], [59], spectral analysis (VFleak, A1-3, bWT) [44], [45], [60], time domain features (MAV, Np, count2) [33], [41], [42], or the sample distributions of the denoised signal (Kurt) and its detail coefficients FQR/IQR [33]. Additional results for the discriminative power of the features using ROC curve analysis are available in the supplementary materials.

Fig. 5 shows the accuracies (balanced and absolute) of the shock decision system as a function of features allowed in the SVM. For a good accuracy the number of features in the clas-
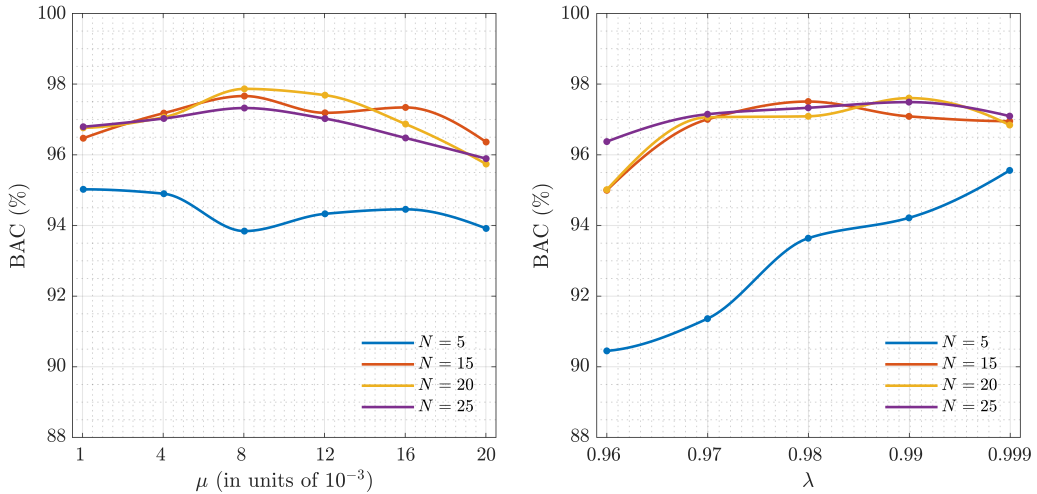
Fig. 4. The mean values of BAC obtained in the 50 repetitions of the nested CV procedure when a LMS (left) or a RLS (right) filter is used to remove the CPR artifact. The performance is given as a function of the coarseness (λ, μ) of the filter for 4 significant values of the filter order, N.

TABLE I
SHOCK DECISION ACCURACIES AND PROCESSING TIMES FOR FILTERING (t_1) AND SHOCK DECISION (t_2) FOR DIFFERENT FILTER ORDERS

	RLS, $\lambda = 0.99$					LMS, $\mu = 8 \cdot 10^{-3}$				
N	Se (%)	Sp (%)	BAC (%)	Acc (%)	t_1/t_2 (ms)	Se (%)	Sp (%)	BAC (%)	Acc (%)	t_1/t_2 (ms)
4	90.6 (1.1)	94.3 (0.7)	92.5 (0.7)	93.6 (0.7)	30/5	92.3 (0.8)	94.6 (0.6)	93.5 (0.5)	94.2 (0.5)	10/6
5	92.8 (1.2)	95.6 (0.6)	94.2 (0.7)	95.1 (0.5)	32/6	91.8 (1.2)	95.9 (0.3)	93.8 (0.7)	95.1 (0.4)	10/6
10	95.4 (0.7)	97.9 (0.4)	96.7 (0.4)	97.4 (0.4)	37/5	96.0 (0.4)	98.6 (0.3)	97.3 (0.3)	98.1 (0.3)	14/7
15	95.8 (0.7)	98.4 (0.3)	97.1 (0.4)	97.9 (0.3)	50/5	96.7 (0.4)	98.6 (0.4)	97.7 (0.3)	98.3 (0.3)	15/7
20	**97.0 (0.5)**	**98.3 (0.2)**	**97.6 (0.2)**	**98.0 (0.2)**	**72/6**	**97.5 (0.4)**	**98.2 (0.4)**	**97.9 (0.3)**	**98.1 (0.3)**	**16/5**
25	96.6 (0.5)	98.5 (0.3)	97.5 (0.2)	98.1 (0.3)	96/4	96.8 (0.4)	97.9 (0.3)	97.3 (0.3)	97.7 (0.3)	17/5
30	96.9 (0.6)	98.0 (0.4)	97.4 (0.4)	97.8 (0.3)	147/6	97.5 (0.4)	97.9 (0.3)	97.7 (0.2)	97.8 (0.3)	18/7

TABLE II
FEATURES RANKED BY N_f, THE NUMBER OF TIMES THEY WERE SELECTED IN THE 500 INNER LOOPS

RLS filter		LMS filter	
Feature	N_f	Feature	N_f
SampEn, d_3	500	SampEn, d_3	500
FQR, d_7	397	VFleak	321
VFleak	337	FQR, d_7	236
A1	275	IQR, d_7	217
CM	255	A2	183
Kurt	248	Kurt	157
A2	207	A3	148
bWT	146	FQR, d_6	119
A3	86	Np	102
IQR, d_7	65	FQR, d_8	85
MAV	60	CM	73
Frqbin	52	count2	67

Fig. 5. Mean values of BAC and Acc as a function of the number of features, K, used in the classifier.

sifier must be between 3 and 7, which gives an Acc and BAC above 97.8%. A classifier with fewer features presented lower BAC and Acc, with a more negative impact on Acc. This means that the most prevalent class, the Sp for nonshockable rhythms,

Fig. 6. Distribution of the performance metrics as a function of the length of the analysis segment (L). The graph shows the median values and the 2.5-97-5 percentile range for Se, Sp and BAC.

Method	Performance metric			
	Se (%)	Sp (%)	BAC (%)	Acc (%)
1-Stg, Dfb[†]				
LMS [30]	98.6 (1.0)	84.0 (1.8)	91.3 (1.2)	86.8 (1.6)
RLS [19]	98.1 (1.0)	87.0 (1.8)	92.5 (1.1)	89.1 (1.5)
Comb [30]	97.1 (2.0)	84.3 (1.8)	90.7 (1.3)	86.8 (1.6)
M-Stg, Dfb[‡]				
LMS [19]	94.4 (3.0)	93.2 (1.2)	93.8 (1.6)	93.4 (1.1)
RLS [19]	91.7 (6.0)	98.1 (1.1)	94.9 (2.6)	96.9 (0.9)
Comb [19]	88.8 (6.0)	96.6 (1.7)	92.7 (2.4)	95.1 (1.1)
1-Stg, SVM				
LMS	97.5 (0.4)	98.2 (0.4)	97.9 (0.3)	98.1 (0.3)
RLS	97.0 (0.5)	98.3 (0.2)	97.6 (0.2)	98.0 (0.2)

[†] **Single stage filtering, shock decision of a commercial defibrillator**.
[‡] **Multistage filtering, shock decision of a commercial defibrillator**.

D. Discussion on the Near-Optimal Solution

The accuracy for the (near)-optimal solutions using an RLS and an LMS filter (see Table I) are compared in Table III to the available methods for shock decision during piston-driven compressions. Feature extraction was 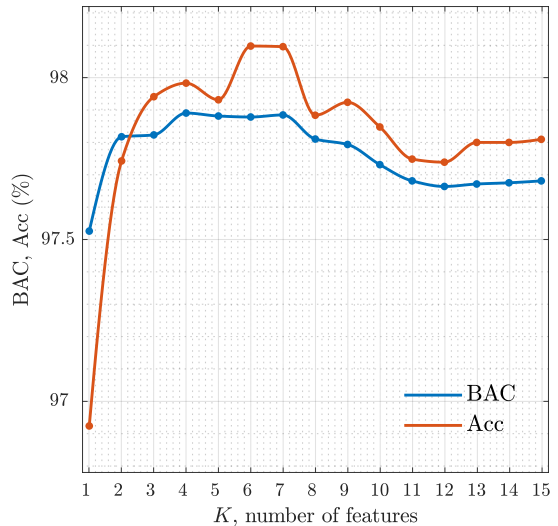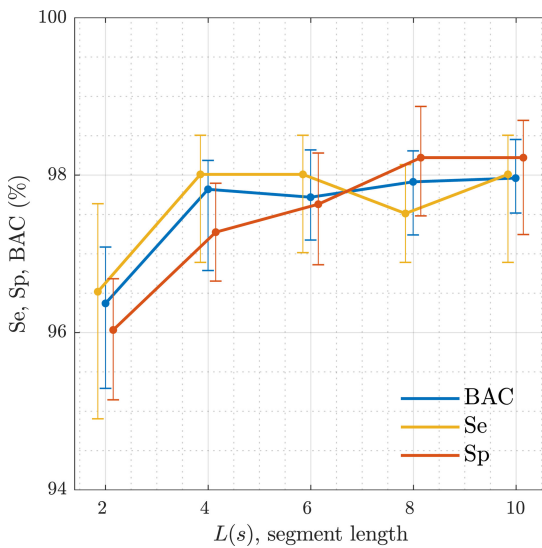done with $L = 8$ s and an SVM with $K = 6$ features was used. The optimal (C, γ) pairs for the SVM were $(17.8 \cdot 10^{-2}, 6.8 \cdot 10^{-2})$ and $(3.162, 1 \cdot 10^{-2})$ for the LMS and RLS filter based solutions, respectively.

The multistage solution introduced in [19] was the most accurate shock decision algorithm for mechanical devices proposed to date. As shown in Table III, the machine learning approach proposed in this study increases the BAC of single filter solutions by over 5-points, and that of the multistage solution by 3-points, and increases the sensitivity substantially, making the solution very reliable for the detection of shockable rhythms. The overall accuracy is also increased by around 1-point, which is a considerable increase because the multistage solution had an overall accuracy of 96.9%. A 1-point increase from that baseline means that around 30% of the errors are now correctly classified. Very importantly, this improvement was achieved together with a drastic reduction of the computation demands of the algorithms. For a solution based on the LMS filter the mean processing time per 8-s segments was 21 ms, an over five fold improvement when compared to the 110 ms required by the multistage solution. This reduction is very important in defibrillators with scarce computation resources.

Finally, Fig. 7 shows three illustrative examples of misclassified segments both for shockable and nonshockable rhythms. In the two examples of nonshockable rhythms the denoised signal and the d_3 detail coefficient (best features) show a disorganized signal, fast in the case of the AS example (middle) and slower for the OR (top). These disorganized signals are interpreted as shockable rhythm by the SVM classifier. In the example of the missed VF, the filter is unable to remove the spiky artifact introduced by the mechanical device at each compression, and these spikes confound the decision algorithm. In any case misclassi-

is negatively affected by using a simpler classifer. Adding more than 7 features sligthly reduces both accuracies, and makes the classifier more complex.

C. Duration of the Analysis Segment

Fig. 6 shows how the performance metrics change as the analysis segment is shortened. The perfomance of the algorithm stabilizes at near-optimal values for analysis segments longer than 4 s, and drops if shorter segments are used. However, for segments as short as 2 s the algorithm still meets the minimum AHA recommendations for Se and Sp, with values of 96.5 (94.9–97.6) and 96.0 (95.1–96.7), respectively. Studies that have developed ad-hoc algorithms for cardiac arrest data have reported minimum segment lengths for an accurate analysis around 3–4 s, both for the analysis of the ECG without CPR artifacts [47], [61] or after suppression of manual CPR artifacts [43]. Previous studies on shock decision during piston-driven chest compressions relied on shock decision algorithms of commercial defibrillators. These algorithms require analysis segments in excess of 5 s in most devices [62]. For instance, in two previous studies on shock decision during mechanical CPR the analysis segment was either 6 s or 9 s long, because the algorithm applied a majority vote to three consecutive 3-s analysis subsegments [19], [30]. Reducing the length of the analysis segments is not critical during compressions, since CPR therapy is not interrupted for the analysis. However, if a rhythm transition analysis is to be performed during CPR [63] short intervals would permit a more accurate time-location of transitions between shockable and nonshockable rhythms, and a reduction of computational burden.
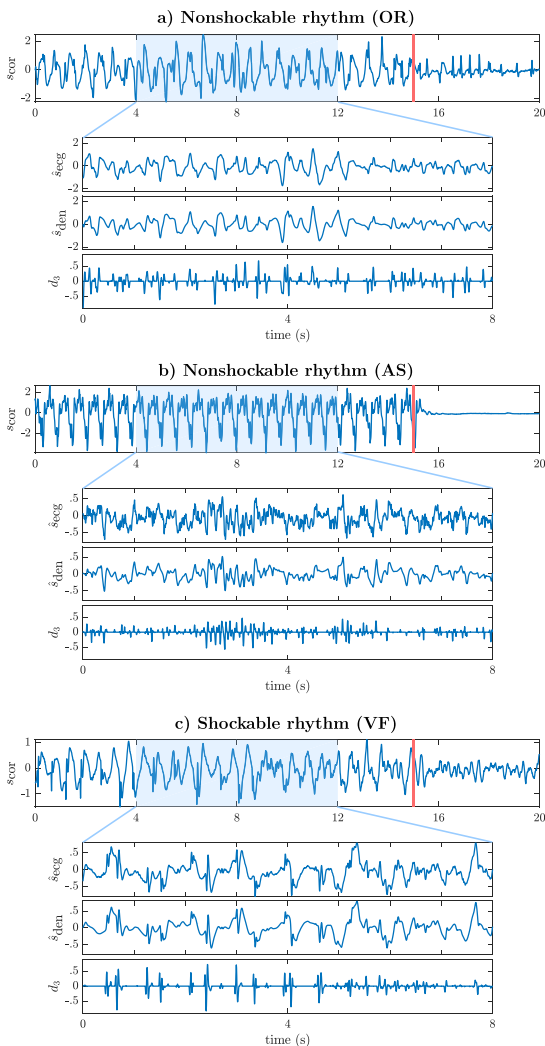
Fig. 7. Three examples of misclassified segments. Panels (a) and (b) depict nonshockable rhythms, OR and AS, respectively, while panel (c) represents a shockable (VF) rhythm. From top to bottom, each panel shows the 20-s ECG segment, and the filtered ECG, the denoised ECG and the detail 3 coefficient of the 8-s interval used by the shock decision algorithm.

fications were very few, around 15 for nonshockable rhythms (Sp $\sim$ 98.2%), and around 5 for VF (Se $\sim$ 97.5%).

VI. Conclusion

This study introduces a machine learning algorithm for shock decisions during piston-driven chest compressions. The algorithm improves the accuracy of the best known solutions to date by 3 points in BAC with an additional 5-fold reduction in computational cost. This makes this solution very accurate and efficient. There are two main reasons for these advances. First, the feature extraction phase based on the stationary wavelet

analysis resulted in new and improved discriminating features. Second, extracting the features after removing the CPR artifact and feeding those features to the SVM improves the accuracy considerably, because the machine learning algorithm is able to learn the characteristics of filtering residuals. Our results show that this approach allows relaxing the characteristics of the compression artifact filters.

The main limitations of this study are associated with the data. The dataset came from a single type of monitor-defibrillator, so the methods may need adjusting to encompass data from other devices with different ECG acquisition characteristics like bandwidth, sampling rates or A/D resolution. Furthermore, the data were compiled from a single emergency service and the LUCAS-2 device may be used differently across emergency services, that may also enforce different resuscitation protocols. Those differences may result in chest compression artifacts with different characteristics. Finally, the (near)-optimal solutions presented in Table I were obtained following a training/validation data partition given the amount of samples available. If more data were available the results should be confirmed using an independent test set.

References

[1] G. Perkins *et al.*, "European resuscitation council guidelines for resuscitation 2015: Section 2. Adult basic life support and automated external defibrillation," *Resuscitation*, vol. 95, pp. 81–99, 2015.

[2] K. B. Kern *et al.*, "Importance of continuous chest compressions during cardiopulmonary resuscitation: Improved outcome during a simulated single lay-rescuer scenario," *Circulation*, vol. 105, no. 5, pp. 645–649, 2002.

[3] C. Vaillancourt *et al.*, "The impact of increased chest compression fraction on return of spontaneous circulation for out-of-hospital cardiac arrest patients not in ventricular fibrillation," *Resuscitation*, vol. 82, no. 12, pp. 1501–1507, 2011.

[4] S. Ruiz de Gauna *et al.*, "Rhythm analysis during cardiopulmonary resuscitation: Past, present, and future," *Biomed. Res. In.*, vol. 2014, 2014, Art. no. 386010.

[5] J. Ruiz *et al.*, "Feasibility of automated rhythm assessment in chest compression pauses during cardiopulmonary resuscitation," *Resuscitation*, vol. 84, no. 9, pp. 1223–1228, 2013.

[6] U. Ayala *et al.*, "Fully automatic rhythm analysis during chest compression pauses," *Resuscitation*, vol. 89, pp. 25–30, 2015.

[7] Y. Li *et al.*, "Identifying potentially shockable rhythms without interrupting cardiopulmonary resuscitation," *J. Crit. Care Medicine*, vol. 36, no. 1, pp. 198–203, 2008.

[8] Y. Li *et al.*, "An algorithm used for ventricular fibrillation detection without interrupting chest compression," *IEEE Trans. Biomed. Eng.*, vol. 59, no. 1, pp. 78–86, Jan. 2012.

[9] H. Kwok *et al.*, "Adaptive rhythm sequencing: A method for dynamic rhythm classification during CPR," *Resuscitation*, vol. 91, pp. 26–31, 2015.

[10] S. O. Aase *et al.*, "CPR artifact removal from human ECG using optimal multichannel filtering," *IEEE Trans. Biomed. Eng.*, vol. 47, no. 11, pp. 1440–1449, Nov. 2000.

[11] J. Husoy *et al.*, "Removal of cardiopulmonary resuscitation artifacts from human ECG using an efficient matching pursuit-like algorithm," *IEEE Trans. Biomed. Eng.*, vol. 49, no. 11, pp. 1287–1298, Nov. 2002.

[12] J. Eilevstjønn *et al.*, "Feasibility of shock advice analysis during CPR through removal of CPR artefacts from the human ECG," *Resuscitation*, vol. 61, no. 2, pp. 131–141, 2004.

[13] K. Rheinberger *et al.*, "Removal of CPR artifacts from the ventricular fibrillation ECG by adaptive regression on lagged reference signals," *IEEE Trans. Biomed. Eng.*, vol. 55, no. 1, pp. 130–137, Jan. 2008.

[14] J. Ruiz *et al.*, "Cardiopulmonary resuscitation artefact suppression using a Kalman filter and the frequency of chest compressions as the reference signal," *Resuscitation*, vol. 81, no. 9, pp. 1087–1094, 2010.

[15] T. Werther *et al.*, "CPR artifact removal in ventricular fibrillation ECG signals using Gabor multipliers," *IEEE Trans. Biomed. Eng.*, vol. 56, no. 2, pp. 320–327, Feb. 2009.

[16] U. Irusta *et al.*, "A least mean-square filter for the estimation of the cardiopulmonary resuscitation artifact based on the frequency of the compressions," *IEEE Trans. Biomed. Eng.*, vol. 56, no. 4, pp. 1052–1062, Apr. 2009.

[17] E. Aramendi *et al.*, "Suppression of the cardiopulmonary resuscitation artefacts using the instantaneous chest compression rate extracted from the thoracic impedance," *Resuscitation*, vol. 83, no. 6, pp. 692–698, 2012.

[18] Y. Gong *et al.*, "An enhanced adaptive filtering method for suppressing cardiopulmonary resuscitation artifact," *IEEE Trans. Biomed. Eng.*, vol. 64, no. 2, pp. 471–478, Feb. 2017.

[19] I. Isasi *et al.*, "A multistage algorithm for ECG rhythm analysis during piston driven mechanical chest compressions," *IEEE Trans. Biomed. Eng.*, vol. 66, no. 1, pp. 263–272, Jan. 2019, doi: 10.1109/TBME.2018.2827304.

[20] U. Ayala *et al.*, "Are dual-channel methods as accurate as multi-channel methods to suppress the CPR artifact?" in *Proc. Comput. Cardioly*, 2011, pp. 509–512.

[21] S. R. de Gauna *et al.*, "A method to remove CPR artefacts from human ECG using only the recorded ECG," *Resuscitation*, vol. 76, no. 2, pp. 271–278, 2008.

[22] R. E. Kerber *et al.*, "Automatic external defibrillators for public access defibrillation: Recommendations for specifying and reporting arrhythmia analysis algorithm performance, incorporating new waveforms, and enhancing safety," *Circulation*, vol. 95, no. 6, pp. 1677–1682, 1997.

[23] S. Rubertsson *et al.*, "Mechanical chest compressions and simultaneous defibrillation vs conventional cardiopulmonary resuscitation in out-of-hospital cardiac arrest: The LINC randomized trial," *J. Amer. Med. Assoc.*, vol. 311, no. 1, pp. 53–61, 2014.

[24] L. Wik *et al.*, "Manual vs. integrated automatic load-distributing band CPR with equal survival after out of hospital cardiac arrest the randomized CIRC trial," *Resuscitation*, vol. 85, no. 6, pp. 741–748, 2014.

[25] G. D. Perkins *et al.*, "Mechanical versus manual chest compression for out-of-hospital cardiac arrest (paramedic): A pragmatic, cluster randomised controlled trial," *Lancet*, vol. 385, no. 9972, pp. 947–955, 2015.

[26] G. Putzer *et al.*, "LUCAS compared to manual cardiopulmonary resuscitation is more effective during helicopter rescue. A prospective, randomized, cross-over manikin study," *Amer. J. Emerg. Med.*, vol. 31, no. 2, pp. 384–389, 2013.

[27] A. I. Larsen *et al.*, "Cardiac arrest with continuous mechanical chest compressions during percutaneous coronary intervention: A report on the use of the LUCAS device," *Resuscitation*, vol. 75, no. 3, pp. 454–459, 2007.

[28] K. Sunde *et al.*, "Quality of mechanical, manual standard and active compression–decompression CPR on the arrest site and during transport in a manikin model," *Resuscitation*, vol. 34, no. 3, pp. 235–242, 1997.

[29] J. Soar *et al.*, "European resuscitation council guidelines for resuscitation 2015: Section 3. Adult advanced life support," *Resuscitation*, vol. 95, pp. 100–147, 2015.

[30] E. Aramendi *et al.*, "Filtering mechanical chest compression artefacts from out-of-hospital cardiac arrest data," *Resuscitation*, vol. 98, pp. 41–47, 2016.

[31] J. Sullivan *et al.*, "A digital filter can effectively remove mechanical chest compression artifact," *Resuscitation*, vol. 85, p. S41, 2014.

[32] A. Langhelle *et al.*, "Reducing CPR artefacts in ventricular fibrillation in vitro," *Resuscitation*, vol. 48, no. 3, pp. 279–291, 2001.

[33] A. B. Rad *et al.*, "ECG-based classification of resuscitation cardiac rhythms for retrospective data analysis," *IEEE Trans. Biomed. Eng.*, vol. 64, no. 10, pp. 2411–2418, Oct. 2017.

[34] M. Holschneider *et al.*, "A real-time algorithm for signal analysis with the help of the wavelet transform," in *Wavelets*. Berlin, Germany: Springer, 1990, pp. 286–297.

[35] J. E. Fowler, "The redundant discrete wavelet transform and additive noise," *IEEE Signal Process. Lett.*, vol. 12, no. 9, pp. 629–632, Sep. 2005.

[36] M. Merah *et al.*, "R-peaks detection based on stationary wavelet transform," *Comput. Methods Programs Biomed.*, vol. 121, pp. 149–160, Oct. 2015.

[37] M. Cesari *et al.*, "A new wavelet-based ECG delineator for the evaluation of the ventricular innervation," *IEEE J. Trans. Eng. Health Med.*, vol. 5, 2017, Art. no. 2000215.

[38] D. L. Donoho, "De-noising by soft-thresholding," *IEEE Trans. Inf. Theory*, vol. 41, no. 3, pp. 613–627, May 1995.

[39] M. A. Arafat *et al.*, "A simple time domain algorithm for the detection of ventricular fibrillation in electrocardiogram," *Signal Image Video Process.*, vol. 5, no. 1, pp. 1–10, 2011.

[40] A. Amann *et al.*, "Reliability of old and new ventricular fibrillation detection algorithms for automated external defibrillators," *Biomed. Eng. Online*, vol. 4, no. 1, p. 60, 2005.

[41] E. M. A. Anas *et al.*, "Sequential algorithm for life threatening cardiac pathologies detection based on mean signal strength and EMD functions," *Biomed. Eng. Online*, vol. 9, no. 1, p. 43, 2010.

[42] I. Jekova and V. Krasteva, "Real time detection of ventricular fibrillation and tachycardia," *Physiol. Meas.*, vol. 25, no. 5, pp. 1167–1178, 2004.

[43] U. Ayala *et al.*, "A reliable method for rhythm analysis during cardiopulmonary resuscitation," *Biomed. Res. Int.*, vol. 2014, 2014, Art. no. 872470.

[44] U. Irusta *et al.*, "A high-temporal resolution algorithm to discriminate shockable from nonshockable rhythms in adults and children," *Resuscitation*, vol. 83, no. 9, pp. 1090–1097, 2012.

[45] S. Barro *et al.*, "Algorithmic sequential decision-making in the frequency domain for life threatening ventricular arrhythmias and imitative artefacts: A diagnostic system," *J. Biomed. Eng.*, vol. 11, no. 4, pp. 320–328, 1989.

[46] S. Kuo, "Computer detection of ventricular fibrillation," in *Proc. IEEE Comput. Cardiology*, 1978, pp. 347–349.

[47] C. Figuera *et al.*, "Machine learning techniques for the detection of shockable rhythms in automated external defibrillators," *PloS One*, vol. 11, 2016, Art. no. e0159654.

[48] F. Alonso-Atienza *et al.*, "Detection of life-threatening arrhythmias using feature selection and support vector machines," *IEEE Trans. Biomed. Eng*, vol. 61, no. 3, pp. 832–840, Mar. 2014.

[49] I. Jekova, "Shock advisory tool: Detection of life-threatening cardiac arrhythmias and shock success prediction by means of a common parameter set," *Biomed. Signal Process. Control*, vol. 2, no. 1, pp. 25–33, 2007.

[50] X.-S. Zhang *et al.*, "Detecting ventricular tachycardia and fibrillation by complexity measure," *IEEE Trans. Biomed. Eng.*, vol. 46, no. 5, pp. 548–555, May 1999.

[51] A. Amann *et al.*, "Detecting ventricular fibrillation by time-delay methods," *IEEE Trans. Biomed. Eng.*, vol. 54, no. 1, pp. 174–177, Jan. 2007.

[52] R. Kohavi and G. H. John, "Wrappers for feature subset selection," *Artif. Intell.*, vol. 97, no. 1/2, pp. 273–324, 1997.

[53] S. Strearns, "On selecting features for pattern classifiers," *Proc. Int. Conf. Pattern Recogniti.*, 1976, pp. 71–75.

[54] A. R. Webb, *Statistical Pattern Recognition*. Hoboken, NJ, USA: Wiley, 2003.

[55] B. Scholkopf *et al.*, "Comparing support vector machines with Gaussian kernels to radial basis function classifiers," *IEEE Trans. Signal Process.*, vol. 45, no. 11, pp. 2758–2765, Nov. 1997.

[56] C.-C. Chang and C.-J. Lin, "LIBSVM: A library for support vector machines," *ACM Trans. Intell. Syst. Technol.*, vol. 2, no. 3, 2011, Art. no. 27.

[57] A. Ben-Hur and J. Weston, "A users guide to support vector machines," in *Proc. Data Mining Techn. Life Sciences*, 2010, pp. 223–239.

[58] I. Isasi *et al.*, "Removing piston-driven mechanical chest compression artefacts from the ECG," in *Proc. Comput. Cardioly*, vol. 44, 2017, pp. 1–4.

[59] B. Chicote *et al.*, "Application of entropy-based features to predict defibrillation outcome in cardiac arrest," *Entropy*, vol. 18, no. 9, 2016, Art. no. 313.

[60] S. Kuo, "Computer detection of ventricular fibrillation," in *Proc. Comput. Cardioly*, 1978, pp. 347–349.

[61] J.-P. Didon *et al.*, "Shock advisory system with minimal delay triggering after end of chest compressions: Accuracy and gained hands-off time," *Resuscitation*, vol. 82, pp. S8–S15, 2011.

[62] D. Snyder and C. Morgan, "Wide variation in cardiopulmonary resuscitation interruption intervals among commercially available automated external defibrillators may affect survival despite high defibrillation efficacy," *J. Crit. Care Medicine*, vol. 32, no. 9 Suppl., pp. S421–S424, Sep. 2004.

[63] A. B. Rad *et al.*, "An automatic system for the comprehensive retrospective analysis of cardiac rhythms in resuscitation episodes," *Resuscitation*, vol. 122, pp. 6–12, Jan. 2018.

Supplementary materials

Iraia Isasi, Unai Irusta*, *Member, IEEE* Andoni Elola, Elisabete Aramendi, Unai Ayala, Erik Alonso, Jo Kramer-Johansen, and Trygve Eftestøl, *Member, IEEE*

I. THE SELECTION OF THE MOTHER WAVELET

The coefficients of the Stationary Wavelet Transform (SWT) represent the projection of the signal over a set of basis functions, $\psi_{j,k}$ generated as translation and dilatation of a protype function, ψ, called mother wavelet. Detail coefficients at different decomposition levels can be obtained by convolving the signal with $\psi_{j,k}$, which for a discrete dyadic decomposition is [1]:

$$\psi_{j,k}(t) = \frac{1}{\sqrt{2^j}}\psi\left(\frac{t - k \cdot 2^j}{2^j}\right) \qquad (1)$$

Where $a = 2^j$ is the scaling parameter associated to each decomposition level j, and $b = k \cdot 2^j$ is the translation parameter.

The selection of the mother wavelet determines the representation of the signal. Therefore, the mother wavelet must carefully be selected so that the reconstructed signal resembles the original ECG as closely as possible.

The aim of this section is to choose the mother wavelet best suited for our machine learning shock decision algorithm. There is no definitive rule for the selection of the mother wavelet and many methodologies have been followed in the literature, most of them based on the maximization of the cross-correlation between the original and the reconstructed ECG [2], [3]. In our work the criterion for mother wavelet selection was the maximization of the BAC of the shock decision algorithm. Six well-known mother families [4], [5] were tested: Haar, Daubechies (db), Symmlet (sym), Coiflet (coif), Fejer-Korovkin (fk) and discrete Meyer (dmey). The analysis was done for the two adaptive filters, the RLS and LMS filters, and results are reported as mean (standard deviation) in Tables I and II, respectively.

The configuration of the filters, (N, λ) for the RLS and (N, μ) for the LMS, was fixed to the optimal filter configurations obtained in our previous works [6], [7]. The model used for feature selection, optimization and evaluation of the shock decision algorithm is the one described in the main manuscript, although simplified to lower the computation cost. In the outer loop a 5-fold cross validation (CV) was used to optimize and evaluate the SVM classifier, incremental feature selection was used to select the best subset of features and only 20 repetitions of the nested CV procedure were

TABLE I
PERFORMANCE OF THE SHOCK DECISION ALGORITHMS FOR DIFFERENT
WAVELET FAMILIES, RLS FILTER WITH $\lambda = 0.99, N = 25$.

MW	Se (%)	Sp (%)	BAC (%)	Acc (%)
haar	97.0 (0.7)	95.7 (0.4)	96.3 (0.4)	96.0 (0.3)
db2	**96.4 (0.5)**	**98.4 (0.3)**	**97.4 (0.3)**	**98.0 (0.3)**
db3	95.8 (0.6)	98.2 (0.3)	97.0 (0.3)	97.7 (0.2)
db4	95.4 (0.7)	97.9 (0.3)	96.6 (0.4)	97.4 (0.3)
db5	96.2 (0.5)	97.6 (0.5)	96.9 (0.3)	97.3 (0.4)
db6	96.3 (0.5)	96.9 (0.5)	96.6 (0.3)	96.8 (0.4)
db7	96.8 (0.5)	96.8 (0.4)	96.8 (0.4)	96.8 (0.4)
db8	96.2 (0.7)	96.7 (0.5)	96.5 (0.5)	96.6 (0.4)
db9	96.8 (0.7)	96.1 (0.3)	96.5 (0.4)	96.3 (0.3)
db10	96.5 (0.7)	96.2 (0.4)	96.3 (0.4)	96.2 (0.3)
sym4	95.9 (0.3)	97.3 (0.4)	96.6 (0.3)	97.0 (0.4)
sym5	95.7 (0.8)	97.4 (0.4)	96.5 (0.4)	97.1 (0.4)
sym6	96.4 (0.4)	96.9 (0.4)	96.6 (0.3)	96.8 (0.3)
sym7	96.7 (0.7)	97.4 (0.4)	97.1 (0.4)	97.3 (0.3)
sym8	96.7 (0.7)	96.0 (0.4)	96.4 (0.4)	96.2 (0.3)
coif1	96.6 (0.5)	98.0 (0.2)	97.3 (0.3)	97.7 (0.2)
coif2	96.0 (0.6)	97.5 (0.3)	96.7 (0.3)	97.2 (0.2)
coif3	96.3 (0.7)	97.6 (0.3)	96.9 (0.3)	97.3 (0.2)
coif4	96.1 (0.6)	97.0 (0.3)	96.6 (0.3)	96.9 (0.2)
coif5	97.1 (0.6)	96.1 (0.4)	96.6 (0.3)	96.3 (0.3)
fk4	96.2 (0.9)	96.7 (0.5)	96.4 (0.6)	96.6 (0.5)
fk6	95.8 (0.6)	97.6 (0.4)	96.7 (0.2)	97.3 (0.3)
fk8	95.9 (0.9)	97.9 (0.4)	96.9 (0.5)	97.5 (0.4)
fk14	95.8 (0.9)	96.6 (0.4)	96.2 (0.4)	96.5 (0.3)
fk18	95.7 (0.7)	95.7 (0.3)	95.7 (0.3)	95.7 (0.3)
fk22	95.9 (0.7)	95.5 (0.6)	95.7 (0.5)	95.6 (0.5)
dmey	95.6 (1.0)	95.8 (0.5)	95.7 (0.5)	95.8 (0.4)

TABLE II
PERFORMANCE OF THE SHOCK DECISION ALGORITHM FOR DIFFERENT
WAVELET FAMILIES, LMS FILTER WITH $\mu = 0.008, N = 20$.

MW	Se (%)	Sp (%)	BAC (%)	Acc (%)
haar	96.6 (0.8)	95.9 (0.4)	96.2 (0.5)	96.0 (0.4)
db2	**97.8 (0.5)**	**97.8 (0.4)**	**97.8 (0.4)**	**97.8 (0.4)**
db3	96.7 (0.4)	97.3 (0.4)	97.0 (0.3)	97.2 (0.3)
db4	96.6 (0.6)	97.1 (0.4)	96.9 (0.4)	97.0 (0.4)
db5	97.1 (0.5)	96.7 (0.5)	96.9 (0.4)	96.8 (0.5)
db6	96.6 (0.8)	96.9 (0.4)	96.8 (0.5)	96.8 (0.4)
db7	97.1 (0.5)	96.6 (0.4)	96.8 (0.3)	96.7 (0.3)
db8	97.2 (0.6)	96.3 (0.5)	96.7 (0.3)	96.5 (0.4)
db9	97.0 (0.7)	95.9 (0.4)	96.4 (0.4)	96.1 (0.3)
db10	96.3 (0.6)	96.1 (0.3)	96.2 (0.3)	96.2 (0.3)
sym4	96.8 (0.6)	97.4 (0.3)	97.1 (0.3)	97.3 (0.2)
sym5	96.1 (0.6)	97.5 (0.4)	96.8 (0.4)	97.2 (0.3)
sym6	97.1 (0.5)	97.2 (0.4)	97.1 (0.3)	97.1 (0.3)
sym7	97.1 (0.5)	96.9 (0.4)	97.0 (0.4)	96.9 (0.4)
sym8	96.9 (0.6)	96.6 (0.5)	96.8 (0.4)	96.7 (0.4)
coif1	97.0 (0.4)	98.1 (0.4)	97.6 (0.3)	97.9 (0.4)
coif2	96.3 (0.6)	97.4 (0.4)	96.8 (0.4)	97.2 (0.4)
coif3	97.2 (0.3)	96.8 (0.5)	97.0 (0.3)	96.8 (0.4)
coif4	96.9 (0.5)	96.7 (0.4)	96.8 (0.3)	96.8 (0.3)
coif5	96.4 (0.8)	97.0 (0.3)	96.7 (0.4)	96.9 (0.3)
fk4	96.6 (1.0)	96.5 (0.5)	96.6 (0.6)	96.6 (0.5)
fk6	96.4 (0.8)	96.9 (0.3)	96.7 (0.4)	96.8 (0.3)
fk8	97.5 (0.7)	97.1 (0.3)	97.3 (0.3)	97.2 (0.2)
fk14	96.6 (0.8)	96.3 (0.4)	96.4 (0.4)	96.3 (0.3)
fk18	96.2 (0.9)	95.9 (0.5)	96.1 (0.5)	96.0 (0.4)
fk22	95.9 (1.0)	95.3 (0.4)	95.6 (0.5)	95.4 (0.3)
dmey	95.5 (0.8)	95.8 (0.5)	95.7 (0.4)	95.8 (0.4)

computed.

The best mother wavelet for both filters was the Daubechies of order 2 (db2), followed by the Coiflet 1 wavelet. Therefore, the db2 wavelet was the one used in the main article for ECG decomposition, denoising and reconstruction. This is consistent with findings in the literature in which the Daubechies wavelet family has been shown to be the family of mother wavelets that most closely resembles the ECG morphology [3], [8], [9]. Fig. 1 shows the morphology of the mother wavelets that achieved the best performance in each family of mother wavelets.
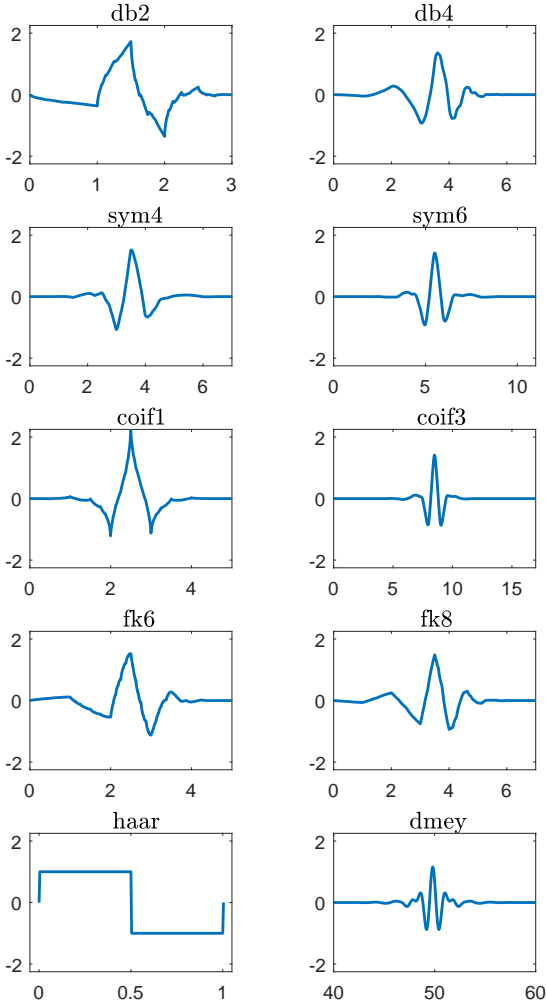

Fig. 1. Mother wavelets of different families with best performance for the shock decision algorithm.

II. DETAILED ANALYSIS OF THE FEATURES

The aim of this section is to analyze the discriminating power of the 38 features used in the main manuscript. The features were obtained after CPR artifact filtering, both from the denoised ECG signal, $\hat{s}_{den}$, and from the wavelet detail coefficients, $d_3 - d_8$.

Table III shows the receiver operating characteristic (ROC) curve analysis of individual features after optimal RLS and LMS filtering. The features are ordered by analysis domain, and the Area Under the Curve (AUC) and the Se/Sp pair for the optimal point in the ROC curve are reported. The optimal working point was defined as the one maximizing the Youden index [10], which is equivalent to maximizing the balanced accuracy (BAC). As for the wavelet decomposition,

TABLE III
ROC CURVE ANALYSIS, AUC AND OPTIMAL POINT.

Feature	LMS $N = 20$, $\mu = 8 \cdot 10^{-3}$			RLS $N = 20$, $\lambda = 0.99$		
	AUC	Se	Sp	AUC	Se	Sp
Detail coeff						
IQR, d_3	87.7	91.5	76.2	88.8	91.0	78.2
IQR, d_4	86.0	89.6	74.6	86.2	89.6	74.8
IQR, d_5	81.3	89.1	65.0	81.2	88.6	64.8
IQR, d_6	68.1	94.5	44.1	68.2	94.5	43.7
IQR, d_7	53.8	91.5	33.3	52.1	93.5	28.9
IQR, d_8	55.4	36.4	86.1	55.8	38.0	86.1
FQR, d_3	87.8	74.5	92.5	88.8	76.4	91.5
FQR, d_4	86.2	73.6	90.5	86.4	73.7	90.5
FQR, d_5	81.0	59.5	93.5	80.8	63.7	89.1
FQR, d_6	68.1	49.1	89.6	68.1	42.9	95.5
FQR, d_7	54.3	32.1	92.5	52.5	30.3	92.0
FQR, d_8	55.5	86.6	35.8	55.9	85.6	37.7
SampEn, d_3	99.5	96.5	98.9	99.4	97.5	97.7
SampEn, d_4	98.6	96.0	95.9	99.1	96.5	95.9
SampEn, d_5	86.9	93.5	70.6	88.1	94.5	73.6
SampEn, d_6	78.4	87.6	63.4	80.0	91.0	63.5
SampEn, d_7	84.5	81.1	78.0	85.4	84.6	73.7
SampEn, d_8	80.6	70.1	81.6	80.4	71.6	79.3
Denoised, $\hat{s}_{den}$						
Time						
Np	91.9	87.6	83.9	89.5	80.1	83.4
TCSC	88.5	93.0	78.8	86.7	93.5	75.1
Expmod	88.8	90.0	72.4	88.9	92.5	70.5
MAV	88.3	89.6	78.2	86.5	90.0	75.7
count1	94.3	93.0	85.4	94.7	91.5	85.8
count2	97.4	93.5	94.1	97.5	96.5	92.1
count3	96.1	95.5	87.9	96.3	93.5	90.8
Spectral						
bWT	94.8	94.0	83.8	95.3	94.0	84.4
A1	61.5	89.6	37.6	68.2	86.6	48.1
A2	82.3	80.1	71.9	81.7	74.6	78.2
A3	82.6	80.2	73.6	83.2	82.3	74.6
VFleak	91.2	85.7	86.1	91.0	87.7	83.6
Slope						
x1	97.8	98.0	92.3	97.8	96.0	94.0
x2	95.2	91.5	89.8	95.0	89.1	90.8
bCP	97.3	92.3	94.0	97.4	92.5	94.5
Complexity						
HILB	89.1	89.6	75.6	88.3	81.6	82.5
CM	84.4	83.6	71.2	85.4	84.1	74.4
Kurt	86.2	75.1	87.6	84.3	78.4	82.1
Frqbin	84.8	96.0	60.2	85.8	86.6	72.5
SampEn	92.8	94.0	80.3	94.2	97.0	80.3

features derived from the detail coefficients $d_3 - d_5$ were the most discriminative ones, which confirms that for shock decision algorithm the 3.9-31.25 Hz frequency band contains most of the relevant information. For the denoised signal, the most discriminative features come from several domains of analysis including the time domain (MAV, Np, count2), the spectral analysis (bWT, VFleak, A1-3) and the complexity of the signal (SampEn, CM, Frqbin). Interestingly, the most discriminative features were obtained after applying SampEn to the detail coefficients of the wavelet decomposition, particularly to d_3 and d_4. For our sampling frequency, these coefficients correspond to a frequency band of 7.81-31.25 Hz, where most of the spectral power of the QRS complexes is concentrated [11]. This is an interesting result that should be analyzed further since it could open a new way to design shock decision algorithms for defibrillators. In our analyses, before computing SampEn the input signals (d_j or $\hat{s}_{\mathrm{den}}$) were resampled to 50 Hz and an embedding dimension of $m = 2$ and a matching threshold of $r = 0.2 \cdot \sigma(s_{\mathrm{in}})$ were used, where

σ stands for the standard deviation.

Table IV shows the complete ranking of the features by the number of times they were selected using the PTA(4,3) in the 50 random repetitions of the 10-fold CV procedure. Optimal filter configurations were used and the procedure was stopped once $K = 6$ features were selected on each inner loop. It is important to stress that this feature ranking is not aligned with the discrimination power of the features as measured through their ROC curve analysis, compare for intance the AUCs in Table III to the feature ranking in Table IV. Many individually strong features are also very correlated and therefore add little new information to the classifier. These feature dependencies are addressed in the PTA feature selection stage. Finally, the ROC curves of the top 6 features are shown in Fig. 2 (LMS) and Fig. 3 (RLS). These figures show the Se/Sp pairs that could be achieved by varying the threshold for a single shock/no-shock decision feature.

TABLE IV
FEATURES RANKED BY N_f, THE NUMBER OF TIMES THEY WERE SELECTED IN THE 500 INNER LOOPS OF 50 RANDOM REPETITIONS OF THE NESTED CROSS VALIDATION PROCEDURE.

| LMS, $N = 20$, $\mu = 8 \cdot 10^{-3}$		RLS, $N = 20$, $\lambda = 0.99$	
Feature	N_f	Feature	N_f
SampEn, d_3	500	SampEn, d_3	500
VFleak	321	FQR, d_7	397
FQR, d_7	236	VFleak	337
IQR, d_7	217	A1	275
A2	183	CM	255
Kurt	157	Kurt	248
A3	148	A2	207
FQR, d_6	119	bWT	146
Np	102	A3	86
FQR, d_8	85	IQR, d_7	65
cm	73	MAV	60
count2	67	Frqbin	52
SampEn, d_6	64	Np	51
FQR, d_5	58	FQR, d_6	39
MAV	57	FQR, d_8	38
bWT	53	HILB	33
FQR, D_3	50	FQR, d_5	29
TCSC	49	TCSC	27
Frqbin	49	SampEn	25
count3	42	x1	21
IQR, d_6	41	FQR, d_3	16
bCP	40	FQR, d_4	15
HILB	32	SampEn, d_4	13
SampEn, d_4	28	count2	11
IQR, d_8	28	SampEn, d_6	8
FQR, d_4	26	IQR, d_8	7
x1	25	IQR, d_6	7
A1	24	SampEn, d_7	6
SamEn, d_7	23	SampEn, d_5	5
count1	23	Expmod	5
Expmod	16	count3	3
SampEn, d_8	15	IQR, d_4	3
IQR, d_4	14	IQR, d_3	3
IQR, d_3	12	x2	2
IQR, d_5	10	count1	2
x2	6	IQR, d_5	2
SampEn	4	SampEn, d_8	1
SampEn, d_5	3		
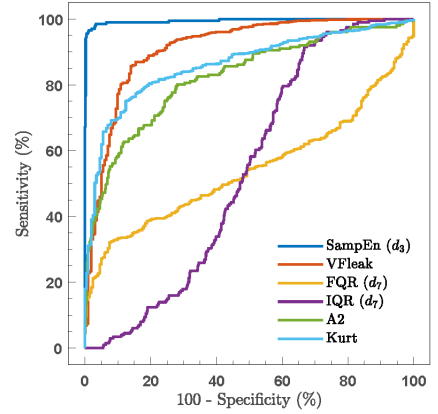
Fig. 2. ROC curves corresponding to the 6 top ranked features when the LMS filter is used to remove the CPR artefact.
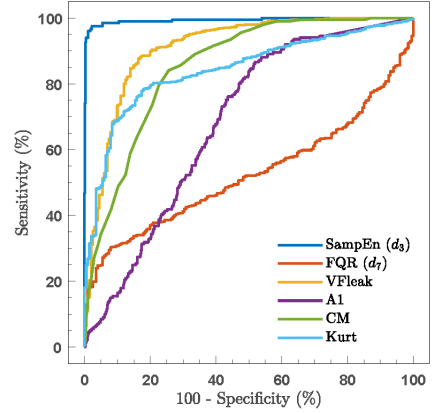

Fig. 3. ROC curves corresponding to the 6 top ranked features when the RLS filter is used to remove the CPR artefact.

REFERENCES

[1] C. E. Agnew *et al.*, "Comparison of rootmusic and discrete wavelet transform analysis of doppler ultrasound blood flow waveforms to detect microvascular abnormalities in type I diabetes," *IEEE Trans. Biomed. Eng.*, vol. 58, no. 4, pp. 861–867, 2011.

[2] B. Castro *et al.*, "ECG feature extraction using optimal mother wavelet," in *Electr. Electron. Eng. Israel. The 21st IEEE convention*. IEEE, 2000, pp. 346–350.

[3] B. N. Singh and A. K. Tiwari, "Optimal selection of wavelet basis function applied to ECG signal denoising," *Digit. Signal Process.*, vol. 16, no. 3, pp. 275–287, 2006.

[4] H. He *et al.*, "Optimal base wavelet selection for ECG noise reduction using a comprehensive entropy criterion," *Entropy*, vol. 17, no. 9, pp. 6093–6109, 2015.

[5] M. Varanis and R. Pederiva, "The influence of the wavelet filter in the parameters extraction for signal classification: An experimental study." *Proc. Braz. Soc. Comp. Appl. Math.*, vol. 5, no. 1, 2017.

[6] I. Isasi *et al.*, "A multistage algorithm for ECG rhythm analysis during piston driven mechanical chest compressions," *IEEE Trans. Biomed. Eng.*, 2018.

[7] E. Aramendi *et al.*, "Filtering mechanical chest compression artefacts from out-of-hospital cardiac arrest data," *Resuscitation*, vol. 98, pp. 41–47, 2016.

[8] M. Merah *et al.*, "R-peaks detection based on stationary wavelet transform," *Comput. Methods Programs Biomed.*, vol. 121, no. 3, pp. 149–160, 2015.

[9] A. B. Rad *et al.*, "ECG-based classification of resuscitation cardiac rhythms for retrospective data analysis," *IEEE Trans. Biomed. Eng.*, vol. 64, no. 10, pp. 2411–2418, 2017.

[10] N. J. Perkins and E. F. Schisterman, "The inconsistency of "optimal" cutpoints obtained using two criteria based on the receiver operating characteristic curve." *Am. J. Epidemiol.*, vol. 163, pp. 670–675, Apr. 2006.

[11] S. Kadambe *et al.*, "Wavelet transform-based QRS complex detector," *IEEE Trans. on Biomed. Eng.*, vol. 46, no. 7, pp. 838–848, 1999.

A.2 PUBLICATIONS ASSOCIATED TO OBJECTIVE 2

A.2.1 JOURNAL PAPER: J1$_2$

Table A.5. Journal paper associated to objective 2.

	Publication in international magazine
Reference	I. Isasi, U. Irusta, A. B. Rad, E. Aramendi, M. Zabihi, T. Eftestøl, J. Kramer-Johansen, L. Wik,"Automatic cardiac rhythm classification with concurrent manual chest compressions", *IEEE Acccess*, vol. 7, pp. 115147-115159, 2019.
Quality indices	• **Type of publication:** Journal paper idexed in JCR and SJR • **Area:** Electrical and Electronic Engineering • **Ranking:** 61/266 (Q1) based on JCR 2019 • **Impact factor SJR:** 0.775 • **Impact factor JCR:** 3.745

Automatic Cardiac Rhythm Classification With Concurrent Manual Chest Compressions

IRAIA ISASI[1], **UNAI IRUSTA**[1], (Member, IEEE), **ALI BAHRAMI RAD**[2], (Member, IEEE),
ELISABETE ARAMENDI[1], (Member, IEEE), **MORTEZA ZABIHI**[3], (Student Member, IEEE),
TRYGVE EFTESTØL[4], (Senior Member, IEEE), **JO KRAMER-JOHANSEN**[5], AND **LARS WIK**[5]

[1]Department of Communications Engineering, University of the Basque Country UPV/EHU, 48013 Bilbao, Spain
[2]Department of Electrical Engineering and Automation, Aalto University, 02150 Espoo, Finland
[3]Department of Computing Sciences, Tampere University, 33720 Tampere, Finland
[4]Department of Electrical Engineering and Computer Science, University of Stavanger, 4036 Stavanger, Norway
[5]Norwegian National Advisory Unit on Prehospital Emergency Medicine (NAKOS), Oslo University Hospital and University of Oslo, 0424 Oslo, Norway

Corresponding author: Iraia Isasi (iraia.isasi@ehu.eus)

ABSTRACT Electrocardiogram (EKG) based classification of out-of-hospital cardiac arrest (OHCA) rhythms is important to guide treatment and to retrospectively elucidate the effects of therapy on patient response. OHCA rhythms are grouped into five categories: ventricular fibrillation (VF) and tachycardia (VT), asystole (AS), pulseless electrical activity (PEA), and pulse-generating rhythms (PR). Clinically these rhythms are grouped into broader categories like shockable (VF/VT), non-shockable (AS/PEA/PR), or organized (ORG, PEA/PR). OHCA rhythm classification is further complicated because EKGs are corrupted by cardiopulmonary resuscitation (CPR) artifacts. The objective of this study was to demonstrate a framework for automatic multiclass OHCA rhythm classification in the presence of CPR artifacts. In total, 2133 EKG segments from 272 OHCA patients were used: 580 AS, 94 PR, 953 PEA, 479 VF, and 27 VT. CPR artifacts were adaptively filtered, 93 features were computed from the stationary wavelet transform analysis, and random forests were used for classification. A repeated stratified nested cross-validation procedure was used for feature selection, parameter tuning, and model assessment. Data were partitioned patient-wise. The classifiers were evaluated using per class sensitivity, and the unweighted mean of sensitivities (UMS) as a global performance metric. Four levels of clinical detail were studied: shock/no-shock, shock/AS/ORG, VF/VT/AS/ORG, and VF/VT/AS/PEA/PR. The median UMS (interdecile range) for the 2, 3, 4, and 5-class classifiers were: 95.4% (95.1-95.6), 87.6% (87.3-88.1), 80.6% (79.3-81.8), and 71.9% (69.5-74.6), respectively. For shock/no-shock decisions sensitivities were 93.5% (93.0-93.9) and 97.2% (97.0-97.4), meeting clinical standards for artifact-free EKG. The UMS for five classes with CPR artifacts was 5.8-points below that of the best algorithms without CPR artifacts, but improved the UMS of latter by over 19-points for EKG with CPR artifacts. A robust and accurate approach for multiclass OHCA rhythm classification during CPR has been demonstrated, improving the accuracy of the current state-of-the-art methods.

INDEX TERMS Out-of-hospital cardiac arrest (OHCA), electrocardiogram (EKG), cardiopulmonary resuscitation (CPR), adaptive filter, stationary wavelet transform (SWT), random forest (RF) classifier.

I. INTRODUCTION

Out-of-hospital cardiac arrest (OHCA) is a leading cause of death in the industrialized world. In Europe the estimated annual average incidence of ambulance treated cases is 41 (range 19-104) per 100 000 persons [1]. Patients in cardiac arrest lose their cardiac and respiratory function, and die within minutes if not treated. Treatment consists of highly time-sensitive interventions such as: recognition, call for help, cardiopulmonary resuscitation (CPR), defibrillation, and post-resuscitation care. Bystanders and lay rescuers can provide CPR to maintain an artificial perfusion of the vital

The associate editor coordinating the review of this manuscript and approving it for publication was Nuno Garcia.

organs through chest compressions, and mouth to mouth breaths for ventilations. Defibrillation by an automated external defibrillator (AED) can be used to revert lethal ventricular arrhythmia and restore the normal function of the heart. Upon the arrival of the medicalized ambulance, specialized treatment becomes available including continued high-quality CPR and defibrillation, but also add intravenous pharmacological treatment (adrenaline and anti-arrhythmic drugs), airway management, and assisted ventilation. If spontaneous circulation is restored, the patient is transported to a hospital for in-hospital treatment and post-resuscitation care [2].

Knowing the patient's cardiac rhythm during resuscitation is important for two reasons. First, awareness of the patient's rhythm may contribute to guide therapy. International guidelines describe treatment pathways based on cardiac rhythm and elapsed time, i.e., rhythm analysis every 2 minutes with defibrillation attempts for ventricular fibrillation (VF) or tachycardia (VT), and consideration of intravenous drugs such as adrenaline every 3-5 minutes for all non-perfusing rhythms [2]. Second, in retrospective analyses, the rhythm transitions of the patient during CPR provide important information about the interplay between therapy and patient response [3]–[5]. This may contribute to identify therapeutic interventions or treatment patterns that improve OHCA survival. One of the limiting factors for such analyses is the lack of datasets with cardiac rhythm annotations due to the manual labor involved. Thus, there is a need for automatic methods for cardiac rhythm annotation. In OHCA rhythms are grouped into five categories [6], [7]: VF, VT, asystole (AS), pulseless electrical activity (PEA), and pulse-generating rhythms (PR). Often, PEA and PR are called organized rhythms (ORG), or rhythms presenting visible QRS complexes in the electrocardiogram (EKG) [8]. PEA is characterized by a disassociation between the mechanical (contraction of the myocardium) and electrical (QRS complexes) activities of the heart, which leads to no palpable pulse [4].

OHCA rhythm classification algorithms are based on the analysis of the EKG, and in most cases address 2-class classification problems. A typical example is AED shock advice algorithms [9]–[11], designed to discriminate shockable (VF/VT) from nonshockable rhythms (AS/ORG). Depending on the clinical context a finer detail is needed. VT treatment may benefit from synchronized electrical cardioversion [12]. Another clinically relevant problem is the detection of spontaneous circulation or pulse, which is framed as a PEA/PR discrimination algorithm once ORG rhythms are identified [8], [13], [14]. So there is clearly a need for different levels of detail in OHCA cardiac rhythm classification. Five-class OHCA rhythm classification using the EKG was introduced by Rad *et al.*, [7], [15] using features obtained from the discrete wavelet transform (DWT) sub-band decomposition of an artifact-free EKG. Most OHCA rhythm classification algorithms consist of an EKG feature extraction stage followed by a machine learning classifier. EKG feature extraction has been approached in the time [16], [17], frequency [18], [19], time-frequency [15], [20], [21],

and complexity domains [22], [23]. The machine learning approaches explored in the classification stage include K-nearest neighbors [15], [24], support vector machines [10], [25], [26], artificial neural networks [13], [19], [27], and ensembles of decision trees [11], [14].

OHCA rhythm classification is further complicated by the presence of CPR artifacts in the EKG. Interruptions in CPR to classify the rhythm lead to interrupted perfusion of vital organs and lowers chances of survival [28]. Efforts have been made to develop accurate OHCA rhythm analysis methods during CPR [29]. The most popular approach is the suppression of the CPR artifact using adaptive filters [30]–[32], followed by an EKG feature extraction stage on the filtered EKG. These approaches have been successfully demonstrated to discriminate shockable (Sh) from nonshockable (NSh) rhythms both during manual CPR [33] and piston driven mechanical CPR [21]. In fact, an improved feature extraction based on the stationary wavelet transform (SWT) sub-band decomposition has yielded improved classification results for shock/no-shock decisions during mechanical CPR, and is the basis for feature extraction in this work. However, there are no studies on multiclass OHCA rhythm classification during CPR. In fact, when 5-class OHCA rhythm classifiers developed using artifact-free EKG were tested during CPR their performance substantially degraded [15], [27]. So there is a need to develop algorithms for multiclass OHCA rhythm classification during CPR.

This study introduces new methods for multiclass OHCA rhythm classification during CPR, using features obtained from the SWT analysis of the EKG after filtering CPR artifacts. The scope of the algorithms is gradually increased from 2-class to 5-class rhythm classification to address the different levels of clinical detail needed depending on the application. The following classification problems were studied: Sh/NSh, Sh/AS/ORG, VF/VT/AS/ORG, and VF/VT/AS/PEA/PR. The paper is organized as follows. The study dataset and its annotation are described in Section II; feature engineering including CPR artifact filtering is described in Section III; Section IV describes the architecture used for the optimization and evaluation of the classification algorithms. Finally, results, discussion, and conclusions are presented in Sections V-VII.

II. DATA COLLECTION AND PREPARATION

Data were extracted from a large prospective OHCA clinical trial designed to measure CPR-quality, and conducted in three European sites between 2002 and 2004: Akershus (Norway), Stockholm (Sweden) and London (UK) [34], [35]. Prototype defibrillators based on the Heartstart 4000 (Philips Medical Systems, Andover, Mass) were deployed in 6 ambulances at each site. The defibrillators were fitted with an external CPR assist pad that measured compression depth [36]. The raw data for our study consisted of the EKG and transthoracic impedance obtained from the defibrillation pads, and the compression depth. All signals were originally sampled at 500 Hz, and then downsampled to a sampling frequency of
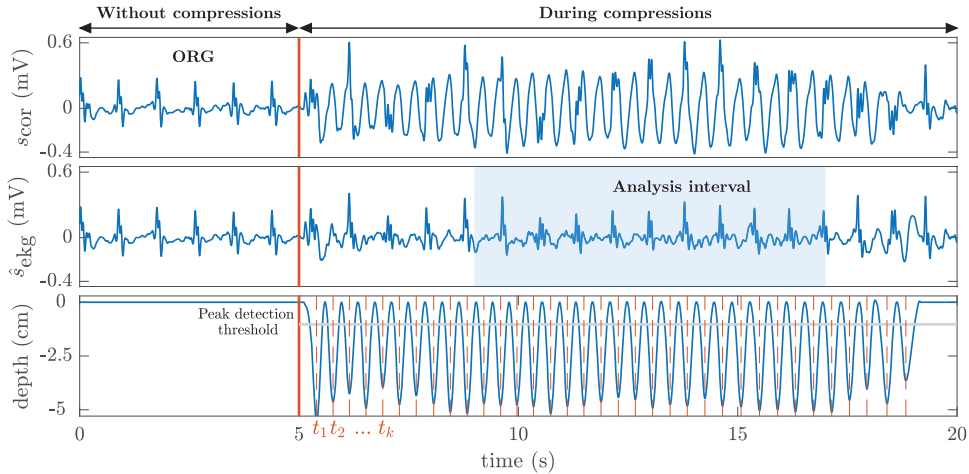
FIGURE 1. One 20-s segment from the dataset corresponding to a patient with an organized rhythm (ORG). In the first 5 s there is no artifact and the ORG rhythm is visible, in the last 15 s the CPR artifact conceals the patient's rhythm. After filtering $\hat{s}_{ekg}$ is obtained (middle panel), and the underlying rhythm is again visible in the artifacted interval. The bottom panel shows the compression depth signal with the chest compression instants (t_k) highlighted using vertical red lines.

$f_s = 250\,Hz$ ($T_s = 4$ ms) for this study. A notch and a Hampel filter were used to remove powerline interferences and spiky artifacts, respectively. Chest compression instants (t_k), were automatically marked in the depth signal using a negative peak detector for depths exceeding 1 cm (see Fig. 1).

All recordings were annotated for the original study into the five OHCA rhythm types, by consensus between an experienced anesthesiologist trained in advanced cardiac life support and a biomedical engineer specialized in resuscitation [34]. VF was defined as an irregular ventricular rhythm with peak-to-peak amplitudes above $100\,\mu V$ and a fibrillation frequency above 2 Hz. Regular ventricular rhythms with rates above $120\,\mathrm{min}^{-1}$ were annotated as VT. AS was annotated in rhythms with peak-to-peak amplitude below $100\,\mu V$ and/or rates below $12\,\mathrm{min}^{-1}$, and ORG rhythms when the heart rate was above 12 min^{-1}. ORG rhythms were further classified into PEA or PR by assessing the presence of blood flow, indicated by clinical annotations of pulse done during resuscitation, or by the presence of fluctuations in the thoracic impedance aligned with the QRS complexes [13], [34].

For this study, we automatically extracted 20-s segments with the following characteristics: unique rhythm type, ongoing compressions during a 15-s interval, and a 5-s interval without compressions either preceding or following chest compressions (see Fig. 1). The interval during compressions was used to develop and evaluate the OHCA rhythm classifiers, and the interval without compression artifacts to confirm the original rhythm annotation. All automatically extracted segments were reviewed by 3 experienced biomedical engineers to discard segments with low signal quality and noise, and to certify by consensus that the original annotations in the dataset were correct. The final dataset contained 2133 segments from 272 patients, whereof 580 were AS (139 patients), 94 PR (31), 953 PEA (167), 479 VF (103), and 27 VT (11).

III. FEATURE ENGINEERING

Feature engineering consisted of 3 stages. First, chest compression artifacts were removed using an adaptive filter. Then, a multi-resolution analysis of the EKG was performed using wavelet transforms, from which the denoised EKG and its sub-band decomposition were obtained. Finally, high-resolution features were extracted from the denoised EKG and its sub-band components. In what follows n is the sample index, so $t = n \cdot T_s$.

A. CPR ARTIFACT FILTER

CPR artifacts were suppressed using a state-of-the-art method based on a recursive least squares (RLS) filter [32] that estimates the CPR artifact, $s_{cpr}(n)$, as a quasiperiodic interference [31]. The fundamental frequency of the artifact, $\omega_0(n)$, is the instantaneous frequency of the chest compressions. The CPR artifact is represented as a truncated Fourier series of N harmonically related components of frequencies $\omega_\ell = \ell \cdot \omega_0$ and slowly time-varying Fourier coefficients [31]:

$$s_{cpr}(n) = A(n) \sum_{\ell=1}^{N} a_\ell(n) \cos(\omega_\ell n) + b_\ell(n) \sin(\omega_\ell n)$$
$$= A(n) \Theta^{\mathsf{T}}(n) \Phi(n) \qquad (1)$$

where

$$\Phi(n = [\cos(\omega_1 n) \ \sin(\omega_1 n) \ldots \cos(\omega_N n) \ \sin(\omega_N n)]^{\mathsf{T}} \quad (2)$$
$$\Theta(n) = [a_1(n) \ b_1(n) \ \ldots \ a_N(n) \ b_N(n)]^{\mathsf{T}} \qquad (3)$$

and $A(n) = 1$ during compressions, and $A(n) = 0$ otherwise. The time-varying coefficients of the RLS filter are the in-phase (a_ℓ) and quadrature (b_ℓ) components in vector $\boldsymbol{\Theta}(n)$. The instantaneous frequency of the compressions was derived from the t_k instants obtained from the depth signal (see Fig. 1):

$$\omega_0(n) = 2\pi \frac{1}{t_k - t_{k-1}} \qquad t_{k-1} \leq nT_s < t_k \qquad (4)$$

The RLS coefficients were adaptively estimated to minimize the mean square error between the corrupted EKG, s_{cor}, and the estimated artifact, $\hat{s}_{\text{cpr}}$, at the frequency of the harmonics. The error signal of the RLS filter is thus the filtered EKG, $\hat{s}_{\text{ekg}}$, which is used to identify the underlying rhythm. The RLS update equations are [37]:

$$\hat{s}_{\text{ekg}}(n) = s_{\text{cor}}(n) - A(n)\boldsymbol{\Theta}^{\mathsf{T}}(n-1)\boldsymbol{\Phi}(n) \qquad (5)$$

$$\mathbf{F}(n) = \frac{1}{\lambda}\left[\mathbf{F}(n-1) - \frac{\mathbf{F}(n-1)\boldsymbol{\Phi}(n)\boldsymbol{\Phi}^{\mathsf{T}}(n)\mathbf{F}(n-1)}{\lambda + \boldsymbol{\Phi}^{\mathsf{T}}(n)\mathbf{F}(n-1)\boldsymbol{\Phi}(n)}\right] \qquad (6)$$

$$\boldsymbol{\Theta}(n) = \boldsymbol{\Theta}(n-1) + \mathbf{F}(n)\boldsymbol{\Phi}(n)\hat{s}_{\text{ekg}}(n) \qquad (7)$$

The gain matrix and coefficients vector were initialized to $F(0) = 0.03 \cdot \mathbf{I}_{2N}$ and $\Theta(0) = \mathbf{0}$, where $\mathbf{I}_{2N}$ is the $2N \times 2N$ identity matrix. The forgetting factor of the RLS algorithm, λ, and the number of harmonics, N, were set to 0.998 and 4, as recommended in [32].

B. STATIONARY WAVELET TRANSFORM

EKG multiresolution analysis was done using the SWT, which differs from the standard DWT in that at each decomposition level the low-pass (approximation) and high-pass (detail) components are not downsampled. Instead, the filters are upsampled so all detail and approximation coefficients have the length of the original signal, producing a translation-invariant representation [38].

Each EKG segment was decomposed into its sub-bands using a pair of quadrature mirror lowpass (h_j) and highpass (g_j) filters, which for level 0 are related by:

$$g_0(L - 1 - n) = (-1)^n h_0(n), \qquad (8)$$

where L is the length of the filters. At stage j the filters were those of stage 0 upsampled by a 2^j factor, $h_j(n) = h_0(n)_{\uparrow 2^j}$. The detail, $d_j(n)$, and approximation, $a_j(n)$, coefficients were recursively obtained through convolution ($*$):

$$a_0(n) = \hat{s}_{\text{ekg}}(n) \qquad (9)$$

$$a_j(n) = h_{j-1}(n) * a_{j-1}(n) \qquad (10)$$

$$d_j(n) = g_{j-1}(n) * a_{j-1}(n) \qquad (11)$$

The time-reversed version of the decomposition filters, that is $\bar{h}(n) = h(L - 1 - n)$, were recursively used to reconstruct the original signal [38]:

$$a_{j-1}(n) = \frac{1}{2}\left(\bar{h_j}(n) * a_j(n) + \bar{g_j}(n) * d_j(n)\right) \qquad (12)$$

from $j = J, \ldots, 1$.

EKG features were extracted using a 2048-sample analysis interval (8.192 s) of $\hat{s}_{\text{ekg}}$ centered in the 15 s during chest

compressions (see Fig. 1). A Daubechies 4 mother wavelet and $J = 7$ decomposition levels were used to generate a_7 and $d_7, \ldots, d_1$. Only detail coefficients $d_3 - d_7$ were used for feature extraction, which is equivalent to retaining the spectral components in the $0.98 - 31.25\,Hz$ band. Soft denoising was applied to $d_3 - d_7$ with a universal threshold rescaled by the standard deviation of the noise [39]. The denoised $d_3 - d_7$ coefficients were used to obtain the denoised EKG, $\hat{s}_{\text{den}}$, by recursively applying eq. (12). The whole decomposition and denoising (reconstruction) processes are illustrated in Fig. 2 for two rhythms, a VF and an ORG.

C. FEATURE EXTRACTION

Ninety three features were extracted from $\hat{s}_{\text{den}}$ and $d_3 - d_7$. These features quantify the most distinctive characteristics of OHCA rhythm subtypes, and encompass the collective knowledge of over 25 years of active research in the field (over 250 features from the available literature were initially analyzed). In what follows, feature naming is that of the original papers, and the MATLAB code for feature calculation is available from (https://github.com/iraiaisasi/OHCAfeatures). The features grouped by analysis domain are:

- *Time domain* (5 features). These were only extracted from $\hat{s}_{\text{den}}$ and include: bCP [18], x1, x2 [33], and the mean and the standard deviation of the heart rate (MeanRate and StdRate) obtained from the QRS detections of a modified Hamilton-Tompkins algorithm [14], [40].
- *Spectral domain* (6 features). Including the classical x3, x4, x5 [33], VFleak [41], and two new features, Enrg, the relative energy content of the signal in the 4-8 Hz frequency band, and SkewPSD, the skewness of the power spectral density of the EKG. All features were computed from $\hat{s}_{\text{den}}$.
- *Complexity analysis* (14 features), including CVbin and Abin [42] of $\hat{s}_{\text{den}}$, and two measures of entropy for $\hat{s}_{\text{den}}$ and $d_3 - d_7$. The entropy measures were the sample entropy (SampEn) of the signal, and the Shannon entropy (ShanEn) of the sign of the first difference [43].
- *Statistical analysis* (54 features). Nine features were calculated to characterize the statistical distribution of the signal amplitude: interquartile ranges (IQR) [15], mean and standard deviation of the absolute value of the amplitudes (MeanAbs and StdAbs) and slopes (MeanAbs1 and StdAbs1), Skewness (Skew), Kurtosis (Kurt) [11], and the Hjorth mobility and complexity (Hmb and Hcmp) [44]. All the features were computed for $\hat{s}_{\text{den}}$ and $d_3 - d_7$.
- *Phase space features* (14 features). Taken's time-delay embedding method [45] with a delay of $\tau = 2$ samples was used to create a two-dimensional phase space representation for $\hat{s}_{\text{den}}$ and $d_3 - d_7$ [46]. An ellipsoid was fitted in the phase-space using the least squares criterion, and its major axis (EllipPS), and the skewness of
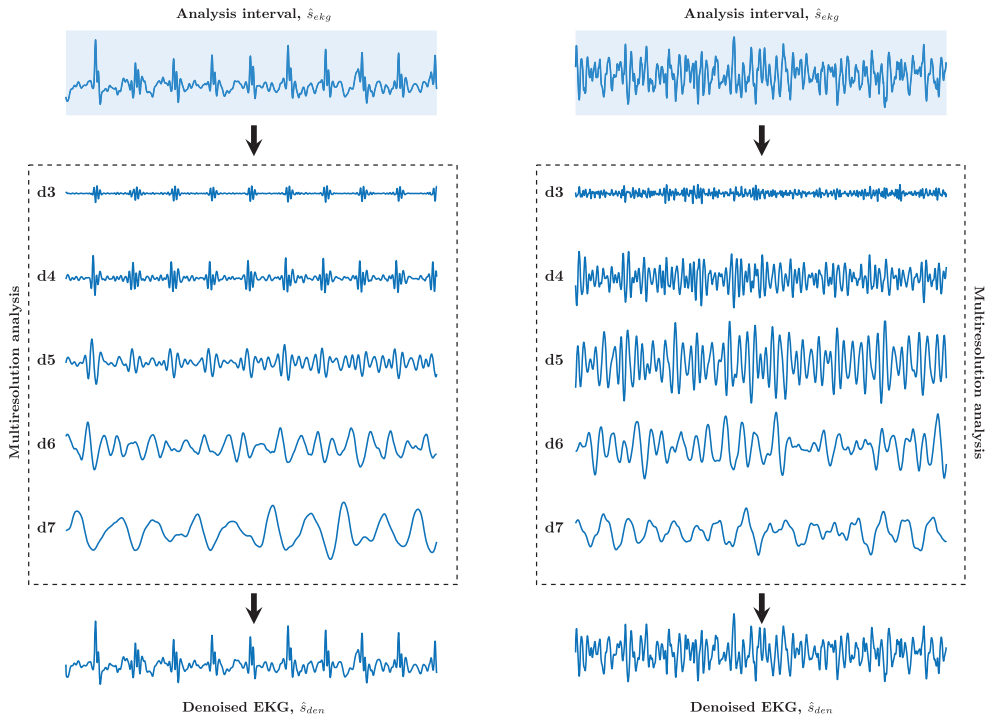
FIGURE 2. SWT sub-band decomposition and denoised EKG reconstruction for the 8.192-s analysis interval of the filtered EKG, $\hat{s}_{ekg}$. The left panel corresponds to an organized rhythm (ORG) and the right panel to a ventricular fibrillation (VF).

the distance distributions in the phase space (SkewPS) were computed. Then a recurrence quantification analysis (RQA) was used to extract and quantify the transition structures of the system dynamics in the phase space. Two RQA measures were computed only for $\hat{s}_{den}$, the length of the longest diagonal line (RQA1), and the recurrence period density entropy (RQA2) [47].

The dataset can thus be represented as a set of instance-label pairs $\{(\boldsymbol{x}_1, y_1), ..., (\boldsymbol{x}_N, y_N)\}$ where y_i are the class labels (for instance $\{0, 1\}$ for a Sh/NSh classification problem), the feature vector $\boldsymbol{x}_i \in \mathbb{R}^K$ contains the values of the $K = 93$ features for EKG segment i, and $N = 2133$ is the number of EKG segments in the database.

IV. CLASSIFIER TRAINING AND EVALUATION

A repeated quasi-stratified nested cross-validation (CV) architecture was used [21], [48], with an outer 10-fold CV for feature selection and model assessment, and an inner 5-fold CV for classifier parameter optimization. First, for each training set of the outer CV, features were selected using recursive feature elimination (RFE) [49]. Then, these features were used in the inner CV to optimize the parameters of the classifier. Finally, the classifier was trained and assessed in the outer loop. Data were always partitioned patient-wise

and in a quasi-stratified manner, by forcing the prevalence of each rhythm in each fold to be at least 70% of the prevalence of that rhythm in the whole set. In this way patient-wise and stratified sampling could be done simultaneously.

Confusion matrices were used to evaluate the performance of the classifiers [15], and four classification problems were addressed: Sh/NSh (2-class), Sh/AS/ORG (3-class), VF/VT/AS/ORG (4-class), and VF/VT/AS/PEA/PR (5-class). For each class i the sensitivity (Se_i) was computed, and the unweighted mean of all sensitivities (UMS) was used as summarizing metric:

$$\mathrm{Se}_i = \frac{\mathrm{TP}_i}{\mathrm{TP}_i + \mathrm{FN}_i}, \quad \mathrm{UMS} = \frac{1}{P} \sum_{i=1}^{P} \mathrm{Se}_i \qquad (13)$$

where TP_i and FN_i are the true positives and false negatives for class i, and P is the number of classes. The nested CV procedure was repeated 50 times to estimate the statistical distributions of Se_i and UMS, and to obtain the stacked confusion matrices for each classification problem.

A. CLASSIFIER

Random forest (RF) classifiers [50] were used to decide the EKG rhythm class. An RF is an ensemble of B decision
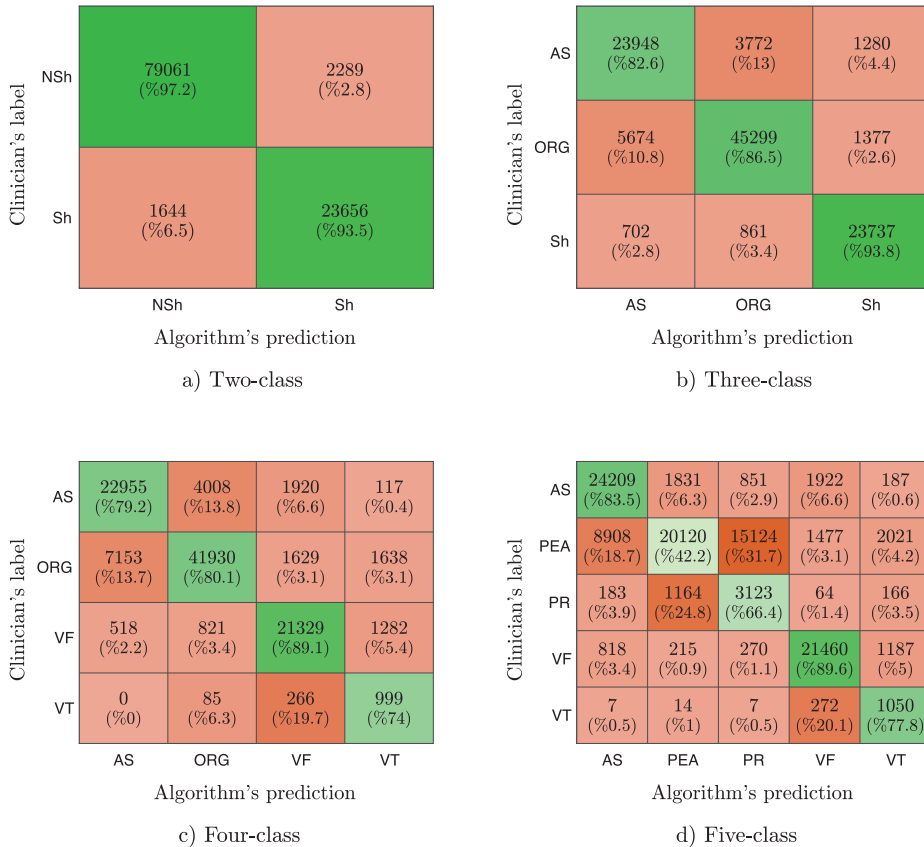
FIGURE 3. Stacked confusion matrices for 50 runs of the nested CV procedure for the different models. The mean sensitivities for each class and model are shown in the diagonals (mean and median sensitivities are slightly different, see table 1).

trees $\{T_1(\boldsymbol{x}), ..., T_B(\boldsymbol{x})\}$ that produces B nearly uncorrelated predictions $\{\hat{y}_1 = T_1(\boldsymbol{x}), ..., \hat{y}_B = T_B(\boldsymbol{x})\}$ of the rhythm type for the EKG segment. Training an RF classifier comprises:

- Generating B training subsets from the original training data by bootstrapping (i.e., random sampling with replacement). We choose each training subset to have the same size as the original training data.
- A classification tree is grown for each training subset by choosing the best split among a randomly selected subset of m_{try} features in each node. The criterion to choose the split was to minimize the cross-entropy.
- The recursive binary splitting continues until each terminal node has fewer than some minimum number of observations, l_{size}.
- The decision of classifier, $\hat{y}_j = F_{RF}(\boldsymbol{x}_j)$, is obtained by the majority vote of the B trees.

Once the models were trained, the predictions in the validation sets were obtained by comparing the predictions of the model $\hat{y}_j$ to the labels assigned by the clinicians y_j, to obtain the confusion matrix of the model and the metrics derived thereof.

We considered three parameters of the RF classifier: B, m_{try}, and l_{size}. The number of trees was initially fixed to $B = 500$. This choice is not critical, a sufficiently large number stabilizes the accuracy and further increasing B does not overfit the model [50]. The number of predictors per split was set to the default value $\sqrt{K}$. The minimum number of observations per leaf, l_{size}, controls the depth of the trees, and was identified as critical in our preliminary tests. We optimized l_{size} in the inner CV by doing a grid-search in the range $1 \leq l_{size} \leq 200$ with the UMS as the objective function. Finally, uniform prior probabilities for each class were assigned during training to address the class imbalance.

B. FEATURE SELECTION

Feature selection was based on an RFE approach using the permutation importance as a ranking criterion [51]–[53]. Permutation importance is a built-in characteristic of the RF
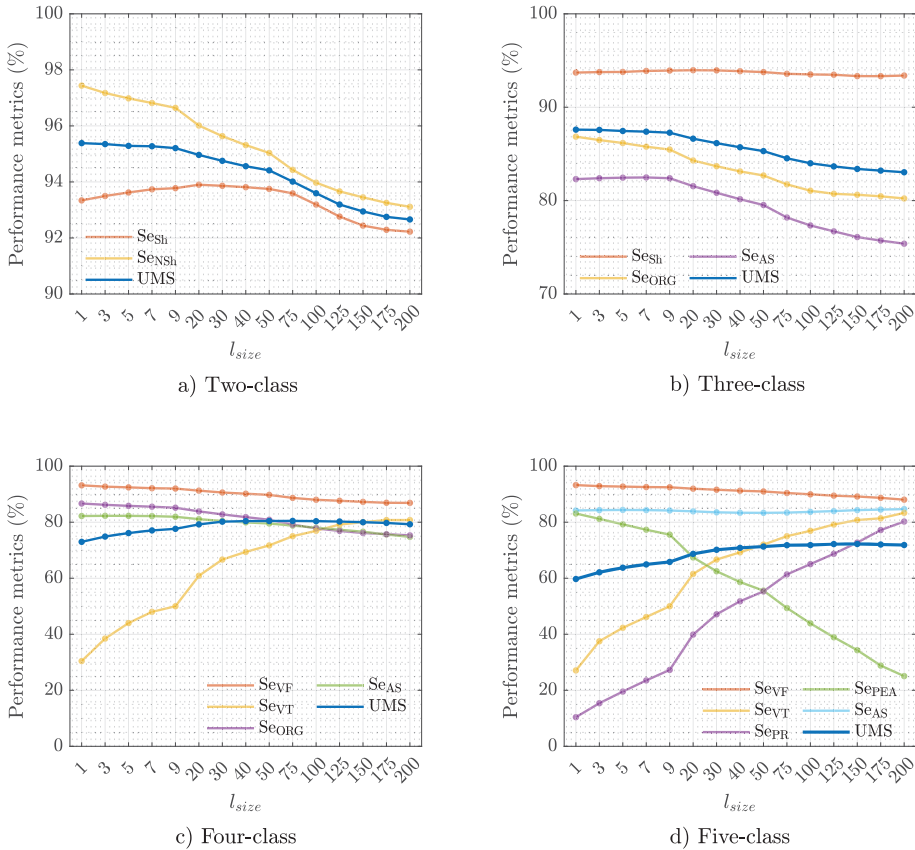
FIGURE 4. Median UMS and Se per class in the 50 repeats of the 10-fold outer CV, as a function of l_{size}.

classifier that ranks feature importance by permuting the values of the feature in the training data and assessing the out-of-bag error. Large errors mean the feature is important for classification. At each iteration of the RFE algorithm, features were ranked and the least important 3% of the features were removed. The process was continued until K_{cl} features were left for classification. The values decided for the different models were: $K_{cl} = 25$ for 2-class, $K_{cl} = 30$ for 3-class, $K_{cl} = 35$ for 4-class, and $K_{cl} = 40$ for 5-class.

V. RESULTS
The results reported in this section are those obtained after running the RFE feature selection algorithm in the 10-fold outer CV until K_{cl} features were left, and fitting the classifiers with the optimal parameters determined in the 5-fold inner CV. The process was repeated in 50 random repetitions of the nested CV procedure, there are thus 50 estimates of the metrics for the whole dataset and 500 algorithmic runs on the validation folds in the outer CV. The metrics are reported as median (interdecile range, IDR) for those 50 evaluations.

A detailed analysis of the classification results for the different class models are shown in Table 1 and Fig. 3. Fig. 3 shows the confusion matrices obtained stacking the predictions from the 50 random repetitions of the nested CV procedure, and provide all the information needed to accurately calculate the performance metrics for each rhythm type and classifier. The median (IDR) of the sensitivities and UMS for each classifier are shown in Table 1. The clinical relevance of the classification results and classification errors is addressed in section VI, the discussion.

As reference, we also computed the classification results when the features were selected exclusively on the feature's permutation importance. That is, the RFE algorithm was substituted by a single feature ranking based on importance from which the K_{cl} most important features were selected. Using a single feature ranking based on importance the median (IDR) UMS for the 2, 3, 4 and 5-class classifiers were 95.3% (95.0-95.5), 87.3% (86.9-87.6), 81.1% (79.5-82.3), and 67.8% (65.7-70.0), respectively. The classification results for 2, 3, and 4 classes were similar to those obtained using

TABLE 1. Median UMS and sensitivity per class for different classifiers. The metrics are reported as median (IDR) for the 50 runs of the nested CV procedure.

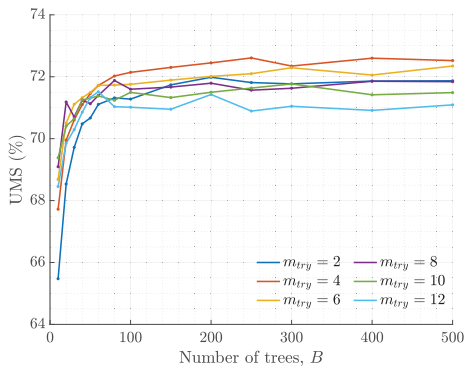| Classifier	Se (%)	UMS (%)
Two-class		
Sh	93.5 (93.0-93.9)	**95.4 (95.1-95.6)**
NSh	97.2 (97.0-97.4)	
Three-class		
AS	82.5 (81.6-83.4)	
OR	86.5 (86.0-87.1)	**87.6 (87.3-88.1)**
Sh	93.9 (93.3-94.3)	
Four-class		
AS	79.0 (78.1-80.3)	
OR	80.1 (78.8-81.3)	**80.6 (79.3-81.8)**
VF	89.1 (88.2-89.8)	
VT	74.1 (70.4-77.8)	
Five-class		
AS	83.4 (81.9-85.1)	
PEA	42.6 (37.6-46.9)	
PR	65.4 (60.1-73.9)	**71.9 (69.5-74.6)**
VF	89.6 (88.5-90.6)	
VT	77.8 (66.7-88.9)	

FIGURE 5. The median UMS (5-class) in the 50 random repetitions, as a function of the number of trees, B, and the number of features per split, m_{try}.

RFE feature selection, but an advanced feature selection approach combining feature importance and sequential feature elimination boosted the 5-class classification results by 4-points.

A. SELECTION OF PARAMETERS

The most critical parameter in our RF classifiers was the minimum number of observations in the terminal nodes, l_{size}, which gives a compromise between bias and variance by controlling how shallow the classification trees are. Larger values of l_{size} produce shallower trees. Fig. 4 shows, for the different classifiers, the median value of the performance metrics for the evaluations of the 50 repeats of the 10-fold outer CV as a function of l_{size}. In the cases where class imbalance is smaller (2 and 3 class) deeper trees increase the UMS, however when the class imbalance is large (4 and 5 class) shallower trees produce better results (see Fig. 4). The median (IDR) value of the optimal l_{size} for the 2 and 3-class classifiers were 3 (1.0-7.0) and 3 (1.0-5.0), but increased considerably to
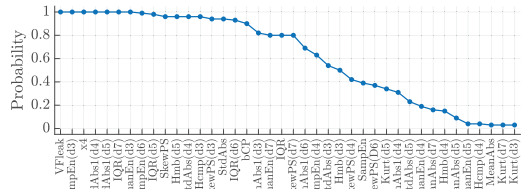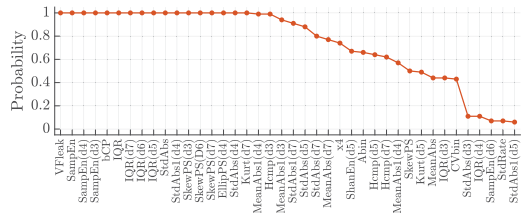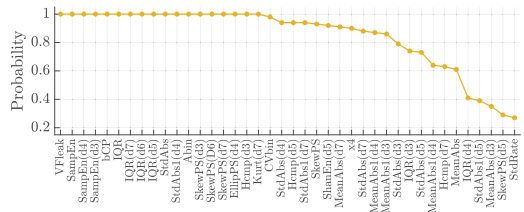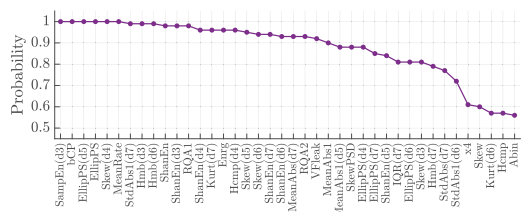
FIGURE 6. Selection probability for the 40 most selected features in the 500 runs of feature selection (outer loop).

80 (30.0-150.0) and 125 (50.0-200.0) for the cases of 4 and 5-classes.

Fig. 4 also shows that the sensitivity for the classes with lower prevalence (VT and PR) increases with shallower trees. In the 4-class classifier the sensitivity for VT increased by more than 40 points when l_{size} was raised from 1 to 100, while the sensitivities of the most prevalent classes (AS, ORG, and VF) decreased very slightly. A similar behavior was observed for the sensitivities of VT and PR in the 5-class problem, although in this case the sensitivity of PEA, the rhythm that borders PR and VT, decreased considerably from 83.1 % to 25.1 %. PEA sensitivity could be better addressed using
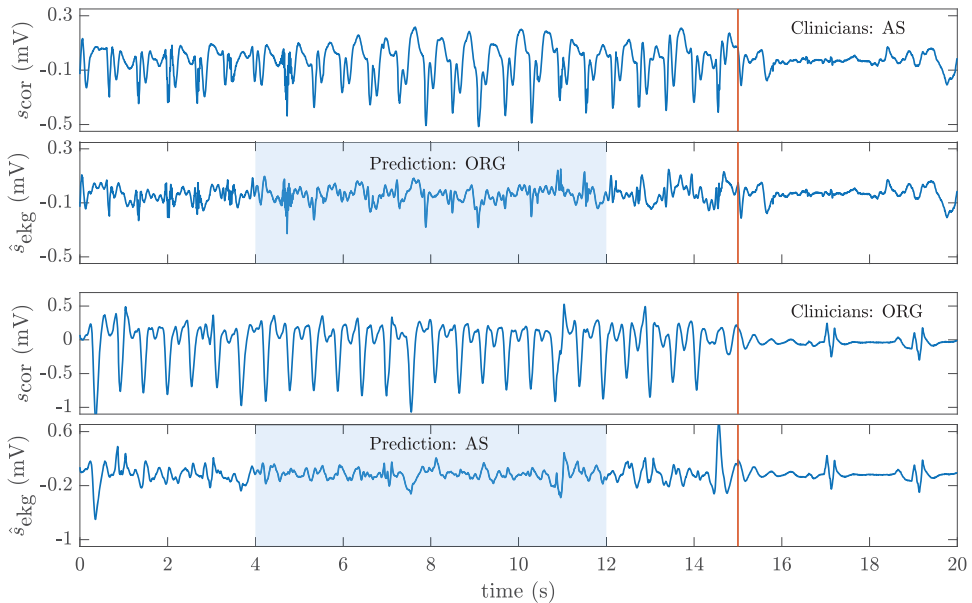
FIGURE 7. Two examples of misclassified segments for the 3-class classifier. In the top panel an AS is classified as ORG, while the bottom panel shows an ORG misclassified as AS.

multimodal analysis by adding information on perfusion from other signals like pulse oximetry, invasive blood pressure, brain oximetry or expired CO_2 when available [54], [55].

Changing the number of trees, B, and the features per split, m_{try}, had less impact on classification. Fig. 5 shows the median UMS of the 50 random repetitions of the 5-class classifier for different choices of B and m_{try}, with $l_{size} = 125$. The figure shows that our preliminary design choices were sound, the UMS stabilizes for $B > 250$ and the effect of m_{try} on the classification results was small with the median UMS varying between 70.9 % and 72.6 %. So the default $m_{try} = \sqrt{K}$ value was a very acceptable choice.

B. FEATURE SELECTION AND RELEVANCE
Feature design is key in classical machine learning. In our approach, we introduced the SWT for multi-resolution analysis because it allows a better amplitude and statistical characterization of the features than the classical DWT used by Rad *et al.* [15]. In addition soft denoising produced a reconstructed signal from which many classical OHCA rhythm classification features could be better estimated. Fig. 6 shows the 40 features with the highest probability of selection (the most important features) for each classification problem. These probabilities were estimated by counting the number of times the features were selected in the 500 runs of feature selection algorithm (50 repeats of 10-fold outer CV). For the 2-class problem the most relevant features

are a mixture of those derived from the detail coefficients and from the denoised signal and correspond to complexity, frequency, time, and statistical domains. For the 3 and 4-class classifiers, features derived from the phase-space reconstruction of the signals were also relevant. Finally, for the most challenging 5-class classifier, the RQA analysis was also needed to improve classification results. Features like `VFleak`, `SampEn` (d_3) and `IQR` (d_7) were selected in all feature selection runs corresponding to the 2, 3 and 4-class classifiers and `SampEn` (d_3) was also selected in all the runs of the 5-class classifier. These results are consistent with our previous findings on shock/no-shock decisions during mechanical CPR [21]. Although CPR artifacts present very different characteristics during mechanical and manual CPR, features derived from the SWT decomposition of the filtered EKG seem to be very robust and independent of the filtering residuals, thus are able to capture the distinctive characteristics of OHCA rhythms.

VI. DISCUSSION
The relevance of the detailed classification results presented in Table 1 and Fig. 3 is better understood in the context of the clinical importance of each classification problem, and by providing illustrative examples of the classification errors that show the limitations of our approach. For the Sh/NSh 2-class problem, the median UMS was 95.4%, with median sensitivity for the shockable and nonshockable rhythms of 93.5 % and 97.2 %, respectively. This is a very important problem
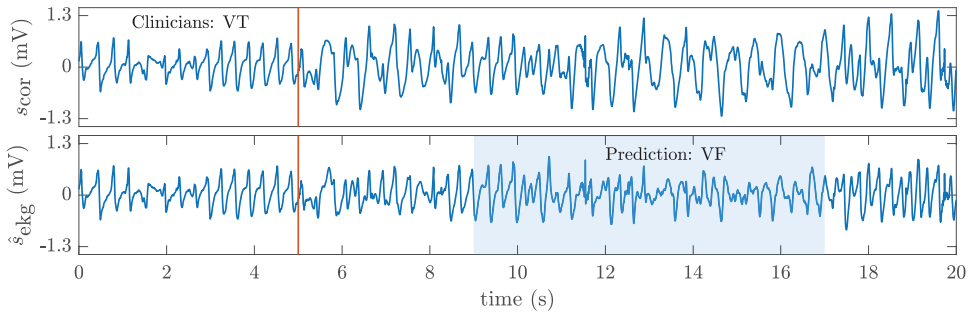
FIGURE 8. An example of a VT classified as VF by the 4-class classifier.
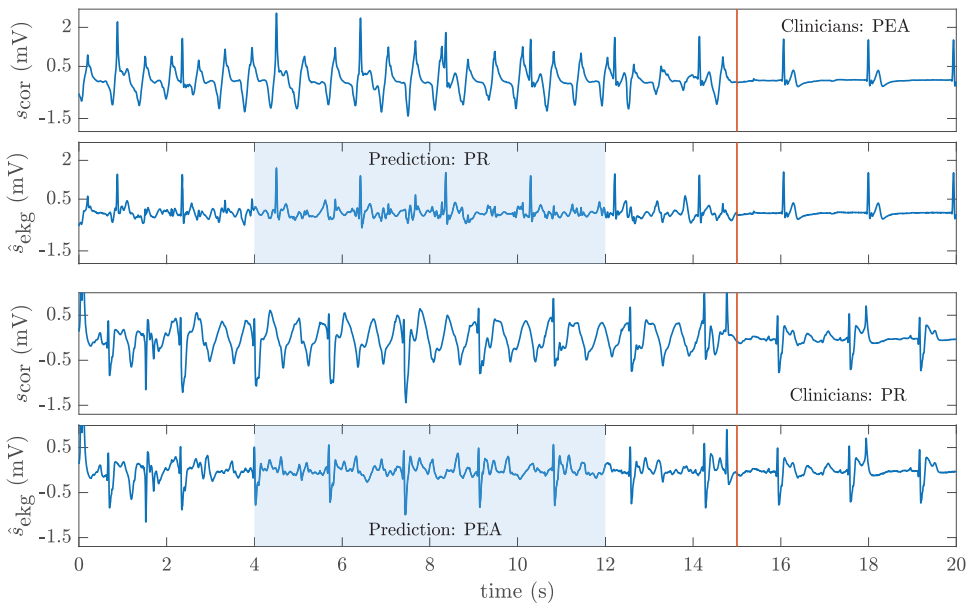
FIGURE 9. Two examples of misclassified PEA/PR rhythms. The last five seconds (clean intervals) of both panels show the difficulty of pulse assessment based only on the EKG.

since it addresses shock advice decisions during CPR. Shock advice algorithms for defibrillators are normally tested on artifact-free data. In that scenario, the American Heart Association requires a minimum sensitivity for shockable and nonshockable rhythms of 90 % and 95 %, respectively [56]. Our solution is above those requirements. Moreover, our results improve by over 1.5-points the UMS reported for the most accurate shock/no-shock algorithms during manual chest compressions [33], [57].

A finer classification of NSh rhythms includes the distinction between AS and ORG rhythms, which can be important to determine pharmacological treatment, or the effect of adrenaline use and dosage during CPR [58]. The UMS for the 3-class classifier was above 87.5 %, and shockable rhythms had a sensitivity of 93.9%. However, the distinction between AS/ORG during CPR was difficult, 13% of AS were incorrectly classified as ORG whereas a 10.8% of ORG rhythms were classified as AS. These finding are in line with those reported by Kwok *et al.*, who on a limited set of patients demonstrated the first 3-class rhythm classification algorithm during CPR [20]. In scenarios without CPR artifact the distinction between AS/ORG is simple and can be addressed using energy and heart-rate measures [33]. During chest compressions spiky filtering residuals may be confounded as QRS complexes during AS (Fig. 7, top panel). Conversely, CPR artifact filtering may reduce R-peak amplitudes in ORG rhythms producing erroneous AS classifications (Fig. 7, bottom panel).

Classifying shockable rhythms into VT or VF may allow synchronized electrical cardioversion on VT, to avoid the R on T phenomenon that may induce VF. However, the sensitivity for VT dropped considerably in the 4-class problem, 19.7% of VT was classified as VF and 6.3 % as ORG. VT rhythms can be confounded as ORG (narrower monomorphic VT) or VF (more irregular Torsades de Pointes). CPR artifacts further complicate the problem since filtering residuals may resemble an irregular VF during VT (see Fig. 8). In any case, the median UMS for the 4-class problem was 80.6%, more than 55-points higher than the 25 % value expected for a random guess.

In the 5-class problem, most of the errors were caused by the PEA/PR distinction (presence of pulse in ORG rhythms). Pulse assessment using only the EKG is hard, and determination of pulse during OHCA frequently relies on additional surrogate variables of perfusion like pulse oximetry signals, invasive blood pressure measurements, or expired CO_2 [55], [59]. Fig. 9 shows two representative examples of the difficulty of determining pulse using only the EKG. However, our 5-class classifier had a median UMS of 71.9% during CPR, which is only 5.8-points lower than the 5-class OHCA rhythm classifier on artifact-free EKG proposed by Rad et al. [15]. Furthermore, when Rad et al. used their algorithms to annotate complete OHCA episodes (no data pruning), the UMS during artifact-free segments was 75 %, but dropped to 52.5 % in intervals during chest compressions, even after filtering the CPR artifact [27]. Our architecture would therefore substantially improve the accuracy of 5-class classifiers during CPR.

VII. CONCLUSIONS

A robust methodology for OHCA rhythm classification during CPR has been presented. The approach consists of an adaptive CPR artifact suppression filter, followed by feature extraction based on the SWT multiresolution analysis of the EKG, the features are finally fed to a random forest to classify the cardiac rhythm. The approach was successfully demonstrated for 2, 3, 4 and 5-class OHCA cardiac rhythm classification, addressing the most important clinical scenarios for rhythm assessment during CPR. Our method improved the state-of-the-art methods in the extensively studied 2-class shock/no-shock decision scenario, meeting the criteria of the American Heart Association for artifact-free EKG. To the best of our knowledge, we introduced the first general framework for multi-class OHCA rhythm classification during CPR with increasing levels of clinical detail, and our approach substantially improved the accuracy of 5-class OHCA cardiac rhythm classifiers during CPR.

REFERENCES

[1] J.-T. Gräsner et al., "EuReCa ONE-27 nations, ONE Europe, ONE registry: A prospective one month analysis of out-of-hospital cardiac arrest outcomes in 27 countries in Europe," Resuscitation, vol. 105, pp. 188–195, Aug. 2016.

[2] G. D. Perkins, A. J. Handley, R. W. Koster, M. Castrén, M. A. Smyth, T. Olasveengen, K. G. Monsieurs, V. Raffay, J.-T. Gräsner, V. Wenzel, G. Ristagno, and J. Soar, "European resuscitation council guidelines for resuscitation 2015: Section 2. Adult basic life support and automated external defibrillation," Resuscitation, vol. 95, pp. 81–99, Oct. 2015.

[3] T. Nordseth, D. E. Niles, T. Eftestøl, R. M. Sutton, U. Irusta, B. S. Abella, R. A. Berg, V. M. Nadkarni, and E. Skogvoll, "Rhythm characteristics and patterns of change during cardiopulmonary resuscitation for in-hospital paediatric cardiac arrest," Resuscitation, vol. 135, pp. 45–50, Feb. 2019.

[4] T. Nordseth, D. Bergum, D. P. Edelson, T. M. Olasveengen, T. Eftestøl, R. Wiseth, B. S. Abella, and E. Skogvoll, "Clinical state transitions during advanced life support (ALS) in in-hospital cardiac arrest," Resuscitation, vol. 84, no. 9, pp. 1238–1244, 2013.

[5] J. T. Kvaløy, E. Skogvoll, T. Eftestøl, K. Gundersen, J. Kramer-Johansen, T. M. Olasveengen, and P. A. Steen, "Which factors influence spontaneous state transitions during resuscitation?" Resuscitation, vol. 80, no. 8, pp. 863–869, 2009.

[6] E. Skogvoll, T. Eftestøl, K. Gundersen, J. T. Kvaløy, J. Kramer-Johansen, T. M. Olasveengen, and P. A. Steen, "Dynamics and state transitions during resuscitation in out-of-hospital cardiac arrest," Resuscitation, vol. 78, no. 1, pp. 30–37, 2008.

[7] A. B. Rad, K. Engan, A. K. Katsaggelos, J. T. Kvaløy, L. Wik, J. Kramer-Johansen, U. Irusta, and T. Eftestøl, "Automatic cardiac rhythm interpretation during resuscitation," Resuscitation, vol. 102, pp. 44–50, May 2016.

[8] E. Alonso, E. Aramendi, M. Daya, U. Irusta, B. Chicote, J. K. Russell, and L. G. Tereshchenko, "Circulation detection using the electrocardiogram and the thoracic impedance acquired by defibrillation pads," Resuscitation, vol. 99, pp. 56–62, Feb. 2016.

[9] U. Irusta, J. Ruiz, E. Aramendi, S. R. de Gauna, U. Ayala, and E. Alonso, "A high-temporal resolution algorithm to discriminate shockable from nonshockable rhythms in adults and children," Resuscitation, vol. 83, no. 9, pp. 1090–1097, 2012.

[10] Q. Li, C. Rajagopalan, and G. D. Clifford, "Ventricular fibrillation and tachycardia classification using a machine learning approach," vol. 61, no. 3, pp. 1607–1613, Jun. 2013.

[11] C. Figuera, U. Irusta, E. Morgado, E. Aramendi, U. Ayala, L. Wik, J. Kramer-Johansen, T. Eftestøl, and F. Alonso-Atienza, "Machine learning techniques for the detection of shockable rhythms in automated external defibrillators," PLoS ONE, vol. 11, no. 7, 2016, Art. no. e0159654.

[12] M. S. Link, L. C. Berkow, P. J. Kudenchuk, H. R. Halperin, E. P. Hess, V. K. Moitra, R. W. Neumar, B. J. O'Neil, J. H. Paxton, S. M. Silvers, R. D. White, D. Yannopoulos, and M. W. Donnino, "Part 7: Adult advanced cardiovascular life support: 2015 American heart association guidelines update for cardiopulmonary resuscitation and emergency cardiovascular care," Circulation, vol. 132, pp. S444–S464, Nov. 2015.

[13] M. Risdal, S. O. Aase, J. Kramer-Johansen, and T. Eftesol, "Automatic identification of return of spontaneous circulation during cardiopulmonary resuscitation," IEEE Trans. Biomed. Eng., vol. 55, no. 1, pp. 60–68, Jan. 2008.

[14] A. Elola, E. Aramendi, U. Irusta, J. D. Ser, E. Alonso, and M. Daya, "ECG-based pulse detection during cardiac arrest using random forest classifier," Med. Biol. Eng. Comput., vol. 57, no. 2, pp. 453–462, 2019.

[15] A. B. Rad, T. Eftestøl, K. Engan, U. Irusta, J. T. Kvaløy, J. Kramer-Johansen, L. Wik, and A. K. Katsaggelos, "ECG-based classification of resuscitation cardiac rhythms for retrospective data analysis," IEEE Trans. Biomed. Eng., vol. 64, no. 10, pp. 2411–2418, Oct. 2017.

[16] I. Jekova and V. Krasteva, "Real time detection of ventricular fibrillation and tachycardia," Physiol. Meas., vol. 25, no. 5, p. 1167, 2004.

[17] N. V. Thakor, Y.-S. Zhu, and K.-Y. Pan, "Ventricular tachycardia and fibrillation detection by a sequential hypothesis testing algorithm," IEEE Trans. Biomed. Eng., vol. 37, no. 9, pp. 837–843, Sep. 1990.

[18] U. Irusta and J. Ruiz, "An algorithm to discriminate supraventricular from ventricular tachycardia in automated external defibrillators valid for adult and paediatric patients," Resuscitation, vol. 80, no. 11, pp. 1229–1233, 2009.

[19] A. Neurauter, T. Eftestøl, J. Kramer-Johansen, B. S. Abella, K. Sunde, V. Wenzel, K. H. Lindner, J. Eilevstjønn, H. Myklebust, P. A. Steen, and H.-U. Strohmenger, "Prediction of countershock success using single features from multiple ventricular fibrillation frequency bands and feature combinations using neural networks," Resuscitation, vol. 73, no. 2, pp. 253–263, 2007.

[20] H. Kwok, J. Coult, M. Drton, T. D. Rea, and L. Sherman, "Adaptive rhythm sequencing: A method for dynamic rhythm classification during CPR," *Resuscitation*, vol. 91, pp. 26–31, Jun. 2015.

[21] I. Isasi, U. Irusta, A. Elola, E. Aramendi, U. Ayala, E. Alonso, J. Kramer-Johansen, and T. Eftestøl, "A machine learning shock decision algorithm for use during piston-driven chest compressions," *IEEE Trans. Biomed. Eng.*, vol. 66, no. 6, pp. 1752–1760, Jun. 2019.

[22] B. Chicote, U. Irusta, R. Alcaraz, J. J. Rieta, E. Aramendi, I. Isasi, D. Alonso, and K. Ibarguren, "Application of entropy-based features to predict defibrillation outcome in cardiac arrest," *Entropy*, vol. 18, no. 9, p. 313, 2016.

[23] B. Chicote, U. Irusta, E. Aramendi, R. Alcaraz, J. J. Rieta, I. Isasi, D. Alonso, M. D. M. Baqueriza, and K. Ibarguren, "Fuzzy and sample entropies as predictors of patient survival using short ventricular fibrillation recordings during out of hospital cardiac arrest," *Entropy*, vol. 20, no. 8, p. 591, 2018.

[24] D. Cabello, S. Barro, J. M. Salceda, R. Ruiz, and J. Mira, "Fuzzy K-nearest neighbor classifiers for ventricular arrhythmia detection," *Int. J. Bio-Med. Comput.*, vol. 27, no. 2, pp. 77–93, 1991.

[25] Y. Alwan, Z. Cvetković, and M. J. Curtis, "Methods for improved discrimination between ventricular fibrillation and tachycardia," *IEEE Trans. Biomed. Eng.*, vol. 65, no. 10, pp. 2143–2151, Oct. 2018.

[26] P. Cheng and X. Dong, "Life-threatening ventricular arrhythmia detection with personalized features," *IEEE Access*, vol. 5, pp. 14195–14203, 2017.

[27] A. B. Rad, T. Eftestøl, U. Irusta, J. T. Kvaløy, L. Wik, J. Kramer-Johansen, A. K. Katsaggelos, and K. Engan, "An automatic system for the comprehensive retrospective analysis of cardiac rhythms in resuscitation episodes," *Resuscitation*, vol. 122, pp. 6–12, Jan. 2018.

[28] S. Cheskes, R. H. Schmicker, J. Christenson, D. D. Salcido, T. Rea, J. Powell, D. P. Edelson, R. Sell, S. May, J. J. Menegazzi, L. Van Ottingham, M. Olsufka, S. Pennington, J. Simonini, R. A. Berg, I. Stiell, A. Idris, B. Bigham, L. Morrison, and R. O. C. R. Investigators, "Perishock pause: An independent predictor of survival from out-of-hospital shockable cardiac arrest," *Circulation*, vol. 124, pp. 58–66, Jul. 2011.

[29] S. R. de Gauna, U. Irusta, J. Ruiz, U. Ayala, E. Aramendi, and T. Eftestøl, "Rhythm analysis during cardiopulmonary resuscitation: Past, present, and future," *BioMed Res. Int.*, vol. 2014, Jan. 2014, Art. no. 386010.

[30] J. Eilevstjønn, T. Eftestøl, S. O. Aase, H. Myklebust, J. H. Husøy, and P. A. Steen, "Feasibility of shock advice analysis during CPR through removal of CPR artefacts from the human ECG," *Resuscitation*, vol. 61, pp. 131–141, May 2004.

[31] U. Irusta, J. Ruiz, S. R. D. Gauna, T. Eftestøl, and J. Kramer-Johansen, "A least mean-square filter for the estimation of the cardiopulmonary resuscitation artifact based on the frequency of the compressions," *IEEE Trans. Biomed. Eng.*, vol. 56, no. 4, pp. 1052–1062, Apr. 2009.

[32] I. Isasi, U. Irusta, E. Aramendi, U. Ayala, E. Alonso, J. Kramer-Johansen, and T. Eftestøl, "A multistage algorithm for ECG Rhythm analysis during piston-driven mechanical chest compressions," *IEEE Trans. Biomed. Eng.*, vol. 66, no. 1, pp. 263–272, Jan. 2019.

[33] U. Ayala, U. Irusta, J. Ruiz, T. Eftestøl, J. Kramer-Johansen, F. Alonso-Atienza, E. Alonso, and D. González-Otero, "A reliable method for rhythm analysis during cardiopulmonary resuscitation," *BioMed Res. Int.*, vol. 2014, Mar. 2014, Art. no. 872470.

[34] L. Wik, J. Kramer-Johansen, H. Myklebust, H. Sørebø, L. Svensson, B. Fellows, and P. A. Steen, "Quality of cardiopulmonary resuscitation during out-of-hospital cardiac arrest," *JAMA*, vol. 293, no. 3, pp. 299–304, 2005.

[35] J. Kramer-Johansen, H. Myklebust, L. Wik, B. Fellows, L. Svensson, H. Sørebø, and P. A. Steen, "Quality of out-of-hospital cardiopulmonary resuscitation with real time automated feedback: A prospective interventional study," *Resuscitation*, vol. 71, no. 3, pp. 283–292, 2006.

[36] S. O. Aase and H. Myklebust, "Compression depth estimation for CPR quality assessment using DSP on accelerometer signals," *IEEE Trans. Biomed. Eng.*, vol. 49, no. 3, pp. 263–268, Mar. 2002.

[37] Y. Xiao, L. Ma, and R. K. Ward, "Fast RLS Fourier analyzers capable of accommodating frequency mismatch," *Signal Process.*, vol. 87, no. 9, pp. 2197–2212, 2007.

[38] J. E. Fowler, "The redundant discrete wavelet transform and additive noise," *IEEE Signal Process. Lett.*, vol. 12, no. 9, pp. 629–632, Sep. 2005.

[39] D. L. Donoho and J. M. Johnstone, "Ideal spatial adaptation by wavelet shrinkage," *Biometrika*, vol. 81, no. 3, pp. 425–455, 1994.

[40] P. S. Hamilton and W. J. Tompkins, "Quantitative investigation of QRS detection rules using the MIT/BIH arrhythmia database," *IEEE Trans. Biomed. Eng.*, vol. BME-33, no. 12, pp. 1157–1165, Dec. 1986.

[41] S. Kuo, "Computer detection of ventricular fibrillation," in *Proc. IEEE Comput. Soc. Comput. Cardiol.*, 1978, pp. 347–349.

[42] I. Jekova, "Shock advisory tool: Detection of life-threatening cardiac arrhythmias and shock success prediction by means of a common parameter set," *Biomed. Signal Process. Control*, vol. 2, no. 1, pp. 25–33, 2007.

[43] F. Alonso-Atienza, E. Morgado, L. Fernández-Martínez, A. García-Alberola, and J. L. Rojo-Álvarez, "Detection of life-threatening arrhythmias using feature selection and support vector machines," *IEEE Trans. Biomed. Eng.*, vol. 61, no. 3, pp. 832–840, Mar. 2014.

[44] L. Gonzalez, K. Walker, S. Challa, and B. Bent, "Monitoring a skipped heartbeat: A real-time premature ventricular contraction (PVC) monitor," in *Proc. IEEE Virtual Conf. Appl. Commercial Sensors (VCACS)*, Jun./Jul. 2017, pp. 1–7.

[45] F. Takens, "Detecting strange attractors in turbulence," in *Dynamical Systems and Turbulence, Warwick* (Lecture Notes in Mathematics), vol. 898. Springer, Oct. 2006, pp. 366–381.

[46] M. Zabihi, A. B. Rad, A. K. Katsaggelos, S. Kiranyaz, S. Narkilahti, and M. Gabbouj, "Detection of atrial fibrillation in ECG hand-held devices using a random forest classifier," in *Proc. Comput. Cardiol. (CinC)*, Sep. 2017, pp. 1–4.

[47] N. Marwan, N. Wessel, U. Meyerfeldt, A. Schirdewan, and J. Kurths, "Recurrence-plot-based measures of complexity and their application to heart-rate-variability data," *Phys. Rev. E, Stat. Phys. Plasmas Fluids Relat. Interdiscip. Top.*, vol. 66, no. 2, 2002, Art. no. 026702.

[48] D. Krstajic, L. J. Buturovic, D. E. Leahy, and S. Thomas, "Cross-validation pitfalls when selecting and assessing regression and classification models," *J. Cheminform.*, vol. 6, no. 1, p. 10, Mar. 2014.

[49] B. Gregorutti, B. Michel, and P. Saint-Pierre, "Correlation and variable importance in random forests," *Statist. Comput.*, vol. 27, no. 3, pp. 659–678, 2017.

[50] L. Breiman, "Random forests," *Mach. Learn.*, vol. 45, no. 1, pp. 5–32, 2001.

[51] R. Díaz-Uriarte and S. A. De Andrés, "Gene selection and classification of microarray data using random forest," *BMC Bioinf.*, vol. 7, no. 1, p. 3, 2006.

[52] H. Pang, S. L. George, K. Hui, and T. Tong, "Gene selection using iterative feature elimination random forests for survival outcomes," *IEEE/ACM Trans. Comput. Biol. Bioinf.*, vol. 9, no. 5, pp. 1422–1431, Sep. 2012.

[53] K. Q. Shen, C. J. Ong, X. P. Li, Z. Hui, and E. P. V. Wilder-Smith, "A feature selection method for multilevel mental fatigue EEG classification," *IEEE Trans. Biomed. Eng.*, vol. 54, no. 7, pp. 1231–1237, Jul. 2007.

[54] P. Hubner, R. W. C. G. R. Wijshoff, J. Muehlsteff, C. Wallmüller, A. M. Warenits, I. A. M. Magnet, K. Nammi, J. K. Russell, and F. Sterz, "A series of case studies on detection of spontaneous pulse by photoplethysmography in cardiopulmonary resuscitation," *Amer. J. Emergency Med.*, to be published.

[55] A. Elola, E. Aramendi, U. Irusta, E. Alonso, Y. Lu, M. P. Chang, P. Owens, and A. H. Idris, "Capnography: A support tool for the detection of return of spontaneous circulation in out-of-hospital cardiac arrest," *Resuscitation*, to be published.

[56] R. E. Kerber, L. B. Becker, J. D. Bourland, R O. Cummins, A. P. Hallstrom, M. B. Michos, G. Nichol, J. P. Ornato, W. H. Thies, R. D. White, and B. D. Zuckerman, "Automatic external defibrillators for public access defibrillation: Recommendations for specifying and reporting arrhythmia analysis algorithm performance, incorporating new waveforms, and enhancing safety: A statement for health professionals from the American heart association task force on automatic external defibrillation, subcommittee on aed safety and efficacy," *Circulation*, vol. 95, no. 6, pp. 1677–1682, 1997.

[57] V. Krasteva, I. Jekova, I. Dotsinsky, and J.-P. Didon, "Shock advisory system for heart rhythm analysis during cardiopulmonary resuscitation using a single ECG input of automated external defibrillators," *Ann. Biomed. Eng.*, vol. 38, no. 4, pp. 1326–1336, 2010.

[58] R. R. Attaran and G. A. Ewy, "Epinephrine in resuscitation: Curse or cure?" *Future Cardiol.*, vol. 6, no. 4, pp. 473–482, 2010.

[59] R. W. C. G. R. Wijshoff, A. M. T. M. van Asten, W. H. Peeters, R. Bezemer, G. J. Noordergraaf, M. Mischi, and R. M. Aarts, "Photoplethysmography-based algorithm for detection of cardiogenic output during cardiopulmonary resuscitation," *IEEE Trans. Biomed. Eng.*, vol. 62, no. 3, pp. 909–921, Mar. 2015.

A.3 Publications associated to objective 3

A.3.1 First conference paper: C1$_3$

Table A.6. Conference paper associated to objective 3.

Publication in international conference
Reference   I. Isasi, Rad, A. B., U. Irusta, M. Zabihi, E. Aramendi, T. Eftestøl, J. Kramer-Johansen, L. Wik,"ECG rhythm analysis during manual chest compressions using an artefact removal filter and random forest classifiers", *Proceedings of the Conference IEEE Computing in Cardiology 2018*, vol. 45, pp. 1-4.
Quality indices   • **Type of publication**: Indexed Congress in SJR   • **Area**: Cardiology and Cardiovascular Medicine   • **SJR factor**: 0.202

ECG Rhythm Analysis During Manual Chest Compressions Using an Artefact Removal Filter and Random Forest Classifiers

Iraia Isasi[1], Ali Bahrami Rad[2], Unai Irusta[1], Morteza Zabihi[3], Elisabete Aramendi[1], Trygve Eftestøl[4], Jo Kramer-Johansen[5], Lars Wik[5]

[1] University of the Basque Country (UPV/EHU), Bilbao, Spain
[2] Aalto University, Espoo, Finland
[3] University of Technology, Tampere, Finland
[4] University of Stavanger, Stavanger, Norway
[5] Oslo University Hospital, Oslo, Norway

Abstract

Interruptions in cardiopulmonary resuscitation (CPR) decrease the chances of survival. However, CPR must be interrupted for a reliable rhythm analysis because chest compressions (CCs) induce artifacts in the ECG. This paper introduces a double-stage shock advice algorithm (SAA) for a reliable rhythm analysis during manual CCs. The method used two configurations of the recursive least-squares (RLS) filter to remove CC artifacts from the ECG. For each filtered ECG segment over 200 shock/no-shock decision features were computed and fed into a random forest (RF) classifier to select the most discriminative 25 features. The proposed SAA is an ensemble of two RF classifiers which were trained using the 25 features derived from different filter configurations. Then, the average value of class posterior probabilities was used to make a final shock/no-shock decision. The dataset was comprised of 506 shockable and 1697 non-shockable rhythms which were labelled by expert rhythm resuscitation reviewers in artifact-free intervals. Shock/no-shock diagnoses obtained through the proposed double-stage SAA were compared with the rhythm annotations to obtain the Sensitivity (Se), Specificity (Sp) and balanced accuracy (BAC) of the method. The results were 93.5%, 96.5% and 95.0%, respectively.

1. Introduction

Minimum "hands-of" intervals during cardiopulmonary resuscitation (CPR) are required to improve the chances of a successful defibrillation [1]. In current practice CPR is interrupted every 2 minutes for a reliable analysis of the heart rhythm. In fact, chest compressions (CCs) provided during CPR induce artifacts in the ECG that impede a reliable rhythm analysis of shock advice algorithms.

Over the last 15 years, many efforts have been made to achieve a continuous rhythm analysis without interruptions to CPR therapy. Different approaches have been proposed, such as rhythm analysis during ventilation pauses [2, 3], however the main approach has been designing adaptive filters to suppress the artifact and then diagnose using a SAA for artifact-free ECG [4]. Nevertheless, the accuracy of this approach is still poor. Adaptive filters substantially reduce CC artifacts with high SNR improvements, however filtering residuals frequently resemble a disorganized rhythm. In these cases, SAAs may produce a wrong shock diagnosis as the majority of the SAAs used are designed for artifact-free ECGs. This is the reason why current methods have a high capacity to detect shockable rhythms, Sensitivity (Se), but a low capacity to detect non-shockable rhythms, Specificity (Sp).

Recently, a multistage algorithm was introduced to increase the Sp [5] (supp materials). In brief, this algorithm uses two recursive least squares (RLS) filters and a SAA of a commercial defibrillator in three decision stages. Although this solution considerably improves the Sp of previous approaches, it still does not meet American Heart Association's criteria for a reliable rhythm diagnosis (Sp>95%, Se>90%) during manual CCs. Another approach to increase the Sp was the use of machine learning techniques to classify the ECG after using an adaptive CPR artifact suppression filter [6].

In this paper, we propose a method for a reliable shock advise during manual CCs, which combines the both aforementioned approaches: a double stage RLS filtering [5] and a SAA algorithm based on random forest (RF) classifiers [6] which benefits from both filtering configurations to reach a reliable shock/no-shock decision.

2. Materials and methods

2.1. Dataset

The data were obtained from a prospective study of out-of-hospital cardiac arrest (OHCA) patients gathered between March 2002 and September 2004 by the emergency services of London, Stockholm and Akershus and coordinated by the Oslo University Hospital. The ECG and the compression depth (CD) signals were acquired using a modified version of Laerdal's Heartstart 4000 defibrillator (4000SP) and were resampled to 250 Hz. A notch and a Hample filter were used to remove 50 Hz noise and spiky artifacts from the ECG, respectively. Finally, the ECG was band limited to 0.5-40 Hz. CC instants (t_k) were automatically marked in the CD signal using a negative peak detector for depths above 1 cm, see figure 1.

The dataset used in this study contained 2203 records obtained from 273 OHCA patients. Each record (see figure 1) consisted of two consecutive intervals: a 15-sec interval which includes continuous CCs, and a 5-sec interval free of artifact. The latter interval was reviewed by expert resuscitation rhythm reviewers to annotate the patient's underlying rhythm as shock/no-shock and use it as ground truth. In total there were 506 shockable and 1697 non-shockable rhythms.

2.2. Filtering the CC Artifact

In this work, the used CC artefact suppression method is based on a recursive least squares (RLS) filter adapted to estimate periodic interferences [5]. The RLS filter estimates the time-varying coefficients ($a_k(n)$ and $b_k(n)$) of a multiharmonic model of the artifact whose fundamental frequency ($f_0(n)$) is derived from the chest compression instants (t_k):

$$s_{\mathrm{cc}}(n) = \sum_{k=1}^{N} a_k(n) \cos(k2\pi f_0(n)nT_s) + \qquad (1)$$
$$b_k(n) \sin(k2\pi f_0(n)nT_s)$$

$$f_0(n) = \frac{1}{t_k - t_{k-1}} \quad t_{k-1} < nT_s \leq t_k \qquad (2)$$

The CC artifact is iteratively estimated ($\hat{s}_{\mathrm{cc}}$) and subtracted from the corrupted ECG (s_{cor}), to obtain the clean ECG ($\hat{s}_{\mathrm{ecg}}$), as shown in figure 1.

In the RLS filter there are two degrees of freedom, the number of harmonics needed to model the artifact (N) and the forgetting factor (λ) which controls the coarseness of the filter. In this paper, the corrupted ECG was filtered for two configurations of the RLS filter (N/λ) following the optimal configuration of the multistage algorithm described in [5] for manual CCs. In the first stage, the corrupted ECG was coarsely filtered ($\hat{s}_{\mathrm{ecg}\lambda_1}$) using a λ of 0.987 whereas in the second stage the ECG was finely filtered ($\hat{s}_{\mathrm{ecg}\lambda_2}$) with a λ fixed to 0.998. In both stages N was set to 4.

2.3. Feature engineering

For each filtered ECG ($\hat{s}_{\mathrm{ecg}\lambda_1}$, $\hat{s}_{\mathrm{ecg}\lambda_2}$), a multi-resolution analysis is employed to extract 244 features. Only the interval from 4 s to 12 s was used to compute features. First 4 s were left out to avoid RLS filtering transients. The 8-second ECG segments were decomposed by discrete wavelet transform (DWT) into its subbands with the Daubechies 4 wavelet and 7 levels of decomposition generating a set of approximation coefficients a_7 and seven sets of detail coefficients d_1 to d_7. The ECG was then reconstructed, $s(n)$, by using detail coefficients $d_3 - d_7$. Reconstructed signals corresponding to each set of detail coefficients (d_3 to d_7) were also generated: $s_3(n)$ to $s_7(n)$.
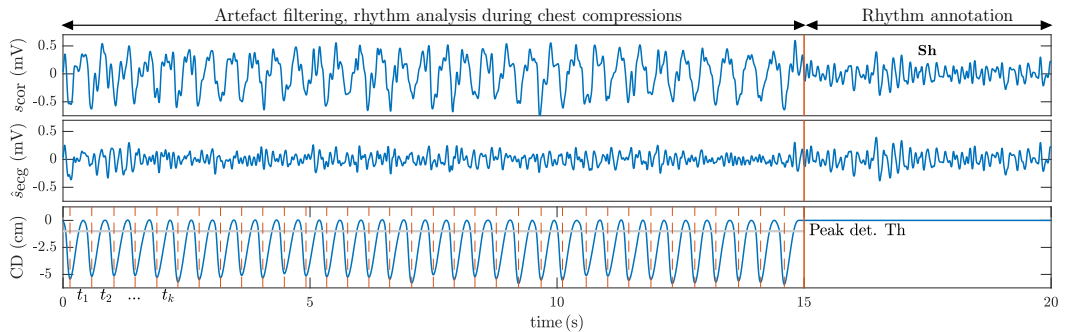

Figure 1. Example of a 20 s episode of the database. The top panel shows the ECG of a patient with a shockable rhythm (Sh): the first 15 s are corrupted by the CC artifact and the last 5 s are free of artifact showing the patient's underlying rhythm. The second pannel shows the filtered ECG and the bottom panel the CD signal with the CC instants (t_k).

For each filtered signal 244 features were computed [7–9] based on the multi-resolution analysis. The features were ranked by importance in each random forest (RF) classifier using the out-of-bag error [10]. For each set the top ranked 25 features were selected for classification.

2.4. Classification

The last step in the proposed SAA is classification. An ensemble of two RF classifiers were combined to reach a shock/no-shock decision, as can be shown in the last block of figure 2. The first classifier was trained using the selected 25 features from $\hat{s}_{ecg\lambda_1}$ whereas the second one was trained using the selected 25 features from $\hat{s}_{ecg\lambda_2}$. The final shock/no-shock decision was made based on the average value of the class posterior probabilities of two RF classifiers. The class with the higher average value of class posterior probabilities was chosen for shock/no-shock decision.

Both RF classifiers had 300 decision trees. Each tree was trained using bootstrapped replicas of the training data and the prior probabilities of each class (shock/no-shock) were balanced for each tree by using resampling. The cost function was defined to penalize the wrong diagnosis of nonshockable rhythms by a factor of 95/90 based on the AHA recommendation.

2.5. Model assessment

A 10-fold cross-validation (CV) scheme was used to train and test the SAA. Folds were partitioned patient-wise ensuring that the rhythm prevalences matched to at least 85% the prevalences for shockable and nonshockable rhythms of the whole dataset (quasi-stratified).

Test segments were diagnosed as shock/no-shock based on the average value of class posterior probabilities (see section 2.4). These diagnoses were compared with the rhythm annotations to obtain the following performance metrics: Se, Sp and Balanced Accuracy (BAC), that is, the mean value of Se and Sp. In order to obtain the statistical distributions of these metrics the process was repeated 100 times. The results were compared to those obtained using the classical approach, filtering followed by a SAA designed for artifact-free ECG [11], in a single stage and multistage configurations.

3. Results

The mean (95% confidence interval) Se, Sp and BAC of the proposed double-stage SAA were 93.5% (92.9-94.0), 96.5% (96.2-96.6) and 95.0% (94.7-95.3), respectively. The classical approach in an optimal multistage configuration, as described in [5], yielded a Se, Sp and BAC of: 91.7%, 93.7% and 92.7%, far below the obtained results using our proposed double-stage SAA.

A classical single stage solution produced an Se, Sp and BAC of 96.3%, 81.3% and 88.8%, respectively. The results for the best single RF-classifier (λ_2) were 92.8% (92.3-93.5), 96.5% (96.2-96.7) and 94.7% (94.4-95.0), respectively. These results meet the minimum 90% Se and 95% Sp performance goals recommended by the American Heart Association (AHA).

Table 1 shows the selected features for $\hat{s}_{ecg\lambda_1}$ and for $\hat{s}_{ecg\lambda_2}$, with the following notation: feature name (signal/wavelet coefficient). The first nine features of both columns are described by Figuera *et al* [7]. Features from 10 to 15 in the left column and from 10 to 12 in the right column were introduced by Rad *et al* [8]. Fuzzy Entropy (FuzzEn), the Signal Integral parameter (SignInt), the Peak Power Frequency (PPF), the Smoothed Nonlinear Energy Operator (SNEO) and the Hjorth Mobility parameter are described in [9, 12], [13], [14], [15] and [16], respectively. The remaining features were designed for this work: the number of QRS-like peaks (Npeak) and the Euclidean distance between the Hjorth Mobility and the Hjorth Mobility of the second degree (Mx2).

4. Discussion

This work introduces a double-stage SAA for a reliable rhythm analysis during CPR inspired by two solutions proposed in the literature to increase the Sp for rhythm analysis during CCs [5, 6]. Our proposed SAA algorithm consists of a double-stage RLS filtering, multiresolution analysis for feature extraction, and two RF classifiers.

A single filtering stage followed by a commercial SAA yielded a Se and a Sp of 96.3% and 81.3% respectively. Using an ad-hoc SAA designed to diagnose filtered ECGs
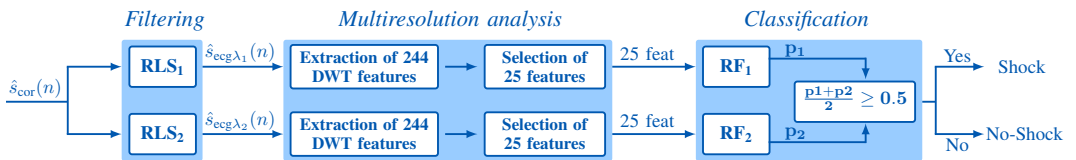

Figure 2. Arquitecture of the proposed double-stage SAA.

Feature	$\hat{s}_{\text{ecg}\lambda_1}$	Feature	$\hat{s}_{\text{ecg}\lambda_2}$
1	x1$(s(n))$	1	x1$(s(n))$
2	x4$(s(n))$	2	x4$(s(n))$
3	SamEn(d_3)	3	SamEn(d_3)
4	SamEn$(s_3(n))$	4	SamEn$(s_3(n))$
5	SamEn$(s_4(n))$	5	SamEn$(s_4(n))$
6	vfleak$(s(n))$	6	vfleak$(s(n))$
7	count2$(s(n))$	7	count2$(s(n))$
8	count3$(s(n))$	8	x3$(s(n))$
9	bCP$(s(n))$	9	bCP$(s(n))$
10	IQR$(\dot{d}(5))$	10	First Quartile(d_5)
11	IQR(d_7)	11	Positive Area$(s(n))$
12	IQR$(\dot{d}_7)$	12	Negative Area$(s(n)$
13	IQR$(\tilde{d}_5)$	13	Mean(d_4)
14	Var(d_5)	14	Mx(d_6)
15	$\mu_2(d_7)$	15	PPF$(s(n))$
16	FuzzEn$(s(n))$	16	FuzzEn$(s(n))$
17	FuzzEn$(s_3(n))$	17	FuzzEn$(s_3(n))$
18	Mx2$(\hat{s}_{\text{ecg}\lambda_1})$	18	FuzzEn$(s_4(n))$
19	SNEO$(s(n))$	19	SNEO$(s(n))$
20	SignInt(d_7)	20	SignInt(d_7)
21	SignInt(d_5)	21	Mean$(s(n))$
22	Std$(\tilde{d}_3)$	22	Std$(\tilde{d}_3)$
23	Mean(d_3)	23	Mean(d_3)
24	Mean$(\tilde{d}_3)$	24	Mean(d_3)
25	Npeak$(s(n))$	25	Npeak$(s(n))$

Table 1. The 25 features selected by the two RF classifiers.

the Sp was increased in 15.2 points although the Se was reduced in 3.5 points. This significant increase in Sp allowed the AHA requirements to be met with an overall BAC of 94.7%. The results were further increased with the addition of the double stage filtering, obtaining a BAC of 95.0%.

In conclusion, this study confirms that ad-hoc decision algorithms for the filtered ECGs provide a reliable rhythm analysis during CPR and that the results would be further improved if the SAA combined the information derived from differently filtered ECG signals.

Acknowledgements

References

[1] Perkins GD, et al. European resuscitation council guidelines for resuscitation 2015: Section 2. adult basic life support and automated external defibrillation. Resuscitation 2015;95:81–99.

[2] Ayala U, Irusta U, Ruiz J, de Gauna SR, González-Otero D, Alonso E, Kramer-Johansen J, Naas H, Eftestøl T. Fully automatic rhythm analysis during chest compression pauses. Resuscitation 2015;89:25–30.

[3] Ruiz J, Ayala U, de Gauna SR, Irusta U, González-Otero D, Alonso E, Kramer-Johansen J, Eftestøl T. Feasibility of automated rhythm assessment in chest compression pauses during cardiopulmonary resuscitation. Resuscitation 2013; 84(9):1223–1228.

[4] Ruiz de Gauna S, et al. Rhythm analysis during cardiopulmonary resuscitation: past, present, and future. BioMed Research International 2014;2014.

[5] Isasi I, et al. A multistage algorithm for ECG rhythm analysis during piston driven mechanical chest compressions. IEEE Transactions on Biomedical Engineering 2018;.

[6] Ayala U, et al. A reliable method for rhythm analysis during cardiopulmonary resuscitation. BioMed Research International 2014;2014.

[7] Figuera C, et al. Machine learning techniques for the detection of shockable rhythms in automated external defibrillators. PloS One 2016;11(7):e0159654.

[8] Rad AB, et al. ECG-based classification of resuscitation cardiac rhythms for retrospective data analysis. IEEE Transactions on Biomedical Engineering 2017; 64(10):2411–2418.

[9] Chicote B, et al. Application of entropy-based features to predict defibrillation outcome in cardiac arrest. Entropy 2016;18(9):313.

[10] Zabihi M, Rad AB, Katsaggelos AK, Kiranyaz S, Narkilahti S, Gabbouj M. Detection of atrial fibrillation in ecg hand-held devices using a random forest classifier. Computing 2017;44:1.

[11] Irusta U, Ruiz J, Aramendi E, de Gauna SR, Ayala U, Alonso E. A high-temporal resolution algorithm to discriminate shockable from nonshockable rhythms in adults and children. Resuscitation 2012;83(9):1090–1097.

[12] Chicote B, Irusta U, Aramendi E, Alcaraz R, Rieta J, Isasi I, Alonso D, Baqueriza M, Ibarguren K. Fuzzy and sample entropies as predictors of patient survival using short ventricular fibrillation recordings during out of hospital cardiac arrest. Entropy 2018;20:591.

[13] Wu X, et al. Signal integral for optimizing the timing of defibrillation. Resuscitation 2013;84(12):1704–1707.

[14] Eftestøl T, et al. Predicting outcome of defibrillation by spectral characterization and nonparametric classification of ventricular fibrillation in patients with out-of-hospital cardiac arrest. Circulation 2000;102(13):1523–1529.

[15] Chicote B, et al. Nonlinear energy operators for defibrillation shock outcome prediction. In Computing in Cardiology Conference (CinC), 2016. IEEE, 2016; 61–64.

[16] Gonzalez L, et al. Monitoring a skipped heartbeat: a real-time premature ventricular contraction (pvc) monitor. In Applications of Commercial Sensors (VCACS), 2016 IEEE Virtual Conference on. IEEE, 2016; 1–7.

Address for correspondence:

Name: Iraia Isasi Liñero
Full postal address: Ingeniero Torres Quevedo Plaza, 1, 48013 Bilbo, Bizkaia, Spain
E-mail address: iraia.isasi@ehu.eus

A.3.2 SECOND CONFERENCE PAPER: C2₃

Table A.7. Conference paper associated to objective 3.

Publication in international conference
Reference I. Isasi, U. Irusta, A. Elola, E. Aramendi, T. Eftestøl, J. Kramer-Johansen, L. Wik,"A robust machine learning architecture for a reliable ECG rhythm analysis during CPR", *Proceedings of the Conference IEEE Engineering and Biology Society 2019*, pp. 1903-1907.
Quality indices   **Type of publication**: Indexed Congress in SJR   **Area**: Biomedical Engineering   **SJR factor**: 0.281

A Robust Machine Learning Architecture for a Reliable ECG Rhythm Analysis during CPR

Iraia Isasi[1], Unai Irusta[1], Andoni Elola[1], Elisabete Aramendi[1], Trygve Eftestøl[2],
Jo Kramer-Johansen[3] and Lars Wik[3]

Abstract— Chest compressions delivered during cardiopulmonary resuscitation (CPR) induce artifacts in the ECG that may make the shock advice algorithms (SAA) of defibrillators inaccurate. There is evidence that methods consisting of adaptive filters that remove the CPR artifact followed by machine learning (ML) based algorithms are able to make reliable shock/no-shock decisions during compressions. However, there is room for improvement in the performance of these methods. The objective was to design a robust ML framework for a reliable shock/no-shock decision during CPR. The study dataset contained 596 shockable and 1697 nonshockable ECG segments obtained from 273 cases of out-of-hospital cardiac arrest. Shock/no-shock labels were adjudicated by expert reviewers using ECG intervals without artifacts. First, CPR artifacts were removed from the ECG using a Least Mean Squares (LMS) filter. Then, 38 shock/no-shock decision features based on the Stationary Wavelet Transform (SWT) were extracted from the filtered ECG. A wapper-based feature selection method was applied to select the 6 best features for classification. Finally, 4 state-of-the-art ML classifiers were tested to make the shock/no-shock decision. These diagnoses were compared with the rhythm annotations to compute the Sensitivity (Se) and Specificity (Sp). All classifiers achieved an Se above 94.5%, Sp above 95.5% and an accuracy around 96.0%. They all exceeded the 90% Se and 95% Sp minimum values recommended by the American Heart Association.

I. INTRODUCTION

High quality cardiopulmonary resuscitation (CPR) and early defibrillation are the most important survival factors in out-of-hospital cardiac arrest [1]. The mechanical activity of chest compressions during CPR introduces artifacts into the ECG. Therefore, current automated external defibrillators require chest compressions to cease to perform a reliable ECG analysis and make a shock/no-shock decision [2]. The lack of myocardial and cerebral blood flow during these "hands-off" periods significantly compromise the survival of the patient [3]. If a reliable ECG rhythm diagnosis could be achieved during compressions, CPR would only be stopped when a shock is advised, avoiding "hands-off" intervals almost completely.

Filtering the CPR artifact has been the major approach to rhythm analysis during CPR [2]. The time-varying characteristics of the chest compression artifact mandate the use of adaptive filters. Recently solutions based on Least Mean Squares (LMS) [4], [5] and Recursive Least Squares (RLS) filters [6], [7] have been proposed. Once the adaptive filters are applied, shock advice algorithms (SAA) of commercial defibrillators have been widely used for the shock/no-shock decision [2]. However, adaptive filters combined with SAAs do not meet American Heart Association's (AHA) accuracy requirements. Commercial SAAs were originally designed to analyze artifact-free ECGs, so filtering residuals are therefore a confounding factor [2]. A recent popular approach is to design machine learning (ML) algorithms after the adaptive filtering stage. ML algorithms learn the characteristics of the filtered ECG, including those of the filtering residuals. These methods have met AHA requirements both for manual [5], [8] and mechanical [6] CPR.

This study proposes a robust ML framework for a reliable shock/no-shock decision during CPR. This framework consists of a high-resolution feature extraction method based on the Stationary Wavelet Transform (SWT), a wrapper-based feature selection algorithm and a shock/no-shock decision classifier. For the shock/no-shock decision 4 state-of-the-art ML were tested: Artificial Neural Network (ANN), Support Vector Machine (SVM), Kernel Logistic Regression (KLR) and Boosting of Decision Trees (BDT). The paper is organized as follows: the dataset is described in Section II; Section III explains the adaptive CPR artifact filter and the feature extraction process; the architecture of the model and the ML classifiers are explained in Section IV and V. Finally, the results and the conclusions are presented in Sections VI and VII, respectively.

II. STUDY DATASET

The data were obtained by the emergency services of London, Stockholm and Akershus (Norway) between March 2002 and September 2004 using a modified version of Laerdal's Heartstart 4000 defibrillator. The recorded ECG and the compression depth (CD) signals were exported to Matlab and resampled to 250 Hz. A notch and a Hampel filter were used to remove powerline interference and the spiky artifacts, respectively. Finally, chest compression instants

(t_k), were automatically marked in the CD signal using a negative peak detector for depths exceeding 1 cm.

The dataset contained 2203 segments from 273 out-of-hospital cardiac arrest patients. The first 15 s included continuous chest compressions and the last 5 s were free of artifacts and were used by expert reviewers to asses the underlying rhythm. The dataset is comprised of 506 shockable and 1697 non-shockable rhythms.

III. FEATURE ENGINEERING

A. CPR artifact filtering

CPR artifacts were suppressed using a state-of-the-art method based on a LMS filter. In this method, the CPR artifact, s_{cpr}, is modeled as a quasiperiodic interference with a time-varying fundamental frequency, $f_0(n)$, which is the instantaneous frequency of the compressions [4]. A CPR artifact composed of N harmonics can therefore be expressed by the following Fourier series representation:

$$s_{cpr}(n) = A(n)\sum_{k=1}^{N} a_\ell(n)cos(k2\pi f_0(n)T_s n) + b_\ell(n)sin(k2\pi f_0(n)T_s n) \quad (1)$$

$$f_0(n) = \frac{1}{t_k - t_{k-1}} \qquad t_{k-1} \le nT_s < t_k \quad (2)$$

where $A(n)$ is an amplitude envelope which differentiates intervals with $(A = 1)$ and without compressions $(A = 0)$.

The in-phase, $a_\ell(n)$, and quadrature, $b_\ell(n)$, components that model the artifact are adaptively estimated to minimize the mean square error between the corrupted ECG, s_{cor}, and the estimated artifact, $\hat{s}_{cpr}$, at the frequency of the harmonics using the LMS algorithm. For further details consult [4].

The parameters governing the LMS filter are the number of harmonics, N, and the step size, μ. The first one determines the order of the filter which is $2N$ since there are a cuadrature and in-phase coefficient per harmonic, whereas the second one controls the coarseness of the filter.

B. Feature extraction

Features were extracted from the SWT [9] decomposition of the filtered ECG, $\hat{s}_{ecg}$, as we recently introduced for mechanical CPR [6]. A signal interval of 8 s of the filtered ECG, as highlighted in Fig. 1, was used for feature extraction.

The 8-s ECG segments were decomposed into subbands with the Daubechies 2 wavelet and 8 levels of decomposition. At each level the SWT can be implemented by a pair of quadrature mirror lowpass/highpass filters, $g(n)/h(n)$, which decompose the signal into the lower and upper halves of the subband. The decomposition process of the filtered ECG segment in $j = 1, \ldots, J$ leves can be therefore obtained by the following equations:

$$a_0(n) = \hat{s}_{ecg}(n) \quad (3)$$
$$a_{j+1}(n) = g_j(n) * a_j(n) \quad (4)$$
$$d_{j+1}(n) = h_j(n) * a_j(n) \quad (5)$$

where a_j and d_j are approximation and detail coefficients of level j and g_{j+1}/h_{j+1} are the up-sampled versions of h_j/g_j achieved using a zero-padding interpolation (with factor 2).

The decomposition was performed into $J = 8$ subbands generating nine sets of coefficients, a_8 and d_8 to d_1. For feature extraction only detail coefficients of levels 3-8 (d_3-d_8) were used, the remaining d_1, d_2 and a_8 were set to 0. Then, a soft denoising was performed in the $d_3 - d_8$ coefficients using the universal tresholding rule proposed by Donoho and Johnstone [10] rescaled by the standard deviation of the noise (estimated from d_1). Finally, the Inverse Stationary Wavelet Transform (ISWT) was applied to reconstruct the denoised ECG signal, $\hat{s}_{den}$, in the 0.5 Hz-31.25 Hz subband.

Thirty eight SWT features were extracted in this study based on $\hat{s}_{den}$ and the denoised detail coefficients, $d_3 - d_8$. These features include time domain, frequency domain and signal complexity characterizations of the ECG [11],
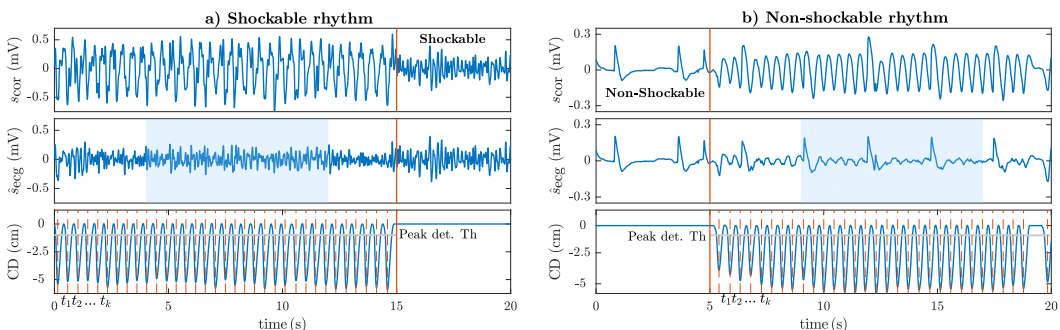
Fig. 1. Two examples of 20 s ECG segments corresponding to a patient with a shockable rhythm (example a) and with a non-shockable rhythm (example b). The first panels show the ECG recorded by the device (the corrupted ECG, s_{cor}) whereas the second panels show the ECG after filtering the CPR artifact, $\hat{s}_{ecg}$. The first 15 s of the panel a) and the last 15 s of panel b) are corrupted by the CPR artifact. The last 5 s of the panel a) and the first 5 s of the panel b) are free of artifact showing the underlying rhythm of the patient. Filtering, (second panels in both examples) reveals the underlying rhythm of the patient. Finally, the third panels show the CD signal, and the compression instants (t_k) are highlighted using vertical red lines.

1904

[12] and are based on the literature on VF detection. The nomenclature of the features used in section VI follows that of [6].

IV. DESIGN AND EVALUATION OF THE SOLUTION

A nested cross-validation (CV) architecture was used for feature selection, main classifier hyperparameter optimization and the evaluation of the model [6], [11]. This architecture involves the use of an inner loop (5-fold CV) for feature selection, and an outer loop (10-fold CV) for the main classifier's optimization and the evaluation of the model. Both inner and outer folds were partitioned patient-wise in a quasi-stratified way, by ensuring that the shock/no-shock case prevalences matched to at least 85% those of the whole dataset. Finally, the performance of the method was evaluated comparing the shock/no-shock diagnoses obtained by the main classifier in the outer test set with ground truth labels. The performance metrics were: Sensitivity (Se), Specificity (Sp), Balanced Accuracy (BAC) and the overall accuracy (Acc). The process was repeated 20 times to statistically characterize these metrics.

A. Optimization of the main classifier and feature selection

The optimization of the hyperparameters of the main classifier was performed in the outer loop doing a grid search and taking BAC as objective function. Two hyperparameters were optimized for each classifier and the optimal pair of hyperparameters selected for the final model (Table II) was the one that achieved the best averaged BAC in the 20 repetitions of the external loop. The results reported in Table I are therefore obtained by training each classifier with that configuration. The cost function of each classifier was weighted to compensate the class imbalance and features were standardized to zero mean and unit variance using the data in the training set.

B. Feature selection strategy

The features used in the main classifier were selected in the inner loop using a wrapper-based approach. In this approach a linear discriminant analysis (LDA) classifier and a PTA(4,3) (plus 4, take away 3) [11], [13] search strategy were used to select the 6 features that maximized the BAC in the 5-fold CV loop.

V. CLASSIFIER MODELS

1) Artificial Neural Network (ANN): A feedfordward ANN was used for the shock/no-shock classification. This network was composed of 6 input neurons (one per selected feature) and 2 output neurons for the two-class classification task. The hyperbolic tangent activation function was used for the neurons. The number of hidden layers was fixed to 2 whereas the number of hidden neurons per layer, which was the same in both layers, was determined in the outer loop $N_h = 10, 15, 20, 25...60$. The number of epochs needed to train the network was also optimized using the 10-fold CV loop and the tested values were $E_p = 20, 30, 40...100$. Finally, the strategy used to train the ANN was resilient

backpropagation and the learning rate used to train the net was fixed to 0.01.

2) Support Vector Machine (SVM): Given a set of instance-label pairs, $\{(\boldsymbol{x}_1, y_1), ..., (\boldsymbol{x}_N, y_N)\} \in \mathbb{R}^6 \times \{\pm 1\}$, where $y_i = 1$ for shockable and $y_i = -1$ for nonshockable rhythm, fitting an SVM is equivalent to minimizing [14]:

$$\frac{1}{N} \sum_{i=1}^{N} (1 - y_i f(\boldsymbol{x_i}))_+ + \lambda \|f\|_{H_k}^2 \tag{6}$$

with $f = b + h$, $h \in H_k$, $b \in \mathbb{R}$. Here the subscript "+" indicates the positive part, λ is the regularization term and H_k is the Kernel Hilbert Spaces (RKHS) generated by the kernel K. The optimal decision function $f(\boldsymbol{x})$ is:

$$f(\boldsymbol{x}) = b + \sum_{i=1}^{N} \alpha_i K(\boldsymbol{x}, \boldsymbol{x_i}) \tag{7}$$

Here α_i are the Lagrange multipliers which are non-zero only for the support vectors $\boldsymbol{x_i}$ and b is the intercept term. Once α_i and b are optimized, the classification rule of the SVM classifier is given by $sign[f(\boldsymbol{x})]$.

A Gaussian kernel was used to find an optimal separating hyperplane in a higher-dimensional feature space:

$$K(\boldsymbol{x}, \boldsymbol{x_i}) = \exp\left(-\gamma \|\boldsymbol{x} - \boldsymbol{x_i}\|^2\right) \tag{8}$$

The two hyperparameters were the kernel width, γ, and the soft margin, $C = \frac{1}{\lambda N}$. The soft margin is a trade-off between maximizing the margin and minimizing errors in the training data.

The values of C and γ were determined in the outer loop doing a 25×25 logarithmic grid search in the ranges $10^{-1} \leq C \leq 10^2$ and $10^{-3} \leq \gamma \leq 10$, respectively.

3) Kernel Logistic Regression (KLR): The minimization problem of the KLR is obtained by replacing $(1 - yf)+$ in equation 6 with $ln(1 + e^{-yf})$ [14]. The fitted decision function and classification rule are those of the SVM. KLR gives an estimate of the probability (logistic function):

$$p(\boldsymbol{x}) = 1/(1 + e^{-f(\boldsymbol{x})}) \tag{9}$$

A Gaussian kernel was used for the feature space conversion, with the kernel with (γ) and regularization parameter (λ) as hyperparameters. The ranges used for the logarithmic grid search were: $10^{-3} \leq \gamma \leq 10$ and $10^{-8} \leq \lambda \leq 10^{\frac{1}{2}}$.

4) Boosting of decision trees (BDT): Boosting consists in sequentially training several $h_m(\boldsymbol{x})$ weak classifiers, each trying to correct its predecessor, $h_{m-1}(\boldsymbol{x})$. So $h_m(\boldsymbol{x})$ focuses on those samples misclassified by $h_{m-1}(x)$. We used the AdaboostM1 reweighting strategy with weighted error for $h_m(x)$ [15]:

$$\epsilon_m = \frac{\sum_{i=1}^{N} d_m(i) I(y_i \neq h_m(\boldsymbol{x_i}))}{\sum_{i=1}^{N} d_m(i)} \tag{10}$$

1905

Here $d_m(i)$ is the weight of observation i at iteration m and I is the indicator function. *AdaBoostM1* increases the weights of the misclassfied instances of $h_m(x)$ by:

$$d_{m+1}(i) = d_m(i) \exp \left[\alpha_m I \big(y_i \neq h_m(\boldsymbol{x_i}) \big) \right] \qquad (11)$$

After training the prediction for new data is given by a weighted vote of the weak learners:

$$f(\boldsymbol{x}) = \text{sign} \left[\sum_{m=1}^{M} \alpha_m h_m(\boldsymbol{x}) \right] \qquad (12)$$

The weights, α_m, of the weak hypotheses are obtained in each iteration by the following equation:

$$\alpha_m = \lambda_b \log \frac{1 - \epsilon_m}{\epsilon_m} \qquad (13)$$

We used decision trees as weak learners. The number of features per split and the minimum leaf size of each tree were fixed to 2 and 10, respectively. The learning rate, λ_b, of the boosting algorithm and the number of boosting iterations, M, were the hyperparameters optimized in the outer loop: $10^{-3} \leq \lambda_b \leq 1$ and $M = 200, 400, 600, 800$.

VI. RESULTS

Fig. 2 shows the mean values of the BAC obtained in the 20 random repetitions of the nested CV procedure for the tested classifiers and different configurations of the LMS filter. The best performance is obtained for $N = 12$ and $\mu = 8 \cdot 10^{-3}$ in all the classifiers, although a wide range of configurations show a BAC above 95%. Table I shows the mean (SD) of the performance metrics for the optimal configuration ($N = 12$ and $\mu = 8 \cdot 10^{-3}$). All the classifiers obtained performances in compliance with AHA (Se > 90%, Sp > 95%). Furthermore, the results obtained for all the classifiers are quite similar, with an accuracy close to 96% and fairly balanced Se and Sp values. This similarity confirms the robustness of the SWT-based features and the feature selection method applied in this work. The optimal pairs of hyperparameters obtained for each classifier are shown in Table II.

Fig. 3 shows the 15 features with higher probabilities of being selected, estimated as the proportion of folds in which they were selected in the inner FS loops. Sample entropy of the detail coefficient d_3 (SampEn, $_{d3}$) and Npeak (the number of peaks in the 8 s interval) were selected in all the 200 inner feature selection loops. The next best parameters were VFleak and IQR, $_{d7}$ with selection probabilities of 97% and 81.5% respectively. Interestingly, these results
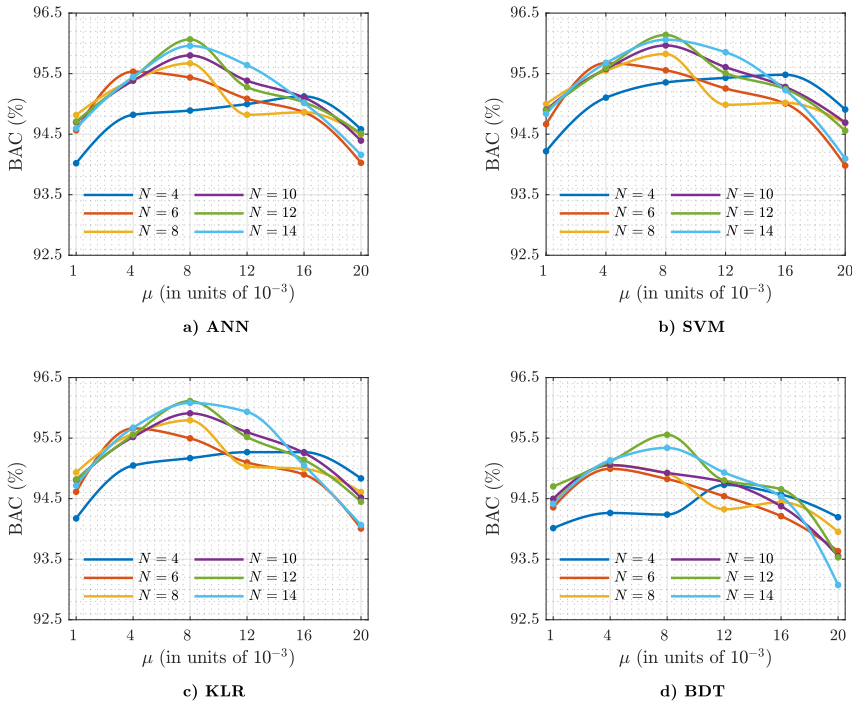

Fig. 2. The mean values of BAC obtained in the 20 repetitions of the nested CV procedure in terms of the adjustable parameters of the LMS filter: the number of harmonics of the CPR model, N, and the step size, μ.

1906

TABLE I
PERFORMANCE METRICS FOR DIFFERENT ML CLASSIFIERS

Classifier	Performance metrics			
	Se (%)	Sp (%)	BAC (%)	Acc (%)
ANN	96.2 (0.5)	95.9 (0.3)	96.1 (0.3)	96.0 (0.2)
SVM	96.7 (0.2)	95.6 (0.2)	96.1 (0.2)	95.9 (0.1)
KLR	96.4 (0.3)	95.8 (0.2)	96.1 (0.2)	96.0 (0.2)
BDT	94.6 (0.5)	96.5 (0.2)	95.6 (0.3)	96.1 (0.2)

TABLE II
THE OPTIMAL PAIRS OF HYPERPARAMETERS

Classifier	Hyper.	Opt. Val.
ANN	N_h/E_p	35/80
SVM	γ/C	$6.8 \cdot 10^{-2}/1.0$
KLR	γ/λ	$4.6/4.4 \cdot 10^{-5}$
BDT	λ_b/M	0.01/600

are consistent with our findings for mechanical CPR [6]. Although CPR artifacts are very different in mechanical and manual CPR [16], the features derived from the SWT decomposition seem to be very robust/independent of the filtering residuals and capture the distinctive characteristics of shockable and nonshockable rhythms [6].
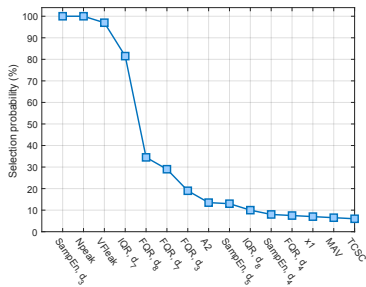

Fig. 3. Selection probability for the 15 most selected features in the 200 inner loops.

VII. CONCLUSIONS

This study introduces a robust ML architecture for a reliable rhythm analysis during manual CPR. All classifiers tested within this architecture obtained very similar performances with a BAC and an Acc close to 96%. Our method improves the BAC and the Acc of the best known solution to date [8] by 1.3 and 0.5 points, respectively. That solution consisted of a RLS filter followed by a Random Forest (RF) classifier and the results are directly comparable since the algorithm was applied on this same database [8].

The improvement in performance is mainly due to two factors. Firstly, the SWT provides higher resolution features than the DWT used in [8] due to the shift-invariance property. Secondly, the wrapper-based approach selects the set of

6 features that maximize the most significant performance metric (BAC), whereas the feature selection used in [8] (based on the feature importance ranking of a RF-classifier) independently evaluates each variable using the out-of-bag error of a RF classifier.

In conclusion, the ML strategy proposed in this study may open the possibility of a reliable shock/no-shock decision without interrupting CPR therapy. Minimizing CPR interruptions reduces no flow periods, and may contribute to increase OHCA survival.

REFERENCES

[1] G. Perkins *et al.*, "European resuscitation council guidelines for resuscitation 2015: Section 2. Adult basic life support and automated external defibrillation," *Resuscitation*, vol. 95, pp. 81–99, 2015.

[2] S. Ruiz de Gauna, U. Irusta, J. Ruiz, U. Ayala, E. Aramendi, and T. Eftestøl, "Rhythm analysis during cardiopulmonary resuscitation: past, present, and future," *BioMed. Res. In.*, vol. 2014, 2014.

[3] K. B. Kern, R. W. Hilwig, R. A. Berg, A. B. Sanders, and G. A. Ewy, "Importance of continuous chest compressions during cardiopulmonary resuscitation: improved outcome during a simulated single lay-rescuer scenario," *Circulation*, vol. 105, no. 5, pp. 645–649, 2002.

[4] U. Irusta, J. Ruiz, S. R. de Gauna, T. Eftestøl, and J. Kramer-Johansen, "A least mean-square filter for the estimation of the cardiopulmonary resuscitation artifact based on the frequency of the compressions," *IEEE Trans. Biomed. Eng.*, vol. 56, no. 4, pp. 1052–1062, 2009.

[5] U. Ayala, U. Irusta, J. Ruiz, T. Eftestøl, J. Kramer-Johansen, F. Alonso-Atienza, E. Alonso, and D. González-Otero, "A reliable method for rhythm analysis during cardiopulmonary resuscitation," *BioMed. Res. In.*, vol. 2014, 2014.

[6] I. Isasi, U. Irusta, A. Elola, E. Aramendi, U. Ayala, E. Alonso, J. Kramer-Johansen, and T. Eftestol, "A machine learning shock decision algorithm for use during piston-driven chest compressions," *IEEE Trans. Biomed. Eng.*, 2018.

[7] I. Isasi, U. Irusta, E. Aramendi, U. Ayala, E. Alonso, J. Kramer-Johansen, and T. Eftestøl, "A multistage algorithm for ECG rhythm analysis during piston-driven mechanical chest compressions," *IEEE Trans. Biomed. Eng.*, vol. 66, no. 1, pp. 263–272, 2019.

[8] I. Isasi, A. B. Rad, U. Irusta, M. Zabihi, E. Aramendi, T. Eftestøl, J. Kramer-Johansen, and L. Wik, "ECG rhythm analysis during manual chest compressions using an artefact removal filter and random forest classifiers," in *Proc. Comput. Cardiol.*, 2018.

[9] J.-C. Pesquet, H. Krim, and H. Carfantan, "Time-invariant orthonormal wavelet representations," *IEEE Trans. Signal Process.*, vol. 44, no. 8, pp. 1964–1970, 1996.

[10] D. L. Donoho and I. M. Johnstone, "Ideal spatial adaptation by wavelet shrinkage," *Biometrika*, vol. 81, no. 3, pp. 425–455, 1994.

[11] A. B. Rad, T. Eftestøl, K. Engan, U. Irusta, J. T. Kvaløy, J. Kramer-Johansen, L. Wik, and A. K. Katsaggelos, "ECG-based classification of resuscitation cardiac rhythms for retrospective data analysis," *IEEE Trans. Biomed. Eng.*, vol. 64, no. 10, pp. 2411–2418, 2017.

[12] C. Figuera, U. Irusta, E. Morgado, E. Aramendi, U. Ayala, L. Wik, J. Kramer-Johansen, T. Eftestøl, and F. Alonso-Atienza, "Machine learning techniques for the detection of shockable rhythms in automated external defibrillators," *PloS one*, vol. 11, no. 7, p. e0159654, 2016.

[13] S. Strearns, "On selecting features for pattern classifiers," *Proc. ICPR, 1976*, pp. 71–75, 1976.

[14] J. Zhu and T. Hastie, "Kernel logistic regression and the import vector machine," in *Adv. Neural Inform. Process. Syst.*, 2002, pp. 1081–1088.

[15] J. Friedman, T. Hastie, and R. Tibshirani, *The elements of statistical learning*. Springer series in statistics New York, NY, USA:, 2001, vol. 1, no. 10.

[16] E. Aramendi, U. Irusta, U. Ayala, H. Naas, J. Kramer-Johansen, and T. Eftestøl, "Filtering mechanical chest compression artefacts from out-of-hospital cardiac arrest data," *Resuscitation*, vol. 98, pp. 41–47, 2016.

A.3.3 JOURNAL PAPER: J1$_3$

Table A.8. Journal paper associated to objective 3.

Publication in international magazine
Reference — I. Isasi, U. Irusta, E. Aramendi, T. Eftestøl, J. Kramer-Johansen and L. Wik,"Rhythm analysis during cardiopulmonary resuscitation using convolutional neural networks", *Entropy*, vol. 22, p. 595, 2020.

Quality indices

- **Type of publication:** Journal paper idexed in JCR and SJR
- **Area:** Multidisciplinary physics
- **Ranking:** 33/85 (Q2) based on JCR 2019
- **Impact factor SJR:** 0.527
- **Impact factor JCR:** 2.494

Article

Rhythm Analysis during Cardiopulmonary Resuscitation Using Convolutional Neural Networks

Iraia Isasi [1,*] , **Unai Irusta** [1] , **Elisabete Aramendi** [1] , **Trygve Eftestøl** [2], **Jo Kramer-Johansen** [3] and **Lars Wik** [3]

1. Department of Communications Engineering, University of the Basque Country UPV/EHU, 48013 Bilbao, Spain; unai.irusta@ehu.eus (U.I.); elisabete.aramendi@ehu.eus (E.A.)
2. Department of Electrical Engineering and Computer Science, University of Stavanger, 4036 Stavanger, Norway; trygve.eftestol@uis.no
3. Norwegian National Advisory Unit on Prehospital Emergency Medicine (NAKOS), Oslo University Hospital and University of Oslo, 0424 Oslo, Norway; jo.kramer-johansen@medisin.uio.no (J.K.-J.); lars.wik@medisin.uio.no (L.W.)
* Correspondence: iraia.isasi@ehu.eus; Tel.: +34-946-01-73-86

check for updates

Abstract: Chest compressions during cardiopulmonary resuscitation (CPR) induce artifacts in the ECG that may provoque inaccurate rhythm classification by the algorithm of the defibrillator. The objective of this study was to design an algorithm to produce reliable shock/no-shock decisions during CPR using convolutional neural networks (CNN). A total of 3319 ECG segments of 9 s extracted during chest compressions were used, whereof 586 were shockable and 2733 nonshockable. Chest compression artifacts were removed using a Recursive Least Squares (RLS) filter, and the filtered ECG was fed to a CNN classifier with three convolutional blocks and two fully connected layers for the shock/no-shock classification. A 5-fold cross validation architecture was adopted to train/test the algorithm, and the proccess was repeated 100 times to statistically characterize the performance. The proposed architecture was compared to the most accurate algorithms that include handcrafted ECG features and a random forest classifier (baseline model). The median (90% confidence interval) sensitivity, specificity, accuracy and balanced accuracy of the method were 95.8% (94.6–96.8), 96.1% (95.8–96.5), 96.1% (95.7–96.4) and 96.0% (95.5–96.5), respectively. The proposed algorithm outperformed the baseline model by 0.6-points in accuracy. This new approach shows the potential of deep learning methods to provide reliable diagnosis of the cardiac rhythm without interrupting chest compression therapy.

Keywords: out-of-hospital cardiac arrest (OHCA); cardiopulmonary resuscitation (CPR); electrocardiogram (ECG); adaptive filter; deep learning; machine learning; convolutional neural network (CNN); random forest (RF) classifier

1. Introduction

Out of hospital cardiac arrest (OHCA) is one of the leading causes of death worldwide [1,2]. The two key life saving therapies are defibrillation (electric shock) when the cardiac rhythm is ventricular fibrillation (VF) or tachycardia (VT), and cardiopulmonary resuscitation (CPR) [3]. The defibrillator monitors the electrocardiogram (ECG), and includes a shock/no-shock algorithm that analyzes the patient's ECG to detect VF/VT [4]. The American Heart Association (AHA) has established the minimum accuracy requirements for these algorithms [5]. Shockable rhythms should be detected with a minimum sensitivity (Se) of 90% to properly identify defibrillation treatment conditions. The specificity (Sp) for detection of nonshockable rhythms must be above 95% to avoid unnecessary shocks that may damage the myocardium or deteriorate the quality of CPR.

The mechanical activity of chest compressions during CPR induces artifacts in the ECG that impede a reliable shock/no-shock decision by the defibrillator [6]. Therefore, defibrillators prompt the rescuers to stop chest compressions for rhythm analysis every 2 minutes [7,8]. These hands off (or no flow) intervals lead to intermittent periods with no cerebral and myocardial blood flow that deteriorate the patient's condition, and compromise survival [7,9–11]. Consequently, many biomedical engineering solutions have been proposed over the years to allow an AHA compliant shock/no-shock decision during CPR [12], but none of these solutions have yet a sufficient positive predictivity to be implemented in commercial defibrillators. These methods are based on adaptive filters to remove CPR artifacts. Adaptive filters are needed to address the time and frequency variability of the artifact and its spectral overlap with OHCA rhythms [13]. These filters use signals recorded by the defibrillator like compression depth (CD) or thoracic impedance (TI) to model the artifact [14,15]. Several adaptive approaches have been demonstrated including Wiener filters [16], Matching Pursuit Algorithms [17], Recursive Least Squares (RLS) [18], Least Mean Squares (LMS) [19], or Kalman filters [20,21]. Once the artifact is removed the ECG is analyzed using the shock/no-shock algorithms in defibrillators, or ad-hoc algorithms specially designed to analyze the filtered ECG [17,19,22]. The latter have shown the highest Se/Sp values by exploiting recent advances in ECG feature extraction and classical machine learning algorithms. ECG features are customarily computed in time, frequency or time-frequency domains [23–26]. These features have been efficiently combined using classical machine learning classification algorithms like support vector machines (SVM) or random forests (RF) [22,25,26].

Recently, deep learning approaches have proven to be superior to classical machine learning algorithms in many biomedical signal applications [27,28], including arrhythmia classification based on the ECG waveform [29–33]. Deep learning algorithms using convolutional neural networks (CNN) are end-to-end solutions in which the algorithm learns efficient internal representations of the data (features) and combines them to solve the classification task [34,35]. Deep learning algorithms have already been shown to outperform classical machine learning algorithms in some OHCA applications, such as detection of VF in artifact free ECG [30,36], or the detection of pulse [37]. However, deep learning has not been applied to design algorithms that give accurate shock/no-shock decisions during CPR.

The objective of this study was to design the first deep learning solution to discriminate shockable from nonshockable rhythms during CPR. The method comprises two stages, an adaptive RLS filter to remove CPR artifacts from the ECG followed by a CNN to classify the filtered ECG. The paper is organized as follows: the study dataset is detailed in Section 2, Section 3 describes the methodology including the CNN architecture and the evaluation procedure. The results are presented in Section 4, discussed in Section 5 and the main conclusions are presented in Section 6.

2. Materials

Data were extracted from a large prospective clinical trial designed to measure CPR quality during OHCA [38]. The study was conducted between March 2002 and September 2004 by the emergency services of London, Stockholm and Akershus (Norway). CPR was performed using prototype defibrillators based on HeartStart 4000 (Philips Medical Systems, Andover, MA, USA) together with a sternal CPR assist pad fitted with an accelerometer (ADXL202e, AnalogDevice, Norwood, Mass). The raw data for this study consisted of the ECG and TI signals acquired through the defibrillation pads and the CD signal derived from accelerometer data [16]. Defibrillator data was anonymized and converted to Matlab (MathWorks Inc, Natick, MA, USA) using a sampling rate of 250 Hz. The ECG had an amplitude resolution of 1.031 µV per least significant bit. A notch filter and a Hampel filter were used to remove powerline interferences and spiky artifacts from the ECG [37]. Finally, chest compressions instants (t_k) were automatically marked using a negative peak detector with a 1 cm threshold on the CD signal (see Figure 1, peak detection Th) [15].
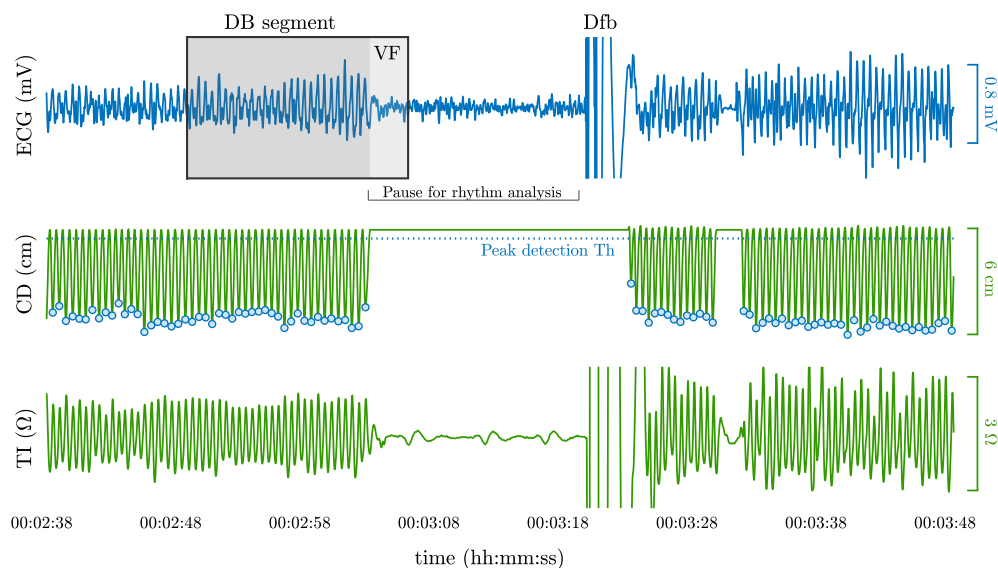
Figure 1. A 70 s interval from an OHCA episode showing the ECG, CD and TI signals. Activity shows CPR followed by a pause for rhythm analysis, the delivery of a defibrillation shock (Dfb) and immediate resumption of CPR. The interval highlighted in grey corresponds to a 15.5 s segment in the dataset. During the first 12.5 s of the segment chest compressions were delivered (see activity in TI and CD), and in the last 3 s there were no compressions and the ground truth rhythm (VF) for the whole segment could be annotated.

The rhythms in the OHCA episodes were originally annotated by two experienced resuscitation researchers/practitioners, a biomedical engineer and an anesthesiologist [38]. For the purpose of this study the rhythm annotations were grouped into shockable and nonshockable. Shockable rhythms comprised lethal ventricular arrhythmia, predominantly VF but also pulseless VT. Non-shockable rhythms included asystole (AS), the absence of electrical activity, and organized rhythms (ORG), or rhythms with visible QRS complexes. The OHCA episodes had median (interquartile range, IQR) durations of 26 min (17–33). From these episodes 15.5 s segments were automatically extracted following these criteria: unique rhythm type in the segment and an interval of 12.5 s with ongoing compressions followed or preceded by a 3 s interval without compressions. The 12.5 s interval with ongoing compressions was used to develop the shock/no-shock decision algorithm, and the 3 s segment was used to confirm the original rhythm annotation in an artifact free ECG. All the data were visually revised (double blind process by authors UI and TE) to ensure compliance with the extraction criteria and the correctness of the rhyhm annotations. The annotated dataset contained 3319 segments from 272 OHCA patients, whereof 586 were shockable and 2733 (1192 AS and 1541 ORG) were nonshockable.

3. Methods

The shock/no-shock decision algorithms proposed in this study are composed of two stages. First, an adaptive RLS filter was used to remove chest compression artifacts from the ECG. Then shock/no-shock decision algorithms were designed to classify the filtered ECG using CNNs. In what follows $t = n \cdot T_s$, where $T_s = 4$ ms is the sampling period ($f_s = 250$ Hz), and n is the sample index.

3.1. CPR Artifact Suppressing Filter

CPR artifacts were suppressed using a state-of-the-art method [26,39] based on a RLS filter designed to remove periodic interferences [40]. The CPR artifact is modeled as a quasi-periodic

interference using a Fourier series truncated to N terms (harmonics). The fundamental frequency of the artifact is that of the chest compressions [19], which is assumed constant during a chest compression, but variable from compression to compression. This means that for an interval between two successive compressions at time points, t_{k-1} and t_k (see Figure 2), the frequency can be expressed as

$$f_0(n) = \frac{1}{t_k - t_{k-1}} \qquad t_{k-1} \leq nT_s < t_k \tag{1}$$

and the N-term Fourier series representation is then:

$$\hat{s}_{\mathrm{cpr}}(n) = A(n) \sum_{\ell=1}^{N} \big(a_\ell(n) \cos(\ell 2\pi f_0(n) T_s n) + b_\ell(n) \sin(\ell 2\pi f_0(n) T_s n) \big) \tag{2}$$

where $A(n)$ is an amplitude envelope which differentiates intervals with $(A = 1)$ and without compressions $(A = 0)$, N is the number of harmonics in the Fourier series and $f_0(n)$ is the instantaneous chest compression frequency.
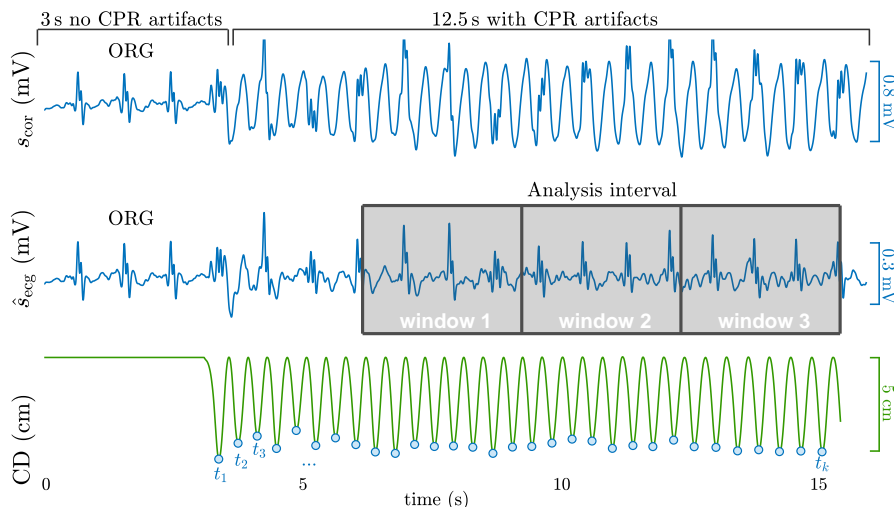
Figure 2. A 15.5 s segment from the study dataset corresponding to a patient in an organized rhythm is shown. In the initial 3 s interval without compressions three QRS complexes are visible, and the nonshockable rhythm annotation was confirmed. The following 12.5 s are corrupted by CPR artifacts (top panel) that conceal the underlying rhythm. The output of the adaptive filter, $\hat{s}_{\mathrm{ecg}}(n)$, reveals the underlying rhythm during chest compressions. CPR activity and the chest compression instants (t_k) can be observed in the CD signal (bottom).

The RLS filter adaptively estimates the time-varying Fourier coefficients, $a_\ell(n)$ and $b_\ell(n)$, of the CPR artifact, $\hat{s}_{\mathrm{cpr}}(n)$, by minimizing in each iteration the error between the corrupted ECG, $s_{\mathrm{cor}}(n)$, and the estimated underlying ECG, $\hat{s}_{\mathrm{ecg}}(n)$, only around the spectral components of the CPR artifact, that is $f_0(n)$ and its harmonics. The underlying ECG is estimated assuming an additive noise model, so $\hat{s}_{\mathrm{ecg}}(n) = s_{\mathrm{cor}}(n) - \hat{s}_{\mathrm{cpr}}(n)$. A detailed description of the RLS filter equations is available in [39], and the values recommended there to suppress CPR artifacts were used in this study, that is, $N = 4$ and a forgetting factor of $\lambda = 0.999$ [39].

The shock/no-shock algorithms trained and evaluated in this study comprise algorithms based on CNNs (core methods of the paper), and a state of the art algorithm based on classical machine learning techniques used as a baseline model for comparison. In both cases, the algorithms were designed to analyze the filtered ECG in the interval from 3–12 s during compressions (see analysis

interval in Figure 2). That is, the algorithms use 9 s of the filtered ECG for a decision, excluding the initial 3 s to avoid RLS filtering transients [39]. The analysis interval was further divided into three non-overlapping analysis windows of 3 s (see Figure 2) and the shock/no-shock decision was obtained as the majority vote. The combination of consecutive analysis windows is a typical design practice in shock/no-shock decision algorithms for defibrillators [41,42], because it increases the reliability of the diagnosis by avoiding the effects of transient lower quality signal intervals, rhythm changes or filtering miss-adjustments.

Algorithm Based on CNNs

Figure 3 shows the architecture of the shock/no-shock decision algorithms based on CNNs. First the 3 s window of the filtered ECG is downsampled to 125 Hz, resulting in a 1-D signal of $N = 375$ samples, $\hat{s}_{\text{ecg}}(n)$. Then the CNN is composed of three convolutional blocks to extract the high level descriptors of the ECG, and two fully connected layers for classification. The b-th convolutional block consists of a convolutional layer with J_b filters of width I_b, followed by a batch normalization layer, a rectified linear unit (ReLU), a max-pooling layer (K = 3) and a dropout layer.
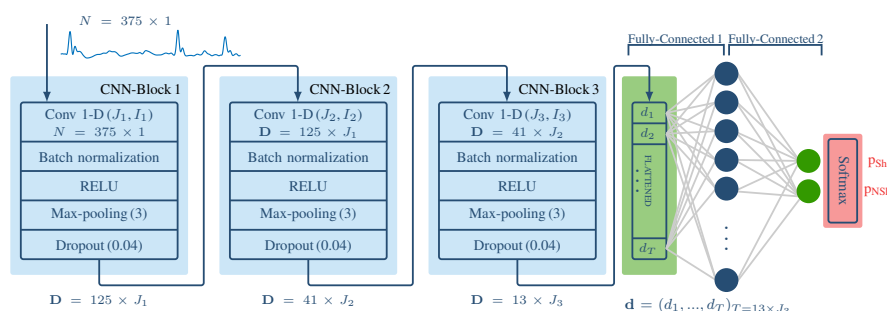
Figure 3. Architecture of the CNN-based shock/no-shock algorithm. It comprises two main stages: a CNN composed of three identical blocks and a classification stage based on two fully connected and a softmax layer.

3.2. Shock/No-Shock Decision Algorithms

Let us denote by $s_{b-1}(n, m)$ the output of block $b - 1$ (input to block b), where n is the time index and m the filter index. In the first block the input is $s_0(n, 1) = \hat{s}_{\text{ecg}}(n)$. The output of the Conv-1D layer at block b can be expressed as

$$c_b(n, m) = f\left(b_m + \sum_{\ell=1}^{J_{b-1}} \sum_{i=1}^{I_b} \omega_{\ell,i}^m s_{b-1}(n + i - 1, \ell) \right) \tag{3}$$

where $\omega_{\ell,i}^m$ are the network weights (convolutional coefficients), and $f(x) = \max(x, 0)$ is the ReLU activation function that makes the network non-linear. The max-pooling layer selects the largest sample in blocks of K samples along the time index n to give the output of block b:

$$s_b(n, m) = \max\{c_b(k, m)\}_{k=(n-1)\cdot K, \cdots, n\cdot K} \tag{4}$$

Padding was applied before the convolutional and the max-pooling layers, so the only reduction of the dimensionality occurs at the max-pooling layers ($K = 3$). This means that the dimensions of the outputs at blocks $b = 1, 2, 3$ where $(125, J_1)$, $(41, J_2)$ and $(13, J_3)$, respectively and that the number of learnable parameters (ω, b) at block b where $J_b \times I_b + J_b$.

The dropout layer at the end of each block has a regularization effect, and is used only during training to avoid overfitting. It temporarily deactivates a randomdly selected proportion of the

network's tunable parameters, and has been shown to improve performance by providing noisy inputs to the fully connected layers that help avoid overfitting [43].

The classification stage takes as input the flattened $13 \times J_3$ features and feeds them into two fully-connected layers. The first one is composed by 10 hidden units whereas the second one uses 2 neurons for the 2-class classification task. In the second fully-connected layer a softmax function is used to convert the output of the last two neurons into two values in the [0,1] range that can be interpreted as the likelihood that the 3 s window is shockable (p_{Sh}) or nonshockable (p_{NSh}).

The weights and biases of every layer were optimized using stochastic gradient descent with a momentum of 0.8. The initial learning rate was fixed to 0.02 and it was reduced by a factor of 0.8 at every epoch. The training data were fed into the CNN in batches of 256, and 20 epochs were used to train the networks [44]. During training data was augmented by splitting each 9 s training segment into overlapping 3 s windows with a linearly spaced start between 0 s and 6 s of the segment. To address class imbalance the augmented number of windows per segment during training was fixed to 100 for shockable and 40 for nonshockable rhythms, respectively. The binary cross entropy was used as loss function during network optimization (training):

$$L = \sum_i y_i \ln(p_{Sh_i}) + (1 - y_i) \ln(1 - p_{Sh_i}) \tag{5}$$

where $y_i = \{0 : NSh, 1 : Sh\}$ corresponds to the rhythm label of 3 s training window i.

Classical Machine Learning Shock/no-Shock Decision Algorithm for Baseline Comparison

The baseline machine learning shock/no-shock algorithm is a state of the art solution described in [25]. In short, the algorithm is based on multiresolution ECG analysis using the Stationary Wavelet Transform (SWT) for feature extraction, followed by a random forest (RF) classifier. The SWT decomposes the 3 s window into 7 sub-bands, and the denoised ECG is reconstructed using detail coefficients d_3 to d_7, i.e. an analysis band of 0.98–31.25 Hz. The daubechies mother wavelet was used for the analysis as recommended in [26]. The selection of the mother wavelet was not a critical for this problem as shown in [26]. The denoised ECG, $s_{den}(n)$, and the detail coefficients d_3-d_7 were used to obtain twenty five ECG features, selected using recursive feature elimination from a set of over 200 features (consult [25] for the details). The most relevant features were classical VF detection features like VFleak or x_4 [22,45] computed from s_{den}, and a rich set of features obtained from the detail coefficients $\{d_i\}_{i=3,\cdots,7}$, such as: sample entropy (SampEn(d_i)), the mean and standard deviation of the absolute value of the signal ($\overline{|d_i|}$, $\sigma(|d_i|)$) and its slope ($\overline{|\Delta d_i|}$, $\sigma(|\Delta d_i|)$), and the Hjorth mobility (Hmb(d_i)) and complexity (Hmc(d_i)) indices [46]. A detailed description of the algorithm is found in [25], with a detailed bibliography for the computation of the features.

The parameters of the RF classifier were fixed to those recommended in [25], that is $B = 500$ trees, 5 predictors per split (standard in RF), and the minimum observations per leaf to 3 (to avoid growing excessively deep or overfit trees). To avoid class imbalance uniform priors were assigned and a cost function was introduced to penalize false shock classifications with a factor of 2.5 (similar to the shock/no-shock augmentation factor used in the CNN).

3.3. Evaluation

All the classification algorithms were trained/tested using 5-fold cross validation (CV). Folds were partitioned patient-wise to avoid training/test data leakage, and in a quasi-stratified way by ensuring that the shock/no-shock prevalences in all folds were at least 80% those of the whole dataset. The performance of the method was evaluated using the standard metrics for binary classification problems, taking the shockable class as positive and the nonshockable class as negative. For a 2×2 confusion matrix with true positives (TP), true negatives (TN), false positives (FP) and false negatives FN) the performance metrics were

$$Se = \frac{TP}{TP + FN} \qquad\qquad PPV = \frac{TP}{TP + FP} \tag{6}$$

$$Sp = \frac{TN}{TN + FP} \qquad\qquad NPV = \frac{TN}{TN + FN} \tag{7}$$

$$Acc = \frac{TP+TN}{TP+FN+TN+FP} \qquad\qquad BAC = \frac{1}{2}(Se + Sp) \tag{8}$$

The Balanced Accuracy (BAC) was used as target performance metric to ensure both shockable and nonshockable rhythms were accurately identified (as recommended by the AHA) despite the large class imbalance in the data.

4. Results

4.1. Parameters of the CNN Architecture

The effect of changing the main parameters of the CNN architecture was first studied taking the BAC as target performance metric (see Figure 4). Three parameters were studied: the number of blocks (B), the size of the filters (I), and the number of filters ($\mathbf{L} = (J_1, ... J_B)$). Four filter configurations were studied with decreasing number of filters (from dense to sparse): $\mathbf{L}_4 = (40, 30, 20, 10)$, $\mathbf{L}_3 = (32, 24, 16, 8)$, $\mathbf{L}_2 = (24, 18, 12, 6)$ and $\mathbf{L}_1 = (16, 12, 8, 4)$. The numbers in parentheses indicate the amount of filters from block 1 to block 4, so for arquitectures with 3 blocks and 2 blocks and $\mathbf{L}_2$ the number of filters would be (24,18,12) and (24,12), respectively.

The results of the analysis are shown in Figure 4, with the median BAC computed over the 5-fold CV partitions. The best classification results were obtained for 3 blocks. Adding a fourth block increases the complexity (number of trainable parameters) and slightly decreases the performance. Using only 2 blocks resulted in a large decrease in performance (over 1-point in BAC), or an overly simplistic model. The best results for a CNN with 3 blocks were obtained with a filter width of $I = 16$, and a filter configuration of $\mathbf{L} = (32, 24, 16)$. This was the CNN configuration adopted for the rest of the analyses.

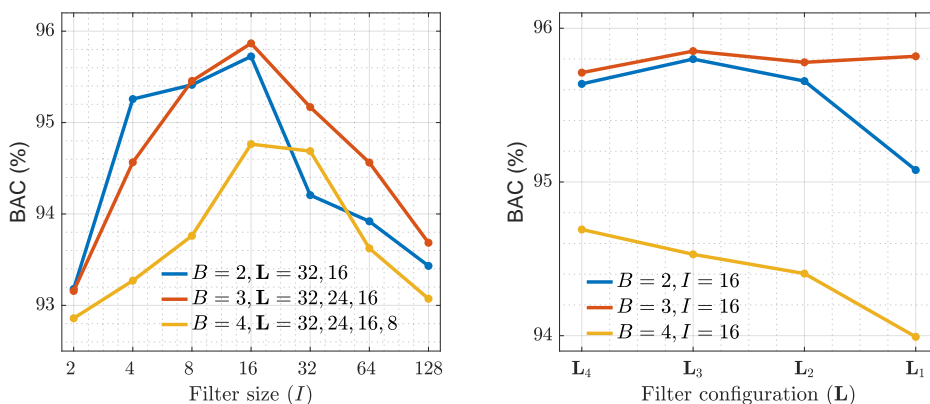**Figure 4.** Performance of the CNN architecture for the configurable parameters of the network: the number of blocks (B), the filter size (I), and the filter configuration ($\mathbf{L}$). The left panel shows the effect of the filter size for networks with $\mathbf{L}_4 = (32, 24, 16, 8)$ filters. The right panel shows the effect of the filter configurations from dense ($\mathbf{L}_4$) to sparse ($\mathbf{L}_1$) for $I = 16$.

4.2. Comparison with the Baseline Machine Learning Model

The shock/no-shock decision algorithms using CNNs and the classical machine learning model were compared. Table 1 shows the results for all the performance metrics. The accuracies were compared using McNemar's test in all 5-fold CV partitions, and the results were considered significant at the 95% level. The CNN model was significantly more accurate (median $p < 0.05$) than the baseline model. As shown in Table 1, the CNN model designed for 9 s improves the best baseline models in 0.6-points in BAC and Acc, and in both cases the algorithms presented balanced Se/Sp values because they were trained to avoid class imbalance. The predictivity is higher for the CNN solution, but the differences are only large for shockable rhythms (PPV) because shockable rhythms have a much lower prevalence in the dataset (1 to 5). The table shows the results for the 3 s windows (where CNN outperforms the baseline model), but also for the combination of three consecutive analyses (9 s). For short windows the algorithms do not meet the minimum 95% value recommended by the AHA for artifact free ECG, but combining diagnoses with a majority vote criterion considerably improves performance and brings both the CNN solution and the baseline algorithm above AHA specifications. The table also shows the shock/no-shock decision performance when the two subgroups of nonshockable rhythms were evaluated separately, AS and ORG rhythms. The results show that no-shock decisions were more inaccurate when the underlying rhythm was asystole. For 9 s segments the CNN architecture yielded results slightly above the AHA's 95% Sp goal for AS, but the baseline model was marginally below.

Table 1. Performance metrics for the CNN and the baseline models. The results are shown as median and 90% confidence interval (CI).

Metric	3 s		9 s	
	CNN	**Baseline**	**CNN**	**Baseline**
Se	93.2 (92.2–94.0)	93.1 (92.6–93.6)	95.8 (94.6–96.8)	95.2 (94.7–95.7)
Sp	94.5 (94.1–94.9)	94.1 (93.9–94.3)	96.1 (95.8–96.5)	95.6 (95.2–95.9)
AS	93.1 (92.6–93.7)	92.5 (92.2–92.8)	95.4 (94.9–96.0)	94.5 (94.1–95.0)
ORG	95.6 (95.1–96.0)	95.3 (95.1–95.6)	96.8 (96.2–97.4)	96.4 (96.0–96.8)
BAC	93.8 (93.4–94.3)	93.6 (93.3–93.9)	96.0 (95.5–96.5)	95.4 (95.0–95.7)
Acc	94.3 (94.0–94.6)	93.9 (93.7–94.1)	96.1 (95.7–96.4)	95.5 (95.2–95.8)
PPV	78.5 (77.2–79.6)	77.2 (76.5–77.7)	84.3 (82.8–85.6)	82.2 (81.0–83.2)
NPV	98.5 (98.3–98.7)	98.5 (98.3–98.6)	99.1 (98.8–99.3)	98.9 (98.8–99.1)

4.3. Effect of the ECG Corruption Level on Classification

CPR artifacts during chest compressions present very different noise levels in the ECG depending on variables like the position of the hands relative to the pads and cables, pad placement, or environmental conditions [47,48]. These variables are difficult to control in a pre-hospital setting, but it is important to know what the observed corruption levels are, and how these corruption levels affect the shock/no-shock decisions. To estimate the signal-to-noise ratio (SNR) the underlying ECG was assumed to be stationary over the 15 s segments, and thus the power of the clean signal (P_{ecg}) was estimated in the 3 s interval without artifacts used to confirm the rhythm annotations. Then, CPR artifact estimated by the RLS filter was used to compute the power of the noise (P_{cpr}), and to obtain the SNR as:

$$\text{SNR} = 10 \cdot \log_{10}\left(\frac{P_{ecg}}{P_{cpr}}\right) \quad (\text{dB}) \tag{9}$$

The noise levels were divided into bins from very large corruption levels (SNR < -18 dB) to very low corruption levels (SNR > 6 dB). The distributions of noise levels and the classification results for the different noise conditions are shown in Figure 5 for shockable (a) and nonshockable (b)

rhythms. As expected the classification results improve as noise conditions improve, but noise affects the classification of shockable and nonshockable rhythms very differently. Nonshockable rhythms are detected with high specificity even in very noisy conditions, and the confidence in a nonshockable diagnosis (NPV) is high because the prevalence of nonshockable rhythms is 5/1 that of shockable rhythms. The sensitivity for shockable rhythms improves considerably as noise conditions improve, and was above the 90% value recommended by the AHA for SNR > -10 dB. However, the confidence on a shock diagnosis (PPV) is good only for SNR > -6 dB because of the lower prevalence of shockable rhythms. The SNR was significantly higher for nonshockable than for shockable rhythms ($p < 0.001$, Mann-Whitney U test), and in approximately 15% of shockable and nonshockable cases the noise level was negligible (SNR > 25 dB, see Figure 5). Although noise levels were lower in nonshockable rhythms, a high specificity was obtained regardless of the noise conditions. Even for the very noisy segments (SNR < -12 dB) the specificity was above 94%.
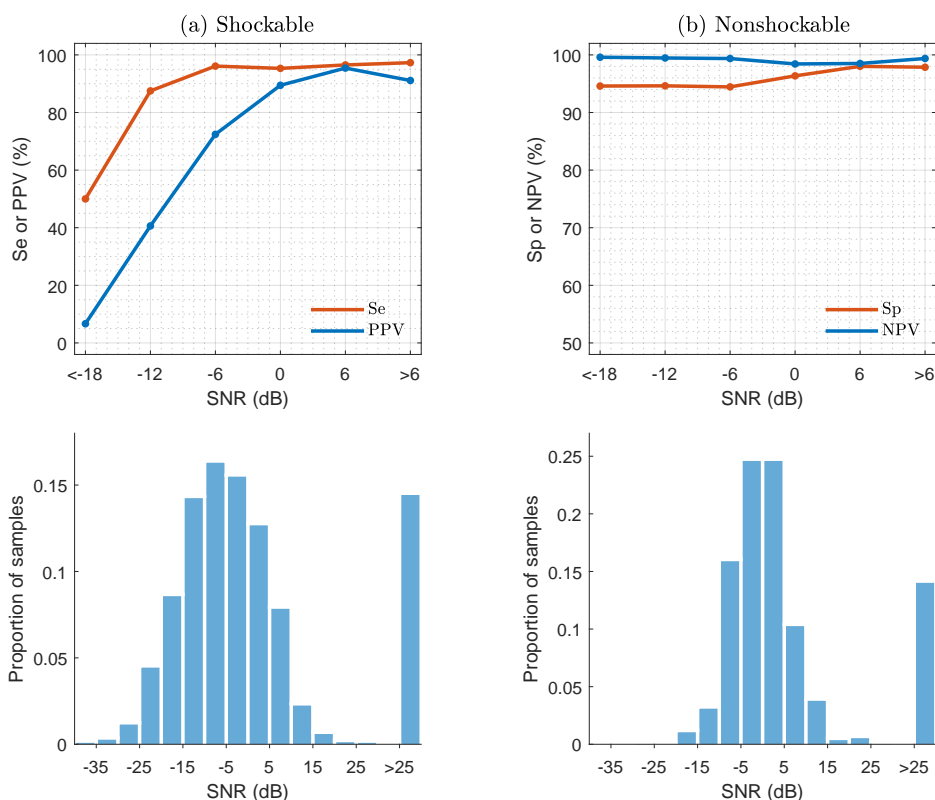
Figure 5. Median values of the performance metrics for shockable and nonshockable rhythms as a function of the SNR. The SNR levels were divided into 6 dB bins for the analysis from high (<-18 dB) to low (>6 dB) corruption levels. The lower panels show the SNR distributions for shockable (**a**) and nonshockable rhythms (**b**).

4.4. Feature Extraction Using CNNs

For these experiments the 10 features at the output of the first fully connected layer were used as the features learned by the algorithm, these features will be named $\{f_i\}_{i=1,\cdots,10}$. To evaluate feature extraction two experiments were conducted [36], and the results were compared to those obtained using the multiresolution features based on the SWT in the baseline model [25]. First, a dimensionality reduction experiment was conducted by projecting the feature space into a 2-D space using the

t-distributed stochastic neighbor embedding (t-SNE) algorithm [49]. The results were visually assessed, and are shown in Figure 6 for the f_i features and the handcrafted multiresolution features. The classes are shown in colors and the nonshockable rhythms are further divided into AS and ORG. As shown in the figure the CNN features produce better defined clusters than the handcrafted features in the 2D space. To numerically evaluate how the classes were clustered the Davies-Boudin index (DBi) was computed to measure the separability of the clusters [50]. The experiment was repeated on 500 bootstrap replicas and the mean (standard deviation) BDi for the CNN and the handcrafted features were 2.28 (0.06) and 4.95 (0.17), respectively ($p < 0.05$, for the paired t-test) [51]. That is, the features learned by the CNN architecture resulted in a more efficient clustering of the classes, and thus to a better separability.
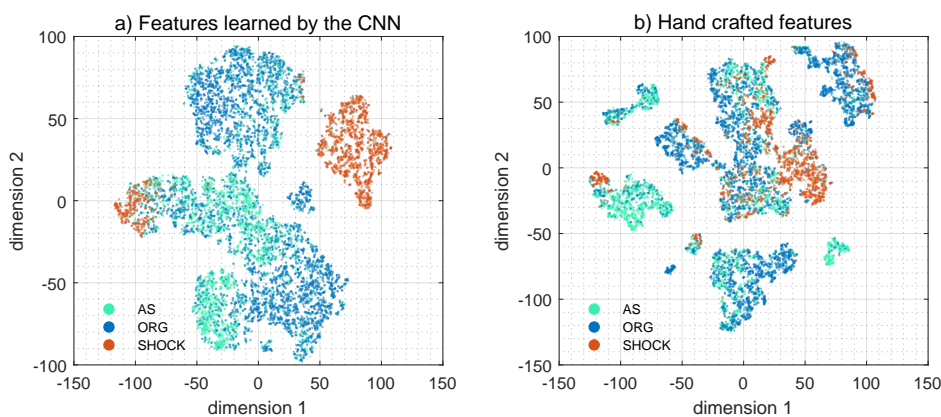
Figure 6. 2D map representation of the separability of the classes for the features learned by the CNN (**a**) and the handcrafted features (**b**). These maps were obtained using the t-SNE algorithm.

Second, the discriminating power of each feature was computed using the area under the receiver characteristics curve (AUC). The results were obtained over 500 bootstrap replicas to statistically characterize the AUCs and compare the AUC distributions for each feature (paired t-test). The results are shown in Table 2, which shows that the four top most discriminating features (f_6, f_{10}, f_1 and f_5) had significantly higher AUCs ($p < 0.05$) than any of the handcrafted features. These results confirm the ability of the CNN to extract high quality discriminating features hidden in the signals.

Table 2. Mean (standard deviation) of the AUCs for the CNN features and the handcrafted features obtained using 500 bootstrap replicas of the data.

CNN Features		Handcrafted Features	
Feature	AUC	Feature	AUC
f_6	97.2 (1.1)	SampEn(d_3)	90.6 (2.0)
f_{10}	96.4 (1.6)	$\sigma(|\Delta d_4|)$	90.3 (1.7)
f_1	95.2 (2.6)	$\sigma(|d_4|)$	87.7 (1.8)
f_5	94.8 (2.3)	$\sigma(|d_3|)$	86.2 (2.3)
f_9	90.7 (3.7)	VFLeak	85.9 (2.7)
f_3	81.2 (11.1)	SampEn(d_4)	84.8 (2.4)
f_8	75.2 (10.6)	$\overline{|\Delta d_3|}$	84.6 (2.8)
f_4	73.9 (8.6)	x4	82.5 (3.6)
f_7	66.9 (6.2)	$\sigma(|s_{den}|)$	82.4 (2.0)
f_2	59.3 (17.1)	SampEn(d_6)	80.6 (2.7)

4.5. Mixed Architectures

To further improve the BAC and accuracy of the CNN model three mixed architectures were also explored. First, the architecture of Figure 3 in which the softmax layer was replaced by a RF classifier to combine the best feature extraction (CNN) and classification (RF) of the the algorithms in Table 1, this solution was named CNN + RF . Second, a RF classifier fed with 25 handcrafted features and the 10 f_i features was tested to see if handcrafted features added information to the CNN features, this was named All-Features. Finally, a basic stacking solution [52] in which the outputs of the CNN+RF (based on f_i) and the baseline model (handcrafted features) were used to form a majority vote (6 analyses, two per window), this solution was called Stacked. The results for 9 s segments are shown in Table 3, which shows that by using more elaborate solutions the BAC and Acc could be further improved in 0.4 and 0.5-points, respectively, either using all features or stacking the classifiers.

Table 3. Performance metrics for 9 s segments of the mixed solutions. The results are shown as median and 90% confidence interval (CI).

Metric	CNN	Mixed Classification Solutions		
		CNN + RF	All-Features	Stacked
Se	95.8 (94.6–96.8)	95.3 (93.9–96.2)	95.6 (94.6–96.4)	96.1 (95.1–96.8)
Sp	96.1 (95.8–96.5)	96.7 (96.3–97.1)	96.8 (96.5–97.1)	96.7 (96.3–97.1)
AS	95.4 (94.9–96.0)	95.9 (95.4–96.5)	96.1 (95.6–96.6)	95.9 (95.3–96.4)
ORG	96.8 (96.2–97.4)	97.2 (96.7–97.7)	97.3 (96.9–97.7)	97.4 (96.9–97.9)
BAC	96.0 (95.5–96.5)	96.0 (95.3–96.5)	96.2 (95.7–96.7)	96.4 (95.9–96.8)
Acc	96.1 (95.7–96.4)	96.4 (96.0–96.7)	96.6 (96.3–96.9)	96.6 (96.3–96.9)
PPV	84.3 (82.8–85.6)	86.0 (84.6–87.4)	86.5 (85.3–87.8)	86.3 (84.8–87.5)
NPV	99.1 (98.8–99.3)	99.0 (98.7–99.2)	99.0 (98.8–99.2)	99.1 (98.9–99.3)

4.6. Analysis of Classification Errors

To conclude the analyses, the classification errors for the CNN based algorithm were identified. Some typical patterns leading to errors are shown in Figure 7. Most of the false positives are caused by the inability of the RLS filter to properly remove artifacts, leading to very disorganized filtering residuals that resemble a VF. Most false negatives occur at low SNR levels with compression rates around $100\,\text{min}^{-1}$. In these cases the filtered ECG still shows an organized activity locked to the compression frequency, incompatible with fast ventricular arrhythmia and thus classified as non-shockable. Interestingly, these errors can be related to the clustering analysis of Section 4.4. Most errors cluster around borderline AS/VF rhythms which appear in the center-left region of the 2D t-SNE map (Figure 6), and ORG/VF rhythms in a much lower proportion in the top-center.

a) False positive, ORG classified as shockable

b) False positive, AS classified as shockable

c) False negative, VF classified as nonshockable

d) False negative, VF classified as nonshockable

1 sec
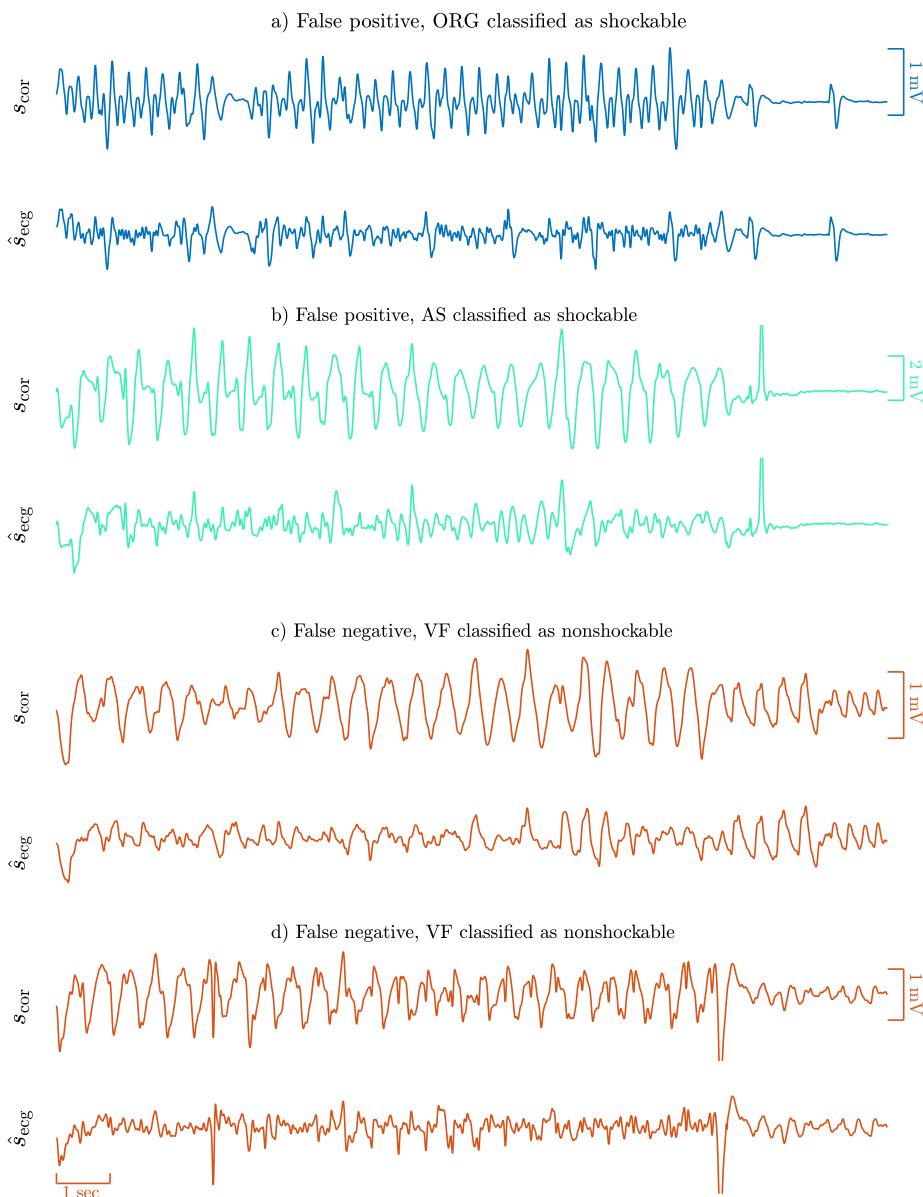
Figure 7. Examples of classification errors. The false positive examples (**a**,**b**) correspond to nonshockable rhythms classified as shockable (ORG panel a and AS panel b). The false negative examples (**c**,**d**) are shockable rhythms classified as nonshockable, and are shown in orange.

5. Discussion

This is, to the best of our knowledge, the first study that uses deep neural network models to discriminate between shockable and nonshockable rhythms during CPR. This algorithm consists of an adaptive RLS filter to remove CPR artifacts followed by a CNN to classify the filtered ECG. The algorithm designed for 9 s improves the performance of the classical machine learning algorithms by 0.6 points in BAC and Acc. This improvement is large considering that the best classical machine learning algorithms had accuracies over 95% and that they are based on more than 20 years of expert

knowledge on ECG feature engineering. Moreover, mixed solutions, obtained by either stacking classifiers or mixing handcrafted and CNN features, could yield further improvements in BAC and Acc, as shown by the preliminary experiments of Section 4.5.

One of the advantages of deep learning solutions is the capacity of the algorithms to learn discriminating features exploiting all information hidden in the ECG. This avoids the time-consuming feature extraction processes and, most importantly, improves the quality of the extracted features. The latter is well reflected by the AUCs on Table 2. Four of the ten features extracted by the deep learning architecture show a higher discrimination capacity than SampEn(d_3), which is the best handcrafted feature for shock/no-shock decisions during CPR in the available literature [25,26].

Two factors were key to improve the performance of the CNN based methods from the preliminary results communicated previously in [53]. First, the design and optimization of the parameters of the CNN to obtain a better model for classification. Second, increasing the size of the database by adding 1186 new annotated samples (a 55% increase in dataset size). These led to 0.5-points and 0.3-points increases in BAC and Acc respectively, of which 0.4-points and 0.1-points are attributable to the larger dataset. And there is further room for improvement from combining the knowledge gained from deep learning and handcrafted ECG feature extraction, basic examples are shown in Table 3 which added an extra 0.5-points in Acc. The performance of deep learning solutions improves as they are exposed to more data, whereas the accuracy of classical machine learning algorithms stagnate past a given sample size. The model presented in this study overfits when more than 3 CNN blocks are used (Figure 4) since from then on the number of trainable parameters is too large for the size of the available dataset. Adding more data would help to develop deeper networks and thus to the extraction of more sophisticated features. There is therefore room to improve the deep learning models for rhythm analysis during CPR, as more and more data is recorded every day and made available in centralized repositories. In research on OHCA, the Resuscitation Outcome Consortium (ROC) network provides the largest OHCA data repository, which includes recordings of eleven regional clinical centers. However, labeled OHCA data are scarce, and obtaining quality controlled rhythm annotations from clinicians is expensive and time consuming. As an alternative, semi-supervised learning could be an efficient way to augment training data and obtain better deep learning models in the future.

As Figure 6 shows, CNN features provide more separate clusters than the handcrafted features for the shock/no-shock classes. Moreover, the deep learning model shows a quite high separability between the features corresponding to AS, OR and shockable rhythms. Therefore, in the future CNN models could improve the accuracy of classical machine learning-based multiclass rhythm classifiers. These classifiers have been demonstrated for clean [24,52] and artifacted ECGs [25], and are multilabel classification algorithms that classify the ECG into the 5 OHCA rhythm types. These algorithms are important for research to analyze large sets of OHCA data [24], and could also help clinicians during OHCA treatment as clinical support tools. The best OHCA multiclass algorithms have unweighted mean sensitivities of 78% for clean ECG [24], and of 72% if the analysis is done during CPR [25]. There is therefore margin for improvement using methods based on deep learning if sufficiently large quality controlled annotated datasets become available.

6. Conclusions

This paper introduces the first shock/no-shock decision algorithm during CPR based on deep learning methods. This solution improves the accuracy of the best classical machine learning models based on handcrafted features, and is able to give a shock/no-shock diagnosis compliant with AHA recommendations for shockable and nonshockable rhythms. Moreover, deep learning algorithms have room for improvement if larger annotated datasets become available allowing the design of deeper networks. This may lead to the first practical solutions for rhythm analysis during CPR, eliminating the no-flow intervals for rhythm analysis and contributing to improve OHCA survival rates.

Author Contributions: Conceptualization, J.K.-J., L.W., I.I., U.I., E.A. and T.E.; methodology, I.I. and U.I; software, I.I.; validation, U.I.; formal analysis, I.I. and U.I.; investigation, I.I., U.I., E.A., T.E., J.K.-J. and L.W.; resources, J.K.-J. and L.W.; data curation, U.I., E.A., T.E. and I.I.; writing—original draft preparation, I.I. and U.I.; writing–review and editing, I.I., U.I., E.A., T.E., J.K.-J. and L.W.; visualization, I.I. and U.I.; supervision, U.I. and E.A.; project administration, U.I. and E.A.; funding acquisition, U.I. and E.A. All authors have read and agreed to the published version of the manuscript.

Conflicts of Interest: The authors declare no conflict of interest.

Abbreviations

The following abbreviations are used in this manuscript:

CPR	cardiopulmonary resuscitation
CNN	convolutional neural network
RLS	recursive least squares
OHCA	out of hospital cardiac arrest
ECG	electrocardiogram
VF	ventricular fibrillation
VT	ventricular tachycardia
ORG	organized
AS	asystole
AHA	American Heart Association
CD	compression depth
TI	thoracic impedance
LMS	least mean squares
SVM	support vector machine
RF	random forest
SWT	stationary wavelet transform
TP	true positive
TN	true negative
FP	false positive
FN	false negative
Se	sensitivity
Sp	specificity
Acc	accuracy
BAC	balanced accuracy
PPV	positive predictive value
NPV	negative predictive value
SNR	signal-to-noise ratio
t-SNE	t-distributed stochastic neighbour embedding
DBi	Davies-Bouldin index
AUC	area under the receiver characteristics curve
ROC	Resuscitaion Outcome Consortium

References

1. Berdowski, J.; Berg, R.A.; Tijssen, J.G.; Koster, R.W. Global incidences of out-of-hospital cardiac arrest and survival rates: Systematic review of 67 prospective studies. *Resuscitation* **2010**, *81*, 1479–1487. [CrossRef] [PubMed]

2. Daya, M.R.; Schmicker, R.H.; Zive, D.M.; Rea, T.D.; Nichol, G.; Buick, J.E.; Brooks, S.; Christenson, J.; MacPhee, R.; Craig, A.; et al. Out-of-hospital cardiac arrest survival improving over time: Results from the Resuscitation Outcomes Consortium (ROC). *Resuscitation* **2015**, *91*, 108–115. [CrossRef] [PubMed]

3.   Perkins, G.; Handley, A.; Koster, R.; Castrén, M.; Smyth, M.; Olasveengen, T.; Monsieurs, K.; Raffay, V.; Gärsner, J.; Wenzel, V.; et al. European Resuscitation Council Guidelines for Resuscitation 2015: Section 2. Adult basic life support and automated external defibrillation. *Resuscitation* **2015**, *95*, 81–99. [CrossRef]

4.   Takata, T.S.; Page, R.L.; Joglar, J.A. Automated external defibrillators: Technical considerations and clinical promise. *Ann. Intern. Med.* **2001**, *135*, 990–998. [CrossRef] [PubMed]

5.   Kerber, R.E.; Becker, L.B.; Bourland, J.D.; Cummins, R.O.; Hallstrom, A.P.; Michos, M.B.; Nichol, G.; Ornato, J.P.; Thies, W.H.; White, R.D.; et al. Automatic external defibrillators for public access defibrillation: Recommendations for specifying and reporting arrhythmia analysis algorithm performance, incorporating new waveforms, and enhancing safety: A statement for health professionals from the American Heart Association Task Force on Automatic External Defibrillation, Subcommittee on AED Safety and Efficacy. *Circulation* **1997**, *95*, 1677–1682.

6.   Snyder, D.; Morgan, C. Wide variation in cardiopulmonary resuscitation interruption intervals among commercially available automated external defibrillators may affect survival despite high defibrillation efficacy. *Crit. Care Med.* **2004**, *32*, S421–S424. [CrossRef]

7.   Van Alem, A.P.; Sanou, B.T.; Koster, R.W. Interruption of cardiopulmonary resuscitation with the use of the automated external defibrillator in out-of-hospital cardiac arrest. *Ann. Emerg. Med.* **2003**, *42*, 449–457. [CrossRef]

8.   Li, Y.; Tang, W. Techniques for artefact filtering from chest compression corrupted ECG signals: Good, but not enough. *Resuscitation* **2009**, *80*, 1219–1220. [CrossRef]

9.   Sato, Y.; Weil, M.H.; Sun, S.; Tang, W.; Xie, J.; Noc, M.; Bisera, J. Adverse effects of interrupting precordial compression during cardiopulmonary resuscitation. *Crit. Care Med.* **1997**, *25*, 733–736. [CrossRef]

10.   Eftestøl, T.; Sunde, K.; Steen, P.A. Effects of interrupting precordial compressions on the calculated probability of defibrillation success during out-of-hospital cardiac arrest. *Circulation* **2002**, *105*, 2270–2273. [CrossRef]

11.   Edelson, D.P.; Abella, B.S.; Kramer-Johansen, J.; Wik, L.; Myklebust, H.; Barry, A.M.; Merchant, R.M.; Hoek, T.L.V.; Steen, P.A.; Becker, L.B. Effects of compression depth and pre-shock pauses predict defibrillation failure during cardiac arrest. *Resuscitation* **2006**, *71*, 137–145. [CrossRef] [PubMed]

12.   Ruiz de Gauna, S.; Irusta, U.; Ruiz, J.; Ayala, U.; Aramendi, E.; Eftestøl, T. Rhythm analysis during cardiopulmonary resuscitation: Past, present, and future. *BioMed Res. Int.* **2014**, *2014*. [CrossRef] [PubMed]

13.   Werther, T.; Klotz, A.; Granegger, M.; Baubin, M.; Feichtinger, H.G.; Amann, A.; Gilly, H. Strong corruption of electrocardiograms caused by cardiopulmonary resuscitation reduces efficiency of two-channel methods for removing motion artefacts in non-shockable rhythms. *Resuscitation* **2009**, *80*, 1301–1307. [CrossRef] [PubMed]

14.   Irusta, U.; Ruiz, J. An algorithm to discriminate supraventricular from ventricular tachycardia in automated external defibrillators valid for adult and paediatric patients. *Resuscitation* **2009**, *80*, 1229–1233. [CrossRef] [PubMed]

15.   Ayala, U.; Eftestøl, T.; Alonso, E.; Irusta, U.; Aramendi, E.; Wali, S.; Kramer-Johansen, J. Automatic detection of chest compressions for the assessment of CPR-quality parameters. *Resuscitation* **2014**, *85*, 957–963. [CrossRef]

16.   Aase, S.O.; Eftestol, T.; Husoy, J.; Sunde, K.; Steen, P.A. CPR artifact removal from human ECG using optimal multichannel filtering. *IEEE Trans. Biomed. Eng.* **2000**, *47*, 1440–1449. [CrossRef]

17.   Eilevstjønn, J.; Eftestøl, T.; Aase, S.O.; Myklebust, H.; Husøy, J.H.; Steen, P.A. Feasibility of shock advice analysis during CPR through removal of CPR artefacts from the human ECG. *Resuscitation* **2004**, *61*, 131–141. [CrossRef]

18.   Berger, R.D.; Palazzolo, J.; Halperin, H. Rhythm discrimination during uninterrupted CPR using motion artifact reduction system. *Resuscitation* **2007**, *75*, 145–152. [CrossRef]

19.   Irusta, U.; Ruiz, J.; de Gauna, S.R.; EftestØl, T.; Kramer-Johansen, J. A least mean-square filter for the estimation of the cardiopulmonary resuscitation artifact based on the frequency of the compressions. *IEEE Trans. Biomed. Eng.* **2009**, *56*, 1052–1062. [CrossRef]

20.   Rheinberger, K.; Steinberger, T.; Unterkofler, K.; Baubin, M.; Klotz, A.; Amann, A. Removal of CPR artifacts from the ventricular fibrillation ECG by adaptive regression on lagged reference signals. *IEEE Trans. Biomed. Eng.* **2007**, *55*, 130–137. [CrossRef]

21. Ruiz, J.; Irusta, U.; de Gauna, S.R.; Eftestøl, T. Cardiopulmonary resuscitation artefact suppression using a Kalman filter and the frequency of chest compressions as the reference signal. *Resuscitation* **2010**, *81*, 1087–1094. [CrossRef] [PubMed]

22. Ayala, U.; Irusta, U.; Ruiz, J.; Eftestøl, T.; Kramer-Johansen, J.; Alonso-Atienza, F.; Alonso, E.; González-Otero, D. A reliable method for rhythm analysis during cardiopulmonary resuscitation. *BioMed Res. Int.* **2014**, *2014*, 872470. [CrossRef] [PubMed]

23. Figuera, C.; Irusta, U.; Morgado, E.; Aramendi, E.; Ayala, U.; Wik, L.; Kramer-Johansen, J.; Eftestøl, T.; Alonso-Atienza, F. Machine learning techniques for the detection of shockable rhythms in automated external defibrillators. *PLOS ONE* **2016**, *11*, e0159654. [CrossRef] [PubMed]

24. Rad, A.B.; Eftestøl, T.; Engan, K.; Irusta, U.; Kvaløy, J.T.; Kramer-Johansen, J.; Wik, L.; Katsaggelos, A.K. ECG-based classification of resuscitation cardiac rhythms for retrospective data analysis. *IEEE Trans. Biomed. Eng.* **2017**, *64*, 2411–2418. [CrossRef] [PubMed]

25. Isasi, I.; Irusta, U.; Rad, A.B.; Aramendi, E.; Zabihi, M.; Eftestøl, T.; Kramer-Johansen, J.; Wik, L. Automatic Cardiac Rhythm Classification With Concurrent Manual Chest Compressions. *IEEE Access* **2019**, *7*, 115147–115159. [CrossRef]

26. Isasi, I.; Irusta, U.; Elola, A.; Aramendi, E.; Ayala, U.; Alonso, E.; Kramer-Johansen, J.; Eftestøl, T. A machine learning shock decision algorithm for use during piston-driven chest compressions. *IEEE Trans. Biomed. Eng.* **2018**, *66*, 1752–1760. [CrossRef]

27. Rim, B.; Sung, N.J.; Min, S.; Hong, M. Deep Learning in Physiological Signal Data: A Survey. *Sensors* **2020**, *20*, 969. [CrossRef]

28. Hong, S.; Zhou, Y.; Shang, J.; Xiao, C.; Sun, J. Opportunities and Challenges in Deep Learning Methods on Electrocardiogram Data: A Systematic Review. *arXiv* **2019**, arXiv:2001.01550.

29. Kiranyaz, S.; Ince, T.; Gabbouj, M. Real-time patient-specific ECG classification by 1-D convolutional neural networks. *IEEE Trans. Biomed. Eng.* **2015**, *63*, 664–675. [CrossRef]

30. Acharya, U.R.; Fujita, H.; Lih, O.S.; Hagiwara, Y.; Tan, J.H.; Adam, M. Automated detection of arrhythmias using different intervals of tachycardia ECG segments with convolutional neural network. *Inf. Sci.* **2017**, *405*, 81–90. [CrossRef]

31. Al Rahhal, M.M.; Bazi, Y.; Al Zuair, M.; Othman, E.; BenJdira, B. Convolutional neural networks for electrocardiogram classification. *J. Med. Biol. Eng.* **2018**, *38*, 1014–1025.

32. Xia, Y.; Wulan, N.; Wang, K.; Zhang, H. Detecting atrial fibrillation by deep convolutional neural networks. *Comput. Biol. Med.* **2018**, *93*, 84–92. [CrossRef] [PubMed]

33. Hannun, A.Y.; Rajpurkar, P.; Haghpanahi, M.; Tison, G.H.; Bourn, C.; Turakhia, M.P.; Ng, A.Y. Cardiologist-level arrhythmia detection and classification in ambulatory electrocardiograms using a deep neural network. *Nat. Med.* **2019**, *25*, 65. [CrossRef] [PubMed]

34. Pourbabaee, B.; Roshtkhari, M.J.; Khorasani, K. Deep convolutional neural networks and learning ECG features for screening paroxysmal atrial fibrillation patients. *IEEE Trans. Syst. Man. Cybern. Syst.* **2018**, *48*, 2095–2104. [CrossRef]

35. Andreotti, F.; Carr, O.; Pimentel, M.A.; Mahdi, A.; De Vos, M. Comparing feature-based classifiers and convolutional neural networks to detect arrhythmia from short segments of ECG. In Proceedings of the 2017 Computing in Cardiology (CinC), Rennes, France, 24–27 September 2017; pp. 1–4.

36. Picon, A.; Irusta, U.; Álvarez-Gila, A.; Aramendi, E.; Alonso-Atienza, F.; Figuera, C.; Ayala, U.; Garrote, E.; Wik, L.; Kramer-Johansen, J.; et al. Mixed convolutional and long short-term memory network for the detection of lethal ventricular arrhythmia. *PLoS ONE* **2019**, *14*, e0216756. [CrossRef]

37. Elola, A.; Aramendi, E.; Irusta, U.; Picón, A.; Alonso, E.; Owens, P.; Idris, A. Deep neural networks for ECG-based pulse detection during out-of-hospital cardiac arrest. *Entropy* **2019**, *21*, 305. [CrossRef]

38. Wik, L.; Kramer-Johansen, J.; Myklebust, H.; Sørebø, H.; Svensson, L.; Fellows, B.; Steen, P.A. Quality of cardiopulmonary resuscitation during out-of-hospital cardiac arrest. *JAMA* **2005**, *293*, 299–304. [CrossRef]

39. Isasi, I.; Irusta, U.; Aramendi, E.; Ayala, U.; Alonso, E.; Kramer-Johansen, J.; Eftestøl, T. A multistage algorithm for ECG rhythm analysis during piston-driven mechanical chest compressions. *IEEE Trans. Biomed. Eng.* **2018**, *66*, 263–272. [CrossRef]

40. Xiao, Y.; Ma, L.; Ward, R.K. Fast RLS Fourier analyzers capable of accommodating frequency mismatch. *Signal Process.* **2007**, *87*, 2197–2212. [CrossRef]

41. Atkins, D.L.; Scott, W.A.; Blaufox, A.D.; Law, I.H.; Dick II, M.; Geheb, F.; Sobh, J.; Brewer, J.E. Sensitivity and specificity of an automated external defibrillator algorithm designed for pediatric patients. *Resuscitation* **2008**, *76*, 168–174.

42. Kwok, H.; Coult, J.; Drton, M.; Rea, T.D.; Sherman, L. Adaptive rhythm sequencing: A method for dynamic rhythm classification during CPR. *Resuscitation* **2015**, *91*, 26–31. [CrossRef] [PubMed]

43. Srivastava, N.; Hinton, G.; Krizhevsky, A.; Sutskever, I.; Salakhutdinov, R. Dropout: A simple way to prevent neural networks from overfitting. *J. Mach. Learn. Res.* **2014**, *15*, 1929–1958.

44. Sutskever, I.; Martens, J.; Dahl, G.; Hinton, G. On the importance of initialization and momentum in deep learning. In Proceedings of the International conference on machine learning, Atlanta, GA, USA, 16–21 June 2013; pp. 1139–1147.

45. Kuo, S. Computer detection of ventricular fibrillation. *Proc. Comput. Cardiol. IEEE Comupt. Soc.* **1978**, 347–349.

46. Gonzalez, L.; Walker, K.; Challa, S.; Bent, B. Monitoring a skipped heartbeat: A real-time premature ventricular contraction (pvc) monitor. In Proceedings of the 2016 IEEE Virtual Conference on Applications of Commercial Sensors (VCACS), Raleigh, NC, USA, 15 June 2016–15 January 2017; pp. 1–7.

47. Langhelle, A.; Eftestøl, T.; Myklebust, H.; Eriksen, M.; Holten, B.T.; Steen, P.A. Reducing CPR artefacts in ventricular fibrillation in vitro. *Resuscitation* **2001**, *48*, 279–291. [CrossRef]

48. Fitzgibbon, E.; Berger, R.; Tsitlik, J.; Halperin, H.R. Determination of the noise source in the electrocardiogram during cardiopulmonary resuscitation. *Crit. Care Med.* **2002**, *30*, S148–S153.

49. Maaten, L.v.d.; Hinton, G. Visualizing data using t-SNE. *J. Mach. Learn. Res.* **2008**, *9*, 2579–2605.

50. Davies, D. DW 1979. A Cluster Separation Measure. *IEEE Trans. Pattern Anal. Mach. Intell.* **1979**, *PAMI-1*, 224–227.

51. Vesanto, J.; Himberg, J.; Alhoniemi, E.; Parhankangas, J. SOM toolbox for Matlab 5. *Hels. Univ. Technol.* **2000**, *216*, 57.

52. Rad, A.B.; Eftestøl, T.; Irusta, U.; Kvaløy, J.T.; Wik, L.; Kramer-Johansen, J.; Katsaggelos, A.K.; Engan, K. An automatic system for the comprehensive retrospective analysis of cardiac rhythms in resuscitation episodes. *Resuscitation* **2018**, *122*, 6–12.

53. Isasi Liñero, I.; López de Larruzea, L.; Irusta Zarandona, U.; Aramendi Ecenarro, E. Diagnóstico del ritmo cardíaco durante la resucitación cardiopulmonar mediante técnicas de aprendizaje profundo. *Actas del XXXVII Congreso Anual de la Sociedad Española de Ingeniería Biomédica* **2019**, *37*, 37–40.

A.4   PUBLICATIONS ASSOCIATED TO OBJECTIVE 4

A.4.1   JOURNAL PAPER: J1$_4$

Table A.9.   Journal paper associated to objective 4.

Publication in international magazine
Reference I. Isasi, U. Irusta, E. Aramendi, A.h. Idris and L. Sörnmo,"Restoration of the electrocardiogram during mechanical cardiopulmonary resuscitation", *Physiological Measurement*, 2020.
Quality indices   **Type of publication:** Journal paper idexed in JCR and SJR   **Area:** Biomedical Engineering   **Ranking:** 49/87 (Q3) based on JCR 2019   **Impact factor SJR:** 0.702   **Impact factor JCR:** 2.309

Restoration of the electrocardiogram during mechanical cardiopulmonary resuscitation

Iraia Isasi[1], Unai Irusta[1], Elisabete Aramendi[1], Ahamed H. Idris[2], Leif Sörnmo[3]

[1]Department of Communications Engineering, University of the Basque Country UPV/EHU, Bilbao, Spain
[2]University of Texas Southwestern Medical Center, Dallas, Texas, USA
[3]Department of Biomedical Engineering and Center of Integrative Electrocardiology, Lund University, Lund, Sweden

E-mail: `iraia.isasi@ehu.eus`

Abstract.
Objective: An artefact-free electrocardiogram (ECG) is essential during cardiac arrest to decide therapy such as defibrillation. Mechanical cardiopulmonary resuscitation (CPR) devices cause movement artefacts that alter the ECG. This study analyzes the effectiveness of mechanical CPR artefact suppression filters to restore clinically relevant ECG information.
Approach: In total, 495 10-s ECGs were used, of which 165 were in ventricular fibrillation (VF), 165 in organized rhythms (OR) and 165 contained mechanical CPR artefacts recorded during asystole. CPR artefacts and rhythms were mixed at controlled signal-to-noise ratios (SNRs), ranging from –20 dB to 10 dB. Mechanical artefacts were removed using least mean squares (LMS), recursive least squares (RLS) and Kalman filters. Performance was evaluated by comparing the clean and the restored ECGs in terms of restored SNR, correlation-based similarity measures, and clinically relevant features: QRS detection performance for OR, and dominant frequency, mean amplitude and waveform irregularity for VF. For each filter, a shock/no-shock support vector machine algorithm based on multiresolution analysis of the restored ECG was designed, and evaluated in terms of sensitivity (Se) and specificity (Sp).
Main results: The RLS filter produced the largest correlation coefficient (0.80), the largest average increase in SNR (9.5 dB), and the best QRS detection performance. The LMS filter best restored VF with errors of 10.3% in dominant frequency, 18.1% in amplitude and 11.8% in waveform irregularity. The Se/Sp of the diagnosis of the restored ECG were 95.1/94.5% using the RLS filter and 97.0/91.4% using the LMS filter.
Significance: Suitable filter configurations to restore ECG waveforms during mechanical CPR have been determined, allowing reliable clinical decisions without interrupting mechanical CPR therapy.

1. Introduction

Out-of-hospital cardiac arrest (OHCA) is a major public health problem claiming over 50 lives per 100 000 persons each year [1]. The latest guidelines from the European Resuscitation Council and the American Heart Association (AHA) identify early defibrillation and high quality cardiopulmonary resuscitation (CPR) as key therapies [2]. In particular, uninterrupted chest compressions, provided either by rescuers or through mechanical devices, are of critical importance [3]. Whereas basic life support responders rely on the defibrillator's automated analysis of the ECG for a shock/no-shock decision, advanced life support (ALS) clinicians visually evaluate the ECG to decide suitable therapeutic interventions. In both cases, chest compressions must be stopped to avoid the confounding effects of CPR artefacts on the ECG. However, such CPR interruptions produce no-flow periods that deteriorate the circulatory state of the patient, reducing the probability of successful defibrillation and subsequent survival [3].

Several adaptive filters have been designed to remove chest compression artefacts during manual CPR so that the ECG is restored [4, 5]. The first solutions used reference signals such as compression depth [6, 7], thoracic impedance [6, 7], compression force [8] or blood pressure [9] to model CPR artefacts. The artefacts were estimated using Wiener filters [7], recursive adaptive matching pursuit algorithms [10], Kalman filters [11], recursive least squares (RLS) [8] and Gabor filters [9], among others. The filters became considerably simplified with the introduction of a quasi-periodic CPR artefact model in which the time-varying Fourier coefficients were estimated using LMS, RLS or Kalman filters [12–14]. In this model, an estimate of the instantaneous chest compression frequency during manual CPR is required, which must be estimated from additional reference channels like depth [12], force [15] and impedance [16]. At present, mechanical CPR devices are increasingly used in resuscitation by ALS clinicians [2, 17, 18]. Such devices deliver chest compressions at a fixed rate and depth and, consequently, no reference channels are needed for adaptive filters based on the Fourier-series model [19, 20].

The preferred approach to evaluating filter performance in terms of ECG waveform restoration is to analyze artificial mixtures of artefact-free ECGs recorded during OHCA and CPR artefacts obtained in the absence of electrical activity of the heart (asystole) [6, 7]. Mixtures are formed at different signal-to-noise-ratios (SNRs), so that the clean ECG and the restored ECG (obtained by filtering) can be compared in terms of performance measures such as the restored SNR [11], or the diagnostic accuracy of an automated shock/no-shock decision algorithm [8]. In the latter case, performance is reported in terms of sensitivity (Se) and specificity (Sp), the proportion of correctly classified shockable and non-shockable rhythms, respectively [14]. Studies based on artificial mixtures, using ECGs recorded during OHCA, have only been conducted during manual CPR, however, little is known on which filter configurations offer good restoration of the ECG waveforms. Moreover, the mixture model is well-suited for evaluating ECG waveform restoration in relation to other diagnostic OHCA scenarios

such as the prediction of defibrillation success [21], the detection of pulse [22] and the prediction of re-arrest [23]. The effect of filtering on ECG restoration for those scenarios has not been yet thoroughly studied.

This study addresses the above-mentioned knowledge gaps by using a mixture model to evaluate the performance of adaptive filters during mechanical CPR in terms of ECG waveform restoration, clinically relevant ECG characteristics and shock/no-shock diagnostic accuracy. The manuscript is organized as follows: Section II describes the study dataset; Section III explains the mixture model, describes the adaptive filters and proposes novel performance measures for filter evaluation; the results, discussion and conclusions are presented in Sections IV and V.

2. Materials

The data were collected by the Dallas-Fort Worth Center for Resuscitation Research between 2012 and 2016, as part of the Resuscitation Outcomes Consortium. A cohort of 393 anonymized OHCA patient data files recorded by the MRx monitor–defibrillator (Philips Medical Systems, Andover, MA, USA) during treatment were used. CPR was administered manually or with the LUCAS-2 (Physio-Control Inc/Jolife AB, Lund, Sweden) piston-driven mechanical CPR device. The LUCAS-2 delivers chest compressions at a fixed rate of $100\,\text{min}^{-1}$ with a fixed depth of 5 cm. The MRx acquires the ECG with a resolution of $1.03\,\mu\text{V}$ per least significant bit, a bandwidth defined by $0\,\text{Hz}$ and $50\,\text{Hz}$, and a sampling frequency of 250 Hz. The ECG and the available signals to monitor chest compression activity (compression depth and impedance) were converted to Matlab (MathWorks Inc, Natick, MA, USA). Chest compressions were automatically detected using standard algorithms on the compression depth or impedance channels [15].

Signal segments of 10-s duration were extracted from the patient files to form mixtures of clean ECG and mechanical CPR artefacts during asystole. Thus, all ECGs (rhythms and CPR artefacts) come from real OHCA data recorded during treatment. The clean ECG segments were extracted in intervals with confirmed absence of chest compressions, and included 165 segments from 96 patients during shockable ventricular fibrillation (VF) and 165 segments from 165 patients in non-shockable organized rhythms (ORs). CPR artefact segments during asystole were obtained during confirmed use of LUCAS-2, indicated by a fix compression rate of $100\,\text{min}^{-1}$ without variability. Asystole was confirmed during pauses in chest compressions whenever the clean ECG had a peak-to-peak amplitude below $100\,\mu\text{V}$ [24]. A total of 165 CPR artefacts from 149 patients were used.

All segments (VF, OR and CPR artefacts) were band-pass filtered between $0.5-40\,\text{Hz}$ to remove baseline wander and high frequency noise. A Hampel filter was used to remove spiky artefacts.

3. Methods

Figure 1 summarizes the procedure followed to evaluate the performance of the adaptive filters. First, using a mixture model, noisy ECGs are formed at controlled SNRs. Then, using different filter types and filter parameter settings, the ECGs are restored. Finally, performance is evaluated in terms of measures quantifying the similarity between the clean and the restored ECG, clinically relevant ECG waveform characteristics and accuracy of shock/no-shock decision.
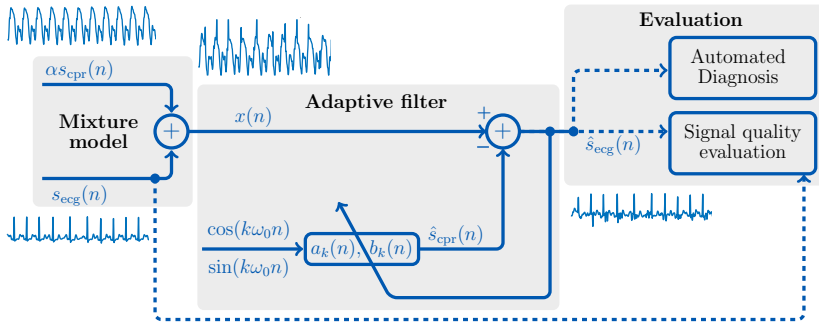
Figure 1. General architecture for CPR artefact removal and evaluation of the quality of the restored ECG, $\hat{s}_{\text{ecg}}(n)$.

3.1. Mixture model with controlled SNR

The noisy ECG signal, $x(n)$, is the mixture of a clean ECG signal, $s_{\text{ecg}}(n)$, and a signal with CPR artefacts, $s_{\text{cpr}}(n)$, recorded during asystole [6, 7]:

$$x(n) = s_{\text{ecg}}(n) + \alpha s_{\text{cpr}}(n). \tag{1}$$

The SNR of $x(n)$ is controlled by the positive-valued weight α [6]:

$$\text{SNR}_{\text{in}} = 10 \cdot \log_{10}\left(\frac{P_{\text{ecg}}}{\alpha^2 P_{\text{cpr}}}\right) \quad \text{(dB)}, \tag{2}$$

where P_{ecg} and P_{cpr} denote the power of $s_{\text{ecg}}(n)$ and $s_{\text{cpr}}(n)$, respectively, which for a segment of L samples are:

$$P_{\text{ecg}} = \frac{1}{L}\sum_{n=1}^{L}|s_{\text{ecg}}(n)|^2 \quad P_{\text{cpr}} = \frac{1}{L}\sum_{n=1}^{L}|s_{\text{cpr}}(n)|^2 \tag{3}$$

The subscript "in" indicates that the SNR applies to the filter input signal $x(n)$. In terms of signal power and SNR_{in}, α is given by

$$\alpha = \sqrt{\frac{P_{\text{ecg}}}{P_{\text{cpr}}} \cdot 10^{-\frac{\text{SNR}_{\text{in}}}{10}}}. \tag{4}$$

Seven different SNR_{in} are tested, ranging from very low ($-20\,\text{dB}$) to high ($10\,\text{dB}$) in steps of $5\,\text{dB}$. For each filter setting, a total of $330 \cdot 165 \cdot 7 = 3.8 \cdot 10^5$ combinations are evaluated, together forming a comprehensive selection of ECGs, CPR artefacts and SNR_{in}. Figure 2 shows an example of $x(n)$ formed using OR and VF rhythms mixed with a CPR artefact at different SNR_{in}.
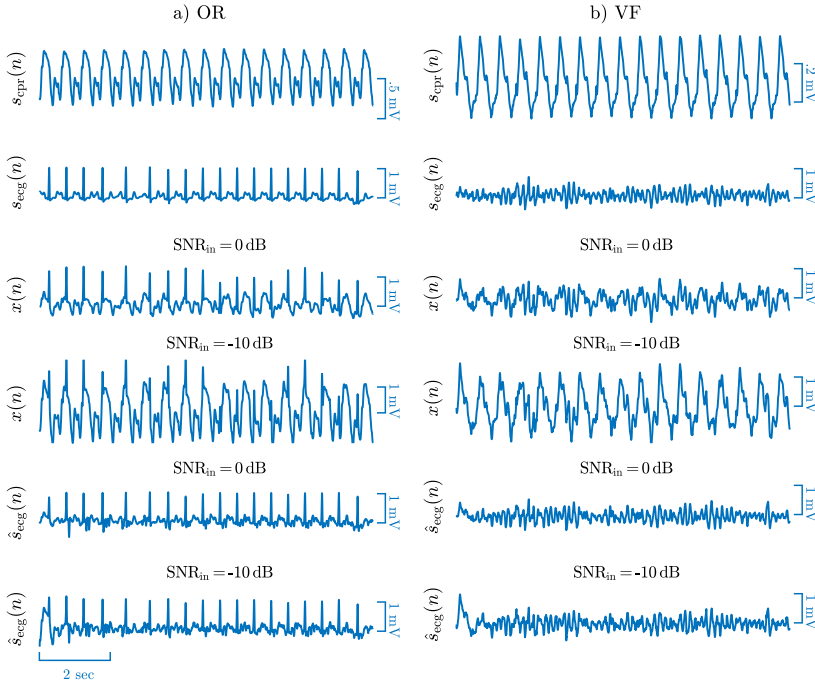
Figure 2. Examples of CPR artefact removal in ECGs with OR (a) and VF (b), using RLS filtering. CPR artefacts (panel 1), clean OR and VF signals (panel 2), mixed signals at SNR_{in} of $0\,\text{dB}$ (panel 3) and $-10\,\text{dB}$ (panel 4) and restored ECGs obtained at 0 dB (panel 5) and $-10\,\text{dB}$ (panel 6).

3.2. Adaptive filters

During mechanical CPR, the chest compression frequency is constant. The LUCAS-2 device delivers compressions at $F_0 = 1.67\,\text{Hz} \equiv 100\,\text{min}^{-1}$, which, for a sampling period of T_{s}, corresponds to a discrete angular frequency of $\omega_0 = 2\pi F_0 T_{\text{s}}$. Under this condition, the CPR artefact can be modeled as a truncated N-term Fourier series with slowly varying amplitude [25, 26]:

$$s_{\mathrm{cpr}}(n) = \sum_{k=1}^{N} c_k(n) \cos(k\omega_0 n + \theta_k(n)) \tag{5}$$

$$= \sum_{k=1}^{N} \big(a_k(n) \cos(k\omega_0 n) + b_k(n) \sin(k\omega_0 n)\big). \tag{6}$$

The Fourier coefficients, $a_k(n)$ and $b_k(n)$, define the adaptive filter that adjust to the time-varying characteristics of the artefact [26]. The restored ECG is obtained by subtracting the model estimate $\hat{s}_{\mathrm{cpr}}(n)$ from the observed signal $x(n)$.

$$\hat{s}_{\mathrm{ecg}}(n) = x(n) - \hat{s}_{\mathrm{cpr}}(n). \tag{7}$$

The LMS, RLS and Kalman filters are explored for estimating $a_k(n)$ and $b_k(n)$. All filter types employ criteria to minimize the error between $x(n)$ and $\hat{s}_{\mathrm{cpr}}(n)$. A detailed description of the filters can be found in [25–28]. Briefly, the LMS filter updates its coefficients at each time n using increments proportional to the squared error and the step-size μ [12]. The RLS filter extends the observation window of the squared error by means of an exponential forgetting factor, λ [13]. The Kalman filter is based on a state-variable model in which the variance of the observation noise, q, controls the adjustment rate of the coefficients [14]. These three parameters control the coarseness of the respective filters. A large forgetting factor (λ), a small step size (μ) and a small noise variance (q) mean lower misadjustment and better filter stability, but reduced tracking capabilities ("fine filtering"). The reverse choice of parameter values means better tracking, but higher misadjustment and poorer stability ("coarse filtering").

In this study, three different settings of the filter parameters μ, λ and q are tested to evaluate the effect of fine, moderate and coarse filtering [14, 26], namely $\lambda = \{0.9999, 0.995, 0.99\}$, $\mu = \{15 \cdot 10^{-4}, 4 \cdot 10^{-3}, 8 \cdot 10^{-3}\}$ and $q = \{5 \cdot 10^{-6}, 1 \cdot 10^{-5}, 5 \cdot 10^{-5}\}$ [14,20,25,26]. For all cases, a model with $N = 20$ harmonics was used [26] meaning that the filters are composed of $2N$ coefficients since each harmonic is defined by a pair of coefficients (a_k, b_k). Figure 2 shows an example of $\hat{s}_{\mathrm{ecg}}(n)$, obtained after removing CPR artefacts from $x(n)$, formed at $0\,\mathrm{dB}$ and at $10\,\mathrm{dB}$ with VF and OR as underlying rhythms.

3.3. Evaluation of filter performance

The performance is evaluated in two ways: First, by comparing $s_{\mathrm{ecg}}(n)$ and $\hat{s}_{\mathrm{ecg}}(n)$ using similarity measures, and by studying the effect of filtering on clinically relevant ECG waveform characteristics. Second, by building a machine learning shock advice algorithm to classify $\hat{s}_{\mathrm{ecg}}(n)$ and thus to evaluate the accuracy of an automated diagnosis at different $\mathrm{SNR}_{\mathrm{in}}$. To avoid the influence of filter transients, performance measures are evaluated using the L samples in the interval [2.5, 9.5] s.

3.3.1. Restored signal quality measures: Three measures are computed, namely the SNR of the restored signal and two signal similarity measures. The restored SNR is defined by [6]:

$$\text{SNR}_{\text{res}} = 10 \cdot \log_{10} \left(\frac{P_{\text{ecg}}}{P_e} \right), \tag{8}$$

where P_{ecg} and P_e are the power of $s_{\text{ecg}}(n)$ and $e(n) = s_{\text{ecg}}(n) - \hat{s}_{\text{ecg}}(n)$, respectively.

Signal quality is quantified by Pearson's correlation coefficient (PCC) computed between $s_{\text{ecg}}(n)$ and $\hat{s}_{\text{ecg}}(n)$ (both signals assumed to be zero mean):

$$\text{PCC} = \frac{\sum_{n=1}^{L} s_{\text{ecg}}(n) \cdot \hat{s}_{\text{ecg}}(n)}{\sqrt{\sum_{n=1}^{L} s_{\text{ecg}}^2(n)} \cdot \sqrt{\sum_{n=1}^{L} \hat{s}_{\text{ecg}}^2(n)}}, \tag{9}$$

which is a standard measure of morphological signal similarity. Values close to ± 1 indicate similarity, while values around 0 indicate dissimilarity. PCC is invariant to differences in signal amplitude, being a disadvantage in our context because filtering affects signal amplitude. For instance, VF waveform amplitude conveys important information on the state of the myocardium during cardiac arrest [21].

The adaptive signed correlation index (ASCI) reflects the amplitude differences between two signals and is defined by [29]:

$$\text{ASCI} = \frac{1}{L} \sum_{n=1}^{L} s_{\text{ecg}}(n) \otimes \hat{s}_{\text{ecg}}(n), \tag{10}$$

where $\otimes$ denotes the signed product of two dichotomized values:

$$s_{\text{ecg}}(n) \otimes \hat{s}_{\text{ecg}}(n) \equiv \begin{cases} 1 & |s_{\text{ecg}}(n) - \hat{s}_{\text{ecg}}(n)| \leq \beta, \\ -1 & |s_{\text{ecg}}(n) - \hat{s}_{\text{ecg}}(n)| > \beta. \end{cases} \tag{11}$$

where the threshold β determines whether the samples at time n are similar. The threshold was set to 10% of the amplitude range of $s_{\text{ecg}}(n)$, as recommended in [30]. ASCI ranges from -1 (i.e. dissimilar signals) to 1 (i.e. similar signals). In this study, ASCI is then normalized to the interval [0,1] to make it comparable to PCC.

3.3.2. Characteristic parameters of OR and VF: The most distinctive characteristic of OR is the presence of QRS complexes. Accurate detection and characterization of QRS complexes are clinically important in cardiac arrest, for example, when detecting spontaneous pulse [31]. However, QRS detection in cardiac arrest is more challenging due to frequently occurring aberrant QRS morphologies [31]. In this study, we evaluate the performance of a wavelet-based QRS detector [32] on both $s_{\text{ecg}}(n)$ and $\hat{s}_{\text{ecg}}(n)$. As ground truth, all QRS complexes in the 165 clean ORs are manually annotated. Finally, the occurrence times are compared to those obtained from $\hat{s}_{\text{ecg}}(n)$ so that the probability of detection (P_D) and the probability of false alarm (P_F) can be estimated:

$$P_D(\%) = 100 \cdot \frac{N_{\text{TP}}}{N_{\text{TP}} + N_{\text{FN}}}, \tag{12}$$

$$P_F(\%) = 100 \cdot \frac{N_{\text{FP}}}{N_{\text{TP}} + N_{\text{FP}}}, \tag{13}$$

where N_{TP}, N_{FP} and N_{FN} denote the number of true positive, false positive and false negative detections, respectively.

Three characteristics of VF are studied: dominant frequency (DF) [33], amplitude [34] and waveform irregularity [21], previously used to predict defibrillation success [21, 35] and to detect VF in shock advice algorithms [13, 26, 36]. The DF is obtained by the location of the largest spectral peak higher than 1.5 Hz. The mean amplitude (MA) is obtained as the mean of $|\hat{s}_{\text{ecg}}(n)|$ [21, 33]. Waveform irregularity is characterized by the sample entropy (SampEn). For the generic parameter K, the absolute relative error, ϵ, is used to evaluate filter performance:

$$\epsilon_K = 100 \times \frac{|K - \hat{K}|}{|K|} \quad \% \tag{14}$$

where K is computed from $s_{\text{ecg}}(n)$ and its estimate $\hat{K}$ from $\hat{s}_{\text{ecg}}(n)$, respectively.

3.4. Accuracy of automated diagnosis

Filter performance is also evaluated in terms of Se for VF and Sp for OR of a shock advice algorithm designed to classify $\hat{s}_{\text{ecg}}(n)$, using a recently introduced machine learning approach for rhythm classification during mechanical CPR [26]. The algorithm is based on high-resolution feature extraction from $\hat{s}_{\text{ecg}}(n)$ using the stationary wavelet transform (SWT), a wrapper-based feature selection, and a radial basis function kernel support vector machine (SVM) classifier. Details on the method for feature extraction and feature selection can be found in [26].

Data is partitioned patient-wise and stratified into training (50%), validation (20%) and test (30%) sets. The training and validation sets are used to select the most discriminative subset of 6 features, and to optimize the hyperparameters of the SVM classifier. The features are standardized to zero mean and unit variance using the data in the training set. This resulted in a training set of M instance-labeled pairs $\{(\boldsymbol{x}_1, y_1), ..., (\boldsymbol{x}_M, y_M)\} \in \mathbb{R}^6 \times \{\pm 1\}$, where $\boldsymbol{x}_i$ is the feature vector and $y_i = 1$ and $y_i = -1$ are the associated shockable and non-shockable rhythm labels, respectively. The decision function of the SVM is found by solving the following maximization problem [37]:

$$W(\alpha) = \sum_{i=1}^{M} \alpha_i - \frac{1}{2} \sum_{i,j=1}^{M} \alpha_i \alpha_j y_i y_j \exp(-\gamma \|\boldsymbol{x}_i - \boldsymbol{x}_j\|^2) \tag{15}$$

subject to the constraints:

$$0 \le \alpha_i \le C \quad \forall i, \quad \text{and} \quad \sum_{i=1}^{M} \alpha_i y_i = 0, \tag{16}$$

where α_i are the Lagrange multipliers which are non-zero only for M_s support vectors, C is the soft margin parameter and γ the width of the Gaussian kernel. Once the support vectors are determined, the decision function is given by:

$$f(\boldsymbol{x}) = \text{sign}\left[\sum_{i=1}^{M_s} \alpha_i y_i \exp(-\gamma\|\boldsymbol{x} - \boldsymbol{x}_i\|^2) + b\right], \tag{17}$$

where the threshold b is determined in the optimization phase and $\boldsymbol{x}$ is the feature vector under evaluation. A rhythm is classified as shockable when $f(\boldsymbol{x}) = 1$ and nonshockable when $f(\boldsymbol{x}) = -1$. The hyperparameters C and γ are determined after feature selection in the training and validation sets, using a 18×18 logarithmic grid search within $10^{-1} \le C \le 10^2$ and $10^{-3} \le \gamma \le 10^1$ to maximize the balanced accuracy (BAC), i.e. the unweighted mean of Se and Sp.

Clean ECGs and CPR artefact segments were treated as two independent databases. Each database was partitioned patient-wise and stratified into training (50%), validation (20%) and test (30%) sets. This means that $\approx 0.5 \cdot 330$ clean ECGs (131 patients) and $\approx 0.5 \cdot 165$ CPR artefact segments (74 patients) were included in the training set. The validation set consisted of $\approx 0.2 \cdot 330$ (52 patients) and $\approx 0.2 \cdot 165$ (30 patients) clean ECGs and CPR artefact segments, respectively. Finally, in the test set $\approx 0.3 \cdot 330$ clean ECGs (78 patients) and $\approx 0.3 \cdot 165$ CPR artefact segments (45 patients) were included. Thus, for each filter setting, the training, validation and test sets consist of all possible combinations of CPR artefacts and clean ECGs, mixed at the SNR_{in} levels resulting in a training set of $\approx 0.5^2 \cdot 165 \cdot 330 \cdot 7$, a validation set of $\approx 0.2^2 \cdot 165 \cdot 330 \cdot 7$ and a test set of $\approx 0.3^2 \cdot 165 \cdot 330 \cdot 7$ signals. The performance on the test set is evaluated in terms of Se, Sp and BAC.

4. Results

4.1. Signal quality

Figure 3 shows the signal quality measures as a function of SNR_{in} for different filter settings. Figure 3a shows, as expected, that $\hat{s}_{\text{ecg}}(n)$ and $s_{\text{ecg}}(n)$ become increasingly similar as SNR_{in} increases. The RLS filter leads to higher PCC and ASCI for almost all SNR_{in} when fine filters are used. However, for the Kalman and LMS filters, coarse filtering leads to higher PCC and ASCI when the CPR artefact is large. In the LMS filter, moderate filtering achieves the highest PCC and ASCI for $\text{SNR}_{\text{in}} \le -10\,\text{dB}$, whereas coarse Kalman filtering gives the best results for $\text{SNR}_{\text{in}} \le -10\,\text{dB}$. Figure 3b shows that coarse filtering leads to higher SNR_{res} at low SNR_{in}. However, for a low SNR_{in}, fine filtering better restores the ECG. The effect of fine and coarse filtering at a high and a low SNR_{in} is exemplified in Figure 4.

a) Signal similarity measures
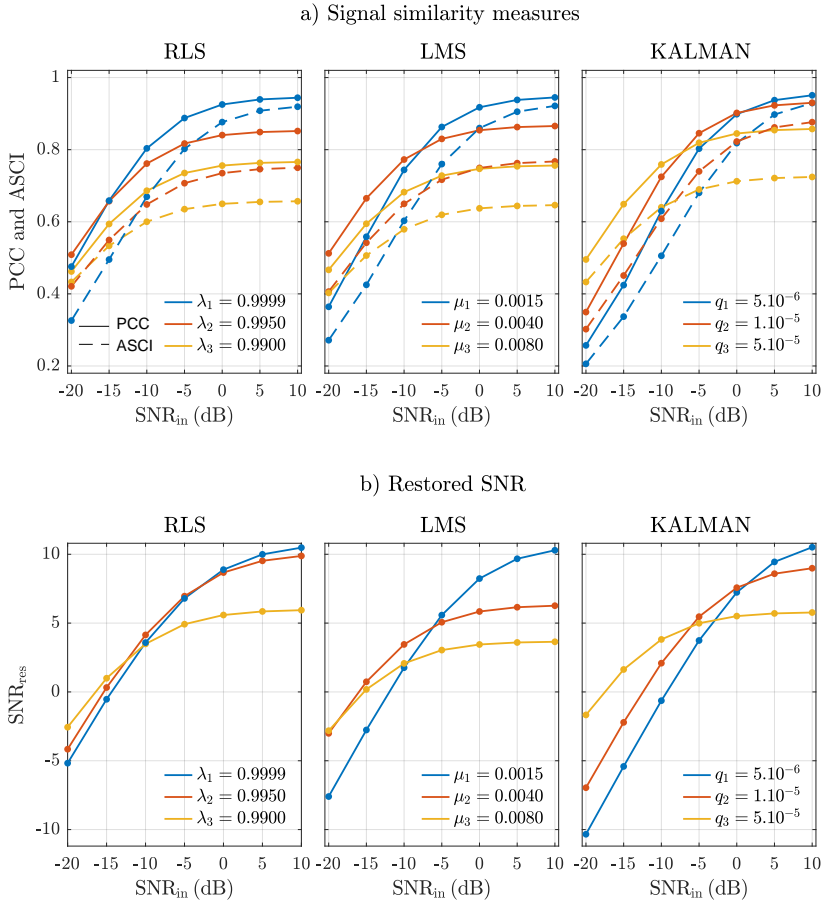

b) Restored SNR

Figure 3. The mean of PCC and ASCI (a) and SNR_{res} (b) for all possible mixing combinations as a function of SNR_{in} for different filter types and settings.

4.2. Waveform characteristics

The performance of the QRS detector on clean ECGs is $P_D = 95.9\%$ and $P_F = 1.9\%$, a result which serves as an upper bound for the results obtained when artefacts are added at different SNR_{in}. Figure 5 shows the QRS detection performance obtained on $\hat{s}_{ecg}(n)$. The best performance at high SNR_{in} is obtained for the Kalman filter, but the best overall performance is obtained for the RLS filter, with P_D exceeding 90% even for an SNR_{in} around -10 dB. As SNR_{in} decreases, P_F degrades considerably for any filter type and setting. For fine RLS filtering, P_F drops from around 10% for $SNR_{in} = 5$ dB to over 30% for $SNR_{in} = -10$ dB.

The effect of filtering on VF waveform characteristics is shown in Figure 6. The absolute relative errors of DF, MA and SampEn are large at low SNR_{in}, unless coarse
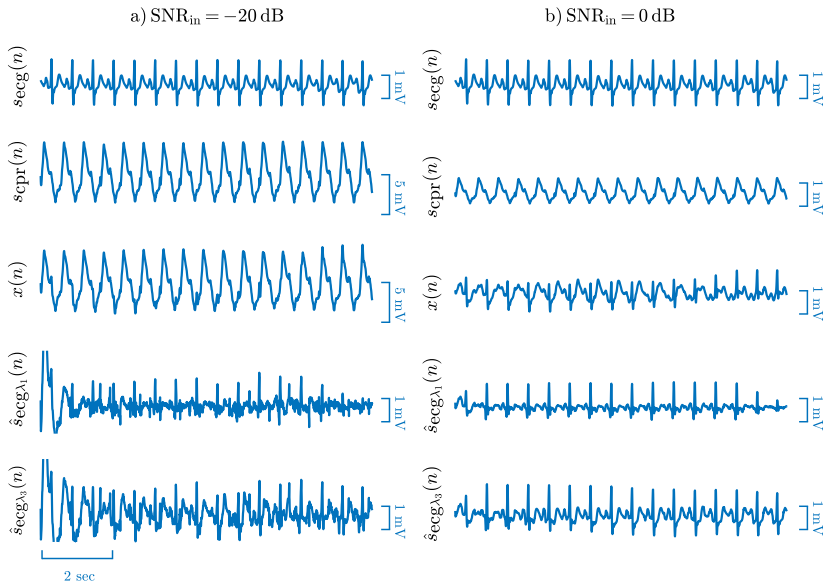
a) $\mathrm{SNR_{in}} = -20\,\mathrm{dB}$ b) $\mathrm{SNR_{in}} = 0\,\mathrm{dB}$

Figure 4. Two examples of RLS filtering of OR at $\mathrm{SNR_{in}} = -20\,\mathrm{dB}$ (a) and $0\,\mathrm{dB}$ (b). Coarse filtering ($\lambda_3 = 0.99$) attenuates QRS amplitude more than fine filtering ($\lambda_1 = 0.9999$) which, on the other hand, produces a larger residual between QRS complexes.
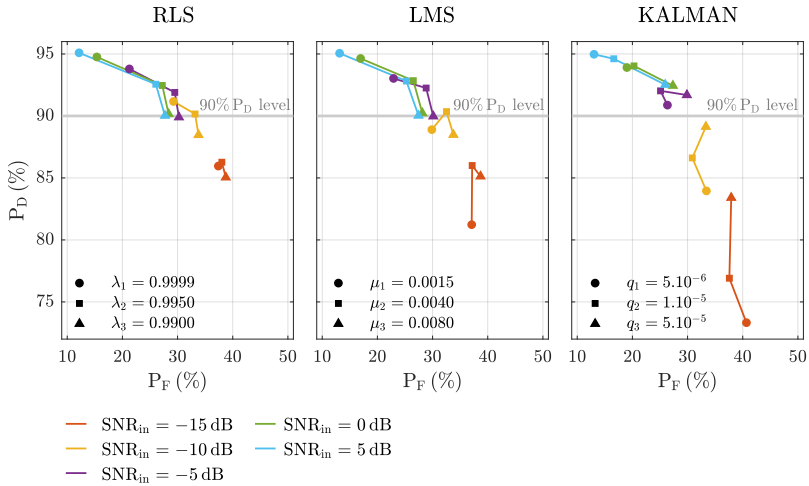
Figure 5. The mean of $\mathrm{P_D}$ as a function of the mean of $\mathrm{P_F}$ for different filter types, filter settings and $\mathrm{SNR_{in}}$. Different filter settings are indicated by marker type whereas $\mathrm{SNR_{in}}$ by line color. The 90% $\mathrm{P_D}$ level is highlighted by a grey line.
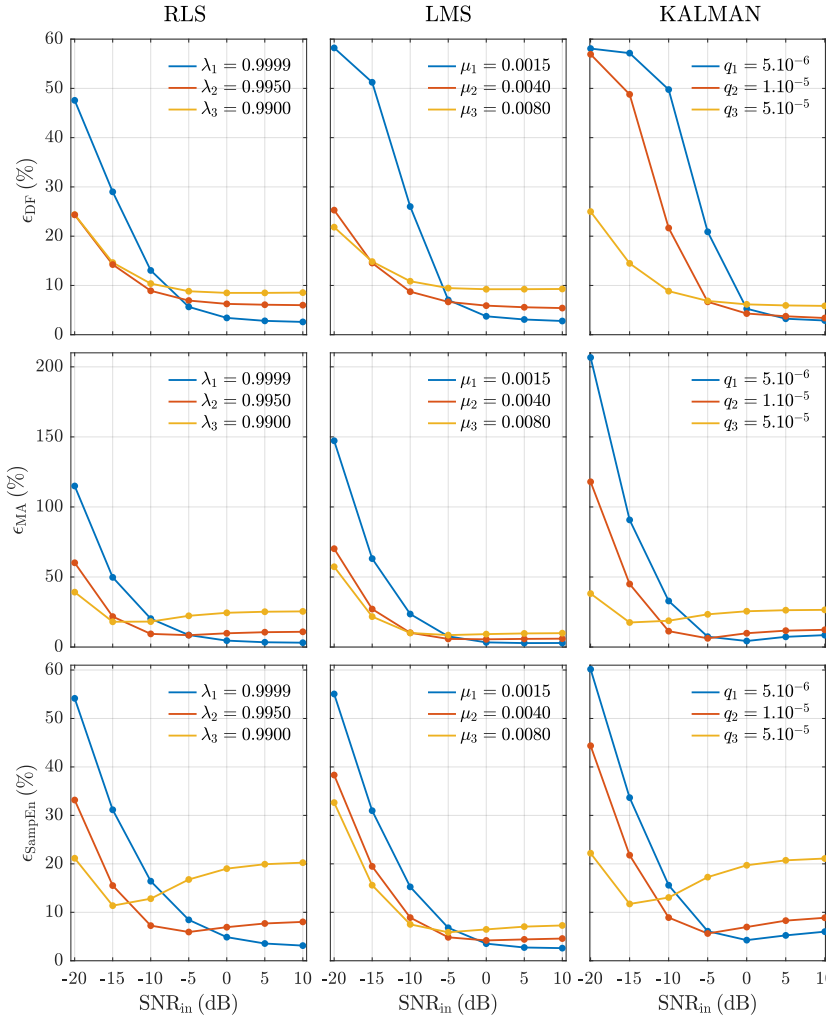
Figure 6. The mean absolute relative error of DF, MA and SampEn as a function of λ, μ, q and SNR_{in} for different filter types and settings.

filtering is used. The error of DF is lower than 30% for $SNR_{in} \leq -5$ when coarse filtering is used. For large SNR_{in}, the DF of the restored VF signal is best preserved using moderate and fine filtering. The errors of MA and SampEn follow a similar pattern, with the LMS filter being the best filter overall, especially for SNR_{in} above -10 dB. The RLS and Kalman filters show a degradation in the estimation of amplitude and complexity for moderate and coarse filtering as SNR_{in} increases, possibly caused by spiky filtering residuals.
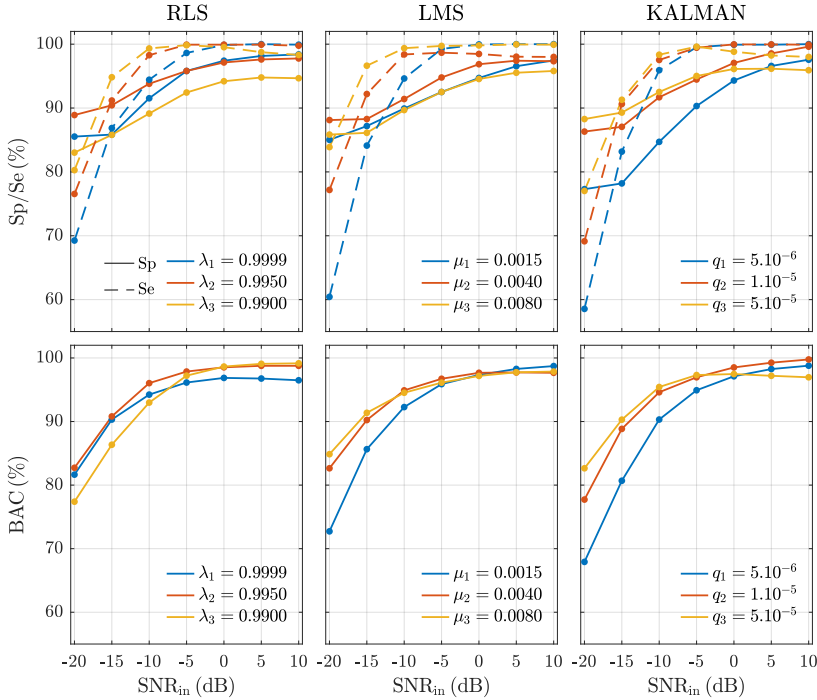
Figure 7. Performance of the shock/no-shock diagnosis for different filter types and settings.
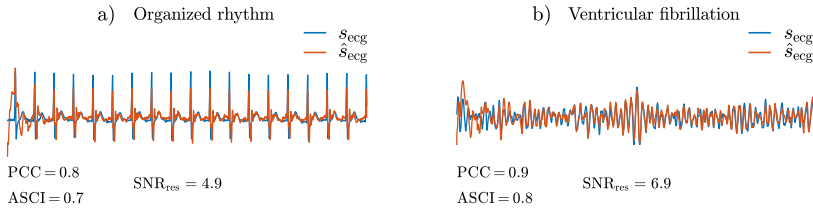
Figure 8. Effect of filtering on the amplitude of $s_{\mathrm{ecg}}(n)$ for OR (a) and VF (b) at $\mathrm{SNR_{in}} = -10\,\mathrm{dB}$.

4.3. Shock/no-shock classification

The performance of the classifiers on the test set is shown in Figure 7 as a function of $\mathrm{SNR_{in}}$. For most filter settings, Se and Sp are almost constant for $\mathrm{SNR_{in}}$ above $-5\,\mathrm{dB}$. Moderate filtering yields better classification of OR (higher Sp), whereas coarse filtering yields better classification of VF (higher Se). The best overall performance in terms of BAC is obtained for the RLS filter, though the differences between the three filter settings are small. The Kalman filter is associated with the worst classification results, suggesting that the state-space model may not be an efficient approach for estimating

the CPR artefact model in (6). For all SNR_{in}, the BAC of the coarse LMS filter is just marginally lower (0.6-percentage points) than that of the best RLS filter.

The accuracy of the shock/no-shock decision algorithm was tested directly on the 165 CPR artefacts (with nonshockable asystole as the underlying rhythm). After filtering the artefact with the RLS filter and $\lambda = 0.995$ (best configuration), the specificity was found to be 99.4%.

Figure 9 shows four illustrative examples of misclassified segments for both shockable (VF) and nonshockable (OR) rhythms. In Figure 9a and b the artefact presents high frequency harmonics causing fast and disorganized filtering residuals in $\hat{s}_{\text{ecg}}(n)$. Thus, the filtered OR rhythm resembles VF. Figure 9c and d shows spiky and high-amplitude filtering residuals resembling an OR rhythm in patients with VF, leading to a misdiagnosis in the shock/no-shock decision algorithm.
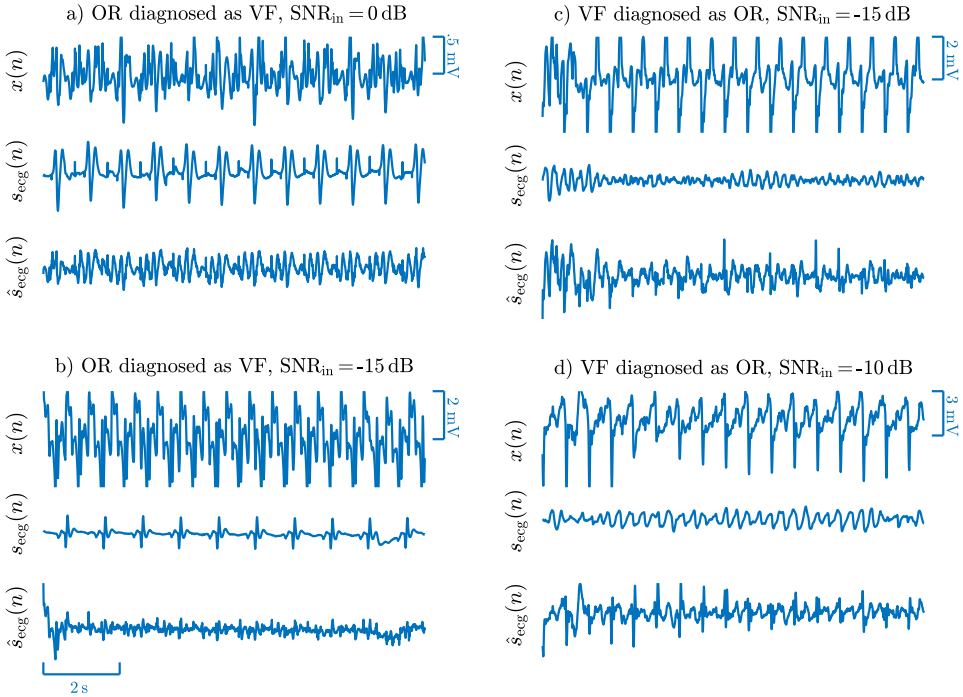

Figure 9. Examples of classification errors. Segments with OR rhythms (a,b) and segments with VF (c,d).

5. Discussion and conclusions

To the best of our knowledge, the present study provides the first thorough evaluation of ECG waveform restoration following adaptive mechanical CPR artefact cancellation

filtering. With this approach, signal quality indices and clinically relevant ECG features can be determined, providing insights into how accurately the underlying ECG rhythms can be restored with filtering. In addition to SNR_{res}, we introduce correlation-based similarity indices [30, 38] and typical OR and VF characteristics of relevance in applications such as shock outcome prediction [21, 35] and detection of pulse [22, 31]. Since ALS clinicians decide on whether to shock the patient by observing $\hat{s}_{\text{ecg}}(n)$, filters that provide the highest signal quality and preserve the salient features of the rhythms are desirable. Moreover, for each filter setting, a 6-feature machine learning algorithm was adjusted to evaluate the viability of an automated shock/no-shock decision and the influence of SNR_{in} on diagnostic accuracy during mechanical CPR.

The high values of SNR_{res} (mean increase of 9.5 dB across all SNR_{in}) presented in Figure 3 show that adaptive filtering considerably reduces CPR artefacts, while the high correlation coefficients indicate that the ECG waveforms are quite accurately preserved in $\hat{s}_{\text{ecg}}(n)$. However, the ASCI values are slightly below the PCC values suggesting an amplitude reduction in the ECG after filtering. This is illustrated in Figure 8 where SNR_{res} is large and both PCC and ASCI are above 0.8, but ASCI is 0.1 smaller than PCC in both cases. The waveform amplitude is lower in $\hat{s}_{\text{ecg}}(n)$ than in $s_{\text{ecg}}(n)$.

Besides waveform alterations, this work shows for the first time that filtering causes changes to the intrinsic properties of OR and VF. The performance of the QRS detector applied to $s_{\text{ecg}}(n)$ is lower when compared to those obtained on standard databases [32]. However, QRS detection in cardiac arrest patients presenting ORs is known to be challenging [31], since QRS complexes may be wide and have aberrant morphologies. As expected, the performance is lower when the QRS detector is applied to $\hat{s}_{\text{ecg}}(n)$. As shown in Figure 5, true QRS complexes are accurately detected after filtering regardless of SNR_{in}. However, as SNR_{in} decreases, the rate of false positives soars due to spiky filtering residuals confounded as actual heartbeats. This may not be a deleterious effect for shock decision algorithms since QRS presence may be enough for a no-shock decision [39], but the effect may confound other algorithms dependent on heart rate and QRS morphology such as the prediction of re-arrest [23] and the detection of spontaneous pulse [31, 40–42]. As for the restoration of VF characteristics, the best results are obtained for coarse filtering; all three types of filtering present a similar trend. At low SNR_{in}, fine filtering inefficiently removes the CPR artefact, causing the dominant frequency of the filtered VF to match the LUCAS-2 rate (1.67 Hz) in about one third of the cases when the best fine filtering is used ($\text{SNR}_{\text{in}} = -20$ dB and RLS with $\lambda = 0.9999$). This is a significant error considering that the mean (standard deviation) DF for clean VF in our data is 5.1 (1.5) Hz. For MA and SampEn, errors are also very large for fine filtering at low SNR_{in}, with relative errors in MA and SampEn in excess of 100% and 50%, respectively. The best overall filter to estimate SampEn is the coarse LMS filter, with an error rate below 30% for $\text{SNR}_{\text{in}} \geq -15$ dB and an error below 10% for $\text{SNR}_{\text{in}} \geq -10$ dB. These results may be of clinical importance as the dominant frequency, amplitude and entropies have been used as predictors of succesful defibrillations [21, 33–35, 43]. Our results suggest that the prediction of

defibrillation success during mechanical CPR may be possible without interrupting the chest compression therapy—a result in line with some recent findings on manual CPR [44].

While an ALS setting requires accurate restoration of $s_{\text{ecg}}(n)$, the shock/no-shock decision of $\hat{s}_{\text{ecg}}(n)$ is also crucial in automatic external defibrillators, used mainly by non-medical personnel. The decision algorithm implemented in this study has Sp below the 95% recommended by the AHA for $\text{SNR}_{\text{in}} < -5\,\text{dB}$. Moreover, Se is in compliance with the 90% recommended by the AHA for $\text{SNR}_{\text{in}} \geq -15\,\text{dB}$. For $\text{SNR}_{\text{in}} \leq -15\,\text{dB}$ Se is very low, meaning many false negatives. This is mostly because spiky and organized filtering residuals are interpreted as QRS complexes of organized rhythms in VF patients [26]. As SNR_{in} increases, a large portion of those false negatives are recovered leading to a significant increase in Se. Specificity remains quite constant for all SNR_{in}. The algorithmic procedure followed for shock/no-shock decision during mechanical CPR was recently demonstrated to have Se/Sp above 95% [26]. Our results suggest that a plausible explanation for those results is that SNR_{in}, in most cases, is high (above $-10\,\text{dB}$).

The SNR_{in} is unknown in real cardiac arrest data, so a filter cannot be adjusted to the SNR_{in}. Thus, the filter that on average shows the best performance should be preferred. Table 1 shows the mean performance across all SNR_{in} for each filter and type of filtering. The RLS filter offers the best preservation of waveform morphology (higher PCC and ASCI), as well as QRS detection performance in terms of P_D-to-P_F ratio. The VF waveform features are best preserved by the LMS filter, using either moderate or coarse filtering, although the results are almost identical to those of moderate RLS filtering. The best results on rhythm classification are obtained for moderate RLS filtering.

In monitor–defibrillators, the computational demands are important to consider because these devices use lower-end microprocessors and FPGAs which run many tasks in parallel. The LMS filter has much lower computational demands than either the RLS or Kalman filters because it only involves an error estimation at time n for the filter update equations. The RLS filter has recursions that involve matrix products [25], and so do the state-space equations. So the choice of adaptive filter should be a compromise between diagnostic accuracy, waveform preservation and computational demands on the monitor–defibrillator.

This study has certain limitations. Data obtained from a single piston driven device were used (LUCAS-2). This is the most widespread mechanical CPR device, whose impact on survival has been studied in two large randomized trials [2,17]. However, there are other piston driven devices on the market [45, 46], and even alternative technologies based on load distribution bands [18]. Our results should generalize well to other piston driven devices, whereas the effect of filtering would need to be studied separately for devices based on load distribution bands for which the artefact characteristics are different [20, 47]. Moreover, data were gathered using one type of monitor–defibrillator and from a single EMS agency. The characteristics of the ECG acquisition circuitry,

Table 1. Mean performance across all SNR_{in} for different filter types and settings.

	PCC	ASCI	P_D/P_F	ϵ_{DF}	ϵ_{MA}	ϵ_{SampEn}	Se	Sp	BAC
RLS									
$\lambda_1 = 0.9999$	**0.80**	**0.71**	**4.9**	14.9	24.7	17.4	92.7	93.2	93.0
$\lambda_2 = 0.9950$	0.76	0.65	2.9	10.4	18.7	12.1	95.1	**94.5**	**94.8**
$\lambda_3 = 0.9900$	0.68	0.59	2.8	12.0	29.2	17.3	95.8	90.6	93.2
LMS									
$\mu_1 = 0.0015$	0.76	0.68	4.6	21.7	35.8	16.7	91.2	91.9	91.6
$\mu_2 = 0.0040$	0.77	0.67	3.0	**10.3**	18.7	12.1	94.4	93.5	93.9
$\mu_3 = 0.0080$	0.68	0.58	2.8	12.1	**18.1**	**11.8**	**97.0**	91.4	94.2
KALMAN									
$q_1 = 5 \cdot 10^{-6}$	0.70	0.62	4.4	28.2	51.1	18.7	91.0	88.4	89.7
$q_2 = 1 \cdot 10^{-5}$	0.74	0.67	3.8	20.8	30.6	15.0	93.8	93.5	93.7
$q_3 = 5 \cdot 10^{-5}$	0.75	0.64	2.9	10.4	25.2	18.0	94.5	93.3	93.9

including sampling frequency, voltage resolution and bandwidths, differ slightly between devices, but should not alter our results substantially. Although different EMS agencies may have different protocols and quality of CPR, the use of a mechanical CPR device standardizes treatment. Finally, an additive mixture model was used to produce a noisy ECG by adding a CPR artefact to a clean ECG at different SNRs. This type of model was proposed in [7] and has since then been used in many studies [6, 10, 25, 26]. However, the model may not accurately reflect the effect of CPR on heart dynamics. Although the additive mixture model is the best available model to evaluate the effect of filtering on ECG characteristics, a better way to evaluate shock/no-shock decision algorithms would be to use noisy ECGs recorded during OHCA. Therefore, a future study is justified to validate the shock/no-shock decision algorithm on real ECGs corrupted by CPR artefacts.

6. Bibliography

[1] C. Atwood, M. S. Eisenberg, J. Herlitz, and T. D. Rea, "Incidence of EMS-treated out-of-hospital cardiac arrest in Europe," *Resuscitation*, vol. 67, no. 1, pp. 75–80, 2005.

[2] G. D. Perkins, A. J. Handley, R. W. Koster, M. Castrén, M. A. Smyth, T. Olasveengen, K. G. Monsieurs, V. Raffay, J.-T. Gräsner, V. Wenzel *et al.*, "European resuscitation council guidelines for resuscitation 2015: Section 2. Adult basic life support and automated external defibrillation," *Resuscitation*, vol. 95, pp. 81–99, 2015.

[3] C. Vaillancourt, S. Everson-Stewart, J. Christenson, D. Andrusiek, J. Powell, G. Nichol, S. Cheskes, T. P. Aufderheide, R. Berg, I. G. Stiell *et al.*, "The impact of increased chest compression fraction on return of spontaneous circulation for out-of-hospital cardiac arrest patients not in ventricular fibrillation," *Resuscitation*, vol. 82, no. 12, pp. 1501–1507, 2011.

[4] S. Ruiz de Gauna, U. Irusta, J. Ruiz, U. Ayala, E. Aramendi, and T. Eftestøl, "Rhythm analysis during cardiopulmonary resuscitation: past, present, and future," *Biomed. Res. Int.*, vol. 2014, 2014.

[5] R. Affatato, Y. Li, and G. Ristagno, "See through ECG technology during cardiopulmonary resuscitation to analyze rhythm and predict defibrillation outcome," *Curr. Opin. Crit. Care*, vol. 22, no. 3, pp. 199–205, 2016.

[6] A. Langhelle, T. Eftestøl, H. Myklebust, M. Eriksen, B. T. Holten, and P. A. Steen, "Reducing CPR artefacts in ventricular fibrillation in vitro," *Resuscitation*, vol. 48, no. 3, pp. 279–291, 2001.

[7] S. O. Aase, T. Eftestøl, J. Husøy, K. Sunde, and P. A. Steen, "CPR artifact removal from human ECG using optimal multichannel filtering," *IEEE Trans. Biomed. Eng.*, vol. 47, no. 11, pp. 1440–1449, 2000.

[8] R. D. Berger, J. Palazzolo, and H. Halperin, "Rhythm discrimination during uninterrupted CPR using motion artifact reduction system," *Resuscitation*, vol. 75, no. 1, pp. 145–152, 2007.

[9] T. Werther, A. Klotz, G. Kracher, M. Baubin, H. G. Feichtinger, H. Gilly, and A. Amann, "CPR artifact removal in ventricular fibrillation ECG signals using Gabor multipliers," *IEEE Trans. Biomed. Eng.*, vol. 56, no. 2, pp. 320–327, 2008.

[10] J. H. Husøy, J. Eilevstjonn, T. Eftestøl, S. O. Aase, H. Myklebust, and P. A. Steen, "Removal of cardiopulmonary resuscitation artifacts from human ECG using an efficient matching pursuit-like algorithm," *IEEE Trans. Biomed. Eng.*, vol. 49, no. 11, pp. 1287–1298, 2002.

[11] K. Rheinberger, T. Steinberger, K. Unterkofler, M. Baubin, A. Klotz, and A. Amann, "Removal of CPR artifacts from the ventricular fibrillation ECG by adaptive regression on lagged reference signals," *IEEE Trans. Biomed. Eng.*, vol. 55, no. 1, pp. 130–137, 2007.

[12] U. Irusta, J. Ruiz, S. R. de Gauna, T. Eftestøl, and J. Kramer-Johansen, "A least mean-square filter for the estimation of the cardiopulmonary resuscitation artifact based on the frequency of the compressions," *IEEE Trans. Biomed. Eng.*, vol. 56, no. 4, pp. 1052–1062, 2009.

[13] I. Isasi, U. Irusta, A. B. Rad, E. Aramendi, M. Zabihi, T. Eftestøl, J. Kramer-Johansen, and L. Wik, "Automatic cardiac rhythm classification with concurrent manual chest compressions," *IEEE Access*, vol. 7, pp. 115 147–115 159, 2019.

[14] J. Ruiz, U. Irusta, S. R. de Gauna, and T. Eftestøl, "Cardiopulmonary resuscitation artefact suppression using a Kalman filter and the frequency of chest compressions as the reference signal," *Resuscitation*, vol. 81, no. 9, pp. 1087–1094, 2010.

[15] U. Ayala, T. Eftestøl, E. Alonso, U. Irusta, E. Aramendi, S. Wali, and J. Kramer-Johansen, "Automatic detection of chest compressions for the assessment of CPR-quality parameters," *Resuscitation*, vol. 85, no. 7, pp. 957–963, 2014.

[16] E. Aramendi, U. Ayala, U. Irusta, E. Alonso, T. Eftestøl, and J. Kramer-Johansen, "Suppression of the cardiopulmonary resuscitation artefacts using the instantaneous chest compression rate extracted from the thoracic impedance," *Resuscitation*, vol. 83, no. 6, pp. 692–698, 2012.

[17] S. Rubertsson, E. Lindgren, D. Smekal, O. Östlund, J. Silfverstolpe, R. A. Lichtveld, R. Boomars, B. Ahlstedt, G. Skoog, R. Kastberg, D. Halliwell, M. Box, H. Johan, and K. Rolf, "Mechanical chest compressions and simultaneous defibrillation vs conventional cardiopulmonary resuscitation in out-of-hospital cardiac arrest: the LINC randomized trial," *JAMA*, vol. 311, no. 1, pp. 53–61, 2014.

[18] L. Wik, J.-A. Olsen, D. Persse, F. Sterz, M. Lozano Jr, M. A. Brouwer, M. Westfall, C. M. Souders, R. Malzer, P. M. van Grunsven *et al.*, "Manual vs. integrated automatic load-distributing band CPR with equal survival after out of hospital cardiac arrest. the randomized CIRC trial," *Resuscitation*, vol. 85, no. 6, pp. 741–748, 2014.

[19] J. Sullivan, R. Walker, A. Esibov, and F. Chapman, "A digital filter can effectively remove mechanical chest compression artifact," *Resuscitation*, vol. 85, p. S41, 2014.

[20] E. Aramendi, U. Irusta, U. Ayala, H. Naas, J. Kramer-Johansen, and T. Eftestøl, "Filtering mechanical chest compression artefacts from out-of-hospital cardiac arrest data," *Resuscitation*,

vol. 98, pp. 41–47, 2016.

[21] B. Chicote, U. Irusta, R. Alcaraz, J. J. Rieta, E. Aramendi, I. Isasi, D. Alonso, and K. Ibarguren, "Application of entropy-based features to predict defibrillation outcome in cardiac arrest," *Entropy*, vol. 18, no. 9, p. 313, 2016.

[22] A. Elola, E. Aramendi, U. Irusta, J. Del Ser, E. Alonso, and M. Daya, "ECG-based pulse detection during cardiac arrest using random forest classifier," *Med. Biol. Eng. Comput.*, vol. 57, no. 2, pp. 453–462, 2019.

[23] A. Elola, E. Aramendi, U. Irusta, N. Amezaga, J. Urteaga, P. Owens, and A. H. Idris, "Machine learning techniques to predict cardiac re-arrest in out-of-hospital setting," *Circulation*, vol. 140, pp. A127–A127, 2019.

[24] A. B. Rad, T. Eftestøl, K. Engan, U. Irusta, J. T. Kvaløy, J. Kramer-Johansen, L. Wik, and A. K. Katsaggelos, "ECG-based classification of resuscitation cardiac rhythms for retrospective data analysis," *IEEE Trans. Biomed. Eng.*, vol. 64, no. 10, pp. 2411–2418, 2017.

[25] I. Isasi, U. Irusta, E. Aramendi, U. Ayala, E. Alonso, J. Kramer-Johansen, and T. Eftestøl, "A multistage algorithm for ECG rhythm analysis during piston-driven mechanical chest compressions," *IEEE Trans. Biomed. Eng.*, vol. 66, no. 1, pp. 263–272, 2018.

[26] I. Isasi, U. Irusta, A. Elola, E. Aramendi, U. Ayala, E. Alonso, J. Kramer-Johansen, and T. Eftestøl, "A machine learning shock decision algorithm for use during piston-driven chest compressions," *IEEE Trans. Biomed. Eng.*, vol. 66, no. 6, pp. 1752–1760, 2018.

[27] S. R. de Gauna, J. Ruiz, U. Irusta, E. Aramendi, T. Eftestøl, and J. Kramer-Johansen, "A method to remove CPR artefacts from human ECG using only the recorded ECG," *Resuscitation*, vol. 76, no. 2, pp. 271–278, 2008.

[28] S. Haykin, *Kalman Filtering and Neural Networks.* John Wiley & Sons, 2004, vol. 47.

[29] J. Lian, G. Garner, D. Muessig, and V. Lang, "A simple method to quantify the morphological similarity between signals," *Signal Process.*, vol. 90, no. 2, pp. 684–688, 2010.

[30] R. Alcaraz, F. Hornero, A. Martínez, and J. J. Rieta, "Short-time regularity assessment of fibrillatory waves from the surface ECG in atrial fibrillation," *Physiol. Meas.*, vol. 33, no. 6, p. 969, 2012.

[31] A. Elola, E. Aramendi, U. Irusta, E. Alonso, Y. Lu, M. P. Chang, P. Owens, and A. H. Idris, "Capnography: A support tool for the detection of return of spontaneous circulation in out-of-hospital cardiac arrest," *Resuscitation*, vol. 142, pp. 153–161, 2019.

[32] J. P. Martínez, R. Almeida, S. Olmos, A. P. Rocha, and P. Laguna, "A wavelet-based ECG delineator: evaluation on standard databases," *IEEE Trans. Biomed. Eng.*, vol. 51, no. 4, pp. 570–581, 2004.

[33] C. G. Brown and R. Dzwonczyk, "Signal analysis of the human electrocardiogram during ventricular fibrillation: frequency and amplitude parameters as predictors of successful countershock," *Ann. Emerg. Med.*, vol. 27, no. 2, pp. 184–188, 1996.

[34] W. D. Weaver, L. A. Cobb, D. Dennis, R. Ray, A. P. Hallstrom, and M. K. Copass, "Amplitude of ventricular fibrillation waveform and outcome after cardiac arrest," *Ann. Intern. Med.*, vol. 102, no. 1, pp. 53–55, 1985.

[35] B. Chicote, U. Irusta, E. Aramendi, R. Alcaraz, J. J. Rieta, I. Isasi, D. Alonso, M. Baqueriza, and K. Ibarguren, "Fuzzy and sample entropies as predictors of patient survival using short ventricular fibrillation recordings during out of hospital cardiac arrest," *Entropy*, vol. 20, no. 8, p. 591, 2018.

[36] C. Figuera, U. Irusta, E. Morgado, E. Aramendi, U. Ayala, L. Wik, J. Kramer-Johansen, T. Eftestøl, and F. Alonso-Atienza, "Machine learning techniques for the detection of shockable rhythms in automated external defibrillators," *PloS ONE*, vol. 11, no. 7, p. e0159654, 2016.

[37] B. Scholkopf, K.-K. Sung, C. J. Burges, F. Girosi, P. Niyogi, T. Poggio, and V. Vapnik, "Comparing support vector machines with Gaussian kernels to radial basis function classifiers," *IEEE Trans. Biomed. Eng.*, vol. 45, no. 11, pp. 2758–2765, 1997.

[38] M. García, M. Martínez-Iniesta, J. Ródenas, J. J. Rieta, and R. Alcaraz, "A novel wavelet-based

filtering strategy to remove powerline interference from electrocardiograms with atrial fibrillation," *Physiol. Meas.*, vol. 39, no. 11, p. 115006, 2018.

[39] U. Irusta, J. Ruiz, E. Aramendi, S. R. de Gauna, U. Ayala, and E. Alonso, "A high-temporal resolution algorithm to discriminate shockable from nonshockable rhythms in adults and children," *Resuscitation*, vol. 83, no. 9, pp. 1090–1097, 2012.

[40] E. Alonso, E. Aramendi, M. Daya, U. Irusta, B. Chicote, J. K. Russell, and L. G. Tereshchenko, "Circulation detection using the electrocardiogram and the thoracic impedance acquired by defibrillation pads," *Resuscitation*, vol. 99, pp. 56–62, 2016.

[41] M. Risdal, S. O. Aase, J. Kramer-Johansen, and T. Eftesøl, "Automatic identification of return of spontaneous circulation during cardiopulmonary resuscitation," *IEEE Trans. Biomed. Eng.*, vol. 55, no. 1, pp. 60–68, 2007.

[42] J. Ruiz, E. Alonso, E. Aramendi, J. Kramer-Johansen, T. Eftestøl, U. Ayala, and D. González-Otero, "Reliable extraction of the circulation component in the thoracic impedance measured by defibrillation pads," *Resuscitation*, vol. 84, no. 10, pp. 1345–1352, 2013.

[43] L. D. Sherman, "The frequency ratio: an improved method to estimate ventricular fibrillation duration based on Fourier analysis of the waveform," *Resuscitation*, vol. 69, no. 3, pp. 479–486, 2006.

[44] J. Coult, J. Blackwood, L. Sherman, T. D. Rea, P. J. Kudenchuk, and H. Kwok, "Ventricular fibrillation waveform analysis during chest compressions to predict survival from cardiac arrest," *Circulation*, vol. 12, no. 1, p. e006924, 2019.

[45] L. Zhang and H. Zhang, "Clinical application of Thumper in emergency cardiopulmonary resuscitation," *Baotou Medical College*, vol. 6, 2008.

[46] W. Wieczorek and H. Kaminska, "Impact of a corpuls CPR mechanical chest compression device on chest compression quality during extended pediatric manikin resuscitation: a randomized crossover pilot study," *Disaster Emerg. Med. J.*, vol. 2, no. 2, pp. 58–63, 2017.

[47] I. Isasi, U. Irusta, E. Aramendi, J. Age, and L. Wik, "Characterization of the ECG compression artefact caused by the Autopulse device," *Resuscitation*, vol. 118, p. e38, 2017.